The methionine biosynthesis operon in *Staphylococcus aureus*: Role of concerted RNA decay in transcript stability and T-box riboswitch turnover

Das Methioninbiosynthese-Operon in *Staphylococcus aureus*: Der Einfluss von koordiniertem RNA Abbau auf Transkriptstabilität und T-Box-Riboswitch-Prozessierung

Doctoral thesis for a doctoral degree (Dr. rer. nat.)
at the Graduate School of Life Sciences,
Julius-Maximilians-Universität Würzburg,
Section: Infection and Immunity

submitted by

Freya Dorothea Ruth Wencker, M. Sc.

from

Castrop-Rauxel

Würzburg, **February 2020**

Reverse page

Submitted on: ……..……..

Office stamp

Members of the *Promotionskomitee*:

Chairperson: Prof Dr Thomas Dandekar

Primary Supervisor: PD Dr Wilma Ziebuhr

Supervisor (Second): PD Dr Knut Ohlsen

Supervisor (Third): Prof Dr Caroline Kisker

Date of Public Defence: ……..……

Date of Receipt of Certificates: …….

Affidavit

I hereby confirm that my thesis entitled ‘The methionine biosynthesis operon in Staphylococcus aureus:
Role of concerted RNA decay in transcript stability and T-box riboswitch turnover’ is the result of my own work. I did not receive any help or support from commercial consultants. All sources and / or materials applied are listed and specified in the thesis.

Furthermore, I confirm that this thesis has not yet been submitted as part of another examination process neither in identical nor in similar form.

‘

Place, Date Signature

Eidesstattliche Erklärung

Hiermit erkläre ich an Eides statt, die Dissertation „Das Methioninbiosynthese-Operon in Staphylococcus aureus:
Der Einfluss von koordiniertem RNA Abbau auf Transkriptstabilität und T-Box-Riboswitch-Prozessierung" eigenständig, d.h. insbesondere selbständig und ohne Hilfe eines kommerziellen Promotionsberaters, angefertigt und keine anderen als die von mir angegebenen Quellen und Hilfsmittel verwendet zu haben.

Ich erkläre außerdem, dass die Dissertation weder in gleicher noch in ähnlicher Form bereits in einem anderen Prüfungsverfahren vorgelegen hat.

Ort, Datum Unterschrift

„Die höchste Form des Glücks ist ein Leben mit einem gewissen Grad an Verrücktheit.“

‘The highest form of bliss is living with a certain degree of folly.’

-Erasmus von Rotterdam-

Summary

Methionine is the first amino acid of every newly synthesised protein. In combination with its role as precursor for the vital methyl-group donor S-adenosylmethionine, methionine is essential for every living cell. The opportunistic human pathogen *Staphylococcus aureus* is capable of synthesising methionine *de novo*, when it becomes scarce in the environment. All genes required for the *de novo* biosynthesis are encoded by the *metICFE-mdh* operon, except for *metX*. Expression is controlled by a hierarchical network with a methionyl-tRNA-specific T-box riboswitch (MET-TBRS) as centrepiece, that is also referred to as *met* leader (RNA). T-box riboswitches (TBRS) are regulatory RNA elements located in the 5'-untranslated region (5'-UTR) of genes. The effector molecule of T-box riboswitches is uncharged cognate tRNA. The prevailing mechanism of action is premature termination of transcription of the nascent RNA in the absence of the effector (*i.e.* uncharged cognate tRNA) due to formation of a hairpin structure, the Terminator stem. In presence of the effector, a transient stabilisation of the alternative structure, the Antiterminator, enables transcription of the downstream genes ('read-through'). Albeit, after the read-through the thermodynamically more stable Terminator eventually forms. The Terminator and the Antiterminator are two mutually exclusive structures. Previous work of the research group showed that in staphylococci the MET-TBRS ensures strictly methionine-dependent control of *met* operon expression. Uncharged methionyl-tRNA that activates the system is only present in sufficient amounts under methionine-deprived conditions. In contrast to other bacterial TBRS, the staphylococcal MET-TBRS has some characteristic features regarding its length and predicted secondary structure whose relevance for the function are yet unkown.

Aim of the present thesis was to experimentally determine the structure of the *met* leader RNA and to investigate the stability of the *met* operon-specific transcripts in the context of methionine biosynthesis control. Furthermore, the yet unknown function of the *mdh* gene within the *met* operon was to be determined.

In the context of this thesis, the secondary structure of the *met* leader was determined employing in-line probing. The structural analysis revealed the presence of almost all highly conserved T-box riboswitch structural characteristics. Furthermore, three additional stems, absent in all T-box riboswitches analysed to date, could be identified. Particularly remarkable is the above average length of the Terminator stem which renders it a potential target of the double-strand-specific endoribonuclease III (RNase III). The RNase III-dependent cleavage of

the *met* leader could be experimentally verified by the use of suitable mutants. Moreover, the exact cleavage site within the Terminator was determined.

The unusual immediate separation of the *met* leader from the *met* operon mRNA via the RNase III cleavage within the Terminator stem induces the rapid degradation of the *met* leader RNA and, most likely, that of the 5'-region of the *met* mRNA. The *met* mRNA is degraded from its 5'-end by the exoribonuclease RNase J. The stability of the *met* mRNA was found to vary over the length of the transcript with an instable 5'-end (*metI* and *metC*) and a longer half-life towards the 3'-end (*metE* and *mdh*). The varying transcript stability is reflected by differences in the available cellular protein levels. The obtained data suggest that programmed mRNA degradation is another level of regulation in the complex network of staphylococcal *de novo* methionine biosynthesis control.

In addition, the MET-TBRS was studied with regard to a future use as a drug target for novel antimicrobial agents. To this end, effects of a dysregulated methionine biosynthesis on bacterial growth and survival were investigated in *met* leader mutants that either caused permanent transcription of the *met* operon ('ON') or prevented operon transcription ('OFF'), irrespective of the methionine status in the cell. Methionine deprivation turned out to be a strong selection pressure, as 'OFF' mutants acquired adaptive mutations within the *met* leader to restore *met* operon expression that subsequently re-enabled growth.

The second part of the thesis was dedicated to the characterisation of the Mdh protein that is encoded by the last gene of the *met* operon and whose function is unknown yet. At first, co-transcription and -expression with the *met* operon could be demonstrated. Next, the Mdh protein was overexpressed and purified and the crystal structure of Mdh was solved to high resolution by the Kisker research group (Rudolf-Virchow-Zentrum Würzburg). Analysis of the structure revealed the amino acid residues crucial for catalytic activity, and zinc was identified as a co-factor of Mdh. Also, Mdh was shown to exist as a dimer. However, identification of the Mdh substrate was, in the context of this thesis, (still) unsuccessful. Nevertheless, interactions of Mdh with enzymes of the *met* operon could be demonstrated by employing the bacterial two-hybrid system. This fact and the high conservation of *mdh*/Mdh on nucleotide and amino acid level among numerous staphylococcal species suggests an important role of Mdh within the methionine metabolism that should be a worthwhile subject of future research.

Zusammenfassung

Methionin ist die erste Aminosäure in jedem neu gebildeten Protein. Zusammen mit seiner Funktion als Vorläufermolekül für die Synthese des essenziellen Methylgruppendonors S-Adenosylmethionin ist Methionin damit für jede lebende Zelle unverzichtbar. *Staphylococcus aureus*, ein opportunistisches Humanpathogen, ist in der Lage, Methionin *de novo* zu synthetisieren, wenn es nicht in ausreichender Menge in der Umgebung vorhanden ist. Mit Ausnahme von MetX sind alle für die Methioninsynthese benötigten Enzyme im *metICFE-mdh*-Operon kodiert. Die Expression des Operons wird durch ein komplexes hierarchisches Netzwerk reguliert, dessen zentrales Steuerelement ein Methionyl-tRNA-spezifischer T-Box-Riboswitch (MET-TBRS) ist, der auch als *met*-leader (RNA) bezeichnet wird. T-Box Riboswitches (TBRS) sind regulatorische RNA-Elemente, die in der untranslatierten Region am 5'-Ende (5'-UTR) ihrer zu kontrollierenden Gene liegen. Sie nutzen unbeladene tRNAs als Effektormoleküle. Die Funktionsweise der meisten TBRS beruht auf dem vorzeitigen Abbruch der Transkription der naszierenden mRNA, der durch die Ausbildung einer Haarnadelstruktur (Terminator) im Transkript herbeigeführt wird, wenn das Effektormolekül (*i.e.* unbeladene tRNA) fehlt. Sobald passende unbeladene tRNA verfügbar ist und bindet, wird eine alternative Struktur, der Antiterminator, kurzzeitig stabilisiert, der die Transkription und damit ein "Durchlesen" in die stromabwärtsliegenden Gene ermöglicht. Terminator und Antiterminator sind zwei sich gegenseitig ausschließende Strukturen, wobei der Terminator die thermodynamisch deutlich stabilere Struktur des TBRS ist, die sich dementsprechend auch in den vollständigen Transkripten erneut ausbildet. Bisherige Vorarbeiten der Arbeitsgruppe zeigten, dass in Staphylokokken der MET-TBRS die Kontrolle der Methioninsynthese in strikter Abhängigkeit von Methionin gewährleistet. Unbeladene Methionyl-tRNA, die nur unter Methioninmangelbedingungen in ausreichenden Konzentrationen vorliegt, aktiviert das System. Im Unterschied zu anderen bakteriellen TBRS weist der Staphylokokken-MET-TBRS (*met*-leader) hinsichtlich seiner Länge und vorhergesagten Struktur einige Besonderheiten auf, deren Bedeutung für die Funktion bislang unklar sind.

Ziel der vorliegenden Arbeit war es daher, die Struktur der *met*-leader-RNA experimentell zu bestimmen und die Stabilität *met*-Operon-spezifischer Transkripte im Kontext der Methioninbiosynthesekontrolle zu untersuchen. Ebenso sollte die bisher unbekannte Funktion des *mdh*-Genes im Operon aufgeklärt werden.

Im Rahmen dieser Doktorarbeit wurde die Sekundärstruktur der *met*-leader-RNA mit Hilfe des so genannten *In-line Probings* bestimmt. Die Sekundärstruktur weist neben fast allen hochkonservierten Strukturmerkmalen eines T-Box-Riboswitches auch drei zusätzliche Haarnadelstrukturen auf, die bisher in keinem anderen T-Box-Riboswitch gefunden wurden. Besonders auffällig ist die überdurchschnittliche Länge des *met*-leader-Terminators, der dadurch zur potentiellen Zielstruktur für die Doppelstrang-spezifische Endoribonuklease RNase III wird. Mittels geeigneter Mutanten konnte die RNase III-abhängige Prozessierung der *met*-leader-RNA experimentell bewiesen werden. Ebenso wurde die exakte Schnittstelle im Terminator bestimmt. Die ungewöhnliche Prozessierung des Terminators durch die RNase III spaltet die *met*-leader-RNA von der *met*-mRNA ab, was den raschen weiteren Abbau der *met*-leader-RNA und sehr wahrscheinlich auch den der *met*-mRNA einleitet. So wird die *met*-mRNA durch die Exoribonuklease RNase J vom 5'-Ende her abgebaut, wobei die Stabilität bezogen auf die Gesamtheit des Moleküls stark variiert: Das 5'-Ende mit den Genen *metI* und *metC* wird äußerst schnell degradiert, während das 3'-Ende mit *metE* und *mdh* deutlich stabiler ist. Die variierende mRNA-Stabilität spiegelt sich auch in Unterschieden hinsichtlich der verfügbaren zellulären Proteinmengen wider. Die Daten legen daher nahe, dass programmierte mRNA-Degradation eine weitere Ebene im komplexen Kontrollnetzwerk darstellt, durch die in Staphylokokken die Methioninbiosynthese sehr exakt den jeweiligen Bedürfnissen angepasst wird.

Des Weiteren wurde der MET-TBRS im Hinblick auf eine zukünftige Nutzung als Angriffspunkt für neue antibakterielle Wirkstoffe untersucht. Dazu wurden die Auswirkungen einer dysregulierten Methioninbiosynthese auf das bakterielle Wachstum und Überleben mit Hilfe von *met*-leader-Mutanten analysiert, die entweder zu einer permanenten Aktivierung („ON“) oder Deaktivierung („OFF“) der *met*-Operon-Transkription, unabhängig vom Methioninstatus in der Zelle, führten. Es zeigte sich, dass Methioninmangel einen starken Selektionsdruck darstellt, da die „OFF“-Mutanten in der Lage waren, durch den Erwerb von adaptiven Mutationen innerhalb der *met*-leader-Sequenz, das *met*-Operon erneut zu aktivieren und wieder zu wachsen.

Der zweite Teil dieser Arbeit widmete sich der Charakterisierung des Mdh-Proteins, das im letzten Gen des *met*-Operons kodiert ist und dessen Funktion derzeit gänzlich unbekannt ist. Zunächst konnte die Kotranskription und -expression von *mdh* mit dem *met*-Operon gezeigt werden. In Zusammenarbeit mit der Arbeitsgruppe Kisker (Rudolf-Virchow-Zentrum Würzburg) wurden anhand von Kristallstrukturanalysen die Aminosäuren identifiziert, die

entscheidend für die katalytische Aktivität des Mdh-Enzyms sind, wobei Zink als ein Kofaktor fungiert. Ebenso zeigte sich, dass Mdh als Dimer vorliegt. Allerdings ist die Identifizierung des Mdh-Substrates im Rahmen dieser Arbeit (noch) nicht gelungen. Mittels eines bakteriellen Zwei-Hybridsystems wurde jedoch nachgewiesen, dass Mdh mit den anderen Enzymen des *met*-Operons interagiert. Dies und die hohe Konservierung von *mdh*/Mdh auf Nukleotid- und Aminosäureebene in verschiedenen Staphylokokkenarten legt eine wichtige Funktion von Mdh im Methioninstoffwechsel nahe, die lohnenswerter Gegendstand weiterer Untersuchungen sein sollte.

List of Figures

List of Tables

Abbreviation Index

(v/v)	(volume/volume)
(w/v)	(weight/volume)
3'-UTR	3'-untranslated region
5'-UTR	5'-untranslated region
aaRS	aminoacyl-synthetase
A	adenine
Amp	ampicillin
approx.	approximately
APS	ammonium persulfate
ATCC	American Type Culture Collection
ATP	adenosine triphosphate
au	arbitrary unit
B. anthracis	*Bacillus anthracis*
B. cereus	*Bacillus cereus*
B. subtilis	*Bacillus subtilis*
B. stearo-thermophilus	*Bacillus stearothermophilus*
BCAA	branched-chain amino acids
BHI	brain heart infusion
BLAST	Basic Local Alignment Search Tool
bp	base pair(s)
BSA	bovine serum albumin
BTHS	bacterial two-hybrid system
C	cytosine
C. glutamicum	*Corynebacterium glutamicum*
cAMP	cyclic AMP (adenosine monophosphate)
CAP	catabolite activator protein
CBL	cystathionine-β-lyase
CDM	chemically defined medium
cDNA	complementary DNA
CFU	colony-forming unit
CGS	cystathionine-γ-synthase

CH_3-THF	N^5-methyl-tetrahydrofolate
CH_3-THPTG	N^5-methyl-tetrahydropteroyl-(tri)glutamate
CIP	calf intestinal phosphatase
Cm	chloramphenicol
conc.	concentration
cRACE	rapid amplification of cDNA ends from circularised RNA
ctrl	control
CyaA	adenylate cyclase
D	aspartic acid
dCTP	deoxycytidine triphosphate
ddH_2O	double deionised water
DEPC	diethylpyrocarbonate
DMSO	dimethyl sulfoxide
DNA	deoxyribonucleic acid
DNase	deoxyribonuclease
dNTP	deoxyribonucleotide triphosphate
ds	double-stranded
E	glutamic acid
E. coli	*Escherichia coli*
e.g.	for example [lat. *exempli gratia*]
EDTA	ethylenediamine tetraacetic acid
Erm	erythromycin
et al.	and others [lat. *et alii*]
EtOH	ethanol
F	phenylalanine
FDH	formate dehydrogenase
F-Glu	N-formyl-L-glutamic acid
Fig.	figure
F-Met	N-formyl-L-methionine
g	gravitational acceleration (9.81 m/s^2)
G	guanine
Glu	glutamic acid
GTP	guanosine triphosphate

H	histidine
h	hour/hours
HAT	homoserine O-acetyltransferase
His	histidine
HST	homoserine O-succinyltransferases
i.e.	that is [lat. *id est*]
IH	isatin hydrolase
IPTG	isopropyl-β-D-1-thiogalactopyranoside
ISC-Nr.	Internal Strain Collection Number
Kana	kanamycin
KEGG	Kyoto Encyclopedia of Genes and Genomes
KFA	kynurenine formamidase
L	leucine
L. aggregata	*Labrenzia aggregata*
L. casei	*Lactobacillus casei*
L. lactis	*Lactococcus lactis*
LB	Luria-Bertani
LC–MS/MS	Liquid Chromatography tandem-Mass Spectrometry
MCS	multiple cloning site
Mdh	metal-dependent hydrolase
MET	L-methionine
+MET	methionine-rich/with methionine
-MET	methionine-deprived/without methionine
MET-TBRS	methionyl-tRNA-specific T-box riboswitch
Me-THF	methyl-tetrahydrofolate
min	minute/minutes
MOPS	4-morpholinepropanesulfonic acid
mRNA	messenger RNA
MRSA	methicillin-resistant *S. aureus*
NA	not applicable
NCBI	National Center for Biotechnology Information
ncRNA	non-coding RNA
NFK	N-formyl-L-kynurenine

nt	nucleotide
NTML	Nebraska Transposon Mutant Library
nts	nucleotides
OD	optical density
ORF	open reading frame
ori	origin of replication
P. aeruginosa	*Pseudomonas aeruginosa*
P/C/I	phenol/chloroform/isoamyl alcohol
PAA	polyacrylamide
PAGE	polyacrylamide gel electrophoresis
PBS	phosphate buffered saline
PCR	polymerase chain reaction
Phe	phenylalanine
PLG	phase lock gel
PNPase	polynucleotide phosphorylase
Q	glutamine
R	arginine
RACE	rapid amplification of cDNA ends
RBS	ribosome binding site
RNA	ribonucleic acid
RNase	ribonuclease
rRNA	ribosomal RNA
RSH	RelA/SpoT synthetases/hydrolases
RT	room temperature
S	serine
SAM	S-adenosylmethionine
S. aureus	*Staphylococcus aureus*
S. suis	*Streptococcus suis*
S. thermophilus	*Streptococcus thermophilus*
SCV	small colony variant
SD	standard deviation
SDS	sodium dodecyl sulfate
SDS-PAGE	sodium dodecyl sulfate-polyacrylamide gel electrophoresis

sec	second/seconds
Ser	serine
sRNA	small RNA
ss	single-stranded
SSC	saline sodium citrate
T	thymine
TF	transcription factor
T.I.R.	translation initiation rate
T_A	annealing temperature (for PCR)
Tab.	table
TAE	tris/acetate/EDTA
TBE	tris/borate/EDTA
TBRS	T-box riboswitch
t_E	elongation time (for PCR)
TEMED	tetramethylethylendiamin
Tm	melting temperature (for PCR)
Tris	tris-(hydroxymethyl)-aminomethan
tRNA	transfer RNA
Trp	tryptophan
TSB	tryptic soy broth
TSS	transcription start site
Tyr	tyrosine
U	uracil
UTR	untranslated region
UV	ultraviolet
wt	wild type
X-gal	5-bromo-4-chloro-3-indolyl-β-D-galactopyranoside

Units and Multiples

%	per cent
°C	degree Celsius
bp	base pair
Ci	Curie
g	gram
g	gravitational acceleration (9.81 m/s^2)
h	hour
J	joule
k	kilo (10^3)
kb	kilo bases
kDa	kilo Dalton
l	liter
M	molar
m	milli (10^{-3})
min	minute
n	nano (10^{-9})
nm	nanometer
nt	nucleotide
rpm	rounds per minute
sec	second
U	unit
V	Volt
W	Watt
µ	micro (10^{-6})

Table of Contents

1. Aim and Organisation of This Thesis

The study presented here deals with different aspects of the methionine (met) biosynthesis operon in the opportunistic human pathogen *Staphylococcus aureus*. The central regulator of *met* operon expression is a MET-T-box riboswitch, hereinafter referred to as '*met* leader'. The aim of the doctoral research was i) to further elucidate the degradation processes of the *met* locus RNA, ii) to investigate effects (molecular and phenotypic) of dysregulated T-box riboswitch control and iii) to determine the secondary structure of the *met* leader RNA. In addition, work on the characterisation of a metal-dependent hydrolase (Mdh) that is part of the *met* operon, but not required for the *de novo* methionine biosynthesis was carried out.

This thesis comprises an 'introduction', a 'results and discussion' chapter which itself has been divided into two separate result parts, each containing its individual discussion at the end, and a common 'conclusion and perspective'.

The introduction provides general background information on methionine and its synthesis and regulation in bacteria, with a focus on the MET-T-box riboswitch-mediated control of methionine biosynthesis (genes) in *S. aureus*. The first 'results and discussion' section addresses the different aspects (structure, processing and dysregulation) of the *met* leader and *met* genes. In the second 'results and discussion' section, the knowledge gained on Mdh and attempts to ascertain its function are presented. The discussion parts provide also ideas for follow-up experiments.

The 'results and discussion' chapter is followed by a common 'conclusion and perspective', which summarises the overall results and presents open questions and possible future directions of the research.

2. Introduction

The text of the following section has been published in a similar form in Wencker and Ziebuhr (2017). Updates due to recent findings have been included.

2.1. Properties of methionine and its *de novo* biosynthesis in bacteria

Methionine is the first N-terminal amino acid of nearly all prokaryotic proteins (in its N-formylated form) and the precursor for S-adenosylmethionine (SAM), the major methyl-group donor in all living cells (Chiang et al., 1996). It is an unbranched, non-polar amino acid with an S-methyl-thioether chain that confers hydrophobicity (**Fig. 1**), (Ferla and Patrick, 2014). In contrast to animals and humans, in which methionine is essential and has to be assimilated with food, most prokaryotes are capable of synthesising the amino acid *de novo*. Usually, homoserine, derived from aspartate, is the starting molecule for methionine synthesis. Sulfur- and methyl-group donors and cofactors are derived from multiple sources. Although, bacteria have evolved different pathways for methionine synthesis, the main biological reactions are nearly identical: i) activation of homoserine by acylation, ii) the sulfuration of the activated homoserine resulting in homocysteine and iii) methylation of homocysteine yielding methionine. However, some bacteria are capable of transferring an entire S-CH_3 group onto the activated homoserine, the so-called 'one-step synthesis' of methionine (**Fig. 1**), (Ferla and Patrick, 2014).

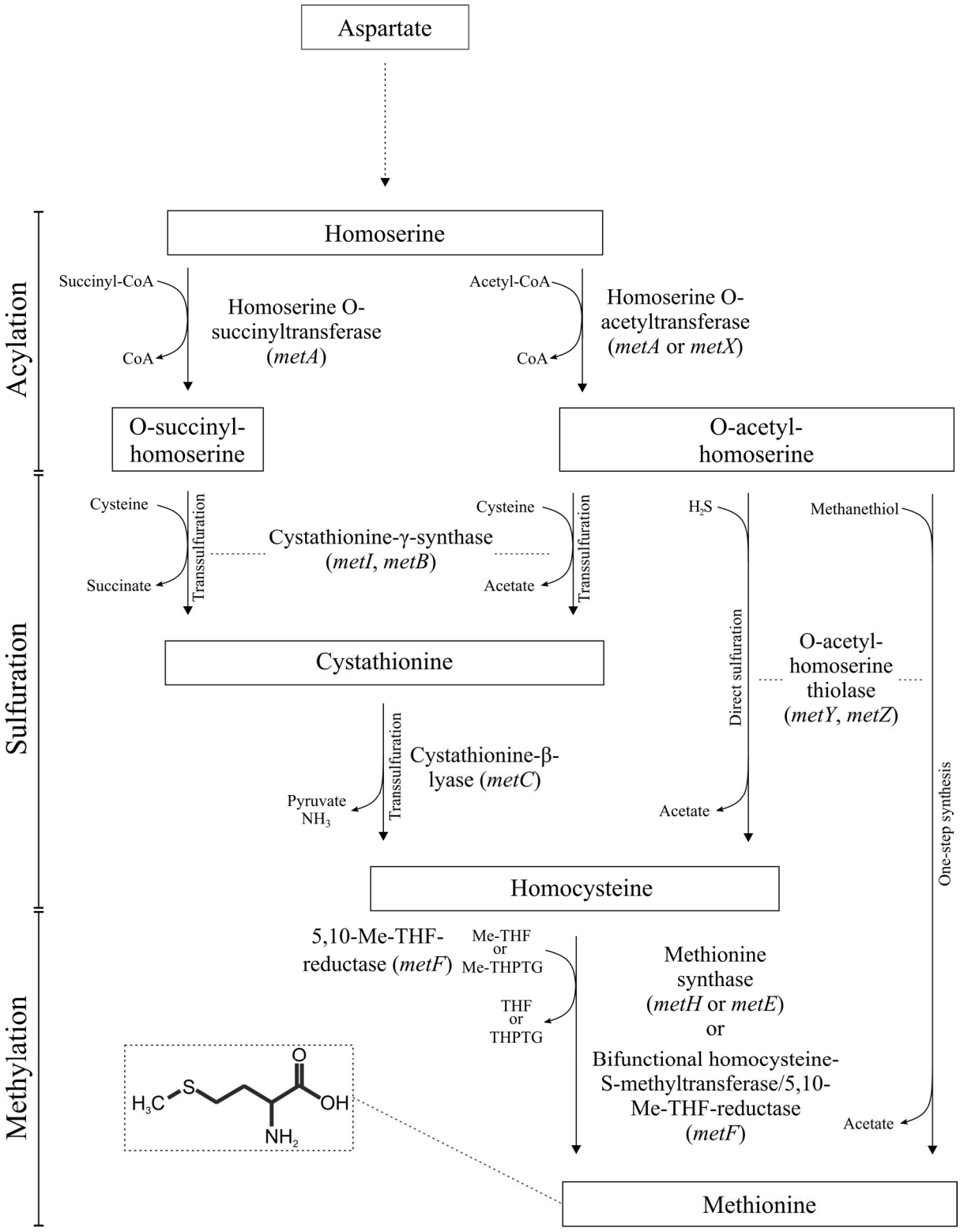

Figure. 1. Methionine biosynthesis in bacteria. Pathway intermediates are shown in rectangles, enzymes are detailed next to arrows and encoding genes are shown in brackets. Structural formula of methionine is given in dashed line box. For details see text.

2.1.1. Acylation: activation of homoserine

Homoserine is activated either by adding an O-succinyl group derived from succinyl-CoA or an O-acetyl group derived from acetyl-CoA (**Fig. 1**). Homoserine O-succinyltransferases (HST) and homoserine O-acetyltransferases (HAT), respectively catalyse this reaction. HSTs are encoded by *metA*, whereas HATs can be encoded by *metA* and *metX* genes.

There is no consistent distribution of these genes among bacteria and many species harbour both the *metA* and *metX* genes emphasising the complexity and importance of methionine biosynthesis (Ferla and Patrick, 2014). In *Bacillus cereus,* the substrate specificity of the homoserine O-succinyltransferases MetA was shown to depend on a single amino acid residue in the active centre of the enzyme. The exchange from glycine to glutamic acid at position (G111E) in MetA was sufficient to switch the substrate specificity from succinyl-CoA to acetyl-CoA, transforming the enzyme into a functional HAT (Zubieta et al., 2008).

Depending on the amino acid present in the active centre, MetA enzymes may therefore represent either HAT or HST enzymes. Thus, the majority of bacterial MetA proteins is classified as HAT enzymes, whereas only a minor proportion is considered as *bona fide* HSTs (Ferla and Patrick, 2014).

MetX is an alternative homoserine transacetylase with no sequence or structural homology to MetA. Up until recently, MetX enzymes have been considered to exclusively use acetyl-CoA as substrate. A recent study by Bastard et al. demonstrated that one-third of the tested MetX enzymes were HSTs. Furthermore, they could show that substrate-specificity depends on one of the amino acid residues in the catalytic centre. An arginine to leucine exchange (R323L) turned a MetX HST into a HAT and *vice versa* (L306R), in a similar manner as had been demonstrated for the MetA enzymes. Their finding that 'Acyl-CoA use is mispredicted for 68% of MetA enzymes and 41% of MetX enzymes in databases' subsequently led to the update of the UniProtKB database (Bastard et al., 2017).

Nevertheless, O-acetylation appears to be the prevailing reaction for homoserine activation in bacteria, as 62 % of all investigated homoserine transacetylase genes (> 8,000) are predicted to use acetyl-CoA as substrate (Bastard et al., 2017).

2.1.2. Sulfuration: from homoserine to homocysteine

During sulfuration, the acylated hydroxyl group of homoserine is replaced by a thiol group to produce homocysteine (**Fig. 1**). Next to direct sulfuration (utilising hydrogen sulfide to provide sulfur), bacteria may employ the transsulfuration pathway (using cysteine as sulfur donor) to generate homocysteine. The methionine one-step synthesis (with methanethiol as sulfur and methyl-group source) omits the homocysteine intermediate and activated homoserine is directly converted into methionine. Which of these pathways is preferred depends on substrate availability and the environmental conditions the bacteria live in.

All bacterial species capable of *de novo* methionine biosynthesis harbour all enzymes for at least one of the pathways. Some species are able to use both the direct and the transsulfuration route, and a few species, such as *Corynebacterium glutamicum*, can, in addition, produce methionine via the one-step synthesis pathway when methanethiol is available.

Direct sulfuration

The direct sulfuration route is most prevalent among bacteria to generate homocysteine.

The O-acetyl group of activated homoserine is replaced by a thiol group using hydrogen sulfide as the sulfur donor to yield homocysteine (**Fig. 1**). The enzymes catalysing this reaction are O-acetylhomoserine thiolases (also referred to as O-acetyl thiol-lyases or O-acetyl aminocarboxypropyl transferases) encoded by *metY* genes which are detectable in nearly all bacterial classes (Ferla and Patrick, 2014). The homologous *metZ* genes have likely evolved by a gene duplication event (Gophna et al., 2005). *metZ* is rare in bacterial genomes and it is supposed to encode O-succinylhomoserine thiolases, catalysing the generation of homocysteine from O-succinyl-activated homoserine (Gophna et al., 2005). However, *metZ*-encoded enzymes are suggested to represent rather O-acetyl homoserine thiolases, because the majority of bacteria employs acetyl-CoA instead of succinyl-CoA for homoserine activation (see above) (Ferla and Patrick, 2014).

Transsulfuration

The transsulfuration route of methionine biosynthesis describes the conversion of activated homoserine into homocysteine generating the thioether cystathionine as intermediate (**Fig. 1**). This two-step reaction utilises cysteine as sulfur source. During the first step cystathionine is generated by transferring cysteine to activated homoserine, thereby removing the O-succinyl

or O-acetyl group from homoserine. The reaction is catalysed by cystathionine-γ-synthases (CGS) encoded by *metB* and *metI* genes. CGS display a certain flexibility in substrate specificity and some may accept both O-succinyl homoserine and O-acetyl homoserine as reaction partners (Hacham et al., 2003).

Hence, MetB of *E. coli* uses O-succinyl homoserine and cysteine as substrates for cystathionine synthesis, whereas the bifunctional MetI enzymes present for example in *B. subtilis* utilise O-acetyl homoserine and cysteine or catalyse a direct sulfuration reaction (with hydrogen sulfide as sulfur donor) to yield homocysteine (Auger et al., 2002). This flexibility is supposed to reflect the origin of CGS and cystathionine-β-lyases (CBL) enzymes (see below) from a common evolutionary ancestor (Gophna et al., 2005). Employing cysteine as sulfur donor in the transsulfuration pathway is metabolically costly, at least in comparison to the low-molecular-weight sulfur compounds employed in one-step synthesis and direct sulfuration. However, cysteine appears to have a better availability than hydrogen sulfide or methanethiol which are rather volatile compounds.

In the second step of transsulfuration, cystathionine is cleaved by *metC*-encoded cystathionine-β-lyases yielding homocysteine and releasing pyruvate and ammonia as by-products. The transsulfuration route is rather uncommon in the bacterial world. Nevertheless, it is the preferred pathway among α- and γ-proteobacteria (Ferla and Patrick, 2014). Besides those, some Gram-positive bacteria, such as *Bacillus subtilis* and staphylococci, employ the transsulfuration route to synthesise methionine.

One-step synthesis

The most direct way to generate methionine from the activated homoserine is the addition of the terminal S-CH_3 group to O-acetyl homoserine in a single transfer reaction omitting homocysteine as intermediate and yielding methionine directly in one step (**Fig. 1**). This reaction is catalysed by the O-acetylhomoserine thiolases (encoded by *metY* and *metZ* genes) described above. For this one-step synthesis, the enzymes employ organosulfur compounds instead of hydrogen sulfide as sulfur donors, such as methanethiol or dimethyldisulfide. (Bolten et al., 2010). This ‘shortcut route’ is mainly used by bacterial species that produce methanethiol or other sulfur compounds as by-products of catabolism.

2.1.3. Methylation: from homocysteine to methionine

The final step in methionine biosynthesis is the methylation of the thiol group of homocysteine (**Fig. 1**). The methionine synthases, catalysing this reaction, are highly conserved. They are expressed even in organisms that do not synthesise methionine *de novo* because recycling of the major methyl-group donor S-adenosyl methionine results in homocysteine which then can be converted to methionine and subsequently to SAM again.

Methylation of homocysteine in bacteria is catalysed by two non-homologous methionine synthases, MetE and MetH, which use tetrahydrofolate (THF) compounds as methyl-group donors. MetH is a cobalamin-dependent enzyme that obtains the methyl-group required for homocysteine S-methylation from the mono-glutamate present in N^5-methyl-tetrahydrofolate (CH_3-THF). In contrast, MetE, which is cobalamin-independent, employs N^5-methyl-tetrahydropteroyl-(tri)glutamate (CH_3-THPTG) with three or more glutamate molecules as methyl-group donors (Figge, 2007). The folate-derived methyl-group donors, in turn, are provided by the methylene-tetrahydrofolate reductase encoded by *metF* that catalyses the conversion of N^5,N^{10}-methylene-tetrahydrofolate or N^5,N^{10}-methylene-tetrahydropteroylglutamate into CH_3-THF and CH_3-THPTG, respectively.

MetH, which uses methylcobalamin as intermediate methyl-carrier, was shown to catalyse the methylation reaction of homocysteine 100-times faster than MetE (Figge, 2006; Rodionov *et al.*, 2004). MetH accepts both CH_3-THF and CH_3-THPTG as substrates, whereas MetE only accepts CH_3-THPTG. With a few exceptions, the majority of bacteria harbours both MetE and MetH enzymes, ensuring a certain flexibility with respect to substrate availability and reflecting the general essentiality of the reaction (Ferla and Patrick, 2014; Gophna et al., 2005) .

Some Gram-positive bacteria, such as *B. subtilis* and staphylococci, are thought to harbour, in addition to MetE, a bifunctional homocysteine S-methyltransferase/5,10-methylene-tetrahydrofolate reductase enzyme with both methionine synthase and methylene-THF reductase activities (Grundy and Henkin, 1998).

However, the assumption of bifunctionality is merely based on similarities and shared domain architectures with both enzyme classes and not experimentally proven yet. MetH of *E. coli* has been characterised as modular enzyme with four functional regions: a homocysteine-binding region (residues 2-353), a methyltetrahydrofolate binding region (residues 354-649), a region responsible for binding the cobalamin prosthetic group (residues 650-896) and a SAM-binding domain (residues 897-1227). The methyl-group from methylcobalamin is transferred onto homocysteine to generate methionine, then CH_3-THF or CH_3-THPTG are used to re-methylate

the cobalamin. SAM is required every 1,000 to 2,000 methylation cycles to reactivate cobalamin that is occasionally oxidised to an inactive form. The isolated homocysteine-binding domain (truncated protein only consisting of this domain) has been shown to be still capable of methylating homocysteine to methionine, when methylcobalamin is present (Goulding et al., 1997). The potentially bifunctional enzymes comprise the homocysteine-binding domain of MetH and the 5,10-methylene-tetrahydrofolate reductase enzyme (MetF) sequence (Grundy and Henkin, 1998). In the *S. aureus* 1,842 bp long *metF* gene, bp 1–852 and bp 969-1806 are predicted to represent the methionine synthase and the reductase enzyme, respectively (blastx search) (Gish and States, 1993). Therefore, bifunctionality is possible, but the enzyme would require exogenous methylcobalamin. The lack of the cobalamin-binding domain would render the reactivation by SAM unnecessary.

Nonetheless, the bifunctional protein is alternately (and confusingly) referred to as MetH or MetF. Due to their structural and functional features, the bifunctional enzymes apparently would represent a special subclass of methionine synthases which would warrant an own nomenclature.

2.2. Regulation of methionine biosynthesis

Methionine is the amino acid with the highest metabolic costs regarding ATP consumption. In *E. coli*, 18 mol of ATP is required to obtain 1 mol methionine (Kaleta et al., 2013). Hence, bacteria require adequate regulation of the methionine biosynthesis genes to avoid unnecessary methionine production and its associated waste of energy and resources. The regulation of (methionine) gene expression can be divided into two general control mechanisms: protein-mediated and RNA-mediated transcription control.

Protein-mediated transcription control is executed by transcription factors (TFs), DNA-binding proteins, that recognise specific DNA target sequences in the promoter regions of genes. Interaction of a TF with a promoter can either activate or repress transcription of the respective gene(s), depending on the TF and its target. Frequently, the affinity of the TF for its binding sequence is modulated by so-called cofactors that are usually metabolites or end products of the TF-regulated pathway. Control of gene expression via TFs enables the cell to co-regulate genes belonging to the same metabolic pathway or cellular response programme even though these are scattered throughout the genome. A variety of TFs are involved in methionine biosynthesis gene expression control. An overview can be found in Wencker and Ziebuhr

(2017). Only the TF CodY will be described in more detail (below) because it is part of the hierarchical regulation network of the methionine biosynthesis genes in *S. aureus*.

CodY is a global transcription repressor that is involved in the regulation of many amino acid biosynthesis pathways, transport of macromolecules, and virulence in Gram-positive bacteria. It has been thoroughly studied in *B. subtilis* and *S. aureus* (Majerczyk et al., 2010; Pohl et al., 2009; Ratnayake-Lecamwasam et al., 2001; Shivers and Sonenshein, 2004). The binding of GTP and branched-chain amino acids (BCAA) (isoleucine, valine, leucine) increases the affinity of CodY for its DNA target sequence (consensus motif: AATTTTCWGAAAATT), with isoleucine demonstrated to have the biggest effect among the BCAA (Guédon et al., 2005; Shivers and Sonenshein, 2004). Next to low BCAA levels, starvation for methionine alone was demonstrated to induce CodY-de-repression in *S. aureus* (Schoenfelder et al., 2013).

RNA-based transcription control of methionine biosynthesis genes is mediated by riboswitches in a protein-independent manner. The fact that the centrepiece of my doctoral research is a MET-T-box riboswitch warrants a separate chapter about riboswitches.

2.2.3. Riboswitches: RNA-mediated transcription or translation control

The term 'riboswitch' has been coined by Nahvi et al. in 2002, when they discovered that the 5'-UTR of the *btuB* gene in *E. coli* selectively binds coenzyme B12 leading to a structural rearrangement of the RNA that prevents ribosome binding and subsequent reduces expression of the cobalamin transporter BtuB (Nahvi et al., 2002). However, the first **T-box riboswitch** had been already discovered in 1992 by Henkin et al. in the 5'-UTR of the *B. subtilis tyrS* gene coding for the tyrosyl-tRNA synthetase (Henkin et al., 1992).

Riboswitches are cis-acting RNA regulatory elements, located in the 5'-untranslated regions (5'-UTRs) of genes that adopt mutually exclusive RNA conformations depending on presence or absence of a specific ligand.

A conformational change of the riboswitch triggered by binding of its specific ligand either induces activation or repression of gene expression depending on the riboswitch type. Generally, repression is caused by premature termination of transcription (Rho-independent) or inhibition of translation initiation of the downstream mRNA. In addition, riboswitches controlling gene expression via Rho-dependent transcription termination or ligand-binding-induced self-cleavage (ribozyme) have been discovered (Hollands et al., 2012; Winkler et al., 2004).

Ligand classes comprise (i) RNA-derived compounds including (a) coenzymes (e.g. SAM, THF or FMN), (b) nucleotide derivatives (e.g. guanine, adenine, 2'-deoxyguanosine) and (c) signalling molecules (e.g. cyclic di-GMP, ZTP or ppGpp), (ii) ions (e.g. Mg^{2+}, Mn^{2+} and F^{-}), (iii) amino acids (lysine, glycine and glutamine), (iv) other metabolites (e.g. glucosamine-6-phosphate) and (v) uncharged tRNAs (Kreuzer and Henkin, 2018; McCown et al., 2017; Sherlock et al., 2018). Usually, the ligands are intermediates or end products of the riboswitch-regulated pathways, in the case of T-box riboswitches cognate uncharged tRNAs.

To date, 40 metabolite- and ion-responsive riboswitch classes have been discovered (Malkowski et al., 2019; McCown et al., 2017; Sherlock et al., 2018). By now, T-box riboswitches recognising cognate tRNAs for 19 of the 20 amino acids (except for glutamine-tRNAs) and T-box riboswitches able to recognise two or even more tRNA species via overlapping Specifier codons (see below) have been identified (Saad et al., 2013; Vitreschak et al., 2008).

The riboswitch types involved in bacterial methionine biosynthesis control are SAM-binding, SAH (S-adenosylhomocysteine)-binding and coenzyme B12-binding and MET-T-box riboswitches (Leyn et al., 2014; Nahvi et al., 2004; Rodionov et al., 2004).

T-box riboswitches

Almost 30 years ago, Henkin and colleagues discovered the first T-box riboswitch. They described a 15 nt long sequence which they designated 'T-box' that was conserved in the *tyrS* genes of *B. subtilis* and *B. stearothermophilus* and the *tryZ* gene of *B. subtilis* immediately upstream of a Rho-independent terminator sequence followed by a string of U residues. Henkin and colleagues found 12 nt of the T-box sequence to be highly conserved in all 5'-UTRs of tRNA synthetase genes of *B. subtilis* available at that time (*thrS*, *thrZ*, *pheST* and *trpS*) and upstream of the *ilv-leu* operon, always co-occurring with the terminator and U-rich sequence. They demonstrated the induction of *tyrS-lacZ* (*lac*Z fused to *tyrS* 5'-UTR) expression upon starvation for tyrosine and loss of this response after mutation of the T-box. Furthermore, they showed via primer extension analysis that the length and levels of the *tyrS* leader itself are not changed after tyrosine deprivation, indicating that gene regulation occurred post transcription initiation. Based on the obtained data they suggested a 'common transcriptional antitermination mechanism' for the regulation of tRNA synthetase genes in *B. subtilis*.

According to their proposed model, tyrosine starvation induces read-through into the *tyrS* gene (antitermination) and high levels of tyrosine cause termination of transcription just upstream of the *tyrS* gene. They hypothesised that the trigger for antitermination could be cognate uncharged tRNA (Henkin et al., 1992). One year later, Grundy and Henkin provided evidence that indeed uncharged tRNA is the effector for tRNA synthetase gene expression. Extensive structural analyses of the tRNA synthetase leaders in *B. subtilis* revealed the presence of three stem-loop structures followed by the T-box sequence and the Terminator. Most strikingly, they discovered a triplet sequence always 'located in a bulged region near the base of the first stem-loop' which corresponded to a 'codon specifying the appropriate amino acid' for a given tRNA synthetase gene. They designated this base triplet 'specifier sequence' (Grundy and Henkin, 1993). Mutation of the tyrosine UAC specifier sequence to a phenylalanine UUC codon was sufficient to change the specificity of the response to amino acid limitation from tyrosine to phenylalanine. In addition, they introduced non-sense codons (amber (UAG) and ochre (UAA)) in the specifier sequence which led to complete unresponsiveness to tyrosine deprivation, further supporting the hypothesis that cognate uncharged tRNA directly interacts with the

leader RNA (Grundy and Henkin, 1993). The 'transcription antitermination mechanism' involving a specifier sequence, the T-box motif and a terminator sequence turned out to be widespread in Gram-positive bacteria for gene regulation. Grundy and Henkin identified these nowadays called T-box riboswitches in the 5'-UTR of the tRNA synthetases genes *valS* of *Lactobacillus casei* and *argS* of *Corynebacterium glutamicum* and in the 5'-UTRs of the amino acid biosynthesis genes *trp* of *L. casei* and *Lactococcus lactis* and *his* of *L. lactis* (Grundy and Henkin, 1994).

T-box riboswitches regulate tRNA synthetase genes and genes involved biosynthesis, metabolism and transport of amino acids (Vitreschak et al., 2008).

T-box riboswitch-mediated control of gene expression is most prevalent in low G+C Gram-positive bacteria and usually based on premature termination of transcription, but a number of T-box leaders have been identified in high G+C Gram-positives and Gram-negative bacteria as well. Here, gene regulation seems to operate at the level of translation initiation (Grundy and Henkin, 2003; Henkin and Grundy, 2006; Merino and Yanofsky, 2005). The first translational T-box riboswitch was discovered and biochemically characterised in Actinobacteria (Sherwood et al., 2015). Nevertheless, the typical T-box riboswitch controls gene expression at the level of transcription. The mode of action is depicted schematically in **Fig. 2** using the example of the methionyl-tRNA-specific T-box riboswitch (MET-TBRS). Under methionine-deprived conditions, levels of uncharged tRNAs are high. Interactions of the tRNA anticodon with the specifier sequence within Stem I and of the tRNA's free 3' CCA end with nucleotides within the T-box bulge of the riboswitch stabilise the riboswitch in its Antiterminator conformation. The Antiterminator structure enables the RNA polymerase to continue transcription and read-through into the downstream gene sequence (**Fig. 2 A**). Under methionine-rich conditions, most of the tRNAs are charged with methionine. Therefore, the tRNA can only interact with its anticodon with the specifier sequence. The bound amino acid prevents base pairing of the tRNA 3'-end with the T-box bulge nucleotides. The lacking interaction causes the riboswitch to adopt the thermodynamically more stable Terminator conformation. This in turn, forces the RNA polymerase to terminate transcription just downstream of the riboswitch sequence and to fall off the DNA strand. Transcription of the downstream gene(s) does not take place (**Fig. 2 B**) (Kreuzer and Henkin, 2018).

Next to this conventional view that a charged tRNA 3'end cannot base pair with the T-box bulge due to steric hindrance, very recently crystal structures of a full length translational (!) T-box riboswitch from *Mycobacterium tuberculosis* in complex with a cognate charged tRNA mimic revealed that base pairing of the 3' CCA tRNA end occurs despite charging. The amino

acid (or the mimic) is suggested to subsequently push a RAG motif out of the tRNA 3'-end binding pocket by simple steric clashing. The complete ejection of the motif likely initiates the conformational change terminating gene expression (Battaglia et al., 2019). Albeit, these data were obtained with a translational T-box riboswitch, 'the aminoacylation sensing mechanism is essentially identical' in transcriptional T-box riboswitches (Battaglia et al., 2019). Additional studies will be required to conclusively determine the interactions and processes that lead to transcription termination or translation inhibition.

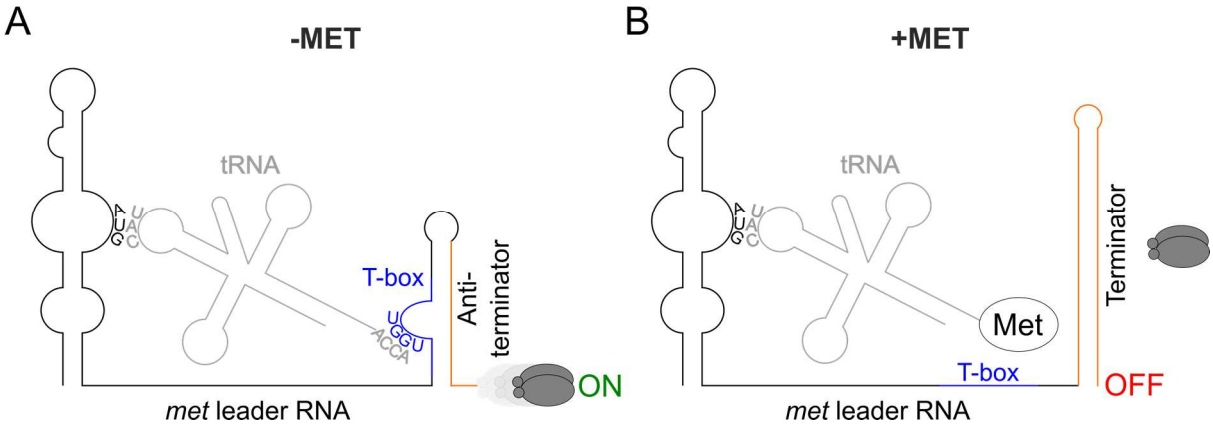

Figure 2. General mechanism of T-box riboswitch transcription control systems. Schematic of the binding interactions between tRNA and *met* leader RNA (T-box riboswitch). (A) System under methionine deprivation ('-MET'): base pairing of the free 3' 'ACCA' end of an uncharged tRNA with the 'UGGU' sequence of the T-box (depicted in blue) stabilises Antiterminator conformation. 'ON': read-through into downstream genes, *met* mRNA transcription. (B) System under high intracellular methionine levels ('+MET'): tRNA charged with methionine (symbolised by circle with 'Met') cannot interact with T-box, Terminator is formed. 'OFF': premature transcription termination, no *met* mRNA transcription. Base pairing of tRNA anticodon ('CAU') with Specifier codon ('AUG') of *met* leader takes place under both conditions. Terminator sequence is highlighted in orange, grey ellipses symbolise RNA polymerase.

2.3. RNA stability as mechanism of gene regulation

Next to the regulation of gene expression on the level of transcription (synthesis), regulation takes place on the level of transcript stability as well. The half-life of an RNA molecule affects its concentration in the cell and therewith protein expression levels (translation). Bacterial mRNAs are generally very short-lived, with half-lives of 2-10 minutes of bulk mRNAs, compared to eukaryotic mRNAs with average half-lives of several hours (Laalami et al., 2014; Sharova et al., 2009). In *S. aureus*, the half-lives of 90 % of log phase mRNAs were determined to be 5 minutes or less (Roberts et al., 2006). However, upon certain stress stimuli or changes in growth (m)RNA stability can greatly vary (Anderson et al., 2006). RNA stability is influenced by various factors: secondary and tertiary structures, RNA binding proteins

(including ribosomes) and regulatory RNAs that create, mask or expose processing and degradation signals (Laalami et al., 2014; Morrison et al., 2012). The enzymes executing RNA processing and degradation are called ribonucleases (RNases). They are classified as endo- or exonucleases according to their specificity. Endonucleases cleave RNA internally, exonucleases digest RNA from the extremities. RNases can be single- or double-strand specific. In bacteria, the major routes to initiate RNA degradation are thought to be either via an endonucleolytic cleavage alone ('direct entry pathway') or via removal of the RNA 5'-end followed by an internal cleavage ('5'-end-dependent pathway') (Bonnin et al., 2015; Durand and Condon, 2018; Laalami et al., 2014). Although the general steps in RNA degradation are similar in all bacteria, the involved enzymes are very different, being a prime example for convergent evolution (Laalami et al., 2014). Most of the knowledge on RNA degradation in bacteria was obtained by studies of the model organisms *E. coli* (Gram-negative) and *B. subtilis* (Gram-positive). This led to the view that in general a distinct set of RNases exists for Gram-negative and Gram-positive bacteria. However, this assumption proved to be too simplistic (see below).

RNA decay in E. coli

In *E. coli*, the main RNase is the essential single-strand specific endonuclease RNase E (Mudd et al., 1990). The enzyme prefers 5'-monophosphorylated RNA that is generated by the pyrophosphohydrolase RppH via dephosphorylation of 5'-triphosphorylated RNA ('5'-end-dependent pathway'), but RNase E can cleave substrates in a 5'-end-independent manner as well ('direct entry pathway') (Anupama et al., 2011; Bouvier and Carpousis, 2011; Deana et al., 2008; Garrey and Mackie, 2011; Mackie, 1998). After the initial endonucleolytic cleavage the RNA molecule is further degraded by 3'-5' exonucleases (RNase II, PNPase, RNase R, oligo-ribonuclease) and successive endonucleolytic cuts. Polyadenylation of RNA 3'-ends by the poly(A) polymerase (PAP I) allows re-engagement of exonucleases required for complete degradation (Laalami et al., 2014).

The membrane-bound RNase E functions as a scaffold for the formation of a membrane-associated multienzyme complex, the RNA degradosome that involves the PNPase (3'-5' exonuclease), the RNA helicase B (RhlB) and a glycolytic enzyme (enolase) next to several other components (e.g. the RNA-binding protein Hfq, protein chaperones and ribosomal proteins) (Carpousis, 2007). The composition of the degradosome can vary in response to environmental changes, e.g. cold shock (Prud'homme-Généreux et al., 2004).

RNA decay in B. subtilis

In *B. subtilis*, RNase E is absent, but functionally substituted by RNase Y and RNase J (J1/J2 complex). Interestingly, the catalytic mechanism is distinct in all three RNases. The homologues RNases J1 and J2 are assumed to form heterodimers or -tetramers (Mathy et al., 2010). RNase J1 of *B. subtilis* has been the first exonuclease described in bacteria with 5' to 3' activity (Mathy et al., 2007). There is good evidence that J1 is required for full catalytic activity and J2 is acting mainly as a structural factor. *In vitro*, J2 of *B. subtilis* exhibited only very poor 5' to 3' exonucleolytic activity compared with J1 (Mathy et al., 2010). RNase J is proposed to be a bifunctional enzyme with strong 5'-3' exonuclease and endonuclease activity. However, the endonuclease function *in vivo* is still under debate (Durand and Condon, 2018). The single-strand specific endonuclease RNase Y is essential in *B. subtilis* and localises to the membrane as RNase E in *E. coli*. It plays a key role in initiation of RNA decay in *B. subtilis* and is regarded as a functional homologue of RNase E (Durand et al., 2012a; Laalami et al., 2013; Lehnik-Habrink et al., 2011a; Lehnik-Habrink et al., 2011b; Shahbabian et al., 2009).

An equivalent of the *E. coli* degradosome has been proposed in *B. subtilis* with RNase Y as scaffolding enzyme based on two-hybrid, co-immunoprecipitation and surface plasmon resonance experiments. Identified components are a DEAD-box helicase (CshA), PNPase and the two glycolytic enzymes enolase and phosphofructokinase (Commichau et al., 2009; Lehnik-Habrink et al., 2010; Newman et al., 2012). However, a recent study surprisingly did not identify any co-localisation of the degradosome enzymes with RNase Y suggesting that the interactions are transitory in *B. subtilis*. Therefore, Durand and Condon propose to describe this instable degradosome rather as a degradosome-like network (DLN) (Durand and Condon, 2018).

RNase E and RNase Y are not exclusively restricted to Gram-negative and Gram-positive bacteria, respectively. Some Gram-positives possess RNase E (e.g. species within Clostridia, Bacillales and Actinomycetales), some Gram-negatives possess RNase Y (e.g. *Helicobacter pylori*) and some species of the δ-proteobacteria and Clostridia possess both endonucleases. Furthermore, the importance of a certain RNase seems to be species-specific as the effect of the deletion of RNase Y (severely impaired growth in *B. subtilis* vs. unaffected growth in *S. aureus*) or the essentiality of RNase III in *B. subtilis* vs. non-essentiality in *S. aureus* demonstrate (Bonnin et al., 2015; Durand et al., 2012b, 2012a; Figaro et al., 2013; Khemici et al., 2015; Marincola et al., 2012).

RNA decay in S. aureus

The key players of mRNA turnover in *S. aureus* are RNase Y, the double-strand-specific RNA endonuclease RNase III and RNase J (J1/J2 heteromer), as well as the 3'-5' exonuclease PNPase (Bonnin et al., 2015; Durand and Condon, 2018). RNase Y is not essential in *S. aureus* and affects less mRNAs than in *B. subtilis*, but plays a major role in virulence gene regulation (Khemici et al., 2015; Marincola et al., 2012). RNase III has shown to be involved in maturation of rRNA operons, processing of non-coding RNAs and degradation of RNA-mRNA duplexes. Furthermore, it cleaves mRNAs including its own (autoregulation) and highly structured 5'-UTRs (Lioliou et al., 2012). The RNase J1/J2 complex is involved in RNA maturation (e.g. 16S rRNA), post-transcriptional regulation and degradation. There is good indication for an *in vivo* endonuclease activity of RNase J in *S. aureus* (Linder et al., 2014). The degradosome-like network is similar to the *B. subtilis* complex with the protein subunit of the RNase P (RnpA) as an additional partner. However, the interactions of the degradosome components seem to be less complex in *S. aureus* (Roux et al., 2011). Detailed information on the respective RNase and its cleavage characteristics in *S. aureus* are provided in the 'Results and Discussion' section where needed.

2.4. The methionine biosynthesis in *Staphylococcus aureus*

2.4.2. General characteristics of *S. aureus*

Staphylococci are Gram-positive, coccoid bacteria belonging to the phylum Firmicutes and the order Bacillales with a low GC content. All staphylococcal species are catalase-positive, non-motile and facultatively anaerobic. At least 56 species are known to date (NCBI Taxonomy Browser https://www.ncbi.nlm.nih.gov/Taxonomy/Browser/wwwtax.cgi). *S. aureus* is a coagulase producer ('coagulase-positive') and can ferment mannitol. It was first identified in 1880 in pus from human abscesses by Sir Alexander Ogston who coined the term 'staphylococcus' (derived from Ancient Greek σταφυλή, Romanised *staphylē*, 'a bunch of grapes' and κόκκος, Romanised *kókkos*, 'grain', 'seed', 'berry') (Ogston, 1882). *S. aureus* (formerly also called *S. pyogenes*) is both, a human commensal and an opportunistic pathogen that permanently colonises the skin and the nasal mucosa of approximately 20 % of the healthy human population, but can cause a plethora of infections ranging from mild skin infections to life-threatening conditions, including osteomyelitis, pneumonia, endocarditis and sepsis (Ananthanarayan, 2006; Foster, 2004; Lowy, 1998; Wertheim et al., 2005; Williams, 1963). *S. aureus* is the leading cause of bacterial infections in the developed world and an emerging health threat due to the (rapid) development of (multi)drug resistances (Haaber et al., 2017). The first penicillin-resistant *S. aureus* has been already reported in 1947, the first methicillin-resistant *S. aureus* (MRSA) in 1961 (Barber, 1947; Jevons, 1961). After a global spread of MRSA, alternative treatments with vancomycin, linezolid and daptomycin had to be employed with increasing frequency. Meanwhile, occurrence of *S. aureus* strains with reduced susceptibility to vancomycin (vancomycin-intermediate *S. aureus*; VISA) or daptomycin or resistance to linezolid is a cause for concern (Chambers and DeLeo, 2009; Dortet et al., 2013; Gu et al., 2013).

Gene regulation in *S. aureus* occurs primarily on the level of transcript synthesis and mRNA processing and decay. Two-component systems (TCS) (e.g *agr*, *sae*, *srr*) and specific transcription factors (e.g. alternative sigma factors, *rot*, *sarS*) enable *S. aureus* to promptly adapt transcription to changing (environmental) conditions (Novick, 2003). In addition, transcript stability and processing are modulated in response to the growth phase and diverse types of shock (stringent response, heat, cold, pH changes) (Anderson et al., 2006, 2010; Roberts et al., 2006).

2.4.3. Biochemistry of methionine biosynthesis and gene organisation in *S. aureus*

S. aureus employs the transsulfuration route with acetyl-CoA activated homoserine for *de novo* methionine biosynthesis. The acetylhomoserine transferase, catalysing the first step of the synthesis pathways, is encoded by *metX* that is under CodY- and SAM-binding riboswitch-control. The remaining genes required for methionine biosynthesis are organised in an operon, the *metICFE-mdh* operon. MetI is the cystathionine-γ-synthase, MetC the cystathionine-β-lyase and MetE the cobalamin-independent methionine synthase. *metF* is annotated as a bifunctional homocysteine S-methyltransferase/5,10-methylene-tetrahydrofolate reductase (Schoenfelder et al., 2013; Wencker and Ziebuhr, 2017).

Interestingly, the order of the genes within the *met* operon matches the order of the biochemical steps (**Fig. 3 A&B**). The organisation of the methionine biosynthesis genes in a single operon is very rare in bacteria. Commonly, the cystathionine-γ-synthase and the -β-lyase or the methylene-THF-reductase and the methionine synthase are co-transcribed in Gram-positive bacteria (Rodionov et al., 2004; Wencker and Ziebuhr, 2017). Only *Bacillus halodurans* and *B. cellulosilyticus* possess a similar *met* operon structure, *Listeria monocytogenes* harbours a *met* operon with the same genes, but in a different order (Rodionov et al., 2004; Taboada et al., 2012). The *met* locus, including the CodY binding site and the *met* leader, is highly conserved among staphylococcal species. Only three of the 16 investigated staphylococcal species did not possess the whole *met* locus (absence of *metI* in *S. carnosus* and *S. simulans*, absence of *mdh* in *S. pseudintermedius*) (own unpublished observations).

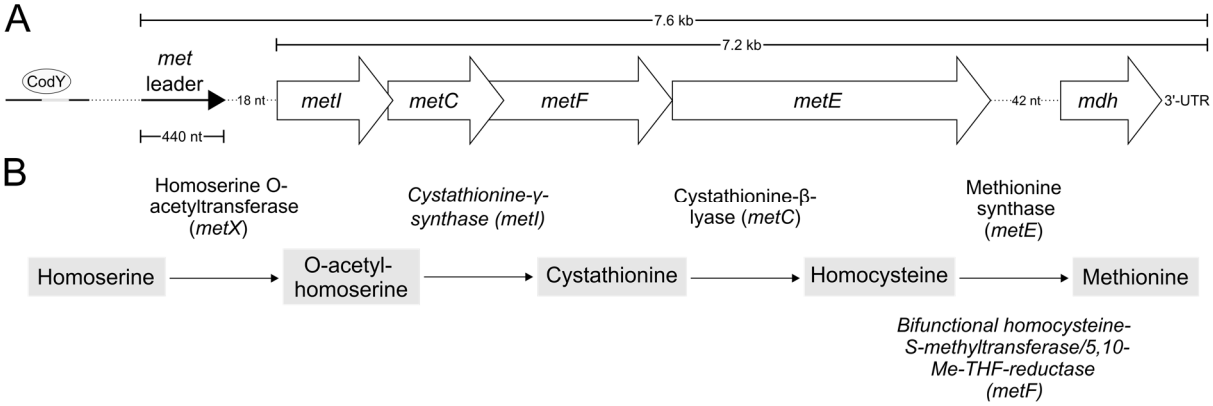

Figure 3. Methionine biosynthesis in *S. aureus*. (A) Schematic view of the organisation of the *met* operon including a CodY binding site and its 5'-UTR (*met* leader), CodY is depicted as ellipse. **(B)** Methionine biosynthesis pathway in *Staphylococcus aureus* with intermediates shown as grey rectangles, enzymes and encoding genes in brackets detailed next to arrows.

2.4.4. Regulation of the *met* operon in *S. aureus*

The *metICFE-mdh* operon is controlled by a hierarchical network with a MET-T-box riboswitch as centrepiece (**Fig. 4**) (Schoenfelder et al., 2013). Hereinafter this MET-T-box riboswitch will be referred to as *met* leader. The *met* operon is under transcriptional control of the *met* leader which in turn is under control of CodY. CodY itself is influenced by the stringent response. The stringent response is a cellular programme, employed by many bacteria, triggered by nutrient limitation to adequately adjust gene expression patterns. It causes the rapid synthesis of the arlamone (p)ppGpp by bifunctional RelA/SpoT synthetases/hydrolases (RSHs) (Geiger et al., 2010). Uncharged tRNAs bound to the ribosome ('stalled ribosomes') due to amino acid starvation activate RSH, (p)ppGpp synthesis lowers the GTP pool that subsequently facilitates the release of CodY from its target DNA (DNA affinity enhancers of CodY: GTP, BCAA) (Ratnayake-Lecamwasam et al., 2001; Shivers and Sonenshein, 2004). Under methionine-rich conditions basal transcription of the *met* leader, but not of the *met* operon genes, takes place. Upon methionine starvation the stringent response and subsequent CodY de-repression are induced which then allows enhanced *met* leader transcription. The high levels of uncharged methionyl-tRNA eventually enable *met* gene expression via antitermination (of the *met* leader) (see **Fig. 2**). Experiments with *rsh* and *codY* mutants nicely demonstrated the hierarchical regulation of the *met* locus (Schoenfelder et al., 2013). Stringent response deficiency (rsh_{Syn}) prevented induction of *met* leader transcription and therewith *met* gene transcription under methionine-deprived conditions due to absence of CodY de-repression (Geiger et al., 2012). In a CodY deletion mutant, *met* leader transcription levels were already strongly elevated under methionine-rich conditions. However, no *met* gene transcription occurred because of the high levels of charged methionyl-tRNA that trigger premature transcription termination (Terminator formation). (m)RNA degradation seems to act as an additional level of *met* operon regulation. First indications for the involvement of RNase III and RNase J were shown by Schoenfelder and colleagues (Schoenfelder et al., 2013).

The operon structure (*met* genes in a single operon, gene order as biosynthesis pathway) in combination with its regulation (CodY and MET-T-box riboswitch) is unique in staphylococci.

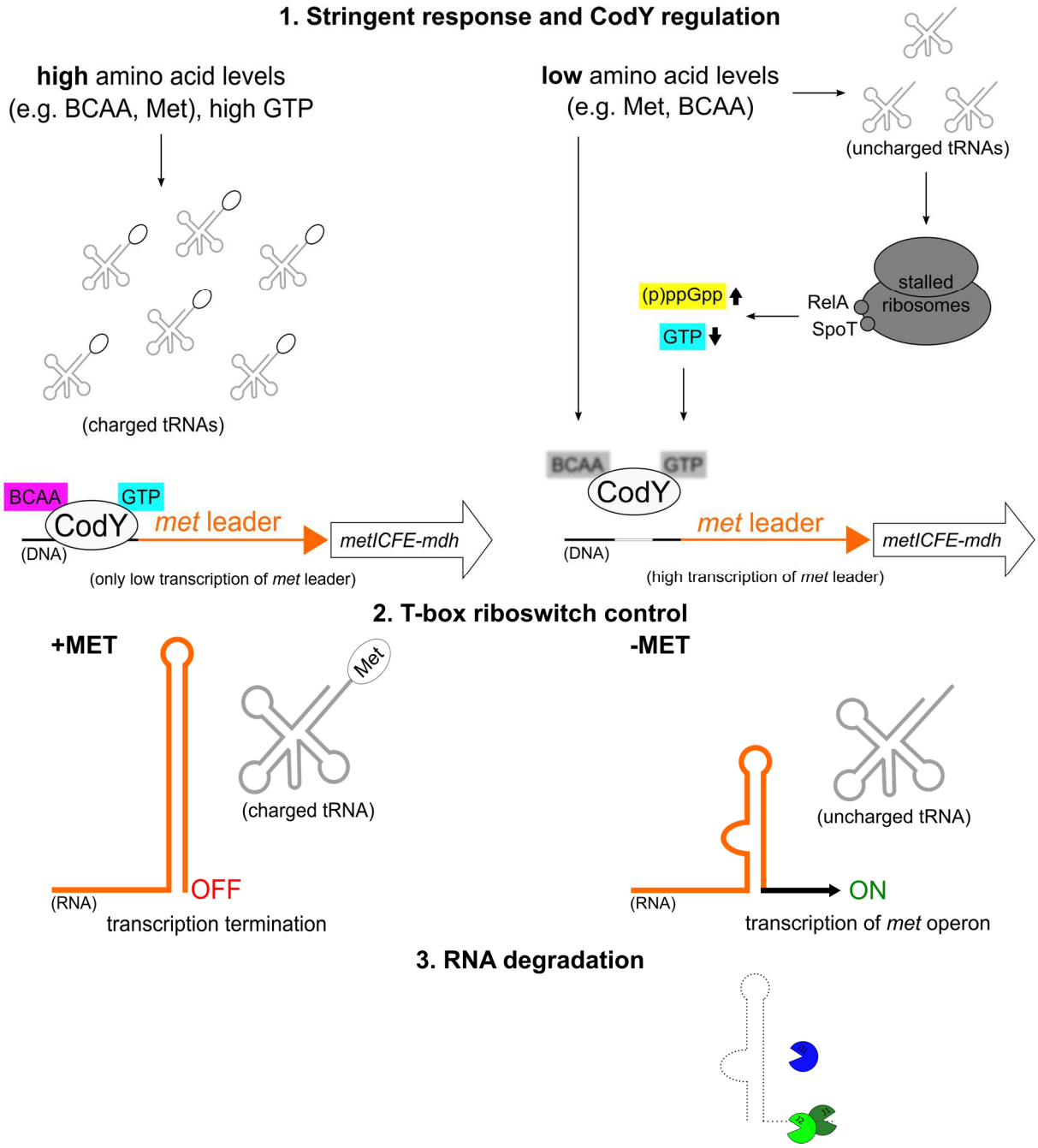

Figure 4. Model of hierarchical network regulating *met* operon expression. Three levels of regulation are shown. 1. Level: Stringent response and CodY. With high amino acid levels, branched-chain amino acids (BCAA) and GTP are bound to the transcription repressor CodY, increasing its affinity for target DNA binding, transcription of *met* leader is repressed, tRNA pools are charged (upper left). With low amino acid levels, tRNAs become uncharged that trigger the stringent response due to stalled ribosomes which leads to an increased RelA-mediated (p)ppGpp alarmone synthesis that in turn lowers GTP levels. CodY, without GTP and BCAA bound, subsequently dissociates from the DNA, strongly enhancing downstream transcription of the *met* leader (upper right). 2. Level: T-box riboswitch control. Under methionine-rich conditions charged methionyl-tRNAs cause the *met* leader RNA to adopt the Terminator conformation and to prematurely terminate transcription; transcription of the *met* genes does not take place 'OFF' (middle left). Under methionine-deprived conditions uncharged methionyl-tRNAs enable Antiterminator formation and transcription of *met* genes 'ON' (middle right). 3. Level: RNA degradation. RNases rapidly degrade *met* leader and *met* mRNA. For details see text.

2.5. The MET-T-box riboswitch as drug target

To date, the only riboswitch class identified in eukaryotes, primarily fungi, plants and algae, is the TPP (thiamine pyrophosphate) riboswitch (McCown et al., 2017). In eukaryotes, in which transcription and translation are two spatially and temporally divided processes, these riboswitches usually regulate alternative splicing of precursor mRNAs (Breaker, 2011). T-box riboswitches appear to be absent in eukaryotes (Zhang and Ferré-D'Amaré, 2015). Therefore, riboswitches represent promising drug targets with low off-target and side-effect potential (Matsui and Corey, 2017).

Riboswitches are, in general, already well recognised as promising antimicrobial drug targets as the discovery and characterisation of several novel compounds demonstrate (Anupam et al., 2008; Blount et al., 2015; Connelly et al., 2019; Frohlich et al., 2019; Mulhbacher et al., 2010a; Perkins et al., 2019; Rekand and Brenk, 2017; Wang et al., 2015).

As described above, methionine is essential for bacterial growth and survival and its *de novo* synthesis is a metabolic costly process. *S. aureus* employs a hierarchical network with a MET-T-box riboswitch as centrepiece to tightly control expression of the methionine biosynthesis operon. The human nose and blood are two niches, where *de novo* synthesis is required due to low methionine levels (Cantor et al., 2017; Krismer et al., 2014). The *met* operon has been demonstrated to be highly upregulated in *S. aureus* in those niches or under conditions mimicking them (Krismer et al., 2014; Mäder et al., 2016) (*S. aureus* expression data browser: http://genome.jouy.inra.fr/cgi-bin/aeb/index.py).

In general, two mechanisms of action are conceivable when targeting the *met* leader (MET-T-box riboswitch) regulating *met* operon expression in *S. aureus*: (i) permanent transcription termination that leads to inhibition of *de novo* methionine biosynthesis and subsequently growth inhibition and cell death under methionine-deprived conditions (nose, blood) or (ii) constant transcription activation that causes permanent methionine production under methionine-rich conditions and therefore resources and energy consumption that eventually leads to weakening of the bacteria.

3. Results and Discussion

3.1. The *met* leader: secondary structure and characteristics

3.1.1. Transcriptional start site (TSS) of *met* leader

cRACE (rapid amplification of cDNA ends from circularised RNA) has been performed to determine the TSS (transcriptional start site) of the *met* leader in *S. aureus* strain Newman (*Staphylococcus aureus* subspecies aureus strain Newman). Briefly, total RNA was isolated from bacteria grown in chemically defined medium (CDM) without methionine to mid-exponential phase, dephosphorylated to generate 5'-monophosphorylated RNA and ensuing self-ligated. Circularised RNA then was used for cDNA synthesis with a primer complementary to a sequence within the *met* leader RNA. Subsequently, generated cDNA was amplified with specific primers and the PCR product was cloned into the pGEM-T-easy vector. Universal vector primers were used to amplify the insert and the PCR product was sequenced to determine the TSS.

The 5'-end of the *met* leader transcript was at position 404 416 in the available genome sequence (NCBI Reference Sequence: NC_009641) in 96 % (n = 52) of sequenced clones, in the remaining 4 % (n = 2) TSS was at position 404 418. Therefore, the *met* leader has a length of 440 nt (including the uracil-rich 3'-end) (**Fig. 5**).

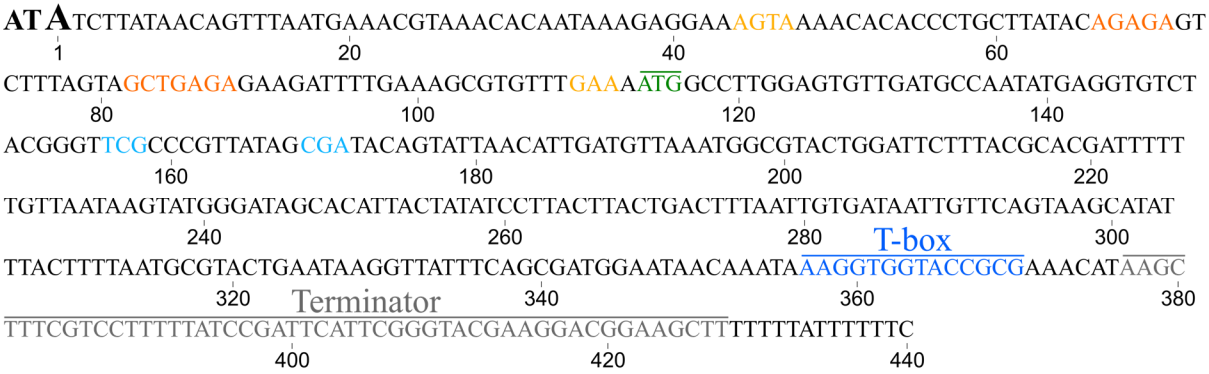

Figure 5. Transcriptional start sites (TSS) and sequence of *met* leader. Transcriptional start sites (TSS) determined by cRACE are shown in bold, major TSS enlarged and numbered with '1', interacting nucleotides of Specifier loop are shown in light orange, base pairing nucleotides of AG-Bulge and apical loop of Stem I in dark orange, Specifier codon in green, potentially interacting nucleotides of Stem IIA/B pseudoknot in light blue, T-box sequence is highlighted in dark blue, Terminator sequence is shown in grey.

3.1.2. Exceptional length of the *met* leader

The *met* leader is with its 440 nt exceptionally long compared to other T-box riboswitches due to its long linker region between Stem II and Stem III described below. It comprises 226 nt instead of around 100 nt as in most of the known MET-T-box riboswitches (Vitreschak et al., 2008). The function of this long linker region remains enigmatic.

3.1.3. 2D structural model of the *met* leader

In order to verify the presence of the highly conserved T-box riboswitch motifs and to find potential RNase target structures, the secondary structure of the *met* leader was determined experimentally. Up until the start of my doctoral research, only a model based on manual folding had been available for the *met* leader RNA (Schoenfelder, 2011).
Here, in-line probing was employed to obtain structural data to subsequently build a 2D model of the riboswitch. Experiments were performed with *met* leader RNA in the 'OFF'/Terminator state (*i.e.* without tRNA ligand).

The in-line probing method uses the natural tendency of RNA to spontaneously differentially degrade according to its secondary structure. This slow, non-enzymatic reaction is a nucleophilic attack of the 2' oxygen of a ribose on its adjacent phosphorous centre that only occurs, when the 2' oxygen, the phosphorous and the 5'-oxygen-leaving group are in 'in-line' geometry (**Fig. 6**). Single-stranded (ss) RNA regions are flexible and switch between different conformations including the in-line state. Double-stranded (ds) RNA is more rigid and locked in a certain conformation, usually not in the in-line conformation. Hence, in ss regions the phosphoester linkages are more prone to cleavage than in ds regions. This differential degradation can be visualised by size separation of spontaneously degrading (40 hours incubation at room temperature) 5'-labelled RNA on a denaturing sequencing gel (Regulski and Breaker, 2008). The gel resolution limit is around 200 nt. In order to resolve the secondary structure of the 3' half of the 440 nt-long *met* leader, a shortened version had to be used in addition to the full-length molecule. The shortened version comprised nts 205 to 440. Obtained structural data were used to build a 2D model assisted by the mfold web server application (Zuker, 2003). Information on single- or double-stranded-ness from the experimental data were entered into the mfold programme as constraints, if needed (**Fig. 7**).

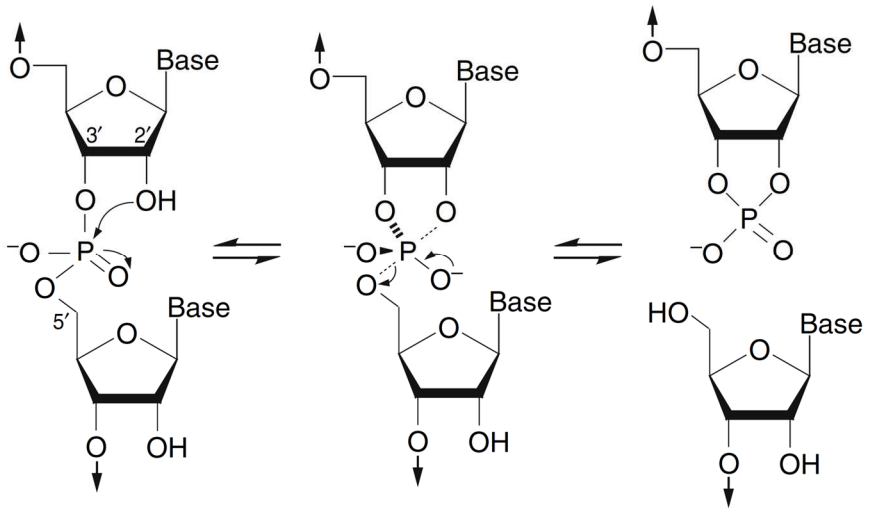

Figure 6. In-line cleavage mechanism. Figure adapted from Regulski and Breaker (2008). 'In-line' nucleophilic attack is necessary for efficient cleavage of an RNA phosphodiester linkage. When the 2' oxygen enters a linear 'in-line' arrangement with the phosphorus and the 5'-oxygen-leaving group of the linkage (dotted line), the 2' oxygen executes a productive nucleophilic attack on the adjacent phosphorous centre, cleaving the RNA linkage.

Because entering the full-length sequence as a whole did not result in a reasonable 2D structure (see **Fig. A1)**, the *met* leader sequence was divided into four parts and subsequently assembled to the complete 2D model. As transcription is a continuous process, regions already existing early during transcription are more likely to base pair with each other than a region from the 5'-end and the 3'end just present late in transcription. Thus, dividing the *met* leader sequence resembles more the situation during transcription. The full-length sequence had been divided into nt 1-129, nt 130-163, nt 164-205 and nt 206-440. The built 2D model is shown in **Fig. 7 B**.

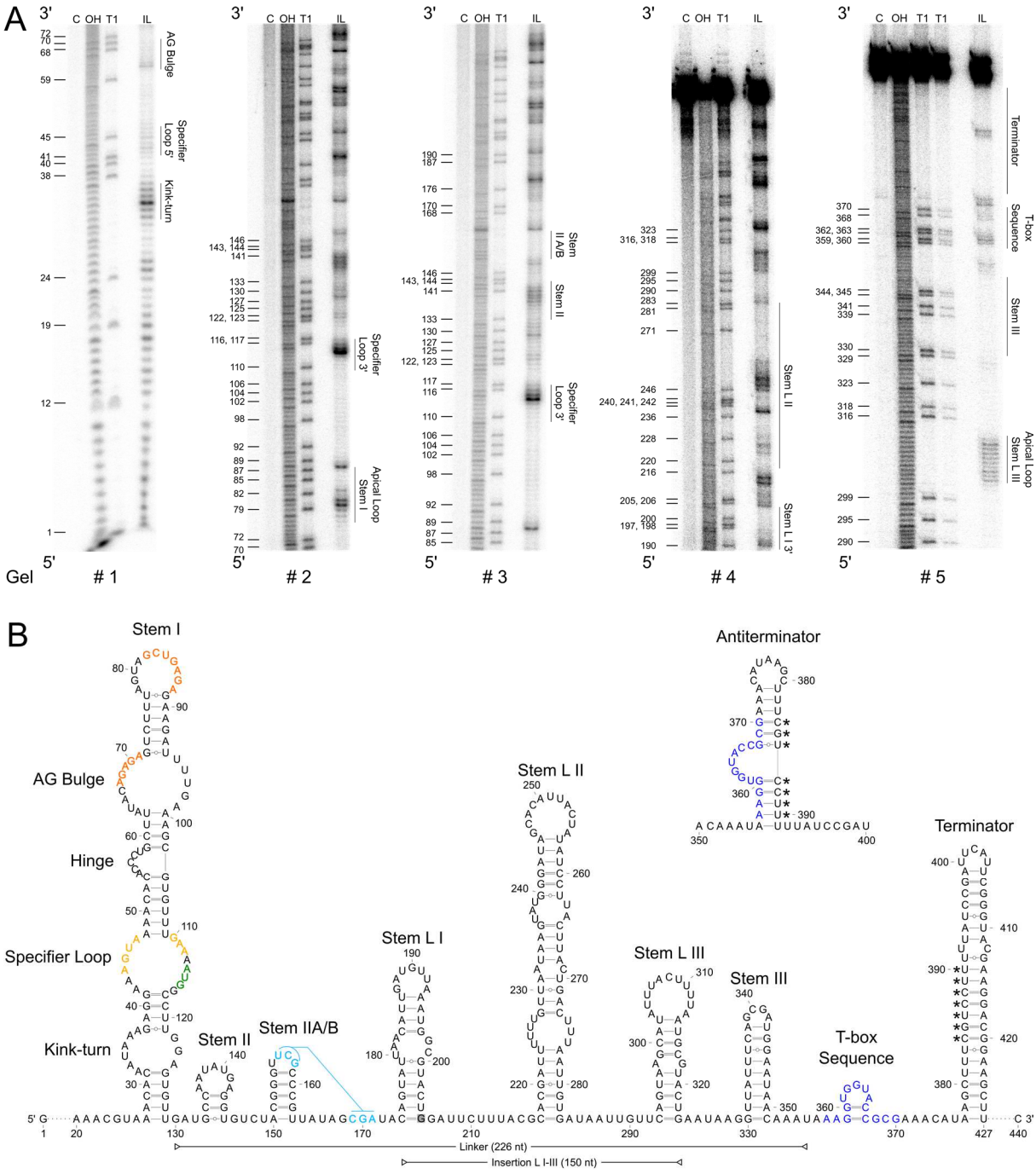

Figure 7. Secondary structure of *met* leader. (A) In-line probing gels used to build 2D model. Nomenclature of structural motifs according to Kreuzer and Henkin (2018). Additional stems within linker region are numbered L I to L III. Position of guanosines (G) is given on the left of each gel. Structural motifs are specified on right side of each gel. *(Continued on next page)*

Figure 7. *continued.* C: control reaction; untreated RNA, OH: alkaline hydrolysis reaction; ladder, T1: RNase T1-treated RNA; G-specific ladder, IL: in-line reaction; RNA incubated for 40 hours at room temperature. 5'-3' orientation is given on the left of each gel. **(B)** 2D structure model of *met* leader in its 'OFF' state, predicted Antiterminator 2D structure is shown above. Interacting nucleotides of Specifier Loop are shown in light orange, base pairing nucleotides of AG-Bulge and apical loop of Stem I in dark orange, Specifier codon in green, potentially interacting nucleotides of Stem II A/B pseudoknot in light blue, T-box sequence in dark blue. Linker region between Stem I and T-box sequence and insertion region of Stem L I-III are indicated by horizontal bars, lengths are specified. Nucleotides of Terminator sequence base pairing with T-box sequence in Antiterminator conformation are marked by asterisks (*). G 205 highlighted in grey indicates 5'-end of short *met* leader RNA used for in-line probing.

The three highly conserved T-box riboswitch motifs in Stem I (Kink-turn, Specifier Loop and AG Bulge) and the structures Stem II, Stem IIA/B pseudoknot, Stem III and Terminator stem were found/identified by in-line probing in the *S. aureus met* leader. In addition, the *met* leader RNA was found to harbour three extra stem-loops (designated L I to III), located between Stem IIA/B pseudoknot and Stem III, that are usually not present in T-box riboswitches. Also, a few minor aberrations within conserved riboswitch elements were detected.

Kink-turn

The asymmetric loop found at the bottom of Stem I (nt 32-37 and nt 122-124) is a common RNA structural element, called Kink-turn or K-turn, that causes the RNA helix backbone axis of the stem to bend by ~120° (Klein et al., 2001). The GA motif that consists of two oppositely oriented 5'-GA-3' dinucleotide sequences within the K-turn is almost completely conserved in all T-box riboswitches (Winkler et al., 2001). However, in the *met* leader the GA within the larger loop portion (5', nt 32-37) is absent (**Fig. 7 B**).

Specifier Loop

The Specifier loop (nt 42-47 and 110-117), located in the proximal part of the Stem I, comprises the AUG codon (nt 114-116, marked in green), that interacts with the anticodon of the tRNA, and two conserved sequences that are known to interact with each other in a non-canonical manner. The 5'-AGUA-3' (nt 44-47) motif interacts with the 5'-GAA-3' (nt 110-112) motif (both marked in light orange). The resulting S-turn increases the accessibility of the Specifier codon for the tRNA anticodon (Chang and Nikonowicz, 2013; Kreuzer and Henkin, 2018; Wang et al., 2010). This interaction was well reflected by the in-line data with these two sequences being (partially) protected from degradation despite the presence of ss regions (loop) (**Fig. 7 A gels #1-3**). The conserved purine immediately 3' of the Specifier codon that has been shown in other T-box riboswitches to be important for stabilising the interaction of the

Specifier codon with the tRNA, is present as a guanine (nt 117) in the *met* leader (**Fig. 7 B**) (Grigg and Ke, 2013; Zhang and Ferré-D'Amaré, 2013).

Stem I platform (AG Bulge and terminal loop)

The distal region of the Stem I includes the AG Bulge (nt 63-71) with the highly conserved 5'-AGAGA-3' motif (nt 67-71, marked in orange) and a terminal loop (nt 78-88) with the 5'-GCUGAGA-3' motif (nt 82-88, marked in orange) that interact with each other to form a platform for a tRNA elbow interaction that has been shown to be crucial for tRNA binding and subsequent antitermination (Grigg et al., 2013; Kreuzer and Henkin, 2018; Zhang and Ferré-D'Amaré, 2013).

The interactions of the AG Bulge with the 3' part of the apical loop of Stem I were well reflected by the in-line results because these two sequences appeared to be protected from degradation despite the presence of a ss region (bulge and loop, respectively) (**Fig. 7 A gels #1&2**).

Hinge

A bulge or an internal loop between the 5'-part of the Specifier Loop and the AG bulge disrupts the RNA helix which introduces structural flexibility that functions as a hinge. This causes the surrounding helices to bend and to kink the distal region of Stem I towards the tRNA elbow (Zhang and Ferré-D'Amaré, 2013). In the *S. aureus met* leader, the Hinge consists of a 5 nt-long bulge (nt 54-58) (**Fig. 7 B**).

Stem II and Stem IIA/B pseudoknot

The Stem II and the Stem IIA/B pseudoknot structures are two additional, conserved T-box riboswitch structural motifs which the in-line data suggested to be present in the *met* leader. However, Stem II (nt 133-145) seems to be very short and without the S-turn motif that is usually found (Kreuzer and Henkin, 2018) (**Fig. 7 A gel #3**). There is indication by the in-line data that the interaction of the apical loop of Stem IIA/B (nt 156-158) with the downstream single-stranded region (nt 169-171), resulting in a pseudoknot, occurs in the *met* leader RNA (marked in light blue) (**Fig. 7 A gel #3**). Despite its single-stranded nature, the predicted apical loop of the Stem IIA/B appeared to be protected from degradation.

Stem III

A Stem III is located just upstream of the T-box sequence in almost all known T-box riboswitches, but sequence and stem length are highly variable (Kreuzer and Henkin, 2018). The *S. aureus met* leader consists of a 9 bp-long stem with a 4 nt-comprising apical loop (nt 330-351) according to the obtained structural data (**Fig. 7 A gel #5**, **Fig. 7 B**).

T-box sequence and Terminator stem

The T-box sequence (nt 357-370, marked in dark blue), located downstream of Stem III, forms a small bulge (nt 361-365) closed by two consecutive G/C base pairs at its basis (in the 'OFF'-state of the *met* leader, *i.e.* without tRNA ligand) (**Fig. 7 A gel #5**).

The Terminator stem is an essential structure of all riboswitches of the transcription termination type as the formation of the Terminator stem under non-inducing conditions causes the RNA polymerase to prematurely terminate transcription.

However, neither sequence nor length is conserved, except for the 7 nt base pairing with the nucleotides of the T-box sequence (marked in dark blue) that are not part of the bulge, during Antiterminator formation (ON-state) (Vitreschak et al., 2008). The *met* leader Terminator stem (nt 377-427) is 23 bp in length and the 7 nt-long sequence interacting with the T-box sequence under activating conditions is CGUCCUU (nt 384-390, marked by asterisks) (**Fig. 7 A gel #5**, **Fig. 7 B**).

The length of the Terminator is above average. Of the 56 MET-T-box riboswitches listed by Vitreschak et al. only 8 have a terminator stem longer than 20 bp, including the *met* leader, whereas a length of 13 to 15 bp is most prevalent (Vitreschak et al., 2008). The loop size varies from 3 to 9 nucleotides and does not correlate with the stem length. The Terminator loop of the *met* leader consists of 5 nt (**Tab. 1**).

As it will be detailed later in this thesis, the length of the Terminator stem seems to influence the type of processing, because the length determines whether it is a suitable target for certain RNases or not.

Table 1. *met* leader Terminator stem length is above average. Terminator stem lengths of 56 MET-T-box riboswitches listed by Vitreschak et al. (2008) are given in descending order in base pairs (bp), value in brackets details sizes of terminal loop in nucleotides (nt), species and T-box regulated gene (if operon, only first gene is listed) is given for each Terminator stem. Terminator stems longer than 20 bp are highlighted in green. Details for *S. aureus* are shown in bold. Unfinished genomes (at the time of publication) are marked by an asterisk (*).

Species	Regulated gene	bp Terminator stem (nt loop)
Lactobacillus plantarum	*yuscba1*	26 (3)
Enterococcus faecalis	*yuscba2*	26 (2)
Lactobacillus plantarum	*metB*	25 (4)
Lactobacillus plantarum	*yuscba2*	24 (4)
S. aureus	***metI***	**23 (5)**
*Lactobacillus brevis**	*yxjh*	22 (4)
*Lactobacillus casei **	*metE*	21 (3)
*Lactobacillus casei **	*yckjki*	21 (3)
Lactobacillus plantarum	*yxjh*	19 (5)
Enterococcus faecalis	*yuscba1*	19 (5)
Lactobacillus johnsonii	*yxjh*	19 (4)
*Pediococcus pentosaceus**	*yuscba*	19 (4)
*Lactobacillus casei **	*yxjh*	18 (4)
*Lactobacillus delbrueckii **	*ytjb*	17 (5)
*Leuconostoc mesenteroides**	*mdh*	17 (5)
Bacillus cereus	*metS*	17 (4)
*Lactobacillus reuteri**	*yusa*	16 (9)
*Lactobacillus reuteri**	*ykruv*	16 (7)
*Lactobacillus reuteri**	*yxjh1*	16 (4)
*Leuconostoc mesenteroides**	*metB*	16 (4)
Clostridium acetobutylicum	*metS*	15 (6)
Enterococcus faecalis	*yxjh*	15 (4)
*Lactobacillus reuteri**	*ytjb*	14 (6)
*Lactobacillus casei **	*yusa*	14 (7)
*Lactobacillus brevis**	*yusacb*	14 (6)
*Oenococcus oeni**	*yusa*	14 (6)
*Oenococcus oeni**	*yusc*	14 (6)
Lactobacillus plantarum	*2751*	14 (6)
*Lactobacillus reuteri**	*mmum*	14 (6)
Clostridium botulinum	*metS*	14 (5)
*Leuconostoc mesenteroides**	*yxjh*	14 (5)
*Lactobacillus reuteri**	*yusacb*	14 (5)
*Lactobacillus delbrueckii **	*mmum*	14 (5)
*Lactobacillus reuteri**	*yxjh2*	14 (4)
*Leuconostoc mesenteroides**	*metF*	14 (4)
Clostridium tetani	*yocr*	14 (4)
*Clostridium beijerincki**	*metS*	13 (6)
Lactobacillus sakei	*yuscba*	13 (6)
Thermoanaerobacter tengcongensis	*metS*	13 (5)
*Pediococcus pentosaceus**	*yxjh*	13 (5)
Clostridium tetani	*metS*	13 (4)
*Lactobacillus delbrueckii **	*yusacb*	13 (4)
Enterococcus faecalis	*opp*	13 (4)
Bacillus clausii	*metS*	13 (3)
*Leuconostoc mesenteroides**	*hcp_mts*	13 (3)
Lactobacillus plantarum	*metE*	12 (9)
*Oenococcus oeni**	*yxjh*	12 (6)
Clostridium difficile	*metS*	11 (6)
Lactobacillus johnsonii	*yusacb*	11 (6)
Lactobacillus plantarum	*yckk2*	11 (6)
*Leuconostoc mesenteroides**	*xxytmklm*	11 (4)
Bacillus halodurans	*metS*	11 (3)
*Lactococcus cremoris**	*yusa*	10 (7)
Clostridium perfringes	*metS*	10 (4)
Lactobacillus plantarum	*metI*	8 (7)
Lactococcus lactis	*yusa*	8 (7)

Linker region Stems L I, II and III

Three hairpin structures, designated Stem L I (nt 174-205), II (nt 217-283) and III (nt 293-323), were identified by in-line probing in the *met* leader linker region (**Fig. 7 A gels #4&5**). Stem L I is a 10 bp-long helix, disrupted by a 3+2 asymmetric loop (nt 180-182 and 198-199), closed by a 7 nt-comprising apical loop (nt 187-193). Stem L II is a 22 nt-long helix, disrupted by a proximal 4+3 (nt 224-227 and 274-276) and a distal 3+2 (nt 237-239 and 263-264) asymmetric loop and an A/C mismatch pair (nt 232&269) between these two loops. Its apical loop consists of 11 nt (nt 246-256). Stem L III is a 10 bp-long helix with an A/G mismatch pair (nt 298&318) and an 11 nt-long apical loop (nt 303-313). These stems are unique structures absent in all known T-box riboswitches structurally described in the literature. The presence of this region expands the size of the linker region between Stem I and the T-box sequence to 226 nt.

3.2. One transcript–distinct stabilities

3.2.1. *met* leader stability and processing

Under transcription-inducing (= methionine-deprived) conditions, formation of the Antiterminator structure in the *met* leader allows the RNA-polymerase to read-through into the *met* operon genes. A read-through implicates the presence of an mRNA that contains the *met* leader and the *met* mRNA. However, we were never able to detect this full-length transcript (~7.6 kb) with a *met* leader-specific probe, but instead only a transcript with the size of the *met* leader alone (about 440 nt) (see **Fig. 3 A**). Re-probing with a *metE* specific probe resulted in a faint signal corresponding to the *met* mRNA without the *met* leader (about 7,200 nts) and a strong signal from a transcript of approx. 4,000 nts (addressed later in this thesis) (**Fig. 8 A**). Accordingly, the *met* leader RNA is immediately separated from the *met* mRNA after the read-through. After separation, the *met* leader RNA is rapidly degraded, as demonstrated by rifampicin assays with the majority of *met* leader transcripts being already degraded after 1 min. Termination events occur also under methionine-deprived conditions. Hence, the *met* leader exists as an independent RNA molecule (+/- 440 nt), visible as faint bands, next to the +/- 390nt-long read-through *met* leader species (after immediate separation) (**Fig. 8 B**).

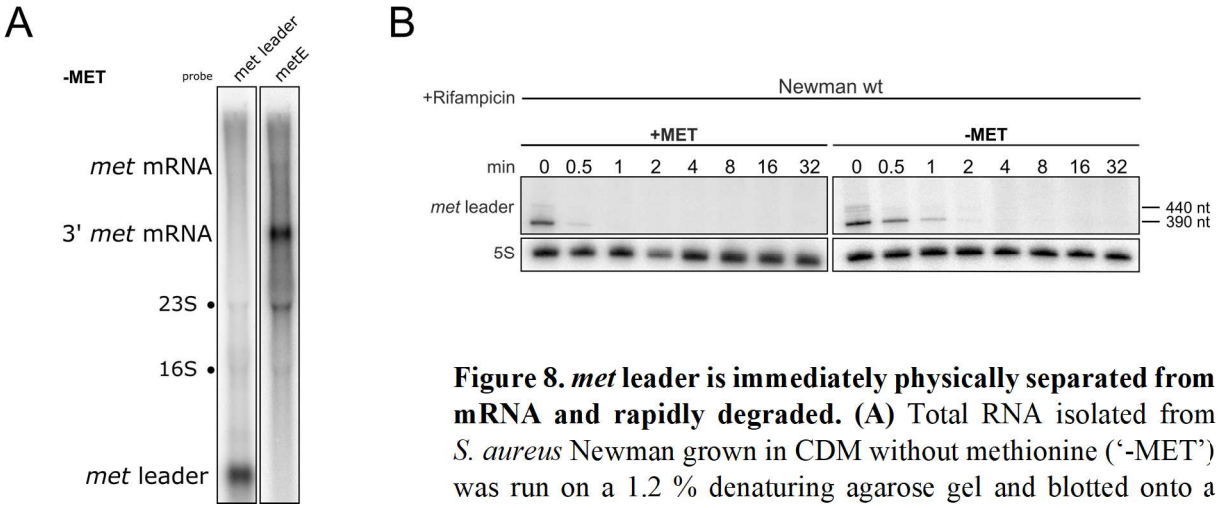

Figure 8. *met* leader is immediately physically separated from mRNA and rapidly degraded. (A) Total RNA isolated from *S. aureus* Newman grown in CDM without methionine ('-MET') was run on a 1.2 % denaturing agarose gel and blotted onto a nylon membrane. Northern blot probed with a *met* leader-specific and then re-probed with a *metE*-specific probe. Positions of *met* leader RNA, *met* mRNA and 3'-region *met* mRNA are indicated on the left, positions of 23S and 16S rRNA are marked by a black dot. **(B)** Total RNA isolated from *S. aureus* Newman grown in CDM with ('+MET') and without methionine ('-MET') over a time course of rifampicin addition (0-32 min) was run on a denaturing 5 % PAA 7 M Urea gel and blotted onto a nylon membrane. Northern blot was hybridised with a *met* leader-specific probe and subsequently re-hybridised with a 5S rRNA-specific probe as loading control.

3.2.2. Cleavage of *met* leader at position 388^389 is RNase III-driven and Terminator is the final conformation independent of methionine-status

The most important RNases for mRNA turnover in *S. aureus* are RNase Y (ss-specific endonuclease), RNase III (ds-specific endonuclease) and RNase J (J1/J2 heteromer) (5'-3' exo- and ss-specific endonuclease), as well as the 3'-5' exonuclease PNPase (Bonnin et al., 2015; Durand and Condon, 2018). RNA degradation is thought to be usually initiated by an endonucleolytic cleavage, followed by exonucleolytic activities from both directions. RNase Y has been shown to cleave several SAM-binding riboswitches in *B. subtilis* and T-box riboswitches in *S. aureus* (Khemici et al., 2015; Shahbabian et al., 2009).
Endonucleolytic cleavage of the *met* leader by either RNase Y, III or J seemed to be conceivable. Therefore, total RNA from Δ*rny*, Δ*rn*c and Δ*rnjB* mutants, grown in CDM without methionine was subjected to Northern blot analysis. At that time, only an RNase J2 (Δ*rnjB*) mutant had been available.
RNase J2 has been shown to play a more structural role in the J1/J2 complex, J1 is required for catalytic activity of the heteromer (Bonnin et al., 2015; Durand and Condon, 2018; Linder et al., 2014).

As shown in **Fig. 9A**, neither in the Δ*rny* nor the Δ*rnjB* strain the *met* leader band pattern differed from that in the wild type, indicating that both RNase Y and the RNase J2 are not involved in endonucleolytic cleavage of the *met* leader, initiating its rapid degradation. (Subsequent experiments with an RNase J1 mutant (Δ*rnjA*) confirmed the conclusion that RNase J is not involved (see **Fig. 14 B**).) However, in the Δ*rnc* mutant the longer RNA species of about 440 nt (terminated *met* leader) was strongly enriched compared to the wild type and at the same time, the smaller RNA species of about 390 nt was diminished. This indicated the involvement of RNase III in the degradation of the *met* leader. Rifampicin assays were performed to investigate the stability of the *met* leader in the RNase mutants. An endonucleolytic cleavage close to the 5'- or 3'-end of the RNA molecule might not be well visible on a PAA gel due to the small size difference between cleaved and non-cleaved, but its occurrence would render the RNA molecule an exonuclease target and thus less stable. Therefore, rifampicin assays were performed to investigate the stability of the *met* leader RNA in the three RNase mutants. In the Δ*rny* as well as in the Δ*rnjB* mutant the total amount of *met* leader RNA appeared to be more in t0, but the stability over time seems not to be affected (**Fig. 9 B&C**). Already after one minute only a minor fraction of the initial transcripts was remaining (**Fig. 9 B**). In contrast, stability of the larger *met* leader RNA molecule was

dramatically increased in the Δ*rnc* mutant compared to the wild type, indicating involvement of RNase III in *met* leader processing (**Fig. 9 C**). After four minutes around 25 % of the initial transcripts were still remaining (**Fig. 9 B**). The presence of a small fraction of the 390 nt processing intermediate in the RNase III mutant most likely stemmed from residual activity of the RNase III as the mutant is not a clean knock-out, but a conditional mutant. Northern blot analyses could only give a rough estimation in which region of the *met* leader RNA the processing might occur. The size of 390 nt of the processing intermediate suggested cleavage within the Terminator stem. At that time, the Terminator was predicted to comprise nts 379-425 (Schoenfelder, 2011). Furthermore, the stem appeared to be a suitable substrate for a ds-RNA specific endonuclease, such as RNase III.

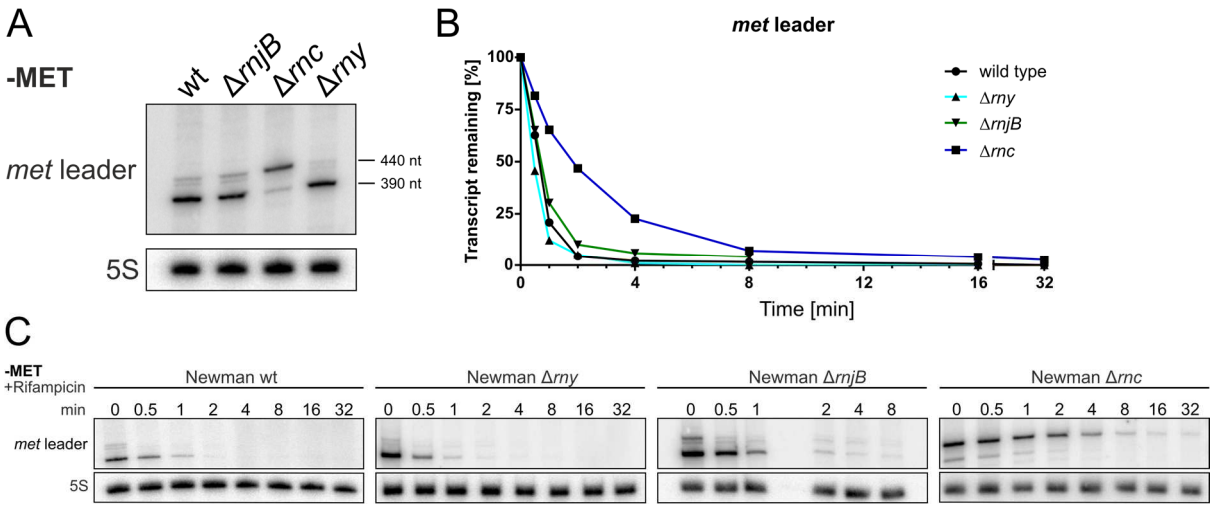

Figure 9. Influence of the main RNases of *S. aureus* on *met* leader stability. (A) Total RNA isolated from *S. aureus* Newman, an RNase J2 (*ΔrnjB*), an RNase III (*Δrnc*) and an RNase Y (*Δrny*) mutant grown in CDM without methionine ('-MET') was run on a denaturing 5 % PAA 7 M Urea gel and blotted onto a nylon membrane. Northern blot was hybridised with a *met* leader-specific probe and subsequently re-hybridised with a 5S rRNA-specific probe as loading control. Approximate transcript lengths are indicated on the right. **(B)** Quantification of *met* leader transcript levels over time from rifampicin stability assays shown in (C). **(C)** Total RNA isolated from strains detailed in (A) grown in CDM without methionine ('-MET') over a time course of rifampicin addition (0-8 and 0-32 min, respectively) was run on a denaturing 5 % PAA 7 M Urea gel and blotted onto a nylon membrane. Northern blot was hybridised with a *met* leader-specific probe and subsequently re-hybridised with a 5S rRNA-specific probe as loading control.

3.2.3. Determination of 5'-and 3'-ends of *met* leader RNA by cRACE reveal position 388^389 as major processing site

The homodimeric RNase III enzyme covers 22 bp of a dsRNA, the usual range of helices cleaved by RNase III is between 20 and 25 bp, resulting in fragments of 9-12 bp in length with a 2 nt-3' overhang. The major cleavage usually occurs within a GC-rich sequence motif of the dsRNA. However, not the cleavage site itself, but surrounding regions have been shown *in vitro* to be crucial for dsRNA recognition and binding, called the proximal (P), middle (M) and distal (D) box, each located both, upstream and downstream of the cleavage site (Gan et al., 2006; Pertzev and Nicholson, 2006; Romilly et al., 2012).

cRACE was performed to determine the exact 5'- and 3'-ends of the *met* leader RNA under inducing (methionine-deprived) conditions. Fusion of the 5'- and 3'-end of the RNA molecule allowed to determine the transcription start site (see **section 3.1.1, page 22**), the processing site, at which the *met* leader is cleaved off from the *metI* mRNA after read-through and other degradation intermediates. Position 388 was with ~ 68 % of all investigated RNA molecules (n = 56) the most prevalent 3'-end of the *met* leader. Therefore, position 388^389 is the major processing site. Additional 15 intermediates were identified with positions 317^318, 387^388 and 425^426 accounting for ~ 4 % each, and all remaining sites for ~ 2 % each, of all investigated *met* leader molecules (**Tab. 2**). Furthermore, cRACE experiments revealed that the Terminator stem is the final structure, even under inducing conditions, because only the presence of the Terminator stem allows RNase III cleavage with a resulting fragment of 388 nt. Presence of the Antiterminator structure would not provide an RNase III substrate (dsRNA with ≥ 11 bp helix between cleavage site and distal box), and cleavage would result in cleavage fragments of 360-370 nt length (**Fig. 9 A**, see **Fig. 7 B**).

5' RACE (rapid amplification of cDNA ends) with a primer binding within the *metI* sequence to investigate the fate of the *met* operon mRNA (see **section 3.3.1, page 43 f.**) nicely confirmed 388^389 as the major cleavage site of the *met* leader, as 50 % (n = 24) of the detected 5'-ends were at position 418 of the *met* leader. Position 417^418 is the RNase III cleavage site on the 3' part of the Terminator stem opposite of 388^389 (**Fig. 10 A**). Consequently, the last 22 nt of the *met* leader remain associated with the *metI* mRNA.

Position	**% of all analysed *met* leader RNA molecules (n = 56)**	**n**
310^311	1.79	1
312^313	1.79	1
316^317	1.79	1
317^318	3.57	2
326^327	1.79	1
331^332	1.79	1
370^371	1.79	1
387^388	3.57	2
388^389	67.86	38
390^391	1.79	1
392^393	1.79	1
397^398	1.79	1
410^411	1.79	1
420^421	1.79	1
425^426	3.57	2
433^434	1.79	1
∑	**100**	**56**

Table 2. cRACE reveals position 388^389 as major processing site of the *met* leader. Position of cleavage within *met* leader is given as 'xxx^yyy' in column one, 'xxx' represents the last, most 3', nucleotide of the *met* leader after cleavage. Respective percentage of cleavage site of all detected cleavage sites is detailed in column two, column three gives number of detected *met* leader RNA molecules for the respective cleavage site. Major processing site 388^389 is highlighted in grey.

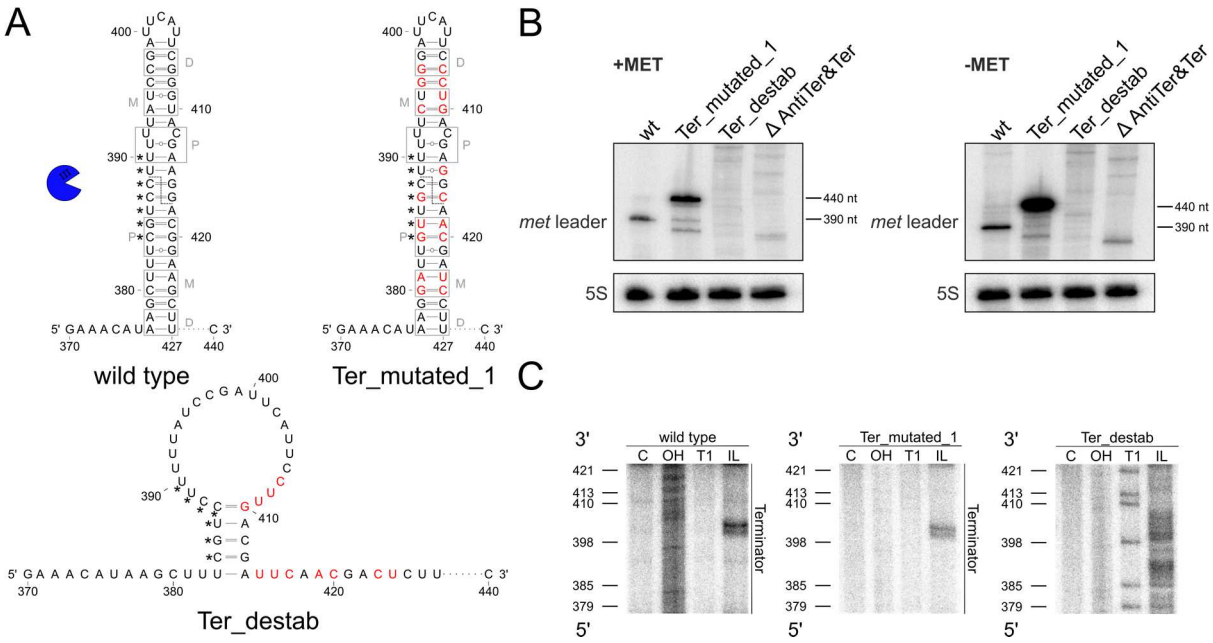

Figure 10. Altered processing of *met* leader in Terminator mutants Ter_mutated_1, Ter_destab and ΔAntiTer&Ter. (A) Predicted secondary structure of Terminator region in *met* leader of wild type and mutants 'Ter_mutated_1' and 'Ter_destab'. Point mutations introduced are highlighted in red, grey boxes indicate regions interacting with RNase III dimer as described in Gan et al. (2006) P: proximal, M: middle, D: distal box. Nucleotides of Terminator sequence base pairing with T-box sequence in Antiterminator conformation are marked by asterisks (*). RNase III is depicted as packman. Position of RNase III cleavage site in wild type *met* leader is indicated by a dashed line. **(B)** Total RNA isolated from *S. aureus* Newman and the *met* leader mutants 'Ter_mutated_1', 'Ter_destab' and 'ΔAntiTer&Ter' grown in CDM with ('+MET') or without methionine ('-MET') was run on a denaturing 5 % PAA 7 M Urea gel and blotted onto a nylon membrane. Northern blot was hybridised with a *met* leader-specific probe and subsequently re-hybridised with a 5S rRNA-specific probe as loading control. **(C)** In-line probing gel sections of the Terminator region of *met* leader wild type, 'Ter_mutated_1' and 'Ter_destab' RNA are shown. Position of guanosines (G) as in 'Ter_destab' is given on the left of each gel. C: control reaction; untreated RNA, OH: alkaline hydrolysis reaction; ladder, T1: RNase T1-treated RNA; G-specific ladder, IL: in-line reaction; RNA incubated for 40 hours at room temperature. 5'-3' orientation is given on the left of each gel.

3.2.4. Absence of cleavage of *met* leader mutants lacking RNase III-recognition characteristics confirm RNase III-dependent processing

In order to confirm RNase III-dependent degradation of the *met* leader RNA, three *met* leader mutants were generated that were expected to not be cleaved by RNase III due to absence of substrate characteristics. Ter_mutated_1 is a *met* leader with altered Terminator sequence, but preserved stem structure and base-pairing strength. Nucleotides of the cleavage site (nt 417) and within the P-, M- and D-boxes were mutated. Ter_destab contains point mutations in the Terminator stem sequence that prevent hairpin formation and ΔAntiTer&Ter is a *met* leader with deletion of the complete Antiterminator and Terminator sequence (nt 352-440) (**Fig. 10 A**).

Bacteria were grown in CDM with or without methionine, total RNA was prepared and subjected to Northern blot analysis. Processing of the *met* leader RNA into the 388 nt fragment was almost completely abolished in the Ter_mutated_1 mutant. The band pattern resembles that of the Δ*rnc* mutant (**Fig.10 B**, see **Fig. 9 A**) corroborating that RNase III cleaves within the *met* leader Terminator stem. In the Ter_destab and the ΔAntiTer&Ter mutants, both unable to form a Terminator stem, no defined processing could be observed, further substantiating the Terminator stem as RNase III substrate (**Fig. 10 B**). Termination events occur also under methionine-deprived conditions. Hence, the *met* leader exists as an independent RNA molecule (440 nt) next to the read-through *met* leader species. In the wild type it is almost immediately cleaved by RNase III into the 388 nt fragment (as the read-through *met* leader). In the Δ*rnc* and Ter_mutated_1 this cleavage does not occur and therefore the terminated *met* leader species is enriched. The Ter_destab and the ΔAntiTer&Ter mutants are termination-deficient due to the absence of the Terminator (via alternative base pairing and deletion, respectively). Thus, neither the terminated *met* leader species (440 nt) exists nor does RNase III cleavage occur, that would result in the 388 nt *met* leader species. Presence and absence of the Terminator stem in the Ter_mutated_1 and Ter_destab mutant, respectively were confirmed *in vitro* by in-line probing (**Fig. 10 C**).

3.2.5. Sequence of cleavage site is neither required for recognition nor activity

Previous studies have shown *in vitro* that the sequence of the cleavage site itself is not required for the recognition by RNase III and its catalytic activity (Romilly et al., 2012). Three additional *met* leader mutants were generated to investigate the minimal cleavage requirements for RNase III *in vivo*.

The cleavage of the *met* leader occurs between nucleotides 388 and 389 and 417 and 418, respectively. Therefore, three *met* leader mutants with point mutations at or adjacent to the cleavage site were generated. Overall base-pairing strength of the Terminator stem was maintained as effectively as possible (**Fig. 11 A**). The *met* leader mutants Ter_mutated_2, 3 and 4 were grown in CDM with or without methionine and total RNA was prepared for Northern blot analyses. As shown in **Fig. 11 B**, cleavage still occurred in all three mutants, confirming that the sequence of the cleavage site itself is not required for the recognition and degradation by RNase III *in vivo* as well. However, in the Ter_mutated_3 mutant the 440 nt transcript signal and that of a slightly smaller transcript species are of higher intensity than in the wild type and the other Ter_mutated mutants that might indicate a less efficient RNase III-cleavage due to the mutations. Further experiments would be required to confirm or disprove this hypothesis. The strongly increased *met* leader transcript levels in the mutants compared to the wild type under methionine-deprived conditions are well explainable by upregulation of the *met* leader transcription due to the inability of these mutants to activate *met* operon gene expression (see below). Presence of the Terminator stem in the Ter_mutated_2, 3 and 4 mutants, respectively were confirmed *in vitro* by in-line probing (**Fig. 11 C**).

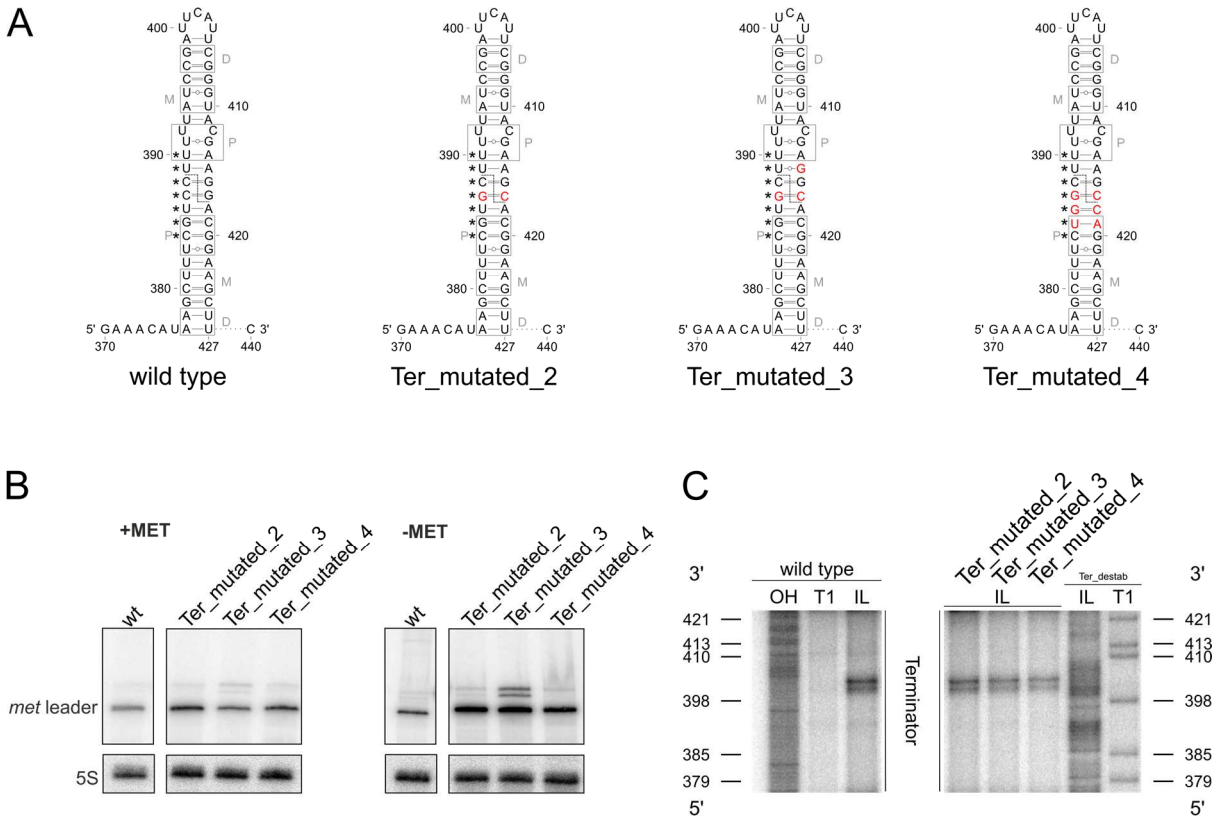

Figure 11. Altered processing of *met* leader in Terminator mutants Ter_mutated_2, 3 and 4. (A) Predicted secondary structure of Terminator region in *met* leader of wild type and mutants 'Ter_mutated_2', 'Ter_mutated_3' and 'Ter_mutated_4'. Point mutations introduced are highlighted in red, grey boxes indicate regions interacting with RNase III dimer as described in Gan et al. (2006) P: proximal, M: middle, D: distal box. Nucleotides of Terminator sequence base pairing with T-box sequence in Antiterminator conformation are marked by asterisks (*). Position of RNase III cleavage site in wild type *met* leader is indicated by a dashed line. **(B)** Total RNA isolated from *S. aureus* Newman and the *met* leader mutants 'Ter_mutated_2', 'Ter_mutated_3' and 'Ter_mutated_4' grown in CDM with ('+MET') or without methionine ('-MET') was run on a denaturing 5 % PAA 7 M Urea gel and blotted onto a nylon membrane. Northern blot was hybridised with a *met* leader-specific probe and subsequently re-hybridised with a 5S rRNA-specific probe as loading control. **(C)** In-line probing gel sections of the Terminator region of *met* leader wild type, 'Ter_mutated_2', 'Ter_mutated_3' and 'Ter_mutated_4' RNA are shown. Position of guanosines (G) as in 'Ter_destab' is given on the left of each gel. OH: alkaline hydrolysis reaction; ladder, T1: RNase T1-treated RNA; G-specific ladder, IL: in-line reaction; RNA incubated for 40 hours at room temperature. 5'-3' orientation is given on the left of each gel.

Cleavage of the *met* leader by RNase III removing the Terminator stem allows the rapid degradation of the RNA and therewith recycling of ribonucleotides under non-inducing (methionine-rich) conditions, but more importantly, it generates an instable 5'-monophosphorylated mRNA under inducing condition after read-through.

Typically, a riboswitch RNA is either not separated from the mRNA after read-through or cleavage occurs 5' of the Terminator stem sequence. Consequently, the mRNA possesses the Terminator stem as a protective structure at its 5'-end (Condon et al., 1996; Khemici et al., 2015; Seif and Altman, 2008; Shahbabian et al., 2009). On the contrary, the *met* leader Terminator stem itself is removed leaving an only 41 nt-long region with a 5'-monophosphate upstream of the *metI* start codon. Therefore, rapid degradation of *met* mRNA was expected.

3.3. Stability of *met* operon mRNA varies over length of transcript

Rifampicin assays were performed to investigate the stability of the *met* operon mRNA (**Fig. 12 A**). Bacteria were grown in CDM without methionine to induce *met* operon gene expression, total RNA was isolated and subjected to Northern blot analysis with various probes (**Fig. 12 B**). Hybridisation with a probe specific for the *metI* gene region resulted rather in a smear than in a sharp band that is rapidly degraded. Only at t0 prior to the addition of rifampicin a blurry band at around 1 kb was detectable (**Fig. 12 B**). Using a *metC*-specific probe did not result in any detectable band. In contrast, hybridisation with a *metE*- or *mdh*-specific probe, both resulted in a sharp band at around 4 kb. This transcript showed a rather high stability compared to the transcript detected with the *metI* probe, as the majority of the transcripts were still present at 4 minutes after rifampicin addition (**Fig. 12 B**). These results demonstrated that the 5'-region of the *met* mRNA is highly unstable, while the 3' region of the transcript has a long half-life. However, the exact nature of this stable transcript remained undetermined.

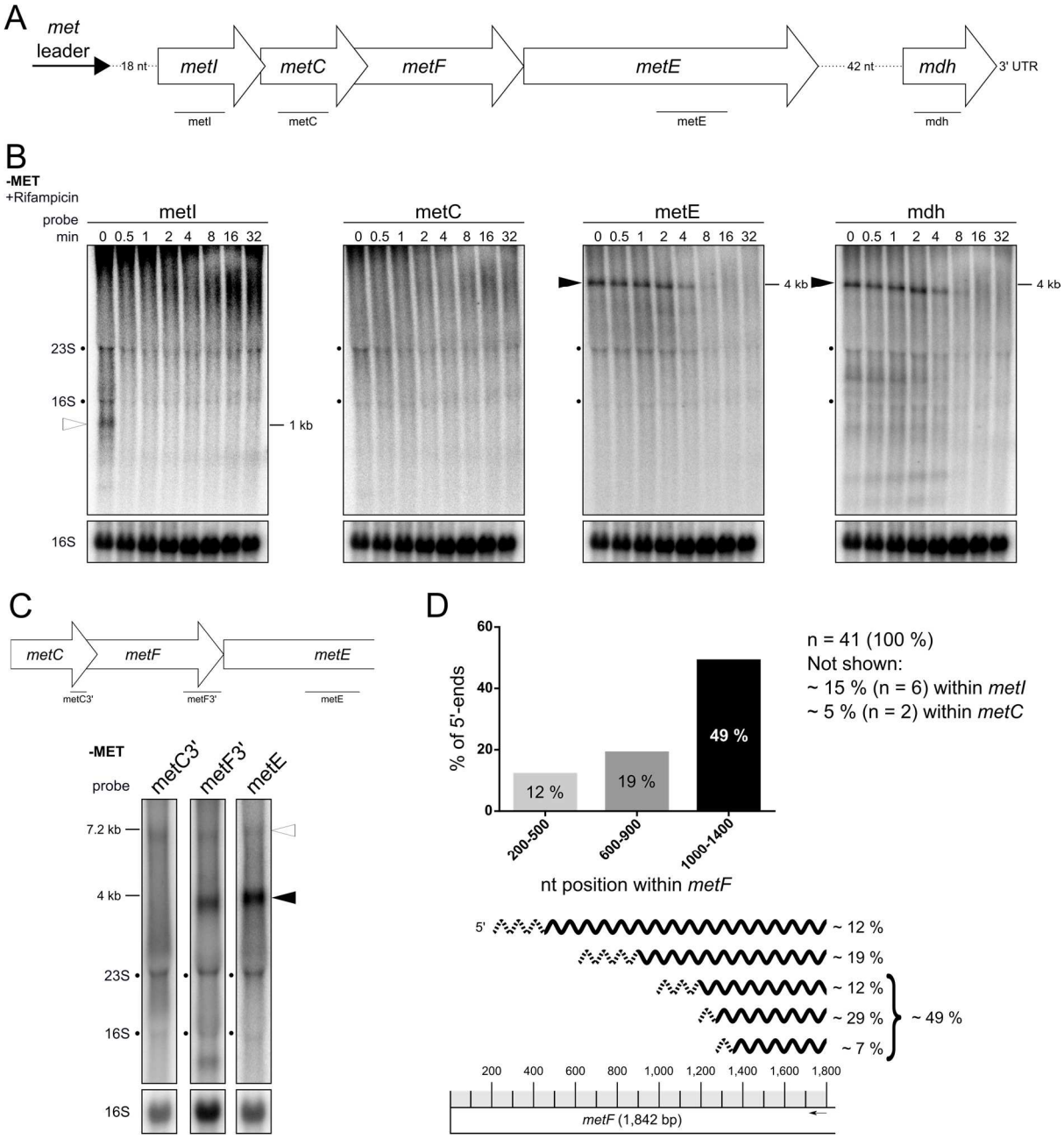

Figure 12. Stability of the *met* operon mRNA varies over length of the transcript. (A) Schematic view of the organisation of the *met* operon including its 5'-UTR (*met* leader). Line below gene arrow indicates relative position of the respective probe used in (B). **(B)** Total RNA isolated from *S. aureus* Newman grown in CDM without methionine ('-MET') over a time course of rifampicin addition (0-32 min) was run on a 1.2 % denaturing agarose gel and blotted onto a nylon membrane. Northern blot was probed for *metI*, *metC*, *metE* and *mdh*. Open arrowhead marks *metI* mRNA and black arrowhead marks 3'-*met* mRNA. Approximate transcript lengths are indicated on the right of the respective blot. Re-hybridisation with a 16S rRNA-specific probe was used as loading control. Positions of 23S and 16S rRNA are marked by a black dot. *(Continued on next page)*

Figure 12. *continued* **(C)** Schematic view of the *met* operon 3'-region without *mdh*. Lines below gene arrows indicate relative position of the probes used. Total RNA isolated from *S. aureus* Newman grown in CDM without methionine ('-MET') was run on a 1.2 % denaturing agarose gel and blotted onto a nylon membrane. Northern blot was probed for 3'-region of *metC* ('metC3''), 3'-region of *metF* ('metF 3'') and *metE*. Open arrowhead marks full-length *met* operon mRNA (without *met* leader) and black arrowhead marks 3'-*met* mRNA. Approximate transcript lengths are indicated on the left. Re-hybridisation with a 16S rRNA-specific probe was used as loading control. Position of 23S and 16S rRNA are marked by a black dot. **(D)** 5' RACE data obtained with primer FW161 for cDNA synthesis. Detected 5'-ends of transcripts were grouped according to the region of *metF*. Graph shows percentage of detected 5'-ends within the respective region of *metF* (nt 200-500, 600-900 or 1000-1400). Graphical representation of 5' RACE data: transcripts characterised by 5' RACE are depicted as wavy lines, dashed region symbolises range of detected 5'-ends within group (300, 200 and 100 nt range, respectively). Percentage of each transcript group of total analysed transcripts (100 %) is detailed in the bar (graph) or on the right (scheme). Size of grey boxes equals 100 nt, each. Approximate position of primer binding site within *metF* sequence is marked by a black arrow.

3.3.1. Stable 3'-region of *met* transcript comprises 3' part of *metF*, *metE* and *mdh*

To characterise the stable transcript, first probes were used that 'walked along' the transcript from 5' to 3' to narrow down the 5'-end of the transcript (**Fig. 12 C**). As shown in **Fig. 12 B**, *metE* and *mdh* are part of the transcript. *metE* and *mdh* together would have a transcript length of only about 3 kb, suggesting the 3'-end of *metF* (1,842 bp) to be part of the 4 kb stable transcript as well. A *metC* 3'-specific probe did, as expected, not allow the detection of a 4 kb transcript resembling the one detected with a *metE*-specific probe. Only the probe specific for the last 500 nucleotides of *metF* (*metF* 3') caused a signal similar to the 4 kb transcript signal (**Fig. 12 D**, see **Fig. 12 B**).

With this knowledge, a primer could be designed for cRACE cDNA synthesis that binds to the stable 4 kb transcript. cRACE was performed to determine the 5'- and 3'-end. Unfortunately, results did not allow any conclusion on the 5'-end position. cRACE appeared to be rather unsuitable for characterisation of long transcripts of several kb. Nevertheless, the 3'-end could be determined to be at position 396 787 of the Newman chromosome. Hence, the 3'-UTR of the *met* operon is suggested to be 81 nucleotides long.

A new approach to determine the 5'-end of the stable transcript was needed. The method of choice was 5' RACE.

Briefly, total RNA was isolated from *S. aureus* Newman grown in CDM without methionine to mid-exponential phase and all 5'-monophosphorylated RNAs present (= only processed transcripts) were ligated with an RNA adapter molecule. Ligated RNA then was used for cDNA synthesis with a primer complementary to a sequence within the last 500 nts of *metF*. Subsequently, generated cDNA was amplified with the RNA adapter and the cDNA primer and the PCR product was cloned into the pCR-XL-2-TOPO vector. Universal vector primers were used to amplify the insert and PCR product was sequenced to determine the 4 kb transcript's 5'-end.

As anticipated, almost 49 % of the analysed transcripts (n = 41) had a 5'-end within the last ~800 nucleotides (nucleotides 1001-1842) of the *metF* gene, but no clear processing site or region could be determined. About 19 % had a 5'-end between nucleotides 600 and 900 of *metF*, around 12 % between nucleotides 200 and 500 of *metF*. Only two analysed transcripts (~5 %) with a 5'-end within the *metC* gene were detected. The remaining 15 % of transcripts had a 5'-end located in the *metI* gene region (**Fig. 12 D**).

In parallel, 5' RACE with a primer binding within the *metI* mRNA region (FW200) was performed. 50 % (n = 24) of the detected 5'-ends started with position 418 of the *met* leader which is precisely one nucleotide 3' of the RNase III cleavage site (see **Fig. 10 A**). Of the remaining 50 %, 45 % of the detected 5'-ends were located within the *metI* sequence.

3.3.2. *metI* mRNA is exonucleolytically degraded by RNase J

The next step was to identify the RNases that drive the rapid degradation of the 5' region of the *met* mRNA.

No clear cleavage site had been detected with the 5' RACE approach. Hence, a 5' to 3' exonucleolytic degradation of the *met* mRNA seemed to be the most likely mechanism. This hypothesis is further supported by the presence of a 5'-monophosphate due to the RNase III-driven separation of the *met* leader from the *metI* mRNA that facilitates exonucleolytic degradation (Durand and Condon, 2018; Laalami et al., 2014). However, it might be possible as well that the mRNA is additionally endonucleolytically cleaved, but these sites are not detectable due to immediate ensuing exonucleolytic 5' to 3' degradation.

The only known 5' to 3' exonuclease in *S. aureus* is the RNase J (J1/J2 complex). Generation of J1 and J1/J2 double mutants failed with the conventional allelic replacement method with inducible counter-selection due to severely impaired growth at 42° C (personal communication Gabriella Marincola, Würzburg), (Bae and Schneewind, 2006; Linder et al., 2014). Linder et al. (2014) eventually succeeded in generating these mutants by using a non-replicative vector with a stringent counter-selection system that does not require the 42° C step for chromosomal integration (Redder and Linder, 2012).

Peter Redder kindly provided us with the Δ*rnjA*, Δ*rnjB* and the Δ*rnjA/B* double mutants and the isogenic wild type strain. The data presented in the following are all obtained with these strains. They have a 'SA564RD' (SA564 *hsdR* type III mutant (restriction deficient)) background and not the Newman background as in the rest of the thesis. These strains are pyrimidine auxotroph due to the deletion of the *pyrFE* genes. SA564 RD Δ*pyrFE* will be referred to as **PR01** and the isogenic RNase J mutant strains SA564 RD Δ*pyrFE* Δ*rnjA*, SA564 RD Δ*pyrFE* Δ*rnjB* and SA564 RD Δ*pyrFE* Δ*rnjA::ermC* & Δ*rnjB* as Δ***rnjA***, Δ***rnjB*** and Δ***rnjA/B***, respectively to simplify matters in this section.

Initial experiments showed that these strains do not sufficiently grow in CDM supplemented with uracil or pyrimidine. Therefore, PR01 and Δ*rnjA* bacteria were grown in MH medium to mid-exponential phase (OD 2.0), washed twice with PBS and resuspended in the same volume of CDM without methionine. After 1 hour of incubation rifampicin assays were performed and subsequently total RNA was subjected to Northern blot analysis. Neither a *met* leader-specific nor a *metE*-specific probe resulted in a clear signal (**Fig. 13**). This indicated that transcription of the *met* leader and consequently the *met* mRNA could not be efficiently initiated in the PR01 and its isogenic Δ*rnjA* strain under inducing conditions. The most likely explanation for the lack of transcription seemed to be mutations in the CodY-binding region or within the *met* leader that either cause constitutive repression of transcription by CodY or premature transcription termination already within the *met* leader, respectively. Since no mutations were observed in this region, transcription inhibition had to be due to a factor more upstream within the regulation cascade.

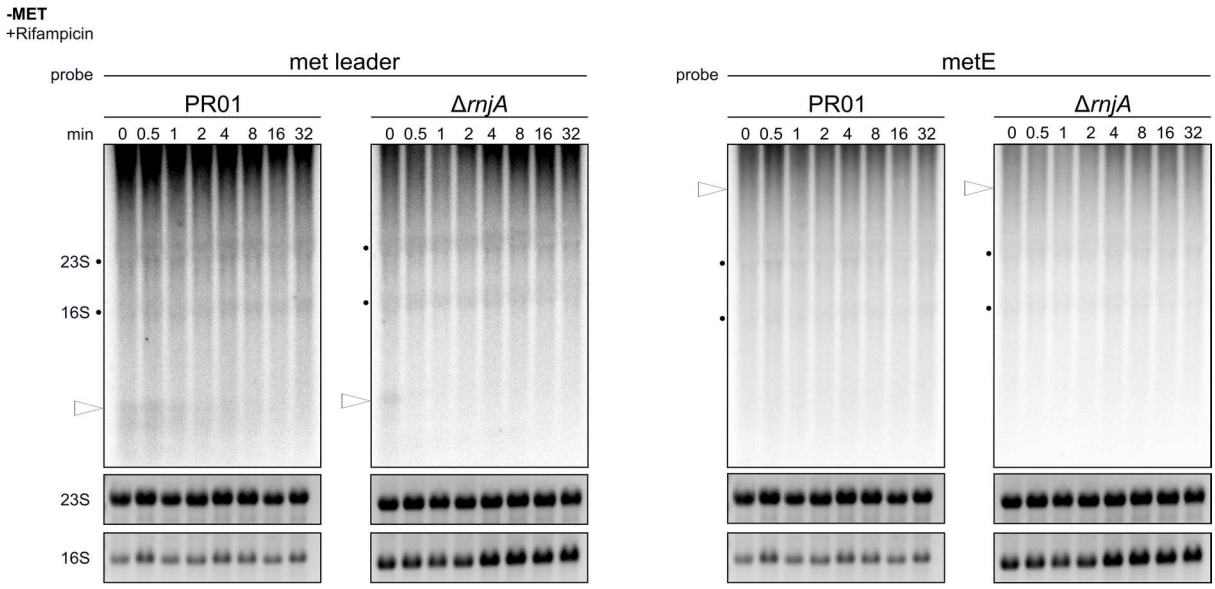

Figure 13. *met* leader and *met* operon are not transcribed in *S. aureus* SA564RD Δ*pyrFE* (PR01) and its isogenic RNase J1 mutant (Δ*rnjA*). Total RNA was isolated from *S. aureus* SA564RD Δ*pyrFE* (PR01) and its isogenic RNase J1 mutant (Δ*rnjA*) grown in MH medium to an OD of 2.0, washed twice with PBS and then shifted into CDM without methionine ('-MET') supplemented with pyrimidine for 1 hour over a time course of rifampicin addition (0-32 min). RNA was run on a 1.2 % denaturing agarose gel and blotted onto a nylon membrane. Northern blot was hybridised with a *met* leader- *and metE*-specific probe, respectively. Open arrowheads indicate expected signal position of *met* leader and 3'-*met* mRNA, respectively. Positions of 23S and 16S rRNA are marked by a black dot. 23S and 16S rRNA detected in Midorigreen-stained gel were used as loading control.

I decided to circumvent the problem by ectopically expressing the *met* leader and the *met* mRNA from a plasmid only under control of the native *met* leader promoter without the upstream CodY-binding region to enable constitutive expression. Unfortunately, approaches to clone the whole *met* locus into a pCN47 vector background failed, most likely due to the large size of 7.7 kb of the insert. As we were mainly interested in the degradation of the very 5'-end of the *met* mRNA, I then decided to generate a construct comprising the *met* leader including its -35 signal and only the first 215 nt of *metI* (**Fig. 14 A**). Cloning was successful and the plasmid was transformed into the PR01 strain and the isogenic Δ*rnjA*, Δ*rnjB* and Δ*rnjA/B* mutant strains. As control the plasmid was transformed into the *S. aureus* Newman wild type strain (data not shown).

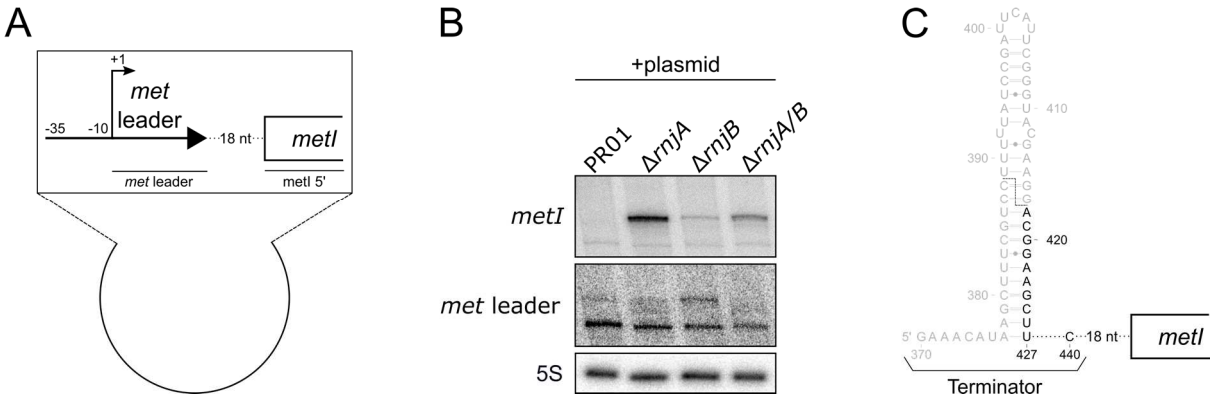

Figure 14. RNase J degrades *metI* mRNA with its 5'-3' exonucleolytic activity. (A) Scheme of plasmid transformed into *S. aureus* SA564RD Δ*pyrFE* (PR01) and its isogenic RNase J1 (Δ*rnjA*), RNase J2 (Δ*rnjB*) and RNase J1/J2 double (Δ*rnjA/B*) mutants, '-35' and '-10': transcription signals, arrow with +1 indicates transcriptional start site of *met* leader, *met* leader sequence depicted as thick, black arrow, first 215 nt of *metI* shown as open rectangle. Lines below gene arrows indicate relative position of probes used in (B). **(B)** Total RNA was isolated from *S. aureus* SA564RD Δ*pyrFE* (PR01) and its isogenic RNase J1 (Δ*rnjA*), RNase J2 (Δ*rnjB*) and RNase J1/J2 double (Δ*rnjA/B*) mutants. Bacteria were grown in MH medium to OD 0.5. Then cultures were washed twice with PBS, bacteria were shifted into CDM without methionine ('-MET') supplemented with pyrimidine for 30 minutes and samples were taken. 5 µg of total RNA was run on a denaturing 5 % PAA 7 M Urea gel and blotted onto a nylon membrane. Northern blot was hybridised with a *met* leader-specific probe, re-probed with a *metI 5'*-specific probe and subsequently re-hybridised with a 5S rRNA-specific probe as loading control. **(D)** Scheme of transcript detected with cRACE in Δ*rnjA*. Region of *met* leader Terminator stem cut off by RNase III and therefore not part of the transcript is depicted in grey, RNase III cleavage site is indicated by dashed line. 5'-region of *metI* mRNA is depicted as open rectangle.

Bacteria were grown in rich medium (Müller-Hinton) to an OD_{600} of 0.5. Then cultures were washed twice with PBS and bacteria were transferred into CDM without methionine and further incubated for 30 minutes to induce *metI* 5' transcription from the plasmid. Total RNA was isolated and subjected to Northern blot analysis with a *met* leader- and a *metI* 5'-specific probe (**Fig. 14 B**). The *met* leader transcript was detectable in all strains and the *metI* 5'-specific probe allowed the detection of a transcript of about 0.55 kb only in the RNase J mutant strains, but not in the PR01 strain (**Fig. 14 B**). cRACE analysis of total RNA of the Δ*rjnA* strain used for the Northern blot described above revealed that the observed transcript comprises the last 23 nt (from position 418 on) of the *met* leader, the *metI* 5' sequence and about 260 nt of the transcription termination sequence of the plasmid (n = 5). Position 418 of the *met* leader is exactly the first nucleotide downstream of the RNase III processing site described in **section 3.2.3, page 34 f.**, (**Fig. 14 C**). The absence of this transcript species in the PR01 bacteria supports the conclusion that this RNA is rapidly degraded by the 5'–3' exonucleolytic activity of the RNase J.

3.3.3. Endonuclease RNase Y is not involved in processing of *met* operon mRNA, but 3' *met* mRNA is strongly enriched in RNase Y mutant

The central single-strand RNA (ss-RNA)-specific endonuclease in *S. aureus* is RNase Y. It has been previously shown to induce differential degradation in polycistronic mRNAs/transcripts. Cleavage of the *saePQRS* operon downstream of *saeP* results in stabilisation of the *saeQRS* transcript region (Marincola et al., 2012).

We had initially (prior availability of RACE results) speculated that the increased stability of the 3' region of the *met* operon might be caused by an RNase Y cleavage. Therefore, a rifampicin assay with an *S. aureus* Newman RNase Y deletion mutant (Δ*rny*) grown to mid-exponential phase in CDM without methionine was performed, total RNA was isolated and subjected to Northern blot analysis with a *metE*-specific probe. The detected transcript resembled that of 3'-*met* mRNA in the wild type in size and stability, indicating that RNase Y does not cleave the *met* mRNA. However, the total transcript amount appeared to be strongly increased in the Δ*rny* strain (**Fig. 15 A**). Transcriptome data confirmed the high transcript abundancy in the RNase Y mutant compared to the wild type (personal communication Gabriella Marincola). In contrast, the *met* leader transcript levels did not differ (**Fig. 15 B**).

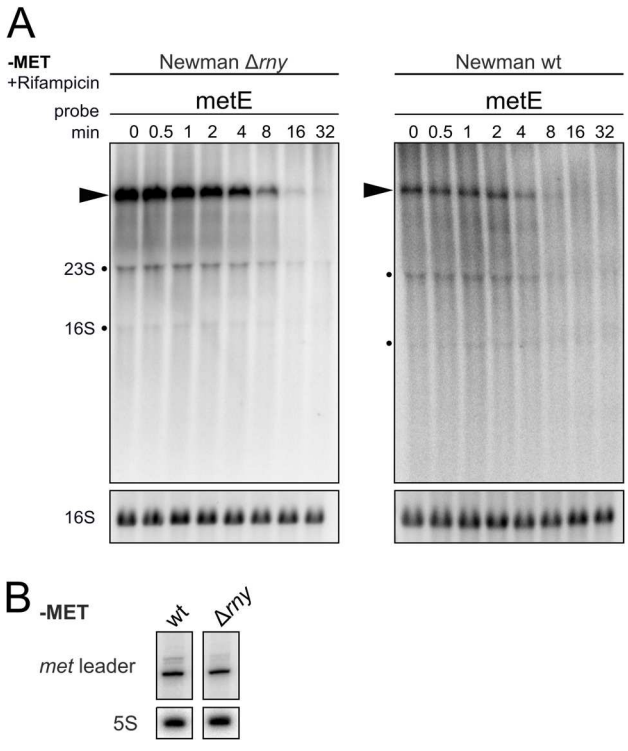

Figure 15. RNase Y is not involved in *met* mRNA processing, but lack of RNase Y leads to massively increased 3'-*met* mRNA levels. (A) Total RNA isolated from *S. aureus* Newman and its isogenic RNase Y mutant (Δ*rny*) grown in CDM without methionine ('-MET') over a time course of rifampicin addition (0-32 min) was run on a 1.2 % denaturing agarose gel and blotted onto a nylon membrane. Northern blot was hybridised with a *metE*-specific probe. Arrowheads mark 3'-*met* mRNA. 16S rRNA detected in Midorigreen-stained gel is shown as loading control. Positions of 23S and 16S rRNA are marked by a black dot. **(B)** Total RNA isolated from *S. aureus* Newman and its isogenic RNase Y mutant (Δ*rny*) grown in CDM without methionine ('-MET') was run on a denaturing 5 % PAA 7 M Urea gel and blotted onto a nylon membrane. Northern blot was hybridised with a *met* leader-specific probe and subsequently re-hybridised with a 5S rRNA-specific probe as loading control.

3.3.4. Other tested RNase mutants did not show changed degradation patterns of the *met* mRNA

More RNases were investigated regarding their involvement in degradation of the *met* locus because an interplay of several RNases is likely and endonucleolytic cleavage of the *met* mRNA by RNase J in addition to exonucleolytic degradation could not be shown by now.

A rifampicin assay with the *S. aureus* Newman RNase III mutant (Δ*rnc*) grown to mid-exponential phase in CDM without methionine was performed, total RNA was isolated and subjected to Northern blot analysis with a *metE*-specific probe. The detected transcript resembled that of 3'-*met* mRNA in the wild type in size and stability (**Fig. 16 A**). This indicates that RNase III does not cleave within the *met* mRNA.

Next to the RNase III mutant, six RNase mutants from the Nebraska Transposon Mutant Library (NTML) were available (Bae et al., 2008a; Fey et al., 2013). Details can be found in **Tab. 3**. The NTML RNase mutants have an *S. aureus* USA_300 JE2 background (Kennedy et al., 2008, 2010). The USA_300 JE2 strain, its isogenic mutants and as reference *S. aureus* Newman strain were grown to mid-exponential phase in CDM without methionine, total RNA was isolated and subjected to Northern blot analyses with a *met* leader- and a *metE*-specific probe, respectively. The detected transcripts resembled in size that of the *met* leader RNA and the 3'-*met* mRNA, respectively in the wild type (**Fig. 16 B&C**). (Note that RNase M5 is involved in 5S rRNA processing. That is why the 5S loading control consisted of four bands instead of one in Δ*rnmV*.) Overall, *met* transcript levels appeared to be lower in the USA_300 JE2 strain compared to the Newman strain and most of the RNase mutants. The degradation pattern of the *met* leader RNA seemed to be similar in all analysed strains, indicating that the tested RNases are not involved in *met* leader processing. Nevertheless, transcript stabilities might differ in the RNase mutants. Further experiments would be required to investigate the RNA half-life.

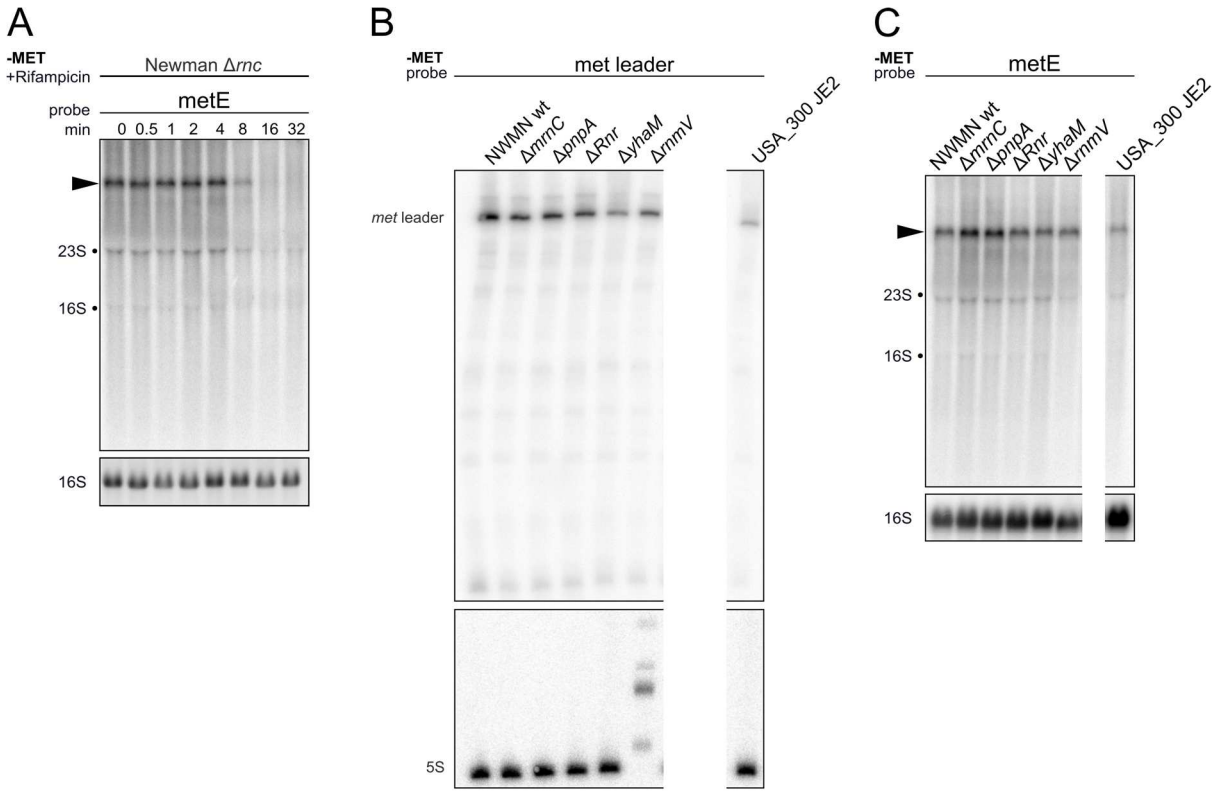

Figure 16. RNase III and tested NTML RNase mutants do not exhibit altered *met* leader RNA and *met* mRNA processing patterns. (A) Total RNA isolated from *S. aureus* Newman Δ*rnc* grown in CDM without methionine ('-MET') over a time course of rifampicin addition (0-32 min) was run on a 1.2 % denaturing agarose gel and blotted onto a nylon membrane. Northern blot was hybridised with a *metE*-specific probe. Arrowhead marks 3'-*met* mRNA. 16S rRNA detected in Midorigreen-stained gel is shown as loading control. Positions of 23S and 16S rRNA are marked by a black dot. **(B)** Total RNA isolated from *S. aureus* Newman, USA_300 JE2 and its isogenic RNase mutants grown in CDM without methionine ('-MET') was run on a denaturing 5 % PAA 7 M Urea gel and blotted onto a nylon membrane. Northern blot was hybridised with a *met* leader-specific probe and subsequently re-hybridised with a 5S rRNA-specific probe as loading control. Note that the RNase M5 (*rnmV*) is involved in 5S rRNA maturation. **(C)** Total RNA isolated from *S. aureus* Newman, USA_300 JE2 and its isogenic RNase mutants grown in CDM without methionine ('-MET') was run on a 1.2 % denaturing agarose gel and blotted onto a nylon membrane. Northern blot was hybridised with a *metE*-specific probe. Arrowhead marks 3'-*met* mRNA. Re-hybridisation with a 16S rRNA-specific probe was used as loading control. Positions of 23S and 16S rRNA are marked by a black dot. White bars indicate omission of irrelevant lanes.

Table 3. Details on NTML RNase mutants. Gene name, function, Locus tag in *S. aureus* Newman and USA_300 of the respective RNase and ID of the corresponding NTML RNase mutant is given. Table adapted from Bonnin et al. (2015).

RNase	**Gene**	**Function**	**Locus Tag Newman**	**Locus Tag USA300**	**NTML entry**
Mini-III	*mrnC*	ds-RNA endonuclease°	0493	0516	NE664
PNPase	*pnpA*	3'-5' exonuclease*	1183	1167	NE259
RNase R	*Rnr*	3'-5' exonuclease°	0749	0764	NE501
YhaM	*yhaM*	3'-5' exonuclease°	1734	1791	NE637
RNase M5	*rnmV*	ds-RNA endonuclease, maturation of 5S rRNA°	0455	0469	NE905

*demonstrated experimentally in *S. aureus*
°function based on results of *B. subtilis* or *E. coli* studies

3.4. Effect of methionine overproduction or prevention of methionine biosynthesis on fitness and virulence (riboswitch permanently 'ON' or 'OFF')

The next objective was to investigate the growth behaviour of *met* leader mutants with a permanently activated ('ON') or permanently terminating ('OFF') riboswitch under methionine-rich and -deprived conditions. The *met* leader mutants Ter_mutated_1, Ter_destab and ΔAntiTer&Ter have been already described in **section 3.2.4, page 37** and **Fig. 10**. Four additional *met* leader mutants were created by allelic replacement: SC2, SC4, SC5 and SC7 (**Fig. 17 A**). Those have either point mutations within the T-box bulge sequence (SC4, SC5 and SC7) or complete deletion of the T-box bulge (SC2) (Schoenfelder et al., 2013).
Ter_destab and ΔAntiTer&Ter were predicted to be 'ON' mutants, SC2 and SC5 to be 'OFF' mutants and for Ter_mutated, SC4 and SC7 wild-type behaviour was expected. Bacterial growth was monitored over a time course of 48 hours by $OD_{595\ nm}$ measurement every 30 minutes. Bacteria were cultivated in a 96-well plate in CDM with or without methionine with shaking at 37° C. Representative data are shown.
Under methionine-rich conditions all mutants behaved like the wild type: OD_{max} of ~0.6 was reached after 5 to 7.5 hours and bacteria entered the stationary growth phase (**Fig. 17 B**). However, under methionine-deprived conditions the mutants showed altered growth behaviour compared to the wild type (**Fig. 17 C**). Most noticeable was lack of growth in the SC4, SC7 and the Ter_mutated_1 mutants (data obtained in three, two and one independent experiments, respectively). The ΔAntiTer&Ter mutant showed a delayed entry into the exponential growth phase of 5 hours compared to the wild type in three different experiments and a slightly higher OD_{max} in two of three experiments. The Ter_destab mutant showed a delayed entry into the exponential growth phase of 5 hours only in one of three experiments (not shown), the OD_{max} varied from experiment to experiment. The SC2 and SC5 mutants both showed a delayed entry into the exponential growth phase of about 5 hours as well, compared to the wild type in two independent experiments, the OD_{max} varied.

In addition to the phenotypic growth behaviour, the *met* leader mutants were investigated on the molecular level. Bacteria were grown in CDM with methionine to mid-exponential phase, sample was taken, and the remaining bacteria were washed twice with PBS and shifted into CDM without methionine for 2 hours, total RNA was prepared and subjected to Northern blot analyses. Shifting was necessary due to the lack of growth of the SC4, SC7 and the Ter_mutated mutants because sufficient amounts of bacteria are required for RNA isolation.

The two *met* leader mutants SC4 and SC7 that are predicted to form the Antiterminator structure as the wild type (**Fig. 17 A**), despite two and one G to C point mutations within the T-box bulge, respectively, showed processing of the *met* leader RNA similar to the wild type under methionine-rich ('+MET') and -deprived ('-MET') conditions (**Fig. 17 D**). However, transcription of the *met* mRNA did not take place under methionine-deprived conditions (**Fig. 17 E**, marked by red hashtags). Lack of *met* operon expression explains the inability of SC4 and SC7 to grow in methionine-free medium (**Fig. 17 C**). SC2 and SC5 showed a band pattern for the *met* leader similar to the wild type under methionine-rich and –deprived conditions. However, the transcript levels were strongly increased compared to the wild type (**Fig. 17 D**). The reason is an enhanced transcript stability as demonstrated by rifampicin assays (**Fig. A2**, see **Fig. 8 B**). In both mutants, transcription of the *met* operon occurred under methionine-rich conditions. In SC2 the transcript levels appeared to be higher than in SC5 (**Fig. 17 E**, marked by green asterisks).

The point mutations introduced into the Terminator sequence of the Ter_mutated_1 mutant did not only impair RNase III-cleavage, but formation of the Antiterminator under methionine-deprived conditions as well (**Fig. 17 D&E**). The 3' part of the Antiterminator stem comprises nucleotides 381-390 that are part of the 5'-Terminator stem region (**Figs. 17 A** and **10 A**). Introduced point mutations prevented proper Antiterminator formation (**Fig. A3**). Hence, *met* operon expression was abrogated and growth inhibited (**Fig. 17 E**, marked by a red hashtag). In ΔAntiTer&Ter and Ter_destab transcription of the *met* operon occurred under methionine-rich conditions (**Fig. 17 E**, marked by green asterisks).

SC4, SC7 and Ter_mutated_1 are 'permanently OFF' *met* leader mutants because transcription of the *met* operon is always shut down independent of the methionine status of the cell. ΔAntiTer&Ter, Ter_destab, SC2 and SC5 are 'permanently ON' *met* leader mutants, as the *met* operon is constantly transcribed despite availability of methionine (**Fig. 17 E**). In SC2 and SC5 transcription levels of the *met* operon appeared to be lower than in Ter_destab and ΔAntiTer&Ter.

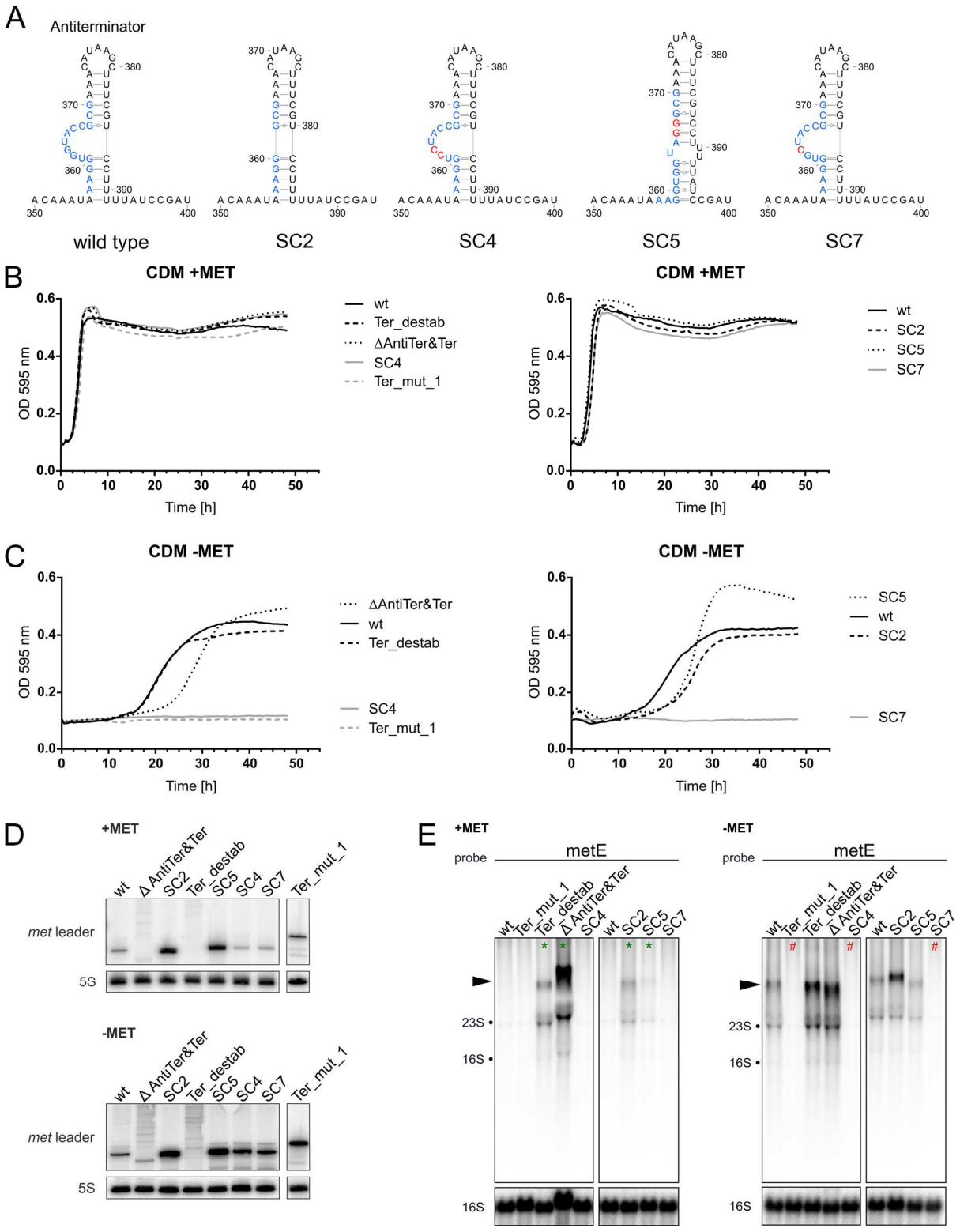

Figure 17. *See next page*

Figure 17. *met* leader mutations impact bacterial growth under methionine-deprived conditions due to *met* operon dysregulation. (A) Predicted secondary structure of Antiterminator region in *met* leader of wild type and mutants 'SC2', 'SC4', 'SC5' and 'SC7'. T-box sequence is highlighted in blue, point mutations introduced are shown in red. **(B)** Growth curves for wild type and *met* leader mutants in CDM with methionine ('+MET') and **(C)** without methionine ('-MET'). Representative data are shown of three (wild type, Ter_destab, ΔAntiTer&Ter, SC4) and two (SC2, SC5, SC7) independent experiments, respectively. The Ter_mutated_1 data are from a single experiment. **(D)** Total RNA isolated from *S. aureus* Newman and its isogenic *met* leader mutants grown in CDM with methionine ('+MET') or grown in CDM +MET, washed twice with PBS and then shifted in CDM without methionine ('-MET') for 2 hours was run on a denaturing 5 % PAA 7 M Urea gel and blotted onto a nylon membrane. Northern blot was hybridised with a *met* leader-specific probe and subsequently re-hybridised with a 5S rRNA-specific probe as loading control. **(E)** Total RNA isolated from *S. aureus* Newman and its isogenic *met* leader mutants as described in (D) was run on a 1.2 % denaturing agarose gel and blotted onto a nylon membrane. Northern blot was probed with *metE*-specific probe. Arrowheads mark 3'-*met* mRNA. Green asterisks (*) indicate 'ON' mutants, red hashtags (#) indicate 'OFF' mutants. For details see text. Re-hybridisation with a 16S rRNA-specific probe was used as loading control. Positions of 23S and 16S rRNA are marked by a black dot. Ter_mutated_1 is abbreviated 'Ter_mut_1'.

The *met* leader mutants Ter_mutated_2,3 and 4, generated to investigate RNase III cleavage requirements described in **section 3.2.5, page 38 f.**, were tested for their ability to activate *met* operon transcription under methionine-deprived conditions as well. Under methionine-rich conditions operon transcription did not occur, as in the wild type, but in the absence of methionine all Ter_mutated mutants were unable to activate operon transcription in contrast to the wild type bacteria (**Fig. 18**).

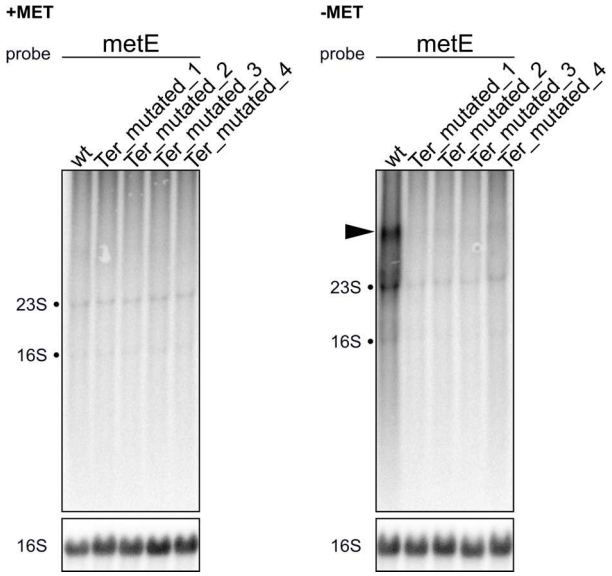

Figure 18. Ter_mutated *met* leader mutants are unable to activate *met* operon transcription under methionine-deprived conditions. Total RNA isolated from *S. aureus* Newman and its isogenic *met* leader mutants Ter_mutated_1, Ter_mutated_2, 3 and 4 grown in CDM with methionine ('+MET') or grown in CDM +MET, washed twice with PBS and then shifted in CDM without methionine ('-MET') for 2 hours was run on a 1.2 % denaturing agarose gel and blotted onto a nylon membrane. Northern blot was probed with *metE*-specific probe. Arrowheads mark 3'-*met* mRNA. Re-hybridisation with a 16S rRNA-specific probe was used as loading control. Positions of 23S and 16S rRNA are marked by a black dot.

3.4.1. Long-term behaviour of permanently 'ON' or 'OFF' *met* leader mutants

Methionine is essential for bacterial growth, the amino acid with the highest metabolic costs regarding ATP consumption and *S. aureus* has only limited capacities to re-use or re-direct excess methionine (Kaleta et al., 2013; Wencker and Ziebuhr, 2017). Therefore, either inhibition or stimulation of methionine *de novo* biosynthesis under methionine-low or -rich conditions, respectively could serve as a potential antimicrobial drug mechanism.

In a pilot experiment, growth and survival of two permanently 'OFF' mutants (SC4 and Ter_mutated_1) and two permanently ON *met* leader mutants (Ter_destab and ΔAntiTer&Ter) were investigated over a time course of 20 days in CDM with and without methionine.
SC4 and Ter_mutated_1 were chosen to investigate the effects of *de novo* methionine biosynthesis inhibition because SC4 has only two point mutations that were expected to be easily reverted to the wild type sequence and Ter_mutated_1 has 18 point mutations that were assumed to be difficult to re-mutate (**Figs. 10 A** and **17 A**). In a previous, unrelated experiment with SC4 and SC7, re-mutations occurred within a couple of days in both mutants (data not shown). Ter_destab and ΔAntiTer&Ter were chosen because they had shown the highest *met* mRNA transcription levels under methionine-rich conditions (**Fig. 17 E**).
Optical density (OD) was measured to determine the approximate cell numbers and the growth dynamics of the culture, the fraction of viable cells was ascertained by colony-forming unit (CFU) counting. Samples were taken at day 0, 1 (24 hours), 2 (48 hours), 4, 8, 12, 16 and 20.
The growth dynamics of Ter_destab and the ΔAntiTer&Ter were very similar to the wild type bacteria under methionine-rich and -deprived conditions (**Fig. 19 A&B**). In CDM with methionine bacteria entered stationary growth phase within the first 24 hours, in CDM without methionine bacteria reached the stationary growth phase during the second day of incubation. The highest numbers of CFU (CFU_{max}) were present in the cultures after 48 hours, except for ΔAntiTer&Ter +MET, where CFU was highest after 24 hours already. Overall, CFU_{max} appeared to be higher in CDM –MET, with values between $3x10^9$ and $4x10^9$ CFU/ml, than in CDM +MET with $2\ x10^8$ to $8x10^8$ CFU/ml only. However, these data need to be evaluated cautiously, because this experiment has been only performed once by now.

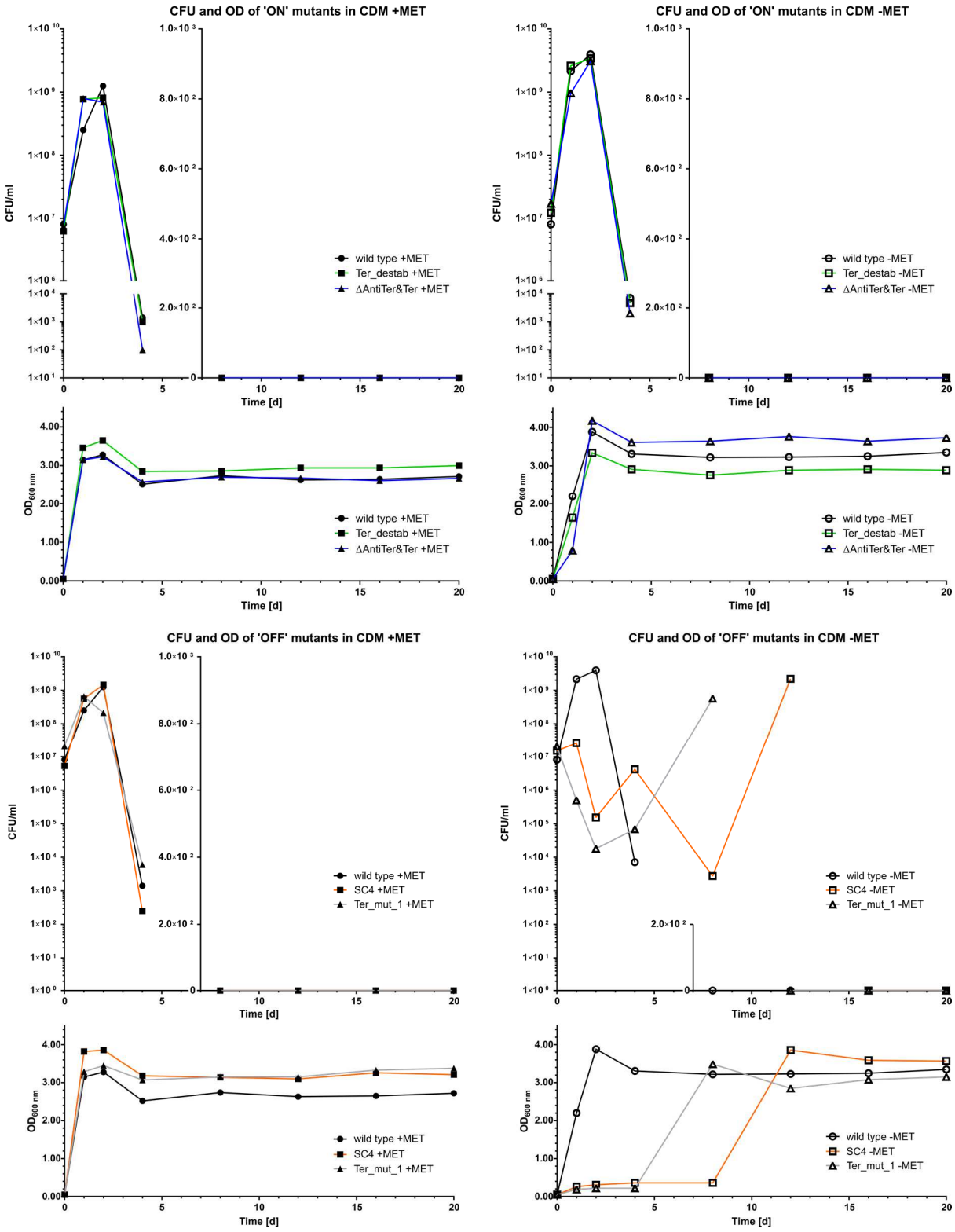

Figure 19. *See next page*

Figure 19. Long-term behaviour of *met* leader 'ON' and 'OFF' mutants under methionine-rich and -deprived conditions. *S. aureus* Newman ('wild type') and its isogenic *met* leader mutants Ter_destab, ΔAntiTer&Ter, SC4 and Ter_mutated_1 were grown in CDM with ('+MET') and without ('-MET') methionine for 20 days. CFU/ml and OD_{600nm} were determined at day 0, 1, 2 and 4, then every 4 days until day 20. CFU/ml values are displayed on a logarithmic scale for all values > 0 and on a linear scale for all values = 0. **(A)** CFU and OD of the wild type and *met* leader mutants with permanently active *met* operon transcription ('ON'), Ter_destab and ΔAntiTer&Ter, in CDM with methionine. **(B)** as (A) in CDM without methionine. **(C)** CFU and OD of the wild type and *met* leader mutants with 'blocked' *met* operon transcription ('OFF'), SC4 and Ter_mutated_1, in CDM with methionine. **(D)** as (C) in CDM without methionine. Data were obtained from a single experiment. Ter_mutated_1 is abbreviated 'Ter_mut_1'.

Between day 2 and 4 the ODs only dropped slightly, but the CFU decreased dramatically to values between $1x10^3$ and $7x10^3$ CFU/ml, for the ΔAntiTer&Ter strain grown in CDM +MET CFU/ml even decreased to $1x10^2$. From day 4 on ODs remained constant, but after day 8 no viable bacteria were present in the cultures.

The growth behaviour of the SC4 and the Ter_mutated_1 strains was very similar to the wild type bacteria under methionine-rich conditions, bacteria entered the stationary growth phase within the first 24 hours (**Fig. 19 C**). The highest numbers of CFU were present in the SC4 +MET culture after 48 hours as in the wild type and the Ter_destab culture, in the Ter_mutated_1 +MET culture CFU were highest already after 24 hours.

Under methionine-deprived conditions Ter_mutated_1 and SC4 did not show any significant growth for 4 and 8 days, respectively (**Fig. 19 D**). The OD increased from 0.05 to around 0.2 within the first 24 hours. The OD of the Ter_mutated_1 culture remained constant until day 4, OD of SC4 slightly increased to OD 0.36 until day 8. However, in the Ter_mutated_1 culture the CFU dropped already after 48 hours from around $1x10^7$ CFU/ml at day 0 to $1.8x10^4$ CFU/ml and $7x10^4$ CFU/ml at day 4. At day 8 CFU_{max} had been reached with about $6x10^8$ CFU/ml and OD_{max} of 3.5, at day 12 no viable cells were present in the culture, OD slightly dropped to 2.85 and remained constant until day 20. In the SC4 culture the CFU remained constant at around $1x10^7$ CFU/ml until day 4, but at day 8 had dramatically dropped to $2.75x10^3$ CFU/ml. At day 12 CFU_{max} had been reached with $2.2x10^9$ CFU/ml and OD_{max} of 3.86, at day 16 no viable cells were present, OD slightly dropped to 3.6 and remained constant until day 20.

Several colonies of day 2 and day 4 samples of SC4 -MET and Ter_mutated_1 -MET appeared smaller than the average colony detected in the other samples. This effect disappeared in the day 8 sample of Ter_mutated_1, when exponential growth had taken place and the culture reached OD_{max} of 3.5. This small colony phenotype had disappeared for SC4 in the day 12 sample after onset of exponential growth between day 8 and 12 (**Fig. A6**).

Onset of growth in the SC4 and Ter_mutated_1 -MET cultures after 4 and 8 days, respectively, indicated the occurrence of re-mutations or adaptive mutations to activate the *met* operon under methionine-deprived conditions. Therefore, the *met* leader region was investigated by sequencing of two colonies, each, from the CFU assay plates of day 0, 8 and 12 for SC4 and day 0, 2, 4 and 8 for Ter_mutated_1. For Ter_mutated_1 the additional time point of day 2 was chosen because gradual re-mutating to the wild type *met* leader sequence might have had occurred.

Sequencing results for the day 0 samples verified the presence of the wanted mutations (GG362,363CC in SC4 and 18 point-mutations in Terminator stem region of Ter_mutated_1). The two SC4 colonies of day 8 both had a 21 nt-deletion within the Antiterminator/Terminator region at position 364/365 (nt 364 and 386 were adjacent then), the same deletion was found in the two colonies of day 12 (**Fig. A7**). The Ter_mutated_1 colonies of day 2 and 4 did not show any changes in the nucleotide sequence of the *met* leader, both colonies of day 8 had a G to U mutation at position 398 of the *met* leader, the 18 point-mutations were unaffected.

3.5. The *met* operon on protein level

The ultimate purpose of gene regulation is the delicate adjustment of protein levels to the current requirements of the cell. Thus, after studying the *met* operon on a transcriptional level we next investigated the protein expression levels with mass spectrometry. We hypothesised that the varying transcript stabilities within the *met* operon have a direct influence on the enzyme levels: high levels of MetE and Mdh and low levels of MetI, C and F. However, not only the mRNA stability, but the translation initiation rate and the half-life time of the protein have an influence on the protein level as well. The fact that translation itself affects transcript stability further complicates matters (Dreyfus, 2009).

Briefly, for protein abundancy determination *S. aureus* Newman was grown in CDM without methionine to mid-exponential phase, culture was washed once and resuspended in CDM without methionine (to keep conditions consistent with half-life determination experiment, see below). t0 sample was taken and methionine was added (final concentration 10 mM, that is ten-times more than in normal CDM) to shut down *met* operon transcription. Samples were taken 15 min, 30 min, 1 h and 4 h after methionine addition, proteins were isolated and subjected to Liquid Chromatography tandem-Mass Spectrometry (LC–MS/MS). (Protein preparation and downstream procedures were carried out by our collaborators of the Becher group in Greifswald. The respective contributions are detailed in **section 6, page 188 f. 'Contributions by Others'**.) In parallel, samples for RNA isolation and subsequent Northern blot analyses were taken to monitor *met* operon transcription (data not shown).

MetE was, with 69 %, the most abundant protein of the *met* operon, Mdh and MetC accounted for 11 and 10 %, respectively, followed by MetI with 6 % and MetF with (only) 4 % (**Fig. 20 A**). Furthermore, half-life times of the *met* operon enzymes were determined (**Fig. 20 D**).

Briefly, for half-life time determination *S. aureus* Newman was grown in CDM without methionine supplemented with 'light' amino acids (^{12}C, ^{14}N) arginine and lysine to mid-exponential phase. Then tx sample was taken, culture washed once and resuspended in CDM without methionine supplemented with 'heavy' labelled amino acids arginine and lysine (^{13}C, ^{15}N) and *vice versa* (from 'heavy' to 'light' arginine and lysine). t0 sample was taken and methionine was added (final concentration 10 mM) to shut down *met* operon transcription. 15 min, 30 min, 1 h and 4 h after methionine addition samples were taken, proteins were isolated and subjected to LC–MS/MS (**Fig. 20 B**).

In parallel, samples for RNA isolation and subsequent Northern blot analyses were taken to monitor *met* operon transcription (**Fig. 20 C**). The addition of methionine to the medium did not fully shut down transcription during the first hour, but within four hours, transcript abundancy decreased from tx to t0 sample (**Fig. 20 C**). Mdh showed the longest half-life with 8.2 hours, followed by MetI with 7.2 hours, MetE had a half-life of 4.8 hours and MetC of 2.2 hours. The half-life time of MetF could not be determined (see discussion) (**Fig. 20 D**).

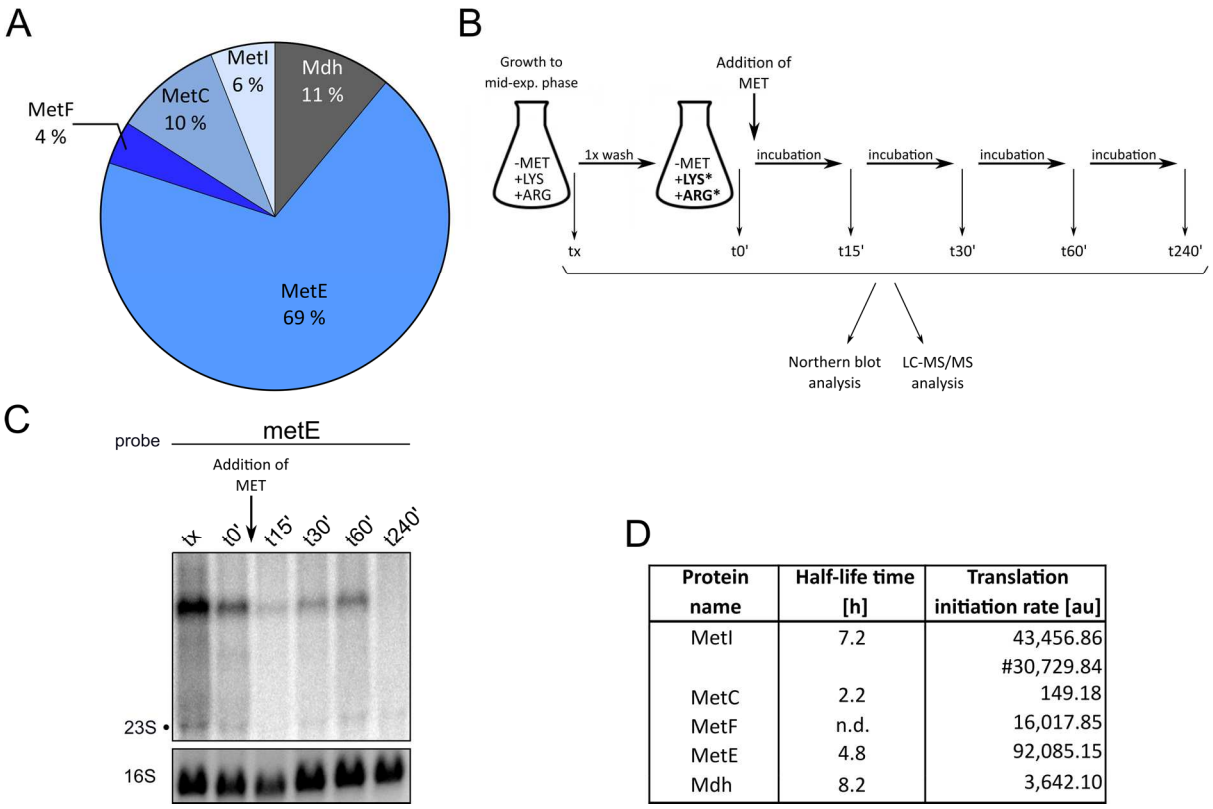

Protein name	Half-life time [h]	Translation initiation rate [au]
MetI	7.2	43,456.86
		#30,729.84
MetC	2.2	149.18
MetF	n.d.	16,017.85
MetE	4.8	92,085.15
Mdh	8.2	3,642.10

Figure 20. The *met* operon on protein level. (A) Relative abundancies of *met* operon enzymes, sum of MetI, C, F, E and Mdh equals 100 %. **(B)** Scheme of experimental procedure for sampling for half-life time determinations and corresponding transcript analysis, asterisks (*) indicate 'heavy' labelled amino acids lysine and arginine. **(C)** Total RNA isolated from *S. aureus* grown as detailed in text and scheme in (B) was run on a 1.2 % denaturing agarose gel and blotted onto a nylon membrane. Northern blot was probed with *metE*-specific probe. Arrow marks addition of methionine to a final concentration of 10 mM. 16S rRNA detected in Midorigreen-stained gel is shown as loading control. Position of 23S rRNA is marked by a black dot. **(D)** Half-life times of *met* operon enzymes determined experimentally in hours, n.d. not determined, and translation initiation rates (T.I.R.) in arbitrary units (au) determined with the RBS Calculator v2.0. Hashtag (#) indicates T.I.R. of *metI* predicted from *met* operon sequence without first 417 nt of *met* leader. T.I.R. in proportional scale from 0.001 to 100,000 au.

Subsequently, the translation initiation rates (T.I.R.) of the methionine biosynthesis operon genes have been determined by prediction, because the T.I.R. directly affects the synthesis rate and therewith has an influence on RNA stability. mRNA densely occupied by ribosomes is usually protected from degradation by RNases due to steric hindrance and masking of cleavage sites (Pedersen et al., 2011). The T.I.R. is an indicator for the strength of a ribosomal binding site (RBS). The higher the T.I.R., the stronger the RBS.

To determine the strength of the respective RBS of the *met* genes, we used the RBS Calculator v2.0 to predict the translation initiation rates (**Fig. 20 D**) (Espah Borujeni et al., 2014; Salis et al., 2009). T.I.R. were predicted on a proportional scale from 0.001 to 100,000 au (arbitrary units) for the input mRNA sequence (Salis, 2011). The full-length operon sequence including the TSS of the *met* leader to the end of the 3'-UTR and the operon sequence starting at nt 418 of the *met* leader have been used as input sequences. *metE* had the highest T.I.R. with 92,085.15 au, followed by *metI* with 43,456.86 au, *metF* with 16,017.85 au and *mdh* with 3,642.1 au. The predicted T.I.R. for *metC* was very low with only 149.18 au. Without taking transcript stability into account, two times more protein would be expressed from *metE* RBS than from *metI* RBS, six times more than from *metF* RBS and 25 times more than from *mdh* RBS. According to the prediction, > 600 times more MetE than MetC would be synthesised. Interestingly, the T.I.R. decreases (43,456.86 au vs. 30,729.84 au), when the first 417 nt of the *met* leader sequence were omitted for prediction of *metI* T.I.R. reflecting conditions *in vivo* after RNase III cleavage. Based on these predictions, *metE* has the strongest RBS, *metC* the weakest.

3.6. Discussion *met* leader and *met* operon

3.6.1. The *met* leader possesses all structural characteristics of a T-box riboswitch albeit length of Terminator stem is above average

The methionyl-tRNA specific T-box riboswitch (‘*met* leader’) upstream of the methionine biosynthesis operon in staphylococci has been identified in a screening of the staphylococcal genome for non-coding RNAs in intergenic regions about a decade ago (Schoenfelder, 2006). Further investigations revealed the *met* leader to be the centrepiece of a hierarchical network controlling *met* operon expression. The *met* leader turned out to be a highly transcribed (under methionine-deprived conditions), but rapidly degraded RNA species with first indications for involvement of RNase J and RNase III (Schoenfelder, 2011; Schoenfelder et al., 2013).

The secondary structure of the *met* leader regulating the methionine biosynthesis operon in *S. aureus* was determined by employing in-line probing (**Fig. 7**). All highly conserved structural elements could be identified in the *met* leader (Kink-turn, Specifier Loop, Stem I platform and hinge in Stem I, Stem IIA/B pseudoknot, Stem III and Terminator stem). The Stem II appeared to be non-canonical in the *met* leader due to its small size and absence of an S-turn motif.

Kink-turn

The Kink-turn has been shown to be important for antitermination (Rollins et al., 1997; Winkler et al., 2001). It is suggested to define the relative orientation of Stem I to the rest of the riboswitch to enable simultaneous binding of the uncharged tRNA with Stem I and the T-box bulge. The asymmetry (5+2 or 6+3) of the loop in combination with the surrounding helices induces the kinking of Stem I by ~120° (Kreuzer and Henkin, 2018). The GA motif, incomplete in the *S. aureus met* leader (GA dinucleotide absent in the 5’ part of the loop), is conserved in the majority of T-box riboswitches. However, Winkler et al. found the GA motif to be very rare in leaders from *Staphylococcus* and *Streptococcus*, in contrast to the Bacillus-Clostridium group (GA motif present in 94 % of leaders) (Winkler et al., 2001). Mutational studies of the *B. subtilis tyrS* GA motif suggested it to be essential for antitermination (Winkler et al., 2001). Some of the mutations might have disrupted the asymmetric loop due to alternative base pairings, though. Therefore, the requirement of the GA motif *per se* for the Kink-turn function is still questionable.

Specifier Loop

The interaction of the two regions of the Specifier Loop (5'-AGUA-3' (nt 44-47) and 5'-GAA-3' (nt 110-112)) causes a distortion in the RNA backbone, an S-turn, that forces the AUG Specifier codon to rotate into the minor groove (Kreuzer and Henkin, 2018). The rotation of the Specifier codon increases its accessibility for the tRNA anticodon and enables accommodation of large post-transcriptional modifications of the tRNA at position 37 of the anticodon (Chang and Nikonowicz, 2013; Kreuzer and Henkin, 2018; Wang et al., 2010).

Stem I platform

The platform created by the AG Bulge and the apical loop of Stem I interacts with the tRNA elbow. The tRNA elbow is formed by tertiary interactions of the D- and T-loop residues of the tRNA in its L-shape conformation. The interaction of the elbow with the docking platform of Stem I has been shown to be crucial for tRNA binding and subsequent antitermination. However, it is still unclear, if the platform-tRNA elbow interaction occurs first and therefore acts as a ruler to enable the interaction of the tRNA anticodon with the Specifier codon, or if the codon-anticodon interaction takes place first and then proper folding of the tRNA is monitored by the platform-tRNA elbow interaction. Currently, the first scenario is favoured, because the platform of Stem I is transcribed prior to the Specifier codon and is therefore available earlier for tRNA binding (Kreuzer and Henkin, 2018; Zhang and Ferré-DAmaré, 2016). Interactions similar to the Stem I platform interaction with the highly conserved elbow region of the tRNA were identified in RNase P and the ribosome (Chetnani and Mondragón, 2017; Korostelev et al., 2006; Reiter et al., 2010).

Hinge

The hinge, located in the middle of Stem I, is also a structural element vital for T-box riboswitch function. Deletion of the 2 nt-bulge in the *glyQS* riboswitch (of *Oceanobacillus iheyensis*) led to reduced tRNA binding to Stem I, indicating the importance of the hinge to proper orientate the Stem I platform and Specifier loop for interactions with the tRNA (Zhang and Ferré-D'Amaré, 2013).

Stem II and Stem IIA/B pseudoknot

The exact function of Stem II and Stem IIA/B pseudoknot is still unclear. *glyQS* riboswitches lack the Stem II and IIA/B domains (Sherwood et al., 2018). In the *B. subtilis trysS* T-box riboswitch, these motifs have been shown to be required for efficient antitermination (Rollins et al., 1997).

A class of T-box riboswitches exists that lack the Stem I platform for tRNA elbow interaction, the so-called ultrashort (US) Stem I variants, where the Specifier codon is located in the terminal loop of Stem I (Sherwood et al., 2018). In these riboswitches, the Stem II and the Stem II A/B pseudoknot domains have been shown to interact with the T- and D- arm of the tRNA, respectively.

The importance of the non-canonical Stem II and the Stem II A/B pseudoknot for proper *met* leader function (= antitermination) would need to be investigated by sequential deletions.

Stem III

Stem III is involved in Antiterminator stabilisation and together with its immediate flanking single-stranded regions, Stem III forms a crucial part of the tRNA 3'-end binding pocket and therefore plays a pivotal role in aminoacylation sensing (Battaglia et al., 2019; Li et al., 2019).

Unusual length of met leader – linker region, Stems L I-L III

The *met* leader is, with its 440 nt, exceptionally long due to its linker region of 226 nt comprising Stem II, Stem II A/B pseudoknot and Stem III and the insertion containing Stems L I to L III (**Fig. 7 B**). Stems L I, II and III are absent in other T-box riboswitches analysed to date. This insertion poses a potential additional interaction surface for the tRNA. To investigate the influence of the respective linker region domains on tRNA binding, sequential deletion of these domains could be performed. If some of these domains turn out to be crucial for antitermination, they would be prime drug target regions for a staphylococcus-specific compound.

Another aspect of the long linker region might be simply extended transcription time between Stem I and the Antiterminator sequence. The tRNA needs to be positioned properly before interaction of the free 3' CCA end with the T-box sequence can occur. Therefore, increased transcription time could facilitate this positioning. With a transcription elongation rate of 40-50 nt/sec the 37 nt-long linker region of the *B. subtilis glyQS* T-box riboswitch would be transcribed in 0.75-1 second, the 226 nt-long *met* leader linker of *S. aureus* would require 4.5-6 seconds (Mosteller and Yanofsky, 1970; Vogel and Jensen, 1994). In this respect, it would be interesting as well to examine the *met* leader for internal RNA polymerase pausing sites. In *B. subtilis glyQS*, a major pausing site has been identified in Stem III that might be crucial for efficient antitermination. Variations in pausing time affected the requirements for the time point of tRNA addition for efficient read-through *in vitro* (Grundy & Henkin 2004).

Deletion of the complete linker region to investigate the influence of the transcription duration and/or potential pausing sites on effective antitermination might lead to misleading results, if

domains of the linker region by themselves already have an influence (see above). Experiments should be performed in parallel with sequential domain deletions and, e.g. a scrambled linker region sequence.

Only two of the 765 T-box riboswitches listed by Vitreschak et al. possess linker regions predicted to be longer than that of the *S. aureus met* leader (226 nt): The LYS-T-boxes upstream of *lysS* and *metS2* in *Clostridium beijernicki* with 262 and 258 nt, respectively. Overall, some T-box classes seem to have shorter linker regions on average than others. GLY T-box linker regions are generally shorter due to absence of Stem II and Stem II A/B pseudoknot (Vitreschak et al., 2008).

In-line probing was performed with *met* leader RNA in the 'OFF'/Terminator state (*i.e.* without tRNA ligand) because previous studies with the *met* leader had already shown that proper interaction of the *met* leader with the uncharged tRNA only occurred, when the *met* leader was transcribed *in vitro* in the presence of the tRNA ('live *in vitro* transcription'). Denaturation with ensuing re-naturation of the *met* leader in presence of the tRNA did not result in *met* leader tRNA binding and Antiterminator formation (Schoenfelder et al. (2013) and personal communication Sonja Schoenfelder, Würzburg). This is in accordance with the induced fit mechanism that has been proposed for the T-box riboswitch tRNA interaction (Zhang and Ferré-D'Amaré, 2015). Furthermore, the *met* leader tRNA interaction is postulated to be only transient because (i) the interaction is only required to stabilise the Antiterminator conformation long enough for the RNA polymerase to pass the Terminator sequence and (ii) permanently bound tRNA would not be available for charging with the amino acid and subsequently for translation (Grundy and Henkin, 2004; Suddala and Zhang, 2019; Suddala et al., 2018; Zhang et al., 2018). Therefore, in-line probing is not suitable to capture transient conformations and interactions as the incubation time is 40 hours and the sample preparation does not allow preservation of *met* leader tRNA interactions occurring during 'live *in vitro* transcription'. However, this method is well suited for secondary structure determinations of stable conformations as the *met* leader in its 'OFF'-state.

A combination of chemical and enzymatic probing could be used to back the structural data obtained with the in-line probing (Ziehler and Engelke, 2000). This method might be even able to detect the transient *met* leader tRNA interactions. However, capturing these interactions would require to *in vitro* transcribe the *met* leader without the 3' part of the Terminator sequence to circumvent the problem with the induced fit as described previously (Chetnani and Mondragón, 2017; Suddala et al., 2018). The *met* leader Terminator stem proved to be a

thermodynamically highly stable structure (ΔG -32.40 kcal/mol) in the course of the in-line probing experiments as even five minutes denaturation at 95° C with immediate addition of RNase T1 on ice did not enable cleavage at the guanosine residues within the Terminator stem sequence (not shown). Only in the Ter_destab *met* leader mutant, unable to form the Terminator stem, RNase T1 cleavage occurred (see **Fig. 7 A gel #5** and **Fig. 10 C**). The *met* leader RNA without the 3' Terminator sequence should properly fold into the antiterminator conformation in presence of the tRNA after denaturation.

Alternatively, the structure of the *met* leader:$tRNA_i$ complex could be characterised employing SAXS (small-angle X-ray scattering). Therefore, *in vitro* co-transcription of the *met* leader (without the 3' Terminator sequence) with the initiator tRNA followed by purification of the natively assembled complex by size exclusion chromatography (SEC) to obtain a homogeneous complex would be required (Chetnani and Mondragón, 2017).

3D structural models of T-box riboswitches

All available 3D structural information in the literature are based on crystal, NMR (nuclear magnetic resonance) and cryo-EM (cryogenic electron microscopy) studies of *glyQS, tyrS* and *ileS* T-box riboswitches (Battaglia et al., 2019; Chang and Nikonowicz, 2013; Grigg and Ke, 2013; Li et al., 2019; Wang et al., 2010; Zhang and Ferré-D'Amaré, 2013). To date, no such data exist for a MET-T-box riboswitch, but the high conservation of structural motifs among T-box riboswitches allows to assume similar tertiary structures in the *met* leader.

As the crystal structure studies revealed, the 3D structure of the T-box riboswitches is important as well to understand the interactions of the riboswitch with its cognate tRNA, especially in the light of utilisation as a drug target (Grigg and Ke, 2013; Zhang and Ferré-D'Amaré, 2013). Thorough understanding of the riboswitch structure and interactions with the tRNA are a pre-requisite for rational drug design.

Terminator stem: above-average length and RNase III cleavage target site

Not only the total length of the *met* leader is exceptional, the length of the Terminator stem is with its 23 bp above average as well among MET-T-boxes (**Tab. 1**) and T-boxes in general (Vitreschak et al., 2008). This length in combination with the GC-rich middle region renders it an RNase III-target.

Commonly, riboswitches are either not cleaved off from the downstream RNA or rather cleaved upstream of the Terminator stem by RNase Y in the case of SAM-binding and T-box

riboswitches (Condon et al., 1996; Khemici et al., 2015; Seif and Altman, 2008; Shahbabian et al., 2009). The *met* leader cleavage at position 388^389 by RNase III was demonstrated by analyses of RNase III- and target-mutants and cRACE in this work (**Figs. 9** and **10**, **Tab. 2**). Cleavage at this position did no longer occur in *met* leader mutants either lacking the Terminator structure (Ter_destab and ΔAntiTer&Ter) or containing mutations likely impairing recognition and cleavage by RNase III (Ter_mutated_1) and cleavage was strongly reduced in an RNase III mutant (Δ*rnc*) (that might have some residual RNase III activity). Residues of the cleavage site itself and immediately adjacent are not essential for recognition or activity of RNase III *in vivo* as proceeding processing of the *met* leader RNA in the Ter_mutated_2, 3 and 4 mutants demonstrates (**Fig. 11 B**). Albeit mutations that lead to a weaker base pairing (U:G instead of U:A at position 389:415) within the Terminator helix right next to the cleavage site might negatively affect RNase III cleavage (see **Fig. 11 A**). This is suggested by Northern blot analyses, where stronger bands of the +/- 440 nt *met* leader RNA in the Ter_mutated_3 mutant occurred compared to the wild type and the Ter_mutated_2 and 4 mutants. Especially under methionine-rich conditions, the increase in signal intensity of the +/-440 nt bands and at the same time decrease in the 390 nt band becomes apparent indicating a reduced cleavage of the *met* leader by RNase III in the Ter_mutated_3 mutant (see **Fig. 11 B**).

None of the Ter_mutated *met* leader mutants (1-4) is antitermination-competent due to the introduced mutations that apparently affect Antiterminator formation; *met* operon transcription does not take place under methionine-deprived conditions (see **Fig. 18**). Strikingly, a single point mutation in the Antiterminator sequence outside the T-box bulge (C387G) seemed to be sufficient to impair proper Antiterminator formation and therewith operon transcription (**Fig. A3**, see **Figs. 11 A** and **18**). This fact emphasises the fine-tuned nature of the riboswitch system. It is a disadvantage when generating mutants to investigate *met* leader processing, but might be an advantage when exploiting the system as a drug target (the system can be easily disabled). Cleavage within the Terminator stem generates an mRNA molecule prone to rapid degradation. This might represent an additional level of regulation of the *met* operon genes because the short half-life of the *metI* transcript directly influences expression levels. A clean RNase III mutant (the used conditional Δ*rnc* mutant likely showed some residual RNase III activity (see **Fig. 9 A&C**)) and/or an RNase III-cleavage deficient *met* leader mutant that is at the same time still antitermination-competent should posses a *metI* mRNA with increased stability due to the still attached *met* leader. However, additional endonucleolytic cleavage events within *metI* likely occur, that would destabilise the *metI* mRNA in the RNase III or cleavage deficient mutant (see below).

Recycling and regulation: the reason for RNase III cleavage within the Terminator stem?

The removal of the Terminator stem might fulfil two functions at the same time: (i) Rapid recycling of nucleotides of *met* leader RNA (no protective structure at 3'-end of *met* leader left that might inhibit, e.g. PNPase) and (ii) regulation of *met* operon expression: prevention of too high protein levels due to long transcript half-life (removal of protective structure 5' of *metI* mRNA).

Furthermore, it was tempting to speculate that the length of the Terminator stem directly influences the transcription termination efficacy. Yet, Carafa et al. showed that not only the length of the stem, but the G-C and A-T distribution within the stem, the terminal loop size and the length of the succeeding U-stretch have an influence on termination efficacy as well (Carafa et al., 1990). Own calculations revealed that the *met* leader and the only 11 bp-long Terminator of the *tyrS* leader of *B. subtilis* would terminate transcription with almost equal efficacy. Hence, the *met* leader does not have higher termination rates and therewith tighter gene regulation due to the extended Terminator stem.

3.6.2. Secondary function of the processed *met* leader?

A secondary or moonlighting function of the *met* leader RNA has been suggested due to its high abundance and unusual RNase III-processing. The short half-life (see **Figs. 8 B** and **9 B&C**) speaks against this hypothesis. To function, e.g. as a small RNA (sRNA) the *met* leader would need sufficient time to bind to its target mRNA. Destabilisation of its target mRNA by RNase III after duplex formation would result in a defined cleavage product of the *met* leader. No such intermediate was detected by Northern blotting or was apparent in available transcriptome data (unpublished data, personal communication Gabriella Marincola, Würzburg).

The intaRNA web application was used to search for potential interactions of the processed *met* leader with mRNAs of *S. aureus* strain Newman (Busch et al., 2008; Mann et al., 2017). An interesting hit is the methionine ABC transporter ATP-binding protein (NWMN_RS02410) that would warrant further investigation.

Though, the high *met* leader abundancies in combination with its rapid degradation rather might be simply a mechanism to keep the opportunity for antitermination high (constant monitoring of methionine levels by continuous basal *met* leader transcription) and then to recycle nucleotides quickly either after termination or after operon activation.

3.6.3. Conservation of *met* leader among staphylococci

The *met* leader sequence is highly conserved among staphylococci. Only the region between the 3'-end of Stem L I, according to the structure in *S. aureus* (**Fig. 7**) and the 5'-end of Stem L III, and the distal region of Stem L III are less well conserved on sequence level (**Fig. A4 A**). This might indicate that at least the sequence of these regions is dispensable for proper riboswitch function as evolution has allowed for mutations there. The *met* leader length varies between 378 nt in *S. sciuri* and 482 nt in *S. capitis*, in most species length ranges around 440 nt as in *S. aureus* (**Fig. A4 B**).

3.6.4. *met* operon transcription

Interestingly, transcription of the *met* operon is quickly turned on after methionine-deprivation (< 30 min), but only slowly (> 1 hour < 4 hours) shut down after addition of methionine (see **Fig. 20 C**), (Schoenfelder et al., 2013). An experiment to narrow down the window of *met* operon transcription shut down should be undertaken. Amino acid starvation has been shown to trigger rapid tRNA degradation in *E. coli* independent of its charging status (Sørensen et al., 2018; Svenningsen et al., 2017). Thus, upon sudden amino acid deprivation the remaining pool of tRNAs becomes quickly uncharged that would explain the fast *met* leader activation. All tRNA pools are affected and this degradation mechanism is thought to decrease translation error frequencies under starvation of a certain amino acid by reducing levels of competing cognate tRNAs. The increase in proper amino acid incorporation would lead to a quicker rise in uncharged tRNAs of the amino acid the bacterium is starved for. T-box riboswitch activation depends on the ratio of uncharged to charged tRNAs and not on absolute levels of uncharged tRNAs (Kreuzer and Henkin, 2018).

3.6.5. Stability of *met* operon mRNA varies over length of transcript

The *met* mRNA turned out to possess distinct stabilities with a very short half-life of the 5'-region and a long half-life of the 3'-transcript-end (see **Fig. 12 B**). The stable 3' region comprises the 3' portion of *metF*, *metE*, *mdh* and the 3'-UTR, determined with probe walking and 5' RACE (**Fig. 12 C&D**). After read-through and immediate separation of the *met* leader RNA (nt 1- 388) from the mRNA, the operon mRNA is present as a whole (~7.2 kb) only for

a short time. The results obtained with a *metI*-specific probe together with the 5' RACE results obtained with primer FW200 (binding within *metI*) suggest the *metI* mRNA to be cleaved off from the mRNA and to exist as a separate entity for less than 30 seconds (see **Fig. 12 B**). RNase J was identified to drive the rapid degradation of the 5'-*metI* mRNA (see **Fig. 14 B**). Cloning of the whole *met* mRNA sequence into the plasmid was unsuccessful (confer **section 3.3.2, page 44 ff.**) To investigate the rest of the *met* mRNA for RNase J cleavage, cloning of longer *met* mRNA fragments into the plasmid would be required.

The absence of clear processing sites, e.g. within the *metI* or *metF* mRNA (confer 5' RACE results described in **section 3.3.1, page 43 f.**), indicates exonucleolytic degradation in 5' to 3' direction preceded by an endonucleolytic cleavage. Neither RNase III nor RNase Y executes endonucleolytic cuts within the *met* mRNA as demonstrated in experiments with Δ*rnc* and Δ*rny* mutants (see **Figs. 15 A and 16 A**). The bifunctional RNase J is likely responsible for the endonucleolytic cuts within the *met* mRNA as well. If RNase J cleaves the *met* mRNA endonucleolytically, a stable transcript consisting of the *met* leader from nt 418 on until the 3'-UTR (~7.2 kb) should be well detectable in an Δ*rnjA* mutant. If other RNases cleave the *met* mRNA endonucleolytically, smaller, stable transcripts should be present in an Δ*rnjA* mutant due to the lacking 5'-3' exonucleolytic activities.

Which factors drive the differential decay of the met operon mRNA?

Dar and Sorek identified hairpin structures 3' of stable transcript regions that act as protective structures against 3'-5' PNPase exonucleolytic activity and RNase E cleavage events just upstream of protective structures that initiate 3'-5' degradation in polycistronic mRNAs of *E. coli* (Dar and Sorek, 2018). Note, that in contrast to *B. subtilis* and *S. aureus*, no 5'-3' exonuclease is known *in E. coli* to date. Due to the 5'-3' exonuclease activity of RNase J, protective structures 5' of the stable transcript region could cause the differential decay of the *met* mRNA as well. However, no clear protective structures could be identified in the *metF* mRNA (1,842 nts) upstream of the stable, around 800 nt-long, 3'-region that comprises the 5,10-methylene-tetrahydrofolate reductase domain (nt 969-1806).

Next to stabilising or protective structures, the ribosome density has been shown to have a direct, positive influence on mRNA stability presumably by blocking RNase cleavage sites (Deana and Belasco, 2005; Iost and Dreyfus, 1995; Lost and Dreyfus, 1994; Yarchuk et al., 1991). Therefore, I hypothesised that the reductase region of *metF* might be translated as an independent open reading frame (ORF). However, no such protein could be identified in the

proteome experiment (personal communication Sandra Maaß, Greifswald). Another aspect that can affect ribosome occupancy is the codon optimality ('codon optimality' refers to the non-uniform decoding rate of each of the 61 codons by the ribosome) (Hanson and Coller, 2018). Rare codons are translated slower (Boël et al., 2016). A stretch of rare codons would cause ribosomes to almost halt at these positions, forming a physical obstacle for the RNase J to proceed 5' -3' exonucleolytic degradation that might explain the range of 5'-ends within *metF* mRNA. Investigating *metF* for regions of rare codons using the graphical codon usage analyser 2.0 (Fuhrmann et al., 2004) revealed that indeed the sequence just upstream of the region, where 29 % of 5'-ends were detected with 5' RACE (see **Fig. 12 D**), contains a stretch of rare codons (**Fig. A5**). A ribosome protects around 30 nucleotides of an mRNA from ribonuclease activity (Steitz, 1969). The probability that nucleotides are protected from degradation by the ribosome should be higher in regions with rare codons due to the extended time the ribosome covers these and downstream nucleotides. The region of *metF* containing the rare codon stretch could be mutated to non-rare codons to investigate, if indeed 'slow ribosomes' confer protection against ribonucleases.

A rather simple experiment to investigate the influence of translation on the *met* mRNA stability would be the inhibition of translation by chloramphenicol with an ensuing rifampicin assay to monitor the transcript stability. If ribosome density is a major contributor to the *metE* mRNA stability, inhibition of translation should lead to a dramatic decrease in *metE* mRNA half-life. A higher ribosome occupancy in the *metE* region than in the *metIC* mRNA region would explain the higher transcript stability and the higher protein levels.

In addition to RNase Y and RNase III, five other RNases were tested for their activity on the *met* mRNA by investigating the transcript in the respective RNase mutants. Absence of RNase III did not have an influence on the 3'-*met* mRNA stability or the nature of the transcript (*i.e.* length) (see **Fig. 16 A**).
Of the tested NTML RNase mutants, Δ*mrnc* (Mini-RNase III) and Δ*pnpA* (PNPase) showed slightly elevated 3'-*met* mRNA levels, but to make a final assertion on the influence of these RNases on the mRNA stability, rifampicin assays would be required (see **Fig. 16 C**).
Absence of RNase Y led to massively increased 3'-*met* RNA transcript levels (see **Fig. 15 A**). In general, transcript levels depend on the ratio of synthesis to degradation rate. As the transcript stability is the same for mutant and wild type (see **Fig. 15 A**), an increased transcription of the *met* locus would be the simplest explanation for the high transcript levels,

but transcription of the *met* leader was not increased in the RNase Y mutant (see **Figs. 9 A** and **15 B**). Per one molecule *met* leader one molecule *met* mRNA is transcribed (read-through after *met* leader activation). No internal promoters and resulting transcript species have been identified in the *met* operon of Δ*rny* in transcriptome data that could explain the strongly increased 3'-*met* mRNA levels (unpublished data, personal communication Gabriella Marincola, Würzburg). Hence, elevated 3'-*met* mRNA transcript levels in the RNase Y mutant still remain inexplicable.

3.6.6. The *met* operon on protein level

A key question is the consequence of the varying transcript stabilities. Why is the 5'-mRNA highly unstable and the 3' region rather long-lived? It has been previously shown, that polycistronic mRNA can undergo differential RNA decay, leaving some genes within the operon more stable than others (Båga et al., 1988; Belasco et al., 1985; Dar and Sorek, 2018; Marincola et al., 2012; Newbury et al., 1987). These distinct transcript stabilities showed to have a direct influence on the respective protein expression levels. The protein required in higher quantities than the other proteins of the operon was encoded by the gene with the highest transcript stability (Newbury et al., 1987).

The *met* mRNA region comprising *metE* (and *mdh*) is most stable. Therefore, we hypothesised that protein levels of MetI, MetC and MetF are low compared to MetE (and Mdh). The proteome data obtained in this work confirmed the high abundance of MetE in *S. aureus* under methionine-deprived conditions (see **Fig. 20 A**). The cobalamin-independent methionine synthase encoded by *metE* has been described as 100 times less efficient in converting homocysteine to methionine than the cobalamin-dependent MetH (Figge, 2007; Rodionov et al., 2004). This 'sluggishness' might explain why MetE is required in large quantities and accounts for around 3 % of total soluble protein in *E. coli* under methionine-deprived conditions (Greene, 1996; Whitfield et al., 1970). The decrease of 3'-*met* mRNA transcript levels from tx to t0 might be due to (temporarily) reduced transcription rates upon washing and subsequent medium shifting of the bacteria (see **Fig. 20 C**). Although, no delay in growth was observed after shifting (data not shown).

In addition to the protein abundancies, the half-life times of the *met* operon enzymes were determined and the translation initiation rates (T.I.R.) were predicted, because not only the

transcript stability, but the enzyme stability and the expression rate have an impact on protein levels as well.

For MetE the data fit well together: a high T.I.R. in combination with a long transcript half-life and a rather stable protein (half-life: 4.8 hours), in comparison to the other *met* operon enzymes, resulted in high protein levels (69 %).

For Mdh the obtained data are coherent as well: a long protein half-life time (8.2 hours) in combination with a rather low T.I.R., but a high transcript stability can explain the protein abundancy of 11 %. Transcript stability might not be that much influenced by the ribosome occupancy here due to the *metE* transcript region present 5' of the *mdh* mRNA. For MetI the data fit moderately well because the relative low abundancy of MetI (6 %) despite the long protein half-life (7.2 hours) and the high T.I.R. could be explained by the low transcript stability. However, usually a well-translated mRNA should have a longer half-life as well.

For MetC the data are inconclusive because a short protein half-life (2.2 hours) in combination with an instable transcript and a very low T.I.R. should result in low protein levels. However, MetC was with 10 % more abundant than MetI and MetF of the operon enzymes (see **Figs. 12 B** and **20 A&D**).

For MetF T.I.R. is only six times less than for MetE, but the 5'-region of the transcript has a short half-life. MetF is the least abundant protein of the *met* operon enzymes, a half-life could not be determined because protein intensity values with the labelled amino acids 'A' used prior to washing (before label switch) increased instead of decreased over time. After the label switch, only labelled amino acids 'B' are available for protein synthesis because labelled amino acids 'A' have been removed by washing. Therefore, levels of proteins with labelled amino acids 'A' usually cannot increase after the label switch. However, this has been the case for MetF. A possible explanation could be the incorporation of labelled amino acids 'A' from degraded proteins within the cell after the label switch. Although, this should occur uniformly in all translated proteins.

Fuchs and colleagues determined the half-lives of MetE and Mdh and the molecules per cell of the *met* operon enzymes in *S. aureus* strain COL. The half-life of MetE was 35.21 hours, of Mdh 13.04 hours and molecules per cell were: MetI 7,918, MetC 7,590, MetF 3,078, MetE 18,051 and Mdh 8,170 (Fuchs et al., 2018; Michalik et al., 2012). Based on these data, MetI and Mdh account for about 18 % of *met* enzymes, MetC for 17 %, MetF for about 7 % and MetE for 40 %. Overall, these proportions are similar to the data presented in **section 3.5, page 61 ff.**. The reason for the deviating half-lives (MetE 4.8 vs. 35.21 hours and Mdh 8.2 vs. 13.04 hours) are most likely due to differences in the experimental set up. The half-lives determined

by Michalik et al. are based on data collected over 20 hours under glucose (and methionine) starvation (Michalik et al., 2012). Our data were collected over 4 hours which required stronger interpolation because our main goal has not been protein half-life determination. Aside from that, samples were taken after addition of 10 mM methionine.

The decreased protein half-lives in our experiment might indicate the existence of a feedback-regulation mechanism. The addition of methionine to the medium renders the *de novo* methionine synthesis unnecessary. The fact that *met* operon transcription is only slowly shut down after addition of methionine (see **Fig. 20 C**) seems to be counterintuitive. However, shutting down *met* operon transcription immediately after availability of methionine would bear the risk to run short of methionine soon after again. The provided levels of methionine (10 mM) seemed not to be sufficient to quickly reach levels of charged tRNAs able to shut down *met* operon transcription.

Feedback regulation on the protein level is an important aspect of methionine biosynthesis in the light of the idea to tackle *S. aureus* via exhaustion by massive methionine overproduction. The influence of methionine on the half-life of the *met* enzymes would need to be investigated in depth.

Ribosome profiling could be employed to investigate the ribosome density on the *met* mRNA and to confirm the predicted translation initiation sites within the *met* mRNA and possibly identify new ones (e.g. in the *metF* 3' region) (Brar and Weissman, 2015; Latif et al., 2015). The varying transcript stabilities of the *met* operon appear to be an additional level of methionine synthesis regulation due to their influence on protein expression levels.

3.6.7. Effect of methionine overproduction or prevention of methionine biosynthesis on fitness and virulence (riboswitch permanently 'ON' or 'OFF')

In a pilot experiment, the growth behaviour of *S. aureus* strains with dysregulated methionine *de novo* biosynthesis has been monitored over a period of 20 days in medium with and without methionine (see **section 3.4.1, page 57 ff.**). Two *met* leader mutants with a permanently activated ('ON') and two *met* leader mutants with a permanently terminating ('OFF') riboswitch were compared with the wild type regarding CFU and OD. Under methionine-rich conditions all strains behaved very similarly: the CFU/ml dramatically dropped from values around 1x 10^9 to 1x 10^2-10^3 at day 4 and no viable bacteria were present in the culture after 8 days, but the OD remained constant from day 4 until day 20 (see **Fig. 19 A&C**). This indicates that no cell lysis occurred. The similar behaviour of all five strains suggests no disadvantage for the 'ON' strains due to the constant methionine *de novo* synthesis under the tested conditions. However, it might be different under nutrient-rich conditions (e.g. TSB medium), in competition with wild type bacteria or in an *in vivo* situation (see below).

Under methionine-deprived conditions the 'ON' mutants behaved like the wild type and no viable bacteria were present at day 8. Overall, the maximum CFU/ml appeared to be slightly higher in medium without methionine, fitting well to the slightly higher OD_{max}. The 'OFF' mutants did not start growing until after 4 and 8 days, respectively (see **Fig. 19 B&D**). The decrease in CFU/ml and the occurrence of small colony variant-like phenotypes until emergence of mutations in the *met* leader sequence and onset of growth, suggests that the bacteria started starving or dying. The acquired mutations obviously allowed to activate methionine synthesis by bypassing the riboswitch system that subsequently enabled the bacteria to grow. In SC4, a 21 nt-long deletion, including the last 6 nt of the T-box sequence and the first 9 nt of the Terminator 5'-region, subsequently enabled bacterial growth (**Fig. A7**). The deletion putatively prevents formation of a stable Terminator stem, thus *met* operon transcription would be permanently active as in the Ter_destab *met* leader mutant.

A single G to U mutation at position 398 in the *met* leader of the Ter_mutated_1 mutant seems to be sufficient to finally enable growth under methionine-deprived conditions. This point mutation is predicted to allow formation of a stem that involves 24 nt of the 5'-Terminator region and might therefore prevent Terminator formation (**Fig. A7**).

Confirmation of these alternative structures by in-line probing and Northern blot analyses with RNA isolated from these mutated variants to verify *met* operon activation are required.

Overall, the *met* leader mutants with a permanent *met* operon transcription (Ter_destab and ΔAntiTer&Ter; 'ON') did not seem to have a fitness disadvantage. A premature drop in CFU under methionine-rich conditions did not occur that might be indicative of a fitness disadvantage. The mutants unable to turn on *met* operon transcription under methionine-deprived conditions (SC4 and Ter_mutated_1; 'OFF') survived long enough to acquire mutations subsequently enabling *met* operon transcription. This pilot experiment provided interesting findings and emphasised the importance of methionine. The lack of methionine appeared to be a strong selection pressure. Nevertheless, this long-term experiment needs to be repeated to obtain statistically reliable data and other conditions would need to be tested to make a final assertion, whether permanent *de novo* methionine biosynthesis or its inhibition has an influence on bacteria fitness.

3.6.8. The *met* leader as drug target

The results of the long-term growth experiment are rather discouraging with regard to the utilisation of the *met* leader as drug target. A compound preventing antitermination and therewith *met* operon transcription that binds to the, e.g. T-box region could easily become ineffective, if the target region of the *met* leader is spontaneously mutated or deleted (as in SC4*, see **Fig. A 7**). However, targeting several T-box riboswitches with the same drug simultaneously would minimise that risk, because i) many T-box regulated genes, such as the tRNA synthetases, are essential and ii) occurrence of adaptive mutations in a number of T-box riboswitches at the same time is highly unlikely. In *S. aureus*, eight tRNA-synthetases (*pheST*, *glyS*, *ileS*, *valS*, *serS*, *thrS*, *alaS*, *cysS*), the anthranilate and tryptophan synthesis components (*trpEGDCFBA*) and a serine O-acetyltransferase (*cysE*, in an operon with *cysS*) are predicted to be T-box regulated in addition to the *met* operon (Fuchs et al., 2018; Vitreschak et al., 2008).

The potential transition into a state of low metabolic activity (small colony variant-like phenotype) due to methionine-starvation after *met* leader inhibition needs to be thoroughly investigated. Low metabolic activity is undesirable because it complicates the treatment of a bacterial infection (Kahl et al., 2016; Lechner et al., 2012; Morikawa et al., 2010; Proctor et al., 2014).

Investigation of the adaptive mutations occurring in the SC4 and the Ter_mutated_1 *met* leader mutants will be of special interest to be able to estimate the range and type (number of

nucleotides, point mutations vs. deletions, possibly insertions?) of feasible mutations. In an experiment not presented in this thesis, the SC4 and SC7 mutants accomplished re-mutation to the wild type T-box sequence to enable growth under methionine-deprived conditions (two and one point mutations, respectively).

Competition experiments with the wild type and the 'ON' *met* leader mutants could give first indications, if constant methionine production under methionine-rich conditions leads to a fitness disadvantage. If this is the case, the wild type bacteria should outcompete the mutants.

In a next step, the larvae of the greater wax moth *Galleria mellonella* could be used as an infection model to determine, if virulence is attenuated in the *met* leader mutants ('ON' and 'OFF') compared to the wild type (Killiny, 2018). Based on these results, mutants that showed reduced fitness and virulence could be investigated in a cotton rat nasal colonisation and murine infection models for their ability to survive in the niche nose and to establish an infection, respectively (Kim et al., 2014; Kokai-Kun, 2008; Krismer et al., 2014; Trübe et al., 2019).

In a cotton rat nasal colonisation study an *S. aureus* Δ*metI* mutant had a reduced colonisation capacity compared to the wild type bacteria, implying that methionine *de novo* biosynthesis is important for *S. aureus* to sustain in the nose, well in agreement with the finding that methionine is only present at very low levels or is absent in the human nose (Krismer et al., 2014). DL-propargylglycine has been shown to efficiently inhibit the staphylococcal cystathionine-γ-synthase (MetI), therewith methionine biosynthesis and ultimately bacterial growth under methionine-deprived conditions (Johnston et al., 1979; Krismer et al., 2014). Unfortunately, DL-propargylglycine turned out to be unsuitable as a drug because it inhibits the human cystathionine-γ-lyase as well with detrimental global effects (Paul and Snyder, 2012). Nevertheless, inhibitors specific for bacterial or staphylococcal CGS could serve as decolonising agents, e.g. in the human nose, with DL-propargylglycine being the proof of concept.

Inhibition of the *met* operon expression by targeting the *met* leader would already act on the level of transcription and might be used for decolonisation as well.

In general, targeting the methionine biosynthesis has been already proven efficient in reducing virulence and weakening bacteria.

A serogroup B *Neisseria meningitidis* strain (leading cause of meningococcal meningitis) with deletion of the methionine synthase II gene (*metH*) and the sialyltransferase gene (*siaD*) required for capsule formation (Δ*siaD* Δ*metH*), was markedly attenuated in its capacity to cause bacteraemia in rodent models and had reduced ability to survive in a human whole-blood assay. Vaccination of adult mice with this live-attenuated strain led to the development of

bactericidal antibodies and conferred sterilising protection against a challenge with homologous live bacteria (Li et al., 2004). (Note that *metH* is the cobalamin-independent methionine synthase (EC 2.1.1.14) in *N. meningitidis*, homologous to *metE* in *S. aureus*. The cobalamin-dependent methionine synthase is not annotated in *N. meningitidis* (Kyoto Encyclopedia of Genes and Genomes (KEGG), https://www.kegg.jp/).)

3.6.9. Current status of drug target research on riboswitches

Riboswitches are meanwhile well recognised as promising antimicrobial drug targets as the discovery and characterisation of novel compounds demonstrate (Blount et al., 2015; Connelly et al., 2019; Mulhbacher et al., 2010b; Perkins et al., 2019; Rekand and Brenk, 2017; Wang et al., 2015).

The advantage of T-box riboswitches over metabolite-binding riboswitches as drug target is their redundant use to regulate multiple essential operons within a single cell (Frohlich et al., 2019).

A number of small molecules specifically targeting T-box riboswitches have been already synthesised (Anupam et al., 2008; Frohlich et al., 2019; Orac et al., 2011; Zhou et al., 2012). Tested triazole or oxazolidinone compounds either decreased antitermination by blocking the interaction of the tRNA with the T-box bulge or stimulated tRNA-independent antitermination *in vitro* (Anupam et al., 2008; Zhou et al., 2012). The substance PKZ18 and some of its analogues were shown to specifically inhibit growth of Gram-positive bacteria by inhibiting transcription of essential aminoacyl-synthetase (aaRS) genes. These aaRS are under T-box riboswitch-mediated control. Binding of the compounds to the Specifier Loop prevented interaction with the tRNA, therewith stimulating termination. Development of resistances was very rare most likely due to the broad target spectrum (e.g. 24 and 10 T-box regulated operons/genes in *Clostridioides difficile* (formerly *Clostridium difficile*) and *S. aureus* (see **section 3.6.8, page 78**), respectively (Frohlich et al., 2019)). The above described studies provide a proof of concept that T-box riboswitches are ‘druggable’ structures.

To date, only one bacterial aaRS inhibitor, mupirocin, that targets the bacterial isoleucyl-tRNA synthetase, is approved as antibiotic for human use, despite a wealth of aaRS inhibitor compounds available due to either off-target effects or high resistance rates (Francklyn and Mullen, 2019; Ho et al., 2018; Silvian et al., 1999). This substantiates that aaRS genes are a suitable drug target due to their essentiality, but that attacking on protein level is problematic

and interfering already at the level of transcription (riboswitch control) would be more favourable.

Besides the discovery of novel T-box-targeting small molecules, well-established protein synthesis inhibitor antibiotics were revisited and shown to interact with riboswitch RNA in addition to their interaction with the ribosome. Some antibiotics (linezolid and chloramphenicol) decreased antitermination of the *glyS* T-box riboswitch of *S. aureus* and some (e.g. neomycin B, tigecycline) stimulated read-through *in vitro* and *in vivo* by blocking and stabilising, respectively, Stem I:tRNA interactions (Stamatopoulou et al., 2017). These findings further encourage the exploitation of T-box riboswitches as drug targets (Deigan and Ferré-D'Amaré, 2011; Suddala and Zhang, 2019).

As a side note, recent studies revealed that antibiotic resistance genes themselves can be under ribo-regulation (Dar et al., 2016; Jia et al., 2013).

Exploiting the met leader as screening system for novel anti-T-box riboswitch compounds

The MET-T-box riboswitch upstream of the methionine biosynthesis genes in *S. aureus* ('*met* leader') could be exploited for an *in vivo* (bacteria) vector-based reporter system to screen for compounds targeting specifically the *met* leader or T-box riboswitches in general (depending on the site of action). A vector containing the *S. aureus* initiator tRNA gene and the *met* leader-*metI* sequence fused to a suicide gene (e.g. *sacB*) is transformed into *Corynebacterium glutamicum*. *C. glutamicum* is a Gram-positive bacterium of biological safety level 1 which is widely used in biotechnology. Except for one tRNA synthetase gene (*ileS*, whose regulation on the chromosome would need to be changed), gene expression in *C. glutamicum* does not undergo T-box riboswitch-mediated control. Accordingly, potential *met* leader targeting compounds will not inhibit growth of the engineered *C. glutamicum* host *per se*. Expression of the suicide gene *sacB* in the presence of sucrose leads to cell death (Jäger et al., 1992). In methionine-rich medium, the riboswitch is 'OFF', no *sacB* expression takes place and bacteria survive. Under methionine-free conditions *sacB* is expressed due to activation of the riboswitch, therefore bacteria die. In the presence of compounds inhibiting riboswitch activation, bacterial growth occurs in methionine-free medium as well. This screening method would allow to identify compounds exclusively targeting the riboswitch.

3.7. Mdh (metal-dependent hydrolase): the unknown of the *met* operon

The *met* operon is bioinformatically predicted to contain an additional ORF with a gene product of yet unknown function at its 3'-end. The gene is annotated as a metal-dependent hydrolase (*mdh*) and its start codon is predicted to be located 42 nt downstream of the *metE* stop codon (**Fig. 12 A**). At the beginning of my doctoral research it was still uncertain, if *mdh* is co-transcribed and expressed with the rest of the *met* operon in *S. aureus* Newman.

3.7.1. Mdh is co-transcribed with *met* genes and expressed

In an initial experiment, total RNA isolated from *S. aureus* Newman grown in CDM without methionine to mid-exponential phase was subjected to Northern blot analysis using a probe specific for the *mdh* sequence. As shown in **Fig. 12 B**, this probe resulted in the same 4 kb signal as with a *metE*-specific probe, verifying co-transcription of *mdh* with the *met* operon. The cRACE experiment performed to characterise the 4 kb transcript, although not successful in determining the 5'-end(s) of this transcript, clearly identified the 3'-end of the mRNA to be 81 nt downstream of *mdh* (see **section 3.3.1, page 43**). This further confirmed co-transcription of *mdh* with the *met* genes. The proteome data presented in **section 3.5, page 61 ff.** demonstrated that *mdh* is not only transcribed but translated as well. Since the presence of the protein (Mdh) had been evidenced, we next sought to find Mdh's substrate(s) and determine its function in the cell.

An initial BLAST search using the amino acid sequence of Mdh revealed homology with a kynurenine formamidase (KFA) of *Pseudomonas aeruginosa* and *Bacillus cereus* encoded by *kynB*. KynB catalyses the second reaction of the aerobic tryptophan catabolism pathway from N-formyl-L-kynurenine (NFK) to L-kynurenine and formic acid (Kurnasov et al., 2003). Based on this reaction, I have developed a hypothesis that could explain why *mdh* is part of the *met* operon and co-regulated with the methionine biosynthesis genes (**Fig. 21**).

Co-expression could couple *de novo* methionine biosynthesis with formylation of methionine bound to the initiator tRNA ($tRNA_i$). $tRNA_i$ charged with N-formyl-L-methionine (hereinafter referred to as F-methionine) is a prerequisite of translation initiation in prokaryotes. During the final step of methionine synthesis, homocysteine is methylated to methionine, the methyl-group donor is methyl-tetrahydrofolate (Me-THF). After the methyl-group transfer from Me-THF to homocysteine, free THF is available. The formyl-THF-synthetase (*fhs*, NWMN_1625, EC 6.3.4.3) converts THF together with formic acid to 10-formyl-THF which is the only known

formyl-group donor to formylate methionine bound to $tRNA_i$ (Kahn et al., 1980; Mader et al., 2013; Meinnel et al., 1993). This reaction is catalysed by the methionyl-tRNA-formyltransferase (*fmt*, NWMN_1126, EC 2.1.2.9). Formic acid can be derived from several cellular processes (e.g. conversion of pyruvate to formic acid to generate acetyl-CoA) (Leibig et al., 2011). Postulating Mdh to be a formamidase, it would convert a formylated amino acid (e.g. N-formyl-L-kynurenine, -methionine, -glutamic acid or -aspartic acid) to formic acid and the respective amino acid. Due to the co-expression of *mdh* and the *met* genes, THF and formic acid would be readily available to generate 10-formyl-THF. Furthermore, newly synthesised methionine would be in close proximity to be loaded onto $tRNA_i$. Based on this hypothesis, experiments have been designed to elucidate Mdh's function.

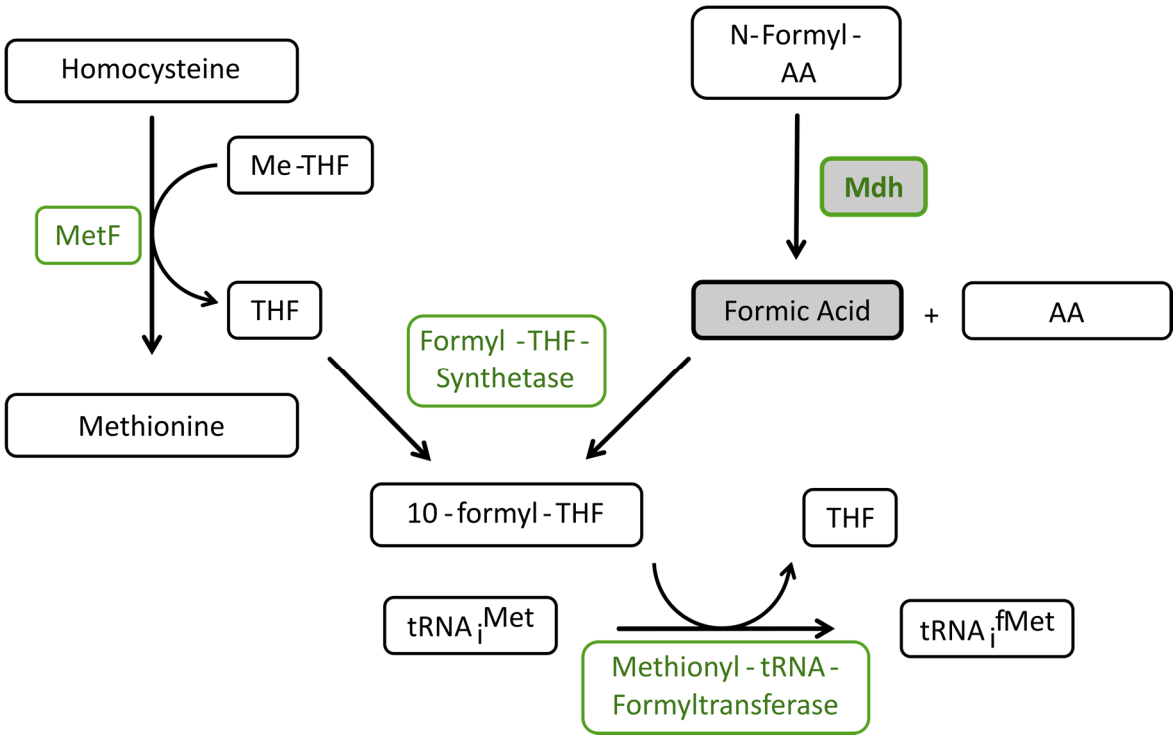

Figure 21. Hypothesised coupling of methionine biosynthesis and initiator tRNA formylation by Mdh. Schematic representation of Mdh's postulated activity and its putative link with methionine biosynthesis. Enzymes are shown in green, intermediate and metabolites are in black. Mdh and formic acid are highlighted in grey. AA: amino acid, THF: tetrahydrofolate, Me-THF: methyl-THF, $tRNA_i^{Met}$: initiator tRNA charged with methionine, $tRNA_i^{fMet}$: initiator tRNA charged with methionine that is formylated. For further details, see text.

The data presented in the following are based on work performed by three master students under my supervision. Daniela Steigerwald and Esther Rogalski worked with me for seven and eight months, respectively and concluded their work by submitting a master thesis.
Matthias Peindl completed an eight-week internship (concluded by an oral presentation).
Crystallisation and structure analyses were performed by Yesid Ramiréz and Wolfgang Kölmel of the Kisker group of the Rudolf-Virchow-Zentrum (RVZ) in Würzburg. The respective contributions are detailed in **chapter 6, page 188 f. 'Contributions by Others'**. Only the key results are described below, for details I herewith refer to the theses of Daniela Steigerwald and Esther Rogalski (Rogalski, 2017; Steigerwald, 2016).

3.7.2. Heterologous overexpression, purification and crystal structure analysis

We overexpressed an N-terminally His-tagged Mdh of *S. aureus* from a plasmid in *E. coli* and purified the enzyme with column-based immobilised metal affinity chromatography and ensuing size exclusion chromatography under native conditions. Buffer- and crystallisation conditions are detailed in Materials and Methods (**section 5.5.2, page 180 ff.**). The isolated Mdh was used for *in vitro* substrate testing described in **section 3.7.5, page 89 f.** of this thesis and for crystallography.

The crystal structure analysis suggested Mdh to predominantly exist as a dimer with zinc as a cofactor (**Fig. 22 A**). The zinc ion in Mdh is coordinated by His65, Asp67, Glu210 and the active site water W1. W1, in turn, is co-ordinated by His71 and Glu198 (**Fig. 22 B**). **Fig. 22 C** shows a top view of an Mdh subunit. The residues His71 (red) and Glu198 (blue) were suggested to be the most essential amino acids of the active centre because His71 is highly conserved among metal-dependent hydrolases (Bjerregaard-Andersen et al., 2014) and involved in nucleophilic hydroxide formation, both residues are required for the active site water co-ordination (**Fig. 22 B**). The residue Phe32 (orange) has been hypothesised to be involved in substrate recognition, as it was not properly resolved in the electron density map. This is indicative of a high flexibility. This flexibility might result from the absence of the substrate as interaction partner that would stabilise the position of Phe32. The localisation of Phe32 above the active centre further supports this hypothesis (personal communication Wolfgang Kölmel, Würzburg). Wolfgang Kölmel and Yesid Ramiréz proposed a catalytic mechanism for Mdh similar to that of bacterial kynurenine formamidases (Díaz-Sáez et al., 2014). The active site water W1 co-ordinated by a basic amino acid (in Mdh His71) donates a proton to the amino acid that generates a nucleophilic hydroxide potent to attack the carbonyl component (later the formic acid) of the substrate (**Fig. 22 D**). Via an intermediate state, the substrate is cleaved and the products (in KFAs L-kynurenine and formic acid) are released. In contrast to KFAs, Mdh seems to possess only a single zinc ion, instead of two in the active centre. In the KFAs the second zinc is required for the co-ordination of the second active site water W2 that regenerates the enzyme after substrate cleavage. The crystal structure of Mdh suggests the second active site water to be co-ordinated by the amino acids Asp182, Glu198 and Glu210 (**Fig. 22 B**).

The data derived from the crystal structure were then used to generate putative catalytically inactive or impaired mutants.

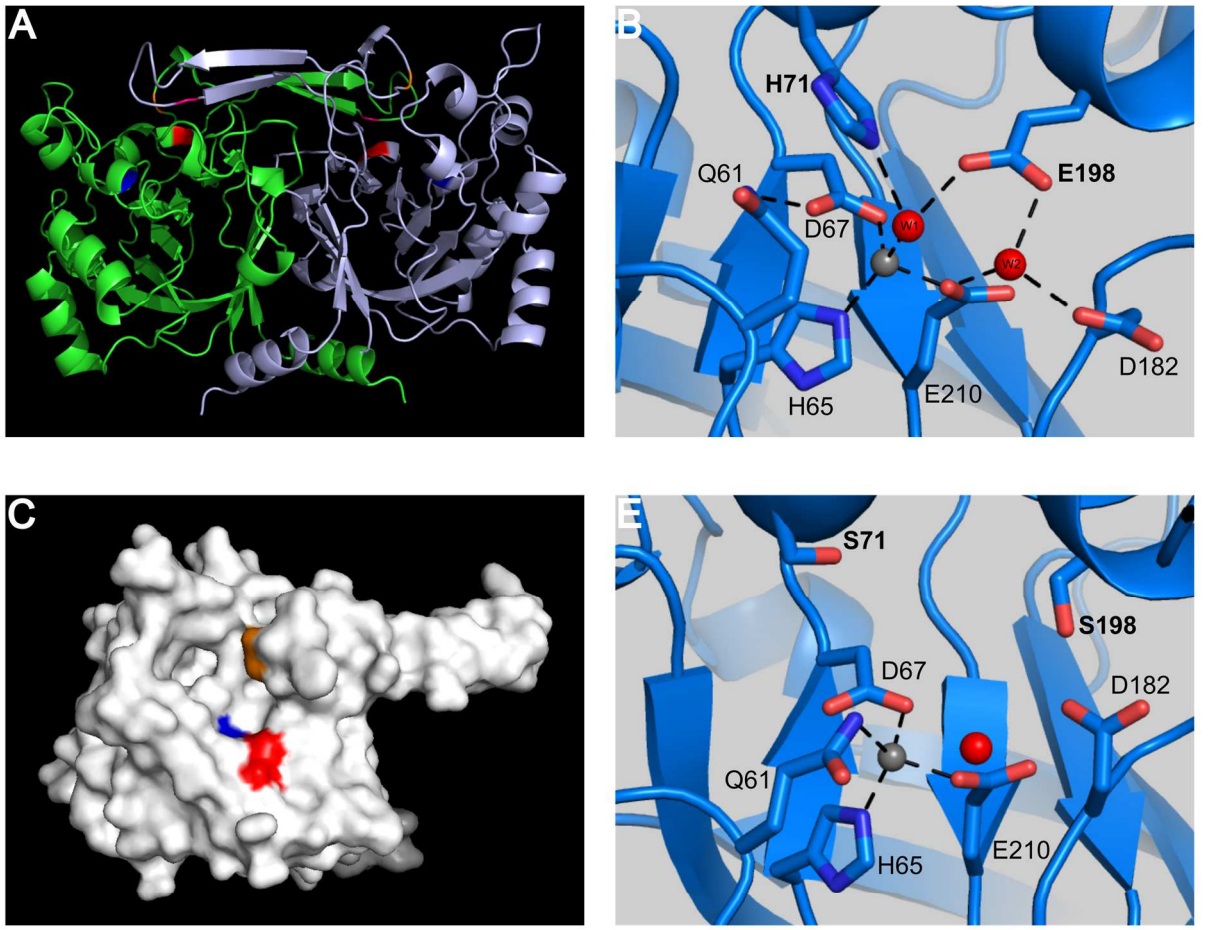

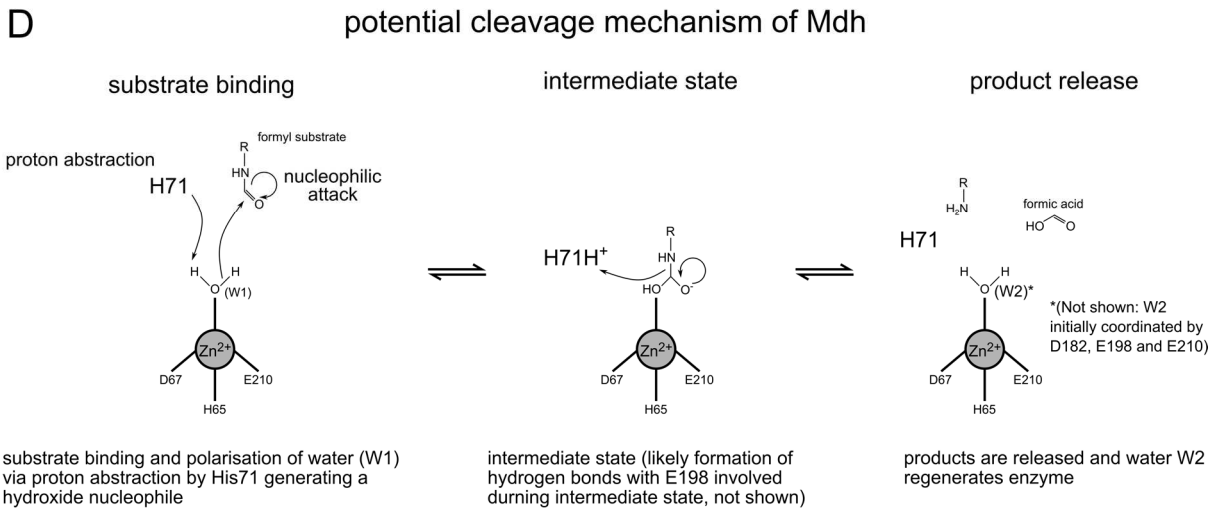

Figure 22. *See next page*

Figure 22. Crystal structure of Mdh and its putative catalytic mechanism. (A) Cartoon representation of Mdh as dimer. Subunits are shown in green and pale purple. Residues His71 and Glu198 of the active centre are highlighted in red and blue, respectively. Residues Phe32 and Tyr52 are highlighted in orange and magenta, respectively. **(B)** Active centre of Mdh. Residues are represented as balls and sticks and labelled according to their position in the amino acid sequence of Mdh. Residues His71 and Glu198 are shown in bold. The catalytic zinc ion is depicted as grey sphere. Active site waters are shown as red spheres and are labelled W1 and W2. Dashed lines indicate interactions. D: aspartic acid, E: glutamic acid, H: histidine, Q: glutamine, S: serine. **(C)** Top view of an Mdh subunit (surface representation). Residues of the active centre His71 and Glu198 are shown in red and blue, respectively. Phe32, postulated to be involved in substrate recognition, is shown in orange. **(D)** Schematic of the proposed catalytic mechanism of Mdh. Catalytic zinc ion is depicted as a grey circle, interactions with the residues D67, H65, E210 and the active site waters W1, W2 or the substrate intermediate are represented by black lines. Curved black arrows indicate electron pair movements. R: rest, formyl(F)-substrate, e.g. F-methionine, F-glutamic acid, F-aspartic acid. For further details, see text and figure text. **(E)** Active centre of the Mdh His71Ser Glu198Ser double mutant. Representation and labelling as in (B). Residues Ser71 and Ser198 are shown in bold.

3.7.3. Dysfunctional Mdh impaired growth, deletion of Mdh did not influence growth

Five different *mdh* mutants were created in *S. aureus* strain Newman to investigate their growth behaviour in comparison to the wild type to further characterise Mdh's function in the cell: a clean deletion mutant (Δ*mdh*), three putative catalytically inactive Mdh variants (His71Ser, Glu198Ser and His71Ser &Glu198) and a putative substrate recognition deficient mutant (Phe32Trp).

The *S. aureus* Newman wild type strain and its five isogenic *mdh* mutants were grown in CDM with and without methionine. Bacterial growth was monitored over a time course of 48 hours by $OD_{595\ nm}$ measurement every 30 minutes. Bacteria were cultivated in a 96-well plate with shaking at 37° C. Representative data are shown.

The *mdh* deletion mutant and the His71Ser mutant both behaved like the wild type in CDM without methionine, bacteria entered stationary phase after approximately 25 hours and reached an OD_{max} of 0.38. The Glu198Ser and the His71Ser & Glu198Ser double mutant entered the stationary growth phase after 25 hours as well. However, the OD_{max} was with about 0.28 lower than that of the wild type (**Fig. 23 A**). The Phe32Trp mutant behaved like the double mutant, the OD_{max} was 0.29 and 0.28, respectively. The wild type reached an OD_{max} of 0.36. In this experiment, all strains entered the stationary phase slightly earlier (**Fig. 23 B**, conf. wild type curve **Fig. 23 A**). Under methionine-rich conditions no differences in growth were expected because *met* operon and therefore *mdh* expression should only take place under methionine-deprivation.

However, the Glu198Ser and the double mutant showed a slightly lower OD in stationary phase than the wild type under methionine-rich conditions (0.49 and 0.47, respectively, vs. 0.52), the His71Ser mutant showed with 0.58 a higher OD than the wild type and the Δ*mdh* mutant a rather similar OD with 0.54 after 48 hours (**Fig. 23 C**). The Phe32Trp mutant grew as the double mutant under methionine-rich conditions, both with a lower OD in the stationary phase than the wild type (0.52 and 0.54, respectively, vs. 0.64) (**Fig. 23 D**). Interestingly, under methionine-deprived conditions the growth curves clustered into two groups (wild type, Δ*mdh*, His71Ser and Glu198Ser, His71Ser & Glu198Ser, Phe32Trp, respectively), whereas under methionine-rich conditions no grouping occurred.

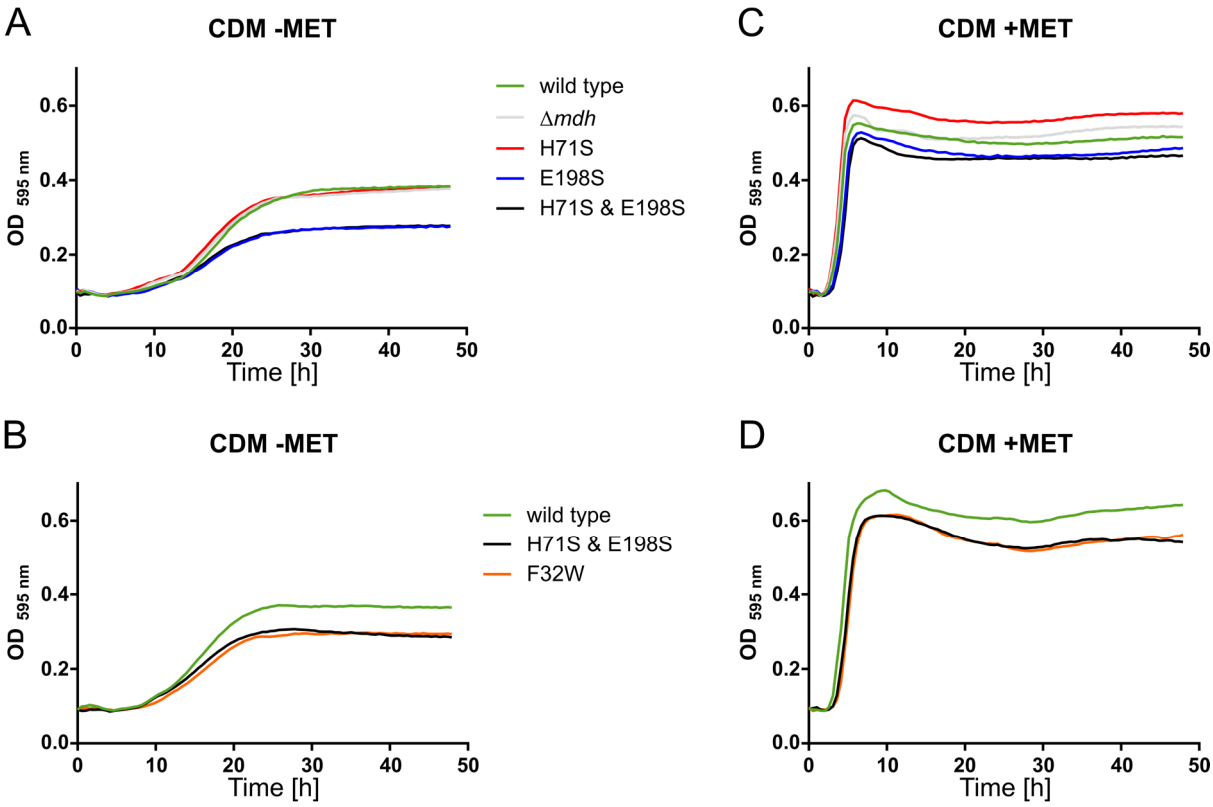

Figure 23. Growth curves of *mdh* mutants. (A) & **(B)** *S. aureus* Newman and its isogenic *mdh* mutants in CDM without methionine. **(C)** & **(D)** *S. aureus* Newman and its isogenic *mdh* mutants in CDM with methionine. Δ*mdh*: deletion of *mdh* gene, H71S: histidine to serine substitution at position 71 of Mdh, E198S: glutamic acid to serine substitution at position 198, H71S & E198S: substitutions as described above, F32W: phenylalanine to tryptophan substitution at position 32. H71S, E198S and H71S & E198S are putative catalytic inactive Mdh mutants, F32W is a postulated substrate-binding deficient Mdh mutant. For legends of (C) and (D), see (A) and (B), respectively.

3.7.4. His71 and Glu198 are crucial for coordination of water ions surrounding the zinc ion in the catalytic centre

Next, we aimed at obtaining crystal structures of the *mdh* mutants that had shown altered (poorer) growth dynamics (Glu198Ser, His71Ser & Glu198Ser and Phe32Trp) compared to the wild type. We succeeded in overexpressing and crystallising the His71Ser & Glu198Ser double *mdh* mutant. Solving the crystal structure revealed that the mutation of residues 71 and 198 from histidine and glutamic acid to serine prevented these residues to properly position the two active site waters (W1 and W2), confirming their essentiality for the active centre (**Fig. 22 E**). The amino acid exchanges in the catalytic centre caused the neighbouring residues Gln61 and Asp182 to change their positions (**Fig. 22 B&E**). Gln61 flipped into the active site to interact with the zinc ion that has been co-ordinated by the active site water W1 in the wild type. W1 is absent in the double mutant Mdh because Ser71 is unable to co-ordinate W1. Asp182 has an altered orientation. These data confirmed the importance of the residues His71 and Glu198 for the active site water co-ordination and therewith for the zinc ion co-ordination.

3.7.5. Establishing an *in vitro* assay for substrate testing

In order to find Mdh's substrate, we tested compounds for their cleavage by Mdh *in vitro*. The first to be tested was N-formyl-L-kynurenine because of the homology of Mdh to kynurenine formamidases. L-kynurenine has an absorption maximum at 365 nm, NFK does not. Therefore, measuring the absorption at 365 nm can be used to detect the formation of L-kynurenine via an increase in absorption. The reaction conditions used are adapted from Díaz-Sáez et al. (2014). For the spectrophotometric assay quartz cuvettes were used. The reaction mixture consisted of the reaction buffer (0.1 M NaH_2PO_4/Na_2HPO_4, pH 7.4), 20 µM zinc chloride, 1mM NFK and, if applicable, 500 ng of KynB or Mdh overexpressed and purified from *E. coli*, as described above, in a final volume of 1 ml. Absorbance at 365 nm was measured for 30 minutes.

As positive control we used KynB of *Pseudomonas aeruginosa* (overexpressed and purified in parallel with Mdh) that has been already experimentally shown to cleave N-formyl-L-kynurenine to kynurenine and formic acid (Díaz-Sáez et al., 2014).

The absorption steadily increased to around 0.1, indicative of the generation of L-kynurenine via the cleavage of NFK by KynB. To exclude that NFK spontaneously degraded to L-kynurenine that would cause an increase in absorption over time as well, a reaction without KynB was set up and measured at t0 and after 30 minutes. The absorbance did not change, therefore production of L-kynurenine had to be due to enzymatic cleavage by KynB (**Fig. 24 A**).

The Mdh sample did not show any increase in absorption over 30 minutes, indicating that no cleavage of the NFK by Mdh occurred (**Fig. 24 A**). These data suggested that NFK is not Mdh's substrate. The aerobic tryptophan catabolism pathway is not annotated in *S. aureus*, therefore NFK might not be available in the cell. However, it could not be excluded that (i) the buffer conditions were not adequate for Mdh, (ii) Mdh was inactive due to the purification procedure or (iii) Mdh heterologously overexpressed in *E. coli* was lacking modifications, such as phosphorylations, required for its activity. The first two assumptions seemed to be rather unlikely because the buffer conditions worked well for the related KynB and the quality of the natively purified Mdh was high enough for crystallisation studies that revealed a dimeric state with zinc in the active centre. A recent phosphoproteomics study revealed the phosphorylation of tyrosine 52 of Mdh in *S. aureus* (Bäsell et al., 2014). In the crystal structure of the dimeric Mdh, Tyr52 (magenta) of one subunit is part of a 'lid-structure' that borders the active centre of the respective other subunit (**Fig. 22 A**). Hence, we decided to purify Mdh from its natural host *S. aureus*. An N-terminal His-tagged version (same as for the overexpression in *E. coli*) and a C-terminal hexa-histidine tagged variant were chromosomally integrated (replacing the wild type *mdh*) into *S. aureus* Newman, respectively. (Overexpression from a plasmid was unsuccessful (data not shown).) C-terminal His-tagged Mdh was purified and used for *in vitro* assays because the N-terminal variant showed impaired growth similar to the catalytically inactive Mdh mutants described above (data not shown), indicating inactive Mdh. Next, N-formylmethionine and N-formylglutamic acid were tested as Mdh substrates with Mdh isolated from *S. aureus* and *E. coli* (heterologous expression).

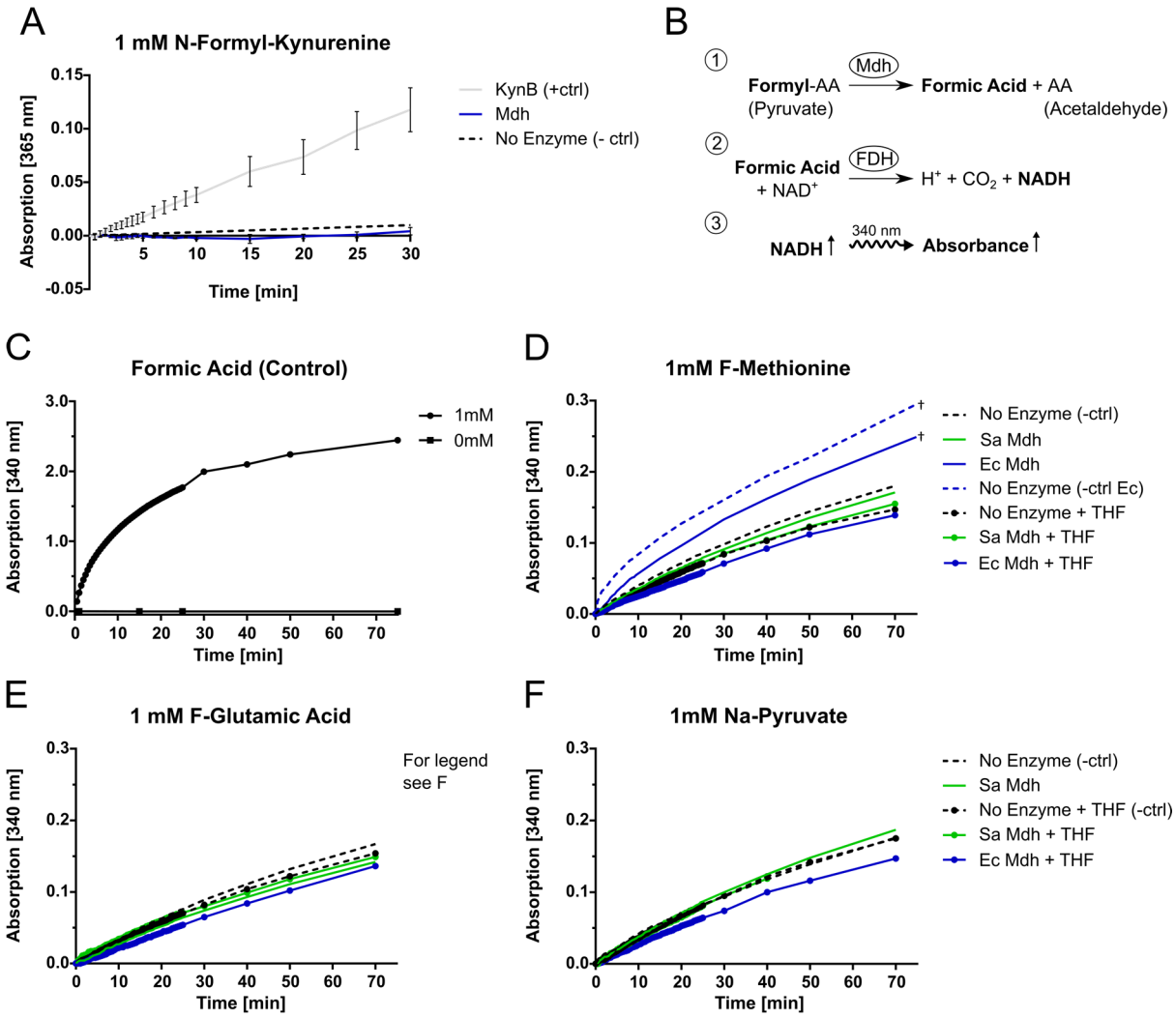

Figure 24. In vitro assays with purified Mdh to determine Mdh's substrate. (A) Absorption curves of kynurenine formamidase KynB of *P. aeruginosa* and Mdh of *S. aureus* overexpressed in *E. coli* incubated with 1 mM N-Formyl-Kynurenine. Absorption measured at 365 nm. Data from three independent measurements. Error bars show SD. **(B)** Principle of coupled *in vitro* assay to measure release of formic acid by Mdh's catalytic activity. AA: amino acid, FDH: formate dehydrogenase, vertical arrow up: increase. For details see text. **(C)** Absorption curves with (1 mM) and without (0 mM) formic acid as control reactions. **(D)** Absorption curves of *S. aureus* Mdh isolated from *E. coli* (Ec) (blue) or *S. aureus* (Sa) (green) incubated with 1 mM F-Methionine in the presence or absence of tetrahydrofolate (THF). Crosses ('†') indicate that those curves are derived from a separate experiment. **(E)** Absorption curves with 1 mM F-Glutamic acid and **(F)** 1 mM Na-Pyruvate, for details see above.

Methionine and glutamic acid and their formylated derivatives cannot be distinguished by differences in their absorbance capacity at a specific wavelength as L-kynurenine and N-formyl-L-kynurenine. This required us to develop a coupled *in vitro* assay (**Fig. 24 B**). The assay is based on the hypothesis that formic acid is released after cleavage of a formylated substrate by Mdh (see **Fig. 21**). The formic acid is then converted to hydrogen ions and carbon dioxide by a formate dehydrogenase (FDH) in the presence of NAD^+ that is reduced to NADH. NADH absorbs light at a wavelength of 340 nm, the extinction at 340 nm increases with rising NADH levels. Therefore, the increase in extinction can be used as a proxy for the release of formic acid. Formic acid is only released, when a formyl-substrate is cleaved by Mdh (**Fig. 24 B**).

The reaction conditions were as described for NFK, 1 U of FDH and NAD^+ to a final concentration of 1 mM were added.

As technical control, 1 mM free formic acid has been added to the reaction mixture consisting of the reaction buffer, FDH and NAD^+ and absorption at 340 nm was measured continuously for 75 minutes. The absorption increased rapidly within the first 25 minutes from 0 to ~1.8, then absorption rose slower to 2.4 at 75 minutes (**Fig. 24 C**). In the absence of formic acid, no increase in absorbance has been observed, verifying that only the conversion of formic acid by FDH results in the reduction of NAD^+ to NADH.

First, F-methionine was tested as substrate (**Fig. 24 D**). 1 mM F-methionine, 1 U of FDH and NAD^+ to a final concentration of 1 mM were mixed with 500 ng Mdh purified from *E. coli* and absorbance at 340 nm was measured for 75 minutes. Absorption steadily increased to ~0.25, indicating release of formic acid into the reaction mixture. However, the control reaction without Mdh resulted in a similar absorbance curve with an absorption value of ~0.3 after 75 minutes. Therefore, release of formic acid was not due to cleavage of F-methionine by Mdh, but rather spontaneous degradation. Next, Mdh isolated from *S. aureus* was incubated with F-methionine as detailed above. Again, absorption values of the Mdh and the control reaction were very similar with 0.17 and 0.18, respectively after 70 minutes. F-methionine has not been cleaved by Mdh. In a further attempt, the reaction mixture was supplemented with tetrahydrofolate because it had been speculated that the formic acid might be either directly transferred onto THF or that the reaction would only take place in the presence of THF as co-factor. Nevertheless, cleavage of F-methionine neither occurred in the reaction with *E. coli*- nor *S. aureus*-purified Mdh (**Fig. 24 D**). The absorption values were almost identical with the control reaction values.

Next, F-glutamic acid was tested (**Fig. 24 E**). Reactions as described for F-methionine were set up, except for the combination *E. coli* Mdh with F-glutamic acid without THF. No cleavage of the substrate by Mdh occurred. All absorption values steadily increased to around 0.14 to 0.17 independent of presence or absence of Mdh.
In a final attempt, pyruvate was tested as substrate of Mdh (**Fig. 24 F**). Pyruvate is released as by-product in methionine biosynthesis during transsulfuration, when cystathionine is converted into homocysteine (see **Fig. 1**). Therefore, pyruvate would be readily available and in proximity of Mdh. Elimination of formic acid from pyruvate would generate acetaldehyde. Reactions as described for F-glutamic acid were set up. No cleavage of pyruvate into formic acid by Mdh occurred. All absorption values steadily increased to around 0.15 to 0.18 independent of presence or absence of Mdh.
Under the tested conditions, neither Formyl-kynurenine, F-methionine, F-glutamic acid nor pyruvate were cleaved by Mdh.

3.7.6. Bacterial-two-hybrid-system identified interactions of Mdh with MetI and MetC

All attempts to determine Mdh's substrate have been unsuccessful to date. A disadvantage of *in vitro* assays is, that they never resemble the *in vivo* situation because potential interaction partners or cofactors are absent. We hypothesised that Mdh might form a complex with other enzymes *in vivo* that are required for its catalytic activity. The bacterial two-hybrid system (BTHS) has been used to identify potential interactions of Mdh with the enzymes of the *met* operon and the formyl-tetrahydrofolate synthetase (*fhs*, NWMN_1625, EC 6.3.4.3). The coupling of transcription and translation in prokaryotes and the co-transcription of *mdh* with the *met* genes enables the enzymes to be immediately in close proximity to each other that would facilitate complex formation.

The BTHS is based on the interaction-mediated restoration of the adenylate cyclase activity in *E. coli*. It makes use of the fact that the catalytic domain of adenylate cyclase (CyaA) from *Bordetella pertussis* comprises two complementary fragments, T25 and T18 (**Fig. 25 A.A**), that are inactive when physically separated (**Fig. 25 A.B**). Fusion of these two fragments to interacting proteins, X and Y, leads to heterodimerisation of these hybrid proteins which results in functional complementation between T25 and T18 fragments and, subsequently, cyclic AMP (cAMP) synthesis (**Fig. 25 A.C**). Cyclic AMP generated by the reconstituted chimeric adenylate cyclase binds to the catabolite activator protein (CAP). The cAMP/CAP complex is

a pleiotropic regulator of gene transcription in *E. coli*. It activates expression of several resident genes, including the *lac* operon involved in lactose catabolism (**Fig. 25 A.D**). This enables the bacteria to utilise lactose as the unique carbon source. Lactose consumption can be easily visualised on indicator agar. To detect *in vivo* interactions between two proteins of interest with the BTHS, the co-expression of these proteins fused to the T25 and T18 fragments is required in bacteria without endogenous adenylate cyclase activity (*E. coli* Δ*cya*). This is accomplished by using two compatible vectors, one expressing the T25 fusion (pKT25 or pKNT25) and the other expressing the T18 fusion (pUT18 or pUT18C). The bacteria are co-transformed with the two plasmids and subsequently plated on LB/X-gal (Luria-Bertani/5-Bromo-4-chloro-3-indolyl-β-D-galactopyranoside) indicator agar to reveal the resulting Cya+ phenotype (for details see Materials and Methods (**section 5.5.4, page 184 f.**), (**Fig. 25 A.1&.2**), (Euromedex BACTH manual).

BTHS interaction data are available for MetI, MetC and MetF with Mdh and Mdh with itself. The dimerisation of Mdh could be confirmed, because all tested combinations resulted in a strong and early positive signal in the BTHS assay, indicative of an interaction of Mdh with itself (**Fig. 25 B**). Furthermore, the assay results suggested an interaction of Mdh with MetI and MetC. The co-transformation of the pUT18C_metI* and the pUT18C_metC* constructs (fusion of the T18 cyclase fragment to the N-terminus of MetI/MetC) with both, the pKNT25_mdh and pKT25C_mdh*, mdh constructs led to strong X-gal positive signals (**Fig. 25 B**). Very weak or no positive X-gal signals were detected after co-transformation of the pUT18N_metI and the pUT18N_metC constructs (fusion of the T18 cyclase fragment to the C-terminus of MetI/MetC) with both mdh constructs. Mdh might interact with MetF as well. However, data are not conclusive because only two out of three co-transformations of pUT18C_metF* with pKNT25_mdh gave X-gal positive results. All remaining combinations resulted in very weak or no positive signals (**Fig. 25 B**).
BTHS data for MetE and Fhs are not available by now.

A

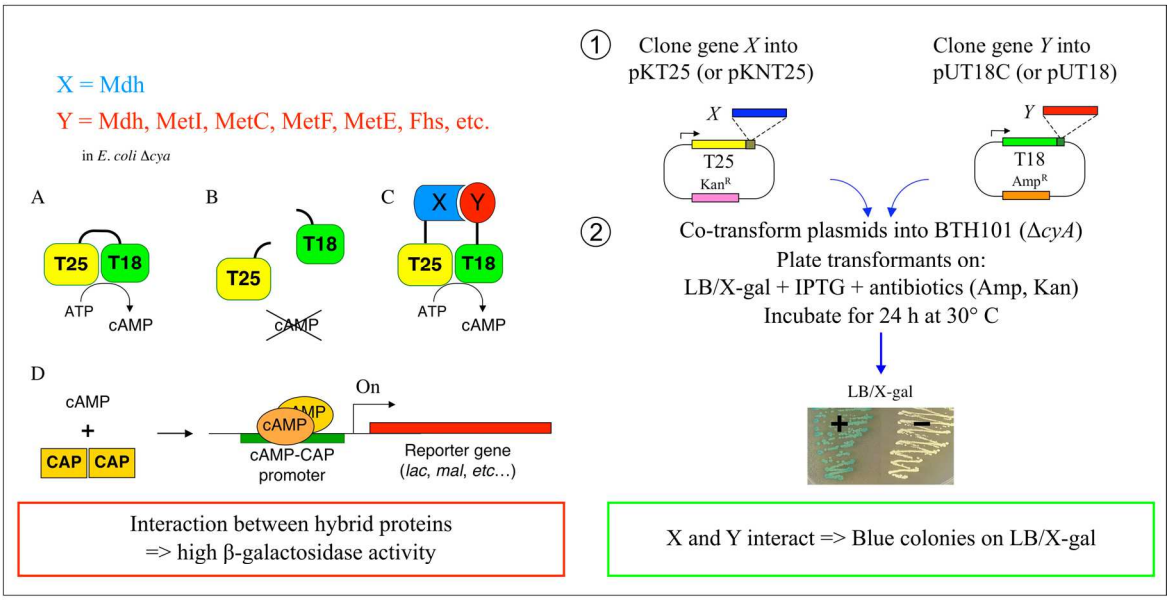

B

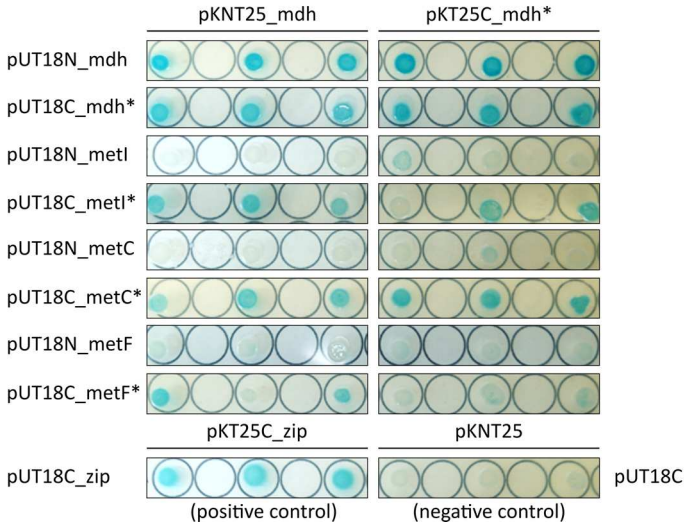

Figure 25. Bacterial-Two-Hybrid-System (BTHS) assay identified protein interactions of Mdh with *met* operon enzymes. (A) Schematic overview of BTHS method and experimental procedure. For details see text. Figure adapted from Euromedex BACTH manual. **(B)** Results of co-transformation of described plasmid combinations with ensuing spotting on indicator agar. Each combination was transformed in triplicates.

3.7.7. Mdh is highly conserved among staphylococci

16 staphylococcal species were investigated regarding existence of *mdh* as gene of the *met* operon and conservation on nucleotide and amino acid sequence level.

In all species with exception of *S. pseudintermedius* the *mdh* gene was present downstream of *metE*. Overall, the similarity between the staphylococcal species was already high on the nucleotide sequence level, with the lowest similarity values being around 67 %. **Tab. 4 A** shows the percent identity of *mdh*'s nucleotide sequence of each tested species in comparison to the others. 50 % identity was set as lowest value and would appear in red, 75 % identity is displayed in yellow, 100 % was set as maximum value and is displayed in dark green. *S. aureus* and *S. argenteus* had with 753 nt the longest *mdh* genes, followed by *S. carnosus* and *S. simulans* with 750 nt. *S. sciuri*, *S. warneri*, *S. pasteuri*, *S. haemolyticus*, *S. lugdunensis*, *S. capitis* and *S. epidermidis* had a gene length of 744 nt. *S. saprophyticus*, *S. xylosus*, *S. succinus* and *S. equorum* had with 741 nt the shortest *mdh* sequences of all investigated staphylococci.

On the amino acid level similarities among species are even higher (**Tab. 4 B** and **Fig. 26**). The amino acids of the catalytic centre His71 (red asterisk) and Glu198 (blue asterisk) and the amino acid Phe32 (orange asterisk) that might be involved in substrate recognition are 100 % conserved. The amino acid Tyr52 (magenta asterisk) that had been found to be phosphorylated in *S. aureus* is conserved in all staphylococci, except for *S. sciuri*, *S. carnosus* and *S. simulans*, in those species position 52 is a phenylalanine. In S. *simulans* position 51 is a tyrosine instead. Mdh is highly conserved among staphylococci on nucleotide and amino acid level.

Table 4. Percent Identity Matrices of nucleotide and amino acid sequences of *mdh*/Mdh for 15 staphylococcal species. A Percent Identity Matrix (PIM) of *mdh* nucleotide sequences. **B** PIM of Mdh amino acid sequences. 50% identitiy (would be) shown in red, 75 % identity shown in yellow, 100 % identity shown in dark green with a colour gradient.

A

	S. sciuri	*S. carnosus*	*S. simulans*	*S. saproph.*	*S. xylosus*	*S. succinus*	*S. equorum*	*S. aureus*	*S. argent.*	*S. warneri*	*S. pasteuri*	*S. haemol.*	*S. lugdun.*	*S. capitis*	*S. epi.*
S. sciuri	100	68.69	67.2	67.34	67.62	67.75	68.29	67.47	69.35	69.77	69.77	68.69	68.96	68.15	67.61
S. carnosus	68.69	100	81.66	71.26	69.37	70.85	70.45	69.33	69.6	70.58	70.58	70.04	71.26	71.66	70.99
S. simulans	67.2	81.66	100	67.21	70.31	68.83	69.23	67.47	69.07	69.35	68.95	69.62	69.89	68.95	68.55
S. saprophyticus	67.34	71.26	67.21	100	81.11	79.08	79.76	71.26	70.45	73.14	73.01	71.12	72.06	71.26	72.6
S. xylosus	67.62	69.37	70.31	81.11	100	80.84	82.73	75.57	74.63	75.3	75.98	74.36	74.63	73.68	73.82
S. succinus	67.75	70.85	68.83	79.08	80.84	100	83.54	73.55	74.22	73.41	73.95	72.47	74.22	71.66	74.49
S. equorum	68.29	70.45	69.23	79.76	82.73	83.54	100	72.6	72.74	75.03	75.44	74.09	75.17	74.09	73.95
S. aureus	67.47	69.33	67.47	71.26	75.57	73.55	72.6	100	91.1	77.82	77.96	79.7	77.28	75.54	77.02
S. argenteus	69.35	69.6	69.07	70.45	74.63	74.22	72.74	91.1	100	77.69	77.42	77.55	76.88	75	76.88
S. warneri	69.77	70.58	69.35	73.14	75.3	73.41	75.03	77.82	77.69	100	96.37	79.97	76.61	77.82	78.63
S. pasteuri	69.77	70.58	68.95	73.01	75.98	73.95	75.44	77.96	77.42	96.37	100	80.38	77.69	79.3	78.23
S. haemolyticus	68.69	70.04	69.62	71.12	74.36	72.47	74.09	79.7	77.55	79.97	80.38	100	80.51	78.76	78.23
S. lugdunensis	68.96	71.26	69.89	72.06	74.63	74.22	75.17	77.28	76.88	76.61	77.69	80.51	100	76.34	77.42
S. capitis	68.15	71.66	68.95	71.26	73.68	71.66	74.09	75.54	75	77.82	79.3	78.76	76.34	100	79.57
S. epidermidis	67.61	70.99	68.55	72.6	73.82	74.49	73.95	77.02	76.88	78.63	78.23	78.23	77.42	79.57	100

B

	S. sciuri	*S. carnosus*	*S. simulans*	*S. saproph.*	*S. xylosus*	*S. succinus*	*S. equorum*	*S. aureus*	*S. argent.*	*S. lugdun.*	*S. warneri*	*S. pasteuri*	*S. epi.*	*S. haemol.*	*S. capitis*
S. sciuri	100	71.26	68.42	70.73	71.14	70.33	71.54	67.21	67.21	68.29	73.58	73.58	70.73	71.14	71.54
S. carnosus	71.26	100	90.73	71.14	72.36	71.54	73.58	69.08	69.48	71.54	73.17	72.76	71.54	73.98	73.17
S. simulans	68.42	90.73	100	70.33	72.76	71.14	72.76	69.48	69.48	70.85	72.87	72.47	71.26	73.68	72.47
S. saprophyticus	70.73	71.14	70.33	100	89.02	86.59	87.8	75.61	75.61	74.8	76.83	76.83	76.42	75.61	75.2
S. xylosus	71.14	72.36	72.76	89.02	100	87.8	90.65	78.86	78.46	76.02	79.27	79.27	76.83	77.64	78.86
S. succinus	70.33	71.54	71.14	86.59	87.8	100	93.09	76.83	77.24	79.27	78.46	78.86	78.46	78.46	79.67
S. equorum	71.54	73.58	72.76	87.8	90.65	93.09	100	78.05	78.46	78.86	81.71	81.71	78.86	79.67	80.89
S. aureus	67.21	69.08	69.48	75.61	78.86	76.83	78.05	100	97.6	83	83.81	83.81	84.21	85.43	83.81
S. argenteus	67.21	69.48	69.48	75.61	78.46	77.24	78.46	97.6	100	83	82.59	82.59	83.81	84.62	83
S. lugdunensis	68.29	71.54	70.85	74.8	76.02	79.27	78.86	83	83	100	84.62	85.02	84.62	87.85	86.23
S. warneri	73.58	73.17	72.87	76.83	79.27	78.46	81.71	83.81	82.59	84.62	100	99.6	86.23	89.88	88.26
S. pasteuri	73.58	72.76	72.47	76.83	79.27	78.86	81.71	83.81	82.59	85.02	99.6	100	86.23	89.47	88.26
S. epidermidis	70.73	71.54	71.26	76.42	76.83	78.46	78.86	84.21	83.81	84.62	86.23	86.23	100	88.26	90.69
S. haemolyticus	71.14	73.98	73.68	75.61	77.64	78.46	79.67	85.43	84.62	87.85	89.88	89.47	88.26	100	91.09
S. capitis	71.54	73.17	72.47	75.2	78.86	79.67	80.89	83.81	83	86.23	88.26	88.26	90.69	91.09	100

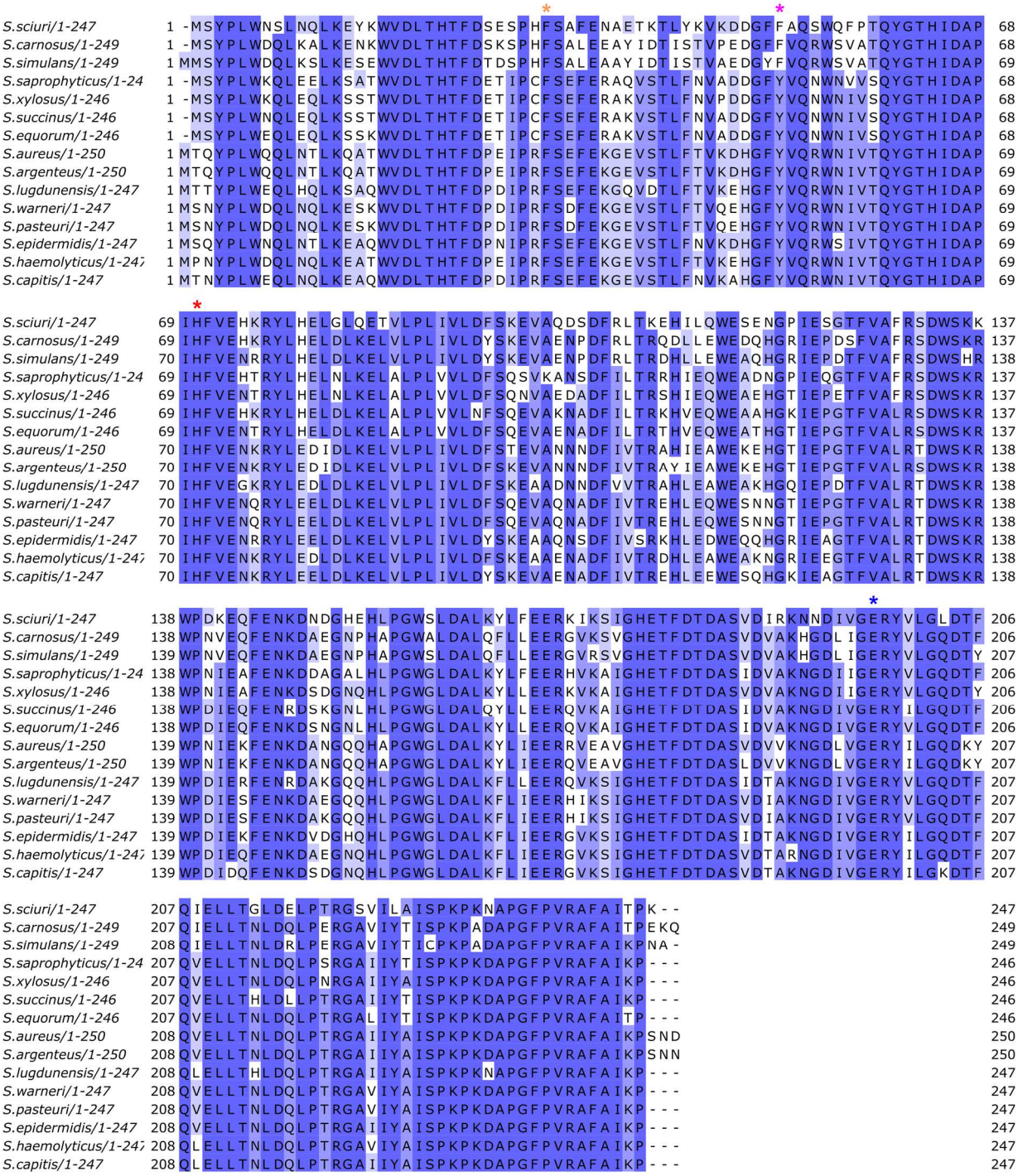

Figure 26. Alignment of Mdh amino acid sequences of 15 staphylococcal species. Mdh sequences of staphylococcal species detailed in the figure were aligned using MUSCLE (**MU**ltiple **S**equence **C**omparison by **L**og- **E**xpectation), graphical representation of alignments was done with Jalview (Waterhouse et al., 2009). Amino acids shaded in dark blue: > 80 % of aligned amino acids at this position agree with the consensus sequence, in blue > 60 % and in light blue > 40 %. Amino acids that differ from consensus are not shaded. Orange asterisk (*): phenylalanine at position 32 of *S. aureus* Mdh, magenta asterisk: tyrosine at position 52, red asterisk: histidine at position 71, blue asterisk: glutamic acid at position 198.

3.7.8. Distance between *metE* and *mdh* varies among staphylococcal species

Data from Esther Rogalski were complemented with additional five staphylococcal species (*S. argenteus*, *S. capitis*, *S. equorum*, *S. simulans*, *S. succinus*). In *S. lugdunensis* the distance between the stop codon of *metE* and the start codon of *mdh* is the longest with 224 bp, in *S. scuri* the distance is the shortest with only 16 bp. The distance in *S. carnosus* is 178 bp, in *S. haemolyticus* 155 bp and in *S. simulans* 104 bp. *S. aureus* and *S. argenteus* have 42 bp distance, *S. equorum* 26 bp, *S. xylosus* and *S. saprophyticus* 24 bp and *S. succinus* 22 bp. *S. capitis*, *S. epidermidis*, *S. pasteuri* and *S. warneri* all have a distance of 21 bp (**Fig. 27**). Whether these differences have an influence on transcription or translation of *mdh* is yet unclear and would need further investigations.

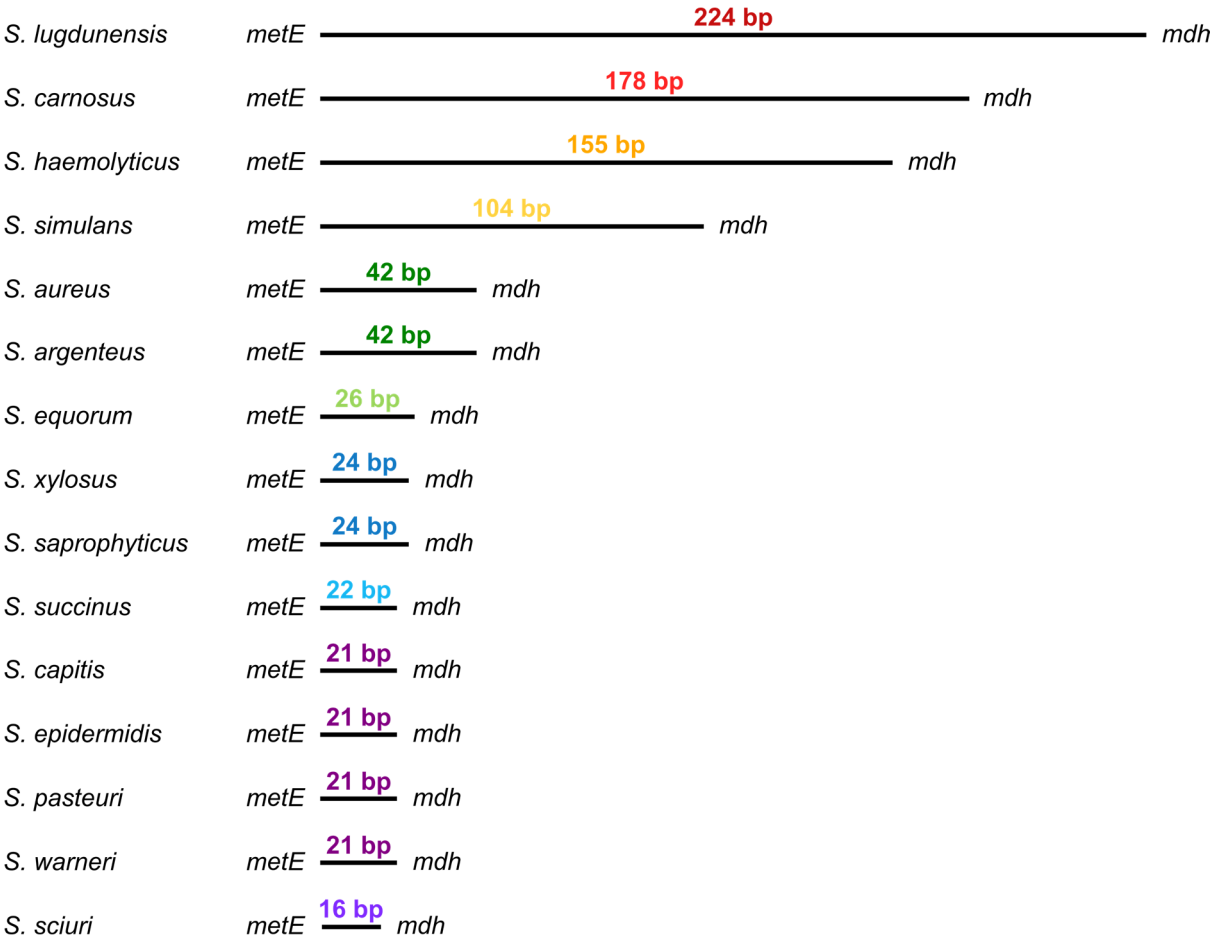

Figure 27. Comparison of distance between *metE* and *mdh* in 15 staphylococcal species. Black bars represent distance between *metE* stop and *mdh* start codon in staphylococcal species detailed in the figure. Length in base pairs (bp) is given on top of each bar. Same colour indicates identical length.

3.8. Discussion Mdh

Already fifteen years ago, Rodionov et al. assumed *mdh* to be part of the *met* operon and therewith under MET-T-box riboswitch control, based on bioinformatics predictions (Rodionov et al., 2004). In this work, I demonstrated co-transcription and –expression of *mdh* with the *met* operon genes in *S. aureus* Newman (see **Figs. 12 B** and **20 A**). The function of Mdh is still unclear. However, a link with methionine metabolism is strongly suggested because association of *mdh* with the *met* operon is highly conserved among staphylococci and *mdh* genes belong to methionine regulons in other bacterial species as well. For example, in *Streptococcus mutans*, *S. thermophilus* and *S. suis mdh* genes are under control of the transcription factor MtaR binding to the so-called 'MET-box' (consensus: 5'-TATAGTTnaAACTATA-3') (Rodionov et al., 2004). On protein level these Mdh enzymes have around 50 % identity, including the important residues Phe32, Tyr52, His71 and Glu198, with the *S. aureus* Mdh (own unpublished observations, protein BLAST). In *Leuconostoc mesenteroides mdh2* is predicted to be under MET-T-box riboswitch control. Mdh2 has 56 % identity with *S. aureus* Mdh and Phe32, His71 and Glu198 are present. *mdh* of *Bacillus cereus* is predicted to be SAM-binding riboswitch-controlled, but amino acid identity to Mdh is, with 26 % low, although residues Phe32, His71 and Glu198 are present (own unpublished observations, protein BLAST, Vitreschak et al., 2008).

3.8.1. *In vitro* assays to determine Mdh's substrate(s)

The homology of *S. aureus* Mdh with kynurenine formamidases (KFA) of *Pseudomonas aeruginosa* and *Bacillus cereus* (identified by an initial BLAST search in 2016) led us to the hypothesis that Mdh cleaves formylated amino acids to obtain formic acid and the respective amino acid (see **Fig. 21**). KFAs catalyse the second reaction of the three-step enzymatic aerobic degradation of L-tryptophan to anthranilate ('anthranilate pathway'): the deformylation of N-formylkynurenine to kynurenine with release of formic acid. This oxidative degradation of tryptophan is rather rare among bacteria. Usually, the non-oxidative degradation pathway via indole and pyruvate is employed (Kurnasov et al., 2003). A KEGG database search revealed that the anthranilate pathway is not annotated in staphylococci, except for *S. sciuri*. In *S. agnetis* and *S. hyicus*, only the kynurenine formamidase is annotated (KEGG). The KFA gene in these staphylococci is unrelated to the *metICFE-mdh* operon and the amino acid similarity with *S. aureus* Mdh is low.

The fact that the anthranilate pathway is absent in *S. aureus* and that the staphylococcal KFAs (*S. sciuri*, *S. agnetis*, *S. hyicus*) are unrelated, made N-formylkynurenine an unlikely substrate for Mdh *in vivo*. However, as enzymes can exhibit a certain promiscuity regarding substrate specificity and generally evolved to catalyse a particular reaction (rather than binding a specific substrate), cleavage of NFK by Mdh *in vitro* seemed initially feasible (Copley, 2003; Jackson et al., 2010).

NFK was the first substrate to be tested with the heterologously overexpressed and purified Mdh. We used the conditions described by Díaz-Sáez et al. as starting point for our functional assays to determine Mdh's substrate(s) (Díaz-Sáez et al., 2014). Cleavage of NFK was only observed with the positive control KynB, the KFA of *P. aeruginosa*, but not Mdh indicating that NFK is not a substrate for Mdh.

None of the tested substrates (NFK, F-methionine, F-glutamic acid, pyruvate) resulted in a positive reaction in the *in vitro* assays (see **Fig. 24**). This might have several reasons: (i) the tested compounds are indeed not substrates for Mdh. This cannot be excluded. However, formylmethionine would well fit into the substrate binding pocket of Mdh (personal communication Wolfgang Kölmel, Würzburg). (ii) the used assay conditions do not facilitate Mdh activity. The used conditions with a zinc-containing buffer enabled activity of KynB and other KFAs as demonstrated in this thesis and by Díaz-Sáez and colleagues (see **Fig. 24 A**, Díaz-Sáez et al., 2014). Zinc was identified as a cofactor of Mdh in the crystal structure analysis (see **Fig. 22 B**). Therefore, at least partial activity of Mdh would be expected. (iii) the purification process (*S. aureus* Mdh isolated from *E. coli* and *S. aureus*) affected enzyme activity. Inactivity due to the purification procedure seems to be unlikely because KynB of *P. aeruginosa* purified under the same conditions was active and the purified Mdh was of sufficient quality to yield in high resolution (1.99 Å) crystal structures. (iv) the N-terminal hexa-histidine tag affected catalytic activity. According to the obtained crystal structure the N-terminal His-tag has to lie outside the actual protein 'core' as the tag is fused to an unstructured region protruding from the dimer (see **Fig. 22 A**). The positive control KynB with a similar overall tertiary structure (PDB entry 4CO9) had the tag attached as well in our experiments, suggesting that this tag does not affect enzyme activity. Díaz-Sáez and colleagues successfully performed *in vitro* assays with similarly tagged KynB as well (Díaz-Sáez et al., 2014). (v) requirement for cofactors (next to zinc) absent in the reaction buffer. Based on the hypothesis that Mdh couples methionine biosynthesis and initiator tRNA formylation (see **Fig. 21**), it had been suggested that THF might be required for Mdh activity due to a direct transfer of the formic acid onto THF to generate 10-formyl-THF. Although highly unlikely, as no THF-

binding site has been identified on Mdh and a second reaction would be required for the formyl-group transfer, Mdh activity was tested in the presence of THF. Addition of THF did not affect Mdh activity. However, requirement of other cofactors cannot be excluded. (vi) absence of *met* enzymes Mdh was shown to interact with (MetI, MetC, likely MetF). Complex formation of Mdh with *met* enzymes *in vivo* would lead to compartmentalisation and a local concentration of substrates (e.g. pyruvate as by-product of the conversion of cystathionine to homocysteine during methionine biosynthesis by MetC (see **Fig. 1**)) and products (e.g. formic acid). Therefore, interactions with other enzymes might be required for Mdh activity that are absent in the *in vitro* assays. (vii) Mdh functions just as a scaffolding protein for the *met* enzyme complex and does not have a catalytic activity itself. The fact that the *mdh* deletion mutant (Δ*mdh*) behaved like the wild type in growth experiments (see **Fig. 22 A**) speaks against this hypothesis because absence of the scaffold should have an effect on bacterial growth due to the impaired methionine biosynthesis.
In the consequence of several potential rather technical obstacles, *in vitro* assays might not be the way to continue to determine Mdh's substrate(s).

3.8.2. New strategies to find Mdh's substrate(s)

Isothermal titration calorimetry (ITC) and microscale thermophoresis (MST) could be used to screen compound libraries for binding to the active site of Mdh. Binding of a substance might point towards a certain class of molecules that could be Mdh's substrate(s). In an isothermal titration calorimeter, the temperature difference between a reference cell and a sample cell (containing the enzyme and the ligand) is (indirectly) measured. Binding of a ligand to its enzyme either causes the release or consumption of energy (heat). Without ligand, or, if the molecule added does not bind to the enzyme, no temperature change occurs (Falconer, 2016; Freyer and Lewis, 2008). Via ITC measurements binding of compounds to Mdh could be identified. Alternatively, MST could be used to screen for Mdh's substrate(s). MST is based on the detection of a temperature-induced change in fluorescence of a target, e.g. a protein, as a function of the concentration of a non-fluorescent ligand. The detectable change in fluorescence is due to two distinct effects. The change is based on (i) a 'temperature-related intensity change' (TRIC) of the fluorescent sample and (ii) on thermophoresis that is the directed motion of a molecule induced by temperature gradients (Wienken et al., 2010). Binding of a ligand can change the fluorescence intensity as well (Asmari et al., 2018). Due to the intrinsic fluorescence of tryptophan, enzyme ligand interactions can be detected label-free

employing MST (Seidel et al., 2012). ITC and MST might be suitable methods to screen for molecules binding to Mdh. Nevertheless, *in vitro* approaches might be unsuccessful due to reasons mentioned above (requirement of complex formation with *met* enzymes, etc.). Therefore, *in vivo* approaches, such as metabolomic analyses of wild type and a *mdh* deletion mutant, could provide new hints towards Mdh's substrate(s) (Meyer et al., 2010). The intra- or extracellular absence, accumulation of altered levels of a certain molecule in the mutant compared to the wild type could enable the substrate identification. The fact that Mdh is not essential, indicates that the reaction catalysed by Mdh can be executed by other enzymes as well. Therefore, rather altered levels than absence or strong accumulation of a certain molecule would be expected in the mutant. In addition to the metabolomic studies, *in silico* docking approaches could be used to characterise Mdh's substrate(s). The obtained crystal structure model (see **Fig. 22 A-C**) allows modelling of compounds into the active centre. Several programmes are available for docking studies (Gioia et al., 2017; Grosdidier et al., 2007; Macalino et al., 2015; Welch et al., 1996).

3.8.3. Interaction of Mdh with other proteins

Initial protein-protein interaction studies using the bacterial two-hybrid system suggested physical contact of Mdh with MetI and MetC of the *met* operon. The detection of X-gal positive signals only with the N-terminal fusion constructs indicates that interaction with Mdh is mediated via MetI's and MetC's C-terminus, respectively (see **Fig. 25 B**). Fusion of the cyclase fragment likely hampers proper interaction by steric hindrance. Therefore, the C-terminal region of MetI and MetC is only freely accessible with the N-terminal cyclase fusion. MetF might interact with Mdh as well, but the results were ambiguous (see **Fig. 25 B**). All interaction experiments need to be repeated to obtain statistically reliable data. In addition, experiments with the cyclase fragments 'switched' (T18 fragment fused to Mdh, T25 fragment fused to proteins of interest) need to be performed to exclude position- and fragment-based bias. Furthermore, MetE (cobalamin-independent methionine synthase), MetX (homoserine-O-acetyltransferase) and Fhs (formyl-THF-synthetase) will be investigated for interactions with Mdh. To confirm the identified interaction partners of Mdh, *in vivo* cross-linking studies could be performed. The SPINE (strep-protein-interaction experiment) procedure allows the isolation of protein complexes. The method combines strep-tag protein purification with reversible *in vivo* protein cross-linking by formaldehyde. After complex isolation, reversion of cross-linking and analysis with SDS-PAGE-(sodium dodecyl sulfate-polyacrylamide gel electrophoresis),

separated complex components can be identified by mass-spectrometry (Herzberg et al., 2007). In addition to the confirmation of interaction partners already identified by the BTHS, further proteins interacting with Mdh (or that are part of the complex) could be identified. Characterising the Mdh complex might provide new hints on Mdh's substrate(s) as well because enzymes of the complex could produce Mdh's substrate and the complex would facilitate a local concentration of the substrate.

3.8.4. Phenotypes of *mdh* mutants

The active site Mdh mutants Glu198Ser and His71Ser&Glu198Ser and the putative substrate binding mutant Phe32Trp reached a lower OD_{max} than the wild type, the deletion mutant (Δ*mdh*) and the His71Ser mutant under methionine-deprived and therewith *mdh* expression conditions (see **Fig. 23 A&B**). Surprisingly, the His71Ser mutant behaved like the wild type. Based on the crystal structure model, the proposed cleavage mechanism and high conservation of His71 among metal-dependent hydrolases, His71 is regarded as crucial for catalytic activity (see **Fig. 22 B&D**) (Bjerregaard-Andersen et al., 2014; Kurnasov et al., 2003). The amino acid exchange Glu198Ser might lead to structural rearrangements that affect substrate release in addition to its proposed effect on catalytic activity. The exchange Phe32Trp is supposed to reduce the space in the active site because the side chain of tryptophan is larger than the side chain of phenylalanine protruding into the active site. This might affect substrate binding and release as well. Crystal structure models of the His71Ser and the Phe32Trp variants could provide further insights. Unfortunately, attempts to obtain crystals and to overexpress the protein, respectively, have been unsuccessful so far.

The growth data indicate that binding and subsequent 'scavenging' of Mdh's substrate is more disadvantageous to the bacteria than absence of the enzyme (Δ*mdh*) or 'sole' catalytic inactivity (His71Ser). It is unclear, why growth of the Phe32Trp (and the His71Ser&Glu198Ser) mutants was affected under methionine-rich conditions in the experiment shown (see **Fig. 23 D**). As *mdh* is only expressed under methionine-deprived conditions, and previous experiments with the other Mdh variants did not show marked differences to the wild type (see **Fig. 23 B**), no difference in growth behaviour was expected under +MET conditions in this experiment as well. For the Phe32Trp mutant the growth experiment has only been performed twice, in contrast to the wild type, Δ*mdh*, His71Ser, Glu198Ser and His71Ser&Glu198Ser variants, for which the experiments have been performed four to seven times. To obtain more reliable data, the growth experiment for Phe32Trp should be repeated. Overall, the observed effects of *mdh*

mutations were rather mild (lower OD_{max}) (Glu198Ser, His71Ser&Glu198Ser, Phe32Trp) to non-detectable (Δ*mdh*, His71Ser) under the investigated conditions (chemically defined medium -MET, 37° C). Nevertheless, it cannot be excluded that, e.g. under infection conditions Mdh plays an important role in the cell that would explain the high conservation among staphylococci as well (see **Fig. 26**).

3.8.5. High conservation of Mdh among staphylococci

The high conservation of *mdh*/Mdh on nucleotide sequence and amino acid level among staphylococcal species and the localisation as last gene of the methionine biosynthesis operon (see **Figs. 26**, **27** and **Tab. 4**) strongly suggest a link to the methionine metabolism and importance of Mdh (under certain conditions) for the bacterium. Interestingly, the distance between the stop codon of *metE* and the start codon of *mdh* varies among staphylococcal species, ranging from 16 to 224 bp (see **Fig. 27**). This might indicate that *mdh* has 'joined' the *met* operon during evolution in a common ancestor of the staphylococcal species. Over time, either deletions or insertions of the region between *metE* and *mdh* might have led to the different distances. As the intergenic region could have an influence on transcription and translation, co-transcription and expression of *mdh* in the staphylococcal species, other than *S. aureus*, would need to be verified by, e.g. Northern and Western blot analyses. To efficiently detect an *mdh* transcript, species-specific probes might be necessary because of certain nucleotide differences among species. However, due to the high amino acids sequence similarity a single antibody specific to all Mdhs seems feasible.

3.8.6. Potential cleavage mechanism of Mdh

The crystal structure revealed similarities of Mdh with the isatin hydrolase of *Labrenzia aggregata* (PDB entry 4MD8) (that has been used to solve Mdh's crystal structure) and with the kynurenine formamidases of *Pseudomonas aeruginosa* (PDB entry 4COB), *Bacillus anthracis* (PBD entry 4CO9) and *Burkholderia cenocepacia* (PDB entry 4COG) on the level of tertiary structure. Wolfgang Kölmel and Yesid Ramiréz identified residues His71 and Glu198 as the crucial amino acids of the active site and the residues Gln61, His65, Asp67, Asp182 and Glu210 to be part of the active centre as well (see **Fig. 22 B**). His65, Asp67 and His71 are conserved among Mdh, KFA of *P. aeruginosa* and isatin hydrolase (IH) of *L. aggregata*, Glu198 of Mdh corresponds to a histidine in KFA and IH. This histidine is involved in the coordination of the second zinc in KFAs. For KFAs a binuclear Zn^{2+} catalytic

centre has been proposed (Díaz-Sáez et al., 2014). In Mdh only a single zinc is present (see **Fig. 22 B**). Only after the determination of Mdh's substrate the proposed cleavage mechanism can be verified.

4. Conclusion and Perspective

The organisation of the methionine biosynthesis genes (matching the order of the synthesis steps) in a single operon in combination with the hierarchical regulation (CodY, T-box riboswitch, RNA decay) are unique to staphylococci. The absence of methionine recycling pathways together with the high metabolic costs of methionine *de novo* synthesis seem to require this complex regulation.

The methionyl-tRNA-specific T-box riboswitch (‘*met* leader’) upstream of the *metICFE-mdh* operon is extraordinary in a number of ways: it is unusually long due to the insertion of three additional stems, its Terminator stem exceeds the average length which, in turn, enables RNase III cleavage uncommon in T-box riboswitches. Cleavage of the Terminator stem initiates degradation of the *met* leader and likely of the *met* mRNA. mRNA decay appears to be an additional level of *met* operon regulation as the stability varying over the length of the transcript has a direct influence on protein (expression) levels. Revealing the further details of this process, especially regarding the mechanisms that stabilise the *met* mRNA towards the 3’-end, are interesting future experimental tasks.

Dysregulation of *met* leader control revealed methionine-deprivation to be a strong selection pressure. The thorough investigation of ‘ON’ and ‘OFF’ *met* leader mutations and their influence on fitness and virulence will be an important future assignment with regard to utilisation of the *met* leader as a staphylococcus-specific drug target. Employing the *met* leader as screening system for novel T-box riboswitch-targeting compounds will initialise an exciting new direction of (MET-)T-box riboswitch research.

The striking association of *mdh* with methionine biosynthesis genes in several bacterial species and the high conservation of *mdh* among staphylococci as part of the *met* operon strongly suggests the involvement of Mdh in methionine metabolism including translation initiation. Co-transcription and -expression of *mdh* with the *met* operon in *S. aureus* were demonstrated, confirming the predicted association with the operon. The obtained crystal structure of Mdh (heterologously overexpressed in *E. coli*) revealed its potential substrate cleavage mechanism involving proton abstraction and a nucleophilic attack. A challenging future task will be the determination of Mdh’s substrate(s).

5. Materials and Methods

5.1. Materials

5.1.1. Technical instruments

Table 5. List of instruments and devices used.

Instrument/device	Manufacturer
ÄKTA protein purification system	GE Healthcare, ÄKTA pure
Biomolecular imager	GE Healthcare, Typhoon™ FLA 7000 laser scanner
Centrifuge	Thermo Scientific, Heraeus Pico 21
Centrifuge	Eppendorf, Centrifuge 5418
Centrifuge	Kendro, Biofuge pico
Centrifuge	Heraeus, Multifuge X1R
Centrifuge	Heraeus, Multifuge X3R
Centrifuge rotor (swing-out)	ThermoScientific, TX-400
Centrifuge rotor (swing-out)	ThermoScientific, BIOShield™ 1000A
Centrifuge, cooling	Eppendorf, Centrifuge 5424R
Electroporator	Equibio, EasyjecT Prima
Freezer, -80°C	ThermoScientific, Hera freezer
Fridge-freezer combinations	Privileg
Fume hood	Renggli Laboratory Systems GmbH, ENTA120
Geiger counter	ThermoScientific, Mini 900 Ratemeter
Gel dryer, radioactivity lab	Bio-Rad, Model 583
Gel electrophoresis chambers, horizontal (for agarose gels)	Bio-Rad
Gel electrophoresis chambers, vertical (for PAA gels)	Peqlab Biotechnologie GmbH
Gel electrophoresis chambers, vertical, long (for in-line probing gels)	C.B.S. Scientific Co., Adjustable Nucleic Acid Sequencing Unit, Model #SG-400-20
Heatable magnetic stirrers	Heidolph, MR3001, Phoenix, RSM-10HS
Heating and cooling block	Bioer, Thermocell Cooling&Heatingblock HB-202
Heating/cooling block with shaking function	Serva, ThermoMix500
Hybridisation ovens	UVP, HB-1000 Hybridizer, Hybaid, Mini 10
Image eraser	GE Healthcare Life Sciences, FLA Image Eraser

Table 5. continued.

Instrument/device	Manufacturer
Imaging plate (storage phosphor screen)	Fujifilm, BAS-IP SR 2040 E (20x40 cm)
Incubator, static 30°C	Heraeus Instruments, Function line
Incubator, static 37°C	Kendro Laboratory Products, HERAcell
Micro centrifuge	Heathrow Scientific® LLC, SPROUT™
Microbiological safety cabinet class II	ThermoScientific, SAFE 2020
Microplate reader	TECAN, infinite F200Pro
Microwave	Privileg
MilliQ system	TKA (Thermo Fisher Scientific), GenPure XCad Dispenser
NanoDrop (spectrophotometer)	ThermoScientific, NanoDrop 2000
pH adjustment	WTW, Inolab pH 720
Pipette controller	Brand, Accu-jetR Pro
Pipettes (100-1000 µl, 20-200 µl, 2-20 µl, 0.5-10 µl, 0.1-2.5 µl)	Brand, Transferpette S
Power supplies	Peqlab Biotechnologie GmbH, Bio-Rad
Rapid Downward Transfer System	Whatman, TURBOBLOTTER™
Scales	Kern & Sohn GmbH, PFB
Shaker	Edmund Bühler GmbH, SM 30, TH 30 control unit
Shaker, orbital shaker with universal mount (RNA assays, protein experiment)	IKA, HS 501 DIGITAL SHAKER
Sonificator, Sonoplus HD70	Bandelin
Special accuracy weighing machine	Chyo Balance Corp. Japan, JL-180
Spectrophotometer	Amersham Biosciences, Ultrospec 3100 pro
Thermocycler	Biometra, T3 Thermocycler
UV chamber, Crosslinker	Peqlab Biotechnologie GmbH
UV imaging system for gel documentation	INTAS, INTAS® GDS
Vortexer	GLW
Waterbath (for RNA isolation)	Polyscience
Wet Blotting System for Northern Blotting (PAA Gels)	Peqlab Biotechnologie GmbH, PerfectBlue Tank Electroblotter WebM

5.1.2. Glass/plastic ware and consumables

Table 6. List of laboratory ware used.

Glass and plastic ware, consumables	Manufacturer and Cat.-No.
Amicon Ultra-15 10 kDa flacon for protein concentration	Merck Millipore, Amicon Ultra-15, PLGC Ultracel-PL Membrane, 10 kDa (UFC90100)
Blotting paper	Whatman, 3mm Chr, 460x570 mmCat-No. 3030-917
Blotting paper, thick, for use with TURBOBLOTTER™	MACHEREY-NAGEL GmbH & Co. KG, MN440B, 580x600 mm, REF: 742125
Bottle (500 ml, single-use) with 0.22 µm filter system	Corning, 430769
Cuvettes (single-use), 1.5 ml	Brand, 759015
Dialysis tubing, diameter 29 mm	SERVA Electrophoresis GmbH, SERVAPOR®, MWCO 12000 - 14000; pore diameter ca. 25 Å, 44146
Electroporation cuvettes, long electrode, red lid, 1 mm gap	Cell Projects Ltd, EP-201
Erlenmeyer flasks, DURAN® or ILMABOR TGI, various volumes	A. Hartenstein, others
Filter membrane, 0.2 µm, non-pyrogenic	Pall Corporation, Acrodisc® 32mm Syringe Filters with 0.2 µM Supor® Membrane, REF 4652
Filter membrane, 0.45 µm, non-pyrogenic	Pall Corporation, Acrodisc® 32mm Syringe Filters with 0.45 µM Supor® Membrane, REF 4654
Filtertips, low binding (1000 µl)	Biozym, SafeSeal SurPhob VT0260
Filtertips, low binding (20 µl)	Biozym, SafeSeal SurPhob VT0220
Filtertips, low binding (200 µl)	Biozym, SafeSeal SurPhob VT0240
Glass bottles, various volumes	Schott
Inoculation loops	A. Hartenstein, IO01
Lysing matrix E tubes 2 ml	MP Biomedicals, Lysing Matrix E
Lysing matrix E tubes 50 ml	MP Biomedicals, Lysing Matrix E
MASTERBLOCK® 96 well, 2 ml	Greiner Bio-One, 780270
Micro spin columns, G-25	GE Healthcare, Illustra MicroSpin G-25
Micro spin columns, G-50	GE Healthcare, Illustra MicroSpin G-50
Microplate, 96 well, flat-bottom, transparent, sterile with lid	Greiner Bio-One, Cellstar® (F-form), Cat.-No. 655180
Nylon membrane	GE Healthcare, Hybond-XL (20 cm ~ 3 m); RPN203S
PCR tubes and caps, strips of 8	BRAND GMBH + CO KG, Brand® #781327
Petri dishes, 92 mm diameter	Nerbe Plus, #09-031-0000
Petri dishes, square, 120x120x17 mm (for BTHS Assay)	Greiner, Z617679
Quartz cuvettes (for Mdh in vitro assays)	Hellma®, Typ 104-QS SA 10 mm, Quarzglas Suprasil

Table. 6 continued.

Glass and plastic ware, consumables	Manufacturer and Cat.-No.
Phase Lock Gel (PLG) tubes, 'heavy', 2ml	5 Prime, #2302830
Pipette tips 1000 µl, neutral	Sarstedt, REF 70.762
Pipette tips 20 µl, neutral	Sarstedt, REF 70.1116
Pipette tips 200 µl, neutral	Sarstedt, REF 70.760.002
Pipettes, serological, sterile (10 ml)	Greiner Bio-One, Cellstar® #607 180
Pipettes, serological, sterile (25 ml)	Greiner Bio-One, Cellstar® #760 180
Reaction tubes, 1.5ml	Sarstedt, #72.690.001
Reaction tubes, 2.0ml safe lock	Sarstedt, #72.695.500
Scalpel, single-use	B. Braun Melsungen AG,
Screw cap micro tube, 2 ml	Sarstedt, REF 72.694.006
Steritop, 500 ml	Sarstedt, 83.1823.101
Syringe, single-use, 2 ml, 5 ml, 10 ml	B. Braun Melsungen AG, Injekt®
Syringe, single-use, 50 ml	BD Plastipak
Test tubes, glass with aluminum cap (for overnight cultures)	A. Hartenstein GmbH,RG14, ALK3
Tube, non-pyrogenic (15 ml)	Sarstedt, REF 62.554.502
Tube, non-pyrogenic (50 ml)	Sarstedt, REF 62.547.254

5.1.3. Chemicals, reagents and size markers

Table 7. List of chemicals, reagents and size markers used.

Chemicals, reagents and size markers	Manufacturer/Brand
10 mM dNTP mix (for cDNA synthesis)	ThermoScientific, R0191
19:1 acrylamide/bis-acrylamide solution (Rotiphorese® Gel 40 (19:1)) (for RNA work)	Carl Roth GmbH + Co. KG
Acetic acid (100 %)	Carl Roth GmbH + Co. KG
Agarose, peqGOLD universal agarose	Peqlab
Amino acids (L-form, unlabeled) for CDM	AppliChem GmbH, Carl Roth GmbH + Co. KG, Merck, Sigma-Aldrich Chemie GmbH
Ammonium persulfate (APS)	AppliChem GmbH
Ammonium-chloride (NH_4Cl)	Carl Roth GmbH + Co. KG
Aqua-Clean, water bath preservative	A. Hartenstein GmbH
Bovine Serum Albumin (BSA, 1 mg/ml))	ThermoScientific
Calcium chloride dihydrate ($CaCl_2*2H_2O$)	Carl Roth GmbH + Co. KG
Chloroform	Carl Roth GmbH + Co. KG
cOmplete™, EDTA-free Protease Inhibitor Cocktail (tablets)	Roche
Diethyl dicarbonate (DEPC)	Carl Roth GmbH + Co. KG
Dimethyl sulphoxide (DMSO)	Sigma-Aldrich Chemie GmbH
Disodium hydrogen phosphate dihydrate ($Na_2HPO_4*2H_2O$)	Carl Roth GmbH + Co. KG
dNTP set, 100 mM solutions	Invitrogen
EDTA 0.5 M, pH 8.0 (for RNA work)	Ambion

Table 7. continued.

Chemicals, reagents and size markers	Manufacturer/Brand
Ethanol	Carl Roth GmbH + Co. KG
Ethanol (for RNA work)	Carl Roth GmbH + Co. KG
Formaldehyde solution 37%	Sigma-Aldrich Chemie GmbH
Formyl-glutamic acid	Synchem UG & Co. KG, BIO039
Formyl-methionine (N-formyl-L-methionine)	Sigma-Aldrich Chemie GmbH, F3377
GeneRuler 1 kb Plus DNA ladder	ThermoScientific, SM1331
D(+)-Glucose monohydrate	Carl Roth GmbH + Co. KG
Glycerol	Sigma-Aldrich Chemie GmbH
GlycoBlue™ Coprecipitant (15 mg/ml)	Ambion
Hydrochloric acid 37% (HCl)	Carl Roth GmbH + Co. KG
Imidazole	Sigma-Aldrich Chemie GmbH, I0125
Isoamyl alcohol	Carl Roth GmbH + Co. KG
Isopropanol (2-Propanol)	Sigma-Aldrich Chemie GmbH, I9516
Isopropyl-β-D-1-thiogalactopyranoside (IPTG)	Carl Roth GmbH + Co. KG, 2316.3
KH2PO4	Carl Roth GmbH + Co. KG
L-arginine HCl (^{13}C,^{15}N) (labelled, 'heavy')	Silantes GmbH
L-lysine HCl (^{13}C, ^{15}N) (labelled, 'heavy')	Silantes GmbH
Magnesium chloride hexahydrate ($MgCl_2*6H_2O$)	Carl Roth GmbH + Co. KG
Magnesium sulfate ($MgSO_4$)	Sigma-Aldrich Chemie GmbH
Midorigreen	Nippon Genetics Europe GmbH
MOPS (4-Morpholinepropanesulfonic acid)	Carl Roth GmbH + Co. KG
N-formyl-L-kynurenine (NFK)	Santa Cruz Biotechnology, Inc., sc-490237
Nickel(II) chloride hexahydrate ($NiCl_2*6H_2O$)	Sigma-Aldrich Chemie GmbH, N6136
Nicotinamide adenine dinucleotide (NAD)	Sigma-Aldrich Chemie GmbH, 10127965001
NTP set, 100 mM solutions	ThermoScientific
Phenol/chloroform/isoamylalcohol solution (25:24:1) (Roti®-Aqua-P/C/I, for RNA work)	Carl Roth GmbH + Co. KG
Potassium acetate	Carl Roth GmbH + Co. KG
Potassium chloride (KCl)	Carl Roth GmbH + Co. KG
Potassium dihydrogen phosphate (KH_2PO_4)	Carl Roth GmbH + Co. KG
Prestained Protein Ladder 10-180 kDa	ThermoScientific
pUC Mix Marker, 8	Fermentas
Pyrimidine	Sigma-Aldrich Chemie GmbH, 131695
RiboRuler High Range RNA Ladder	ThermoScientific, SM1821
RNA Gel Loading Dye (2x)	ThermoScientific
RNase-ZAP® (for RNA work)	Invitrogen
Roti® Hybri Quick	Carl Roth GmbH + Co. KG
Roti®-Aqua Phenol (for RNA work)	Carl Roth GmbH + Co. KG

Table 7. continued.

Chemicals, reagents and size markers	Manufacturer/Brand
D(+)-Saccharose (D-Sucrose)	Carl Roth GmbH + Co. KG
SDS (sodium dodecyl sulfate), ultra-pure	Carl Roth GmbH + Co. KG
SDS, 20% solution (for RNA work)	Ambion
Sodium acetate (3 M), pH 5.5 (for RNA work)	Ambion
Sodium chloride (NaCl)	Carl Roth GmbH + Co. KG
Sodium hydroxide, in pellets	Carl Roth GmbH + Co. KG
Sodium perchlorate ($NaClO_4$)	Carl Roth GmbH + Co. KG
Sodium-pyruvate	Sigma-Aldrich Chemie GmbH, P2256
TEMED (tetramethylethylendiamin)	Carl Roth GmbH + Co. KG
Tetrahydrofolate (THF)	Sigma-Aldrich Chemie GmbH, T3125
Trace Metal Mix A5 with Co	Sigma-Aldrich Chemie GmbH, 92949
Tris 1M, pH 8.0 (for RNA work)	Ambion
TRIS hydrochloride (Tris-HCl)	Carl Roth GmbH + Co. KG
trisodium citrate	Carl Roth GmbH + Co. KG
Urea	Carl Roth GmbH + Co. KG
Vitamins for CDM	AppliChem GmbH, Merck, Sigma-Aldrich Chemie GmbH
Water (ddH_2O), RNase-free (for RNA work)	Ambion
X-gal (5-Bromo-4-chloro-3-indolyl-β-D-galactopyranoside)	Carl Roth GmbH + Co. KG , 2315.4
Zinc chloride ($ZnCl_2$)	AppliChem GmbH, A2076

5.1.4. Buffers and solutions

Table 8. List of buffers and solutions used.

Buffer/solution	Composition/Manufacturer
0.1 M $CaCl_2$ solution	5.55g $CaCl_2$ ddH_2O ad 500 ml
0.1 M $CaCl_2$/15 % (v/v) glycerol solution	0.22 g CaCl2 3.49 ml 86% glycerol ddH_2O ad 20 ml
24:1 chloroform/isoamyl alcohol mix	23 parts chloroform 1 part isoamyl alcohol
2x colourless loading dye	10 M urea 1.5 mM EDTA (pH 8.0)
2x In-line reaction buffer (for 1 ml)	100 µl 1 M Tris (pH 8.0) 400 µl 100 mM $MgCl_2$ 200 µl 1 M KCl 300 µl RNase-free water
30:1 ethanol/sodium acetate mix (for RNA work)	30 or 29 parts of 100 % ethanol 1 part 3 M sodium acetate (pH 5.5)

Table 8. continued.

Buffer/solution	**Composition/Manufacturer**
Alkaline hydrolysis buffer (for in-line probing)	Ambion, supplied with RNase T1 (AM2283)
'Buffer I' (for plasmid preparation)	2.5 ml 1 M Tris (pH7.5) 1 ml 0.5 M EDTA ddH_2O ad 50 ml + 1 µl RNase A per 1 ml 'Buffer I'
'Buffer II' (for plasmid preparation)	200 µl 10 N NaOH 1 ml 10 % (w/v) SDS ddH_2O ad 10 ml
'Buffer III' (pH 5.5) (for plasmid preparation)	29.45 g potassium acetate ddH_2O ad 100 ml (pH adjusted with acetic acid)
LEW buffer (pH 8.0)	50 mM NaH_2PO_4 0.3 M NaCl
MOPS buffer (10x stock) (pH 7.0):	41.85 g MOPS 6.8g sodium acetate*3H_2O 20 ml EDTA (0.5 M) DEPC ddH_2O ad 1 l (pH adjusted with DEPC-NaOH)
Na_2HPO_4/NaH_2PO_4 protein buffer (pH 7.4)	774 ml of 0.1 M Na_2HPO_4 226 ml of 0.1 M NaH_2PO_4
PBS (10x stock) (pH7.4)	80 g NaCl 2g KH_2PO_4 2g KCl 7.12 gNa_2HPO_4*2H_2O ddH2O ad 1 l (pH adjusted with NaOH)
Phage buffer	LB medium with 5 mM $CaCl_2$
RNA elution buffer (for 10 ml)	333,3 µl 3M sodium acetate (pH 5.5) 100 µl 10 % (w/v) SDS solution 200 µl 0.5 M EDTA 9,366.7 µl RNase-free water
RNA Sequencing buffer (for in-line probing)	Ambion, supplied with RNase T1 (AM2283)
RNA Stop Mix (95 % ethanol, 5 % Roti-Aqua-Phenol) (for 80 ml)	76 ml 100 % EtOH 4 ml Roti-Aqua-Phenol
SDS solution (10 % (w/v)) (for 14 ml)	7 ml 20 % (w/v) SDS solution 7 ml DEPC ddH_2O
SSC buffer (20x stock) (pH7.0)	175.3 g NaCl 88.2 g tri-sodium citrate*2H_2O Purified ('VE') H_2O ad 1 l (pH adjusted with HCl)
TAE buffer (50x stock)	242 g Tris 57.1 ml acetic acid 100 ml 0.5 M EDTA Purified ('VE') H_2O ad 1 l

Table 8. continued.

Buffer/solution	Composition/Manufacturer
TBE buffer (10x stock)	108 g Tris base 55 g boric acid 20 mM EDTA (pH 8.0) Purified ('VE') H_2O ad 1 l
TE buffer	5 ml 1 M Tris (pH8.0) 1 ml 0.5 M EDTA Purified ('VE') $H2_O$ ad 500 ml
TE buffer (for 40 ml, RNA work)	400 µl 1 M Tris (pH8.0) 80 µl 0.5 M EDTA 39.52 ml DEPC ddH_2O
TS buffer	0.5 ml 1M Tris (pH 7.5) 12.5 g saccharose ddH_2O ad 50 ml

5.1.5. Commercial kits

Table 9. List of kits used in this work.

Kit	Manufacturer	Purpose
Amersham Megaprime DNA Labeling System	Amersham, GE Healthcare, UK (RPN1606)	radioactive labelling of DNA
innuPREP PCRpure Kit	Analytikjena (Endress+Hauer Company)	clean-up of PCR products
MEGAscript® T7	ThermoFisher Scientific Inc. (Ambion; AM1333)	*in-vitro* transcription of RNA
NucleoSpin® Gel and PCR Clean-up kit	MACHEREY-NAGEL GmbH & Co. KG (REF 740609.250)	clean-up of PCR products
NucleoSpin® Plasmid	MACHEREY-NAGEL GmbH & Co. KG (REF 740588.250)	plasmid isolation
pGEM®-T Easy Vector System I	Promega, USA (#A1360)	cloning of PCR products
Protino® Ni-TED 2000 Packed Columns Kit	MACHEREY-NAGEL GmbH & Co. KG (REF 745120)	Affinity chromatography of His-tagged proteins
QuickLigation™ Kit	New England BioLabs (M2200S)	Cloning (vector ligation)
TOPO™ XL-2 Complete PCR Cloning Kit, with One Shot™ OmniMAX™ 2 $T1^R$ Chemically Competent *E. coli* Cells	ThermoFisher Scientific Inc. (K8050-10, Invitrogen™)	5' RACE, cloning of extra-long PCR products

5.1.6. Enzymes

Table 10. List of enzymes used.

Enzyme	Manufacturer
Alkaline Phosphatase, Calf Intestine (CIP, 10 U/µl)	New England Biolabs, M0290
Antarctic Phosphatase (AnP, 5 U/µl)	New England Biolabs, M0289
DNase I (RNase-free)	Ambion, AM2222
DNase I, recombinant (rDNase I, 2 U/µl)	Ambion, AM2235
DpnI (20 U/µl)	New England Biolabs, R0176
DpnI FD	ThermoScientific, FD1703
DreamTaq DNA Polymerase (5 U/µl)	ThermoScientific, EP0703
Formate-Dehydrogenase from *Candida boidinii* (~50 U/ml)	Sigma-Aldrich Chemie GmbH, 47753-1ML-F
Lysostaphin (2 mg/ml)	Genmedics GmbH
Phusion High-Fidelity DNA Polymerase (2 U/µl)	ThermoScientific, F530S
Platinum SuperFi Green PCR Master Mix (part of the TOPO™ XL-2 Complete PCR Cloning Kit)	ThermoScientific
Proteinase K (from *Tritirachium album*, chromatographically purified lyophilized 30 mAnson-U/mg)	Merck Millipore, 1.24568
Restriction enzymes (XhoI)	New England Biolabs
Restriction enzymes Fast Digest (BamHI BglII, KpnI, NdeI, NotI, Pfl23II, XbaI)	ThermoScientific
RevertAid Premiumn Reverse Transcriptase (200 U/µl)	ThermoScientific, EP0442
RiboLock RNase Inhibitor (40 U/µl)	ThermoScientific, EO0382
RNA 5' Pyrophosphohydrolase (RppH, 5 U/µl)	New England Biolabs, M0356S
RNase A (10 mg/ml)	ThermoScientific, EN0531
RNase T1 (1 U/µl)	Ambion, AM2283
SUPERase*In™ RNase Inhibitor	Ambion, Invitrogen, AM2694
T4 DNA Ligase (400 U/µl)	New England Biolabs, M0202
T4 Polynucleotid Kinase (T4 PNK, 10 U/µl)	ThermoScientific, EK0031
T4 RNA Ligase (10 U/µl)	ThermoScientific, EL0021
T7 RNA Polymerase (20 U/µl)	ThermoScientific, EP0111

5.1.7. Oligonucleotides

Table 11. List of oligonucleotides used.

Purpose	Template	Name	Sequence
General primers			
PCR and sequencing pGEM-T-easy, pCR-XL-2-TOPO		M13-Fow	GTAAAACGACGGCCAG
		M13-Rev	CAGGAAACAGCTATGAC
PCR and sequencing pBASE constructs		pBASE_MCS_F	GATGCCTCAAGCTAGAGAGTCATTACC
		pBASE_MCS_R	CCATGTATTCACTACTTCTTTCAAACTCTCTC
pEB01 constructs		pCN33_seq_for	CTGATTCTGTGGATAACCGTATTACC
		pCN47_seq_rv	CTCGAAAATAATAGAGGGAAAATCAGT
cRACE			
met leader	-	FW144	CACTCCAAGGCCATTTTCAA
	-	FW145	GTGATAATTGTTCAGTAAGCAT
metI	-	FW156	CCTGTCGATTGTCCTAGTTT
	-	FW157	CACGTACTAAAAATCCTACA
whole *met* operon (3'-UTR determined)	-	FW149	GCGATGTTGAAGTGTGTACGTTT
	-	DSt012	CGTGCGCATATAGAAGCAT
5'RACE			
		5' RACE **RNA** adapter	CUAGUACUCCGGUAUUGCGGUACCCUUGUACGCCUGUUUUAUA
		5' RACE RNA adapter primer	GTATTGCGGTACCCTTGT
metI	-	FW200	CGTGGCTGAATGTAAGACTATA
	-	Sa_lgsm02-Lext-Rev	TCAGCACCTTCTGCTAGTGGT
metF	-	FW149	GCGATGTTGAAGTGTGTACGTTT
	-	FW161	CGGTGTGATAATGTATAAACCATT

Table 11. continued.

Purpose	Template	Name	Sequence
Templates *in vitro transcription* for in-line probing			
T7 *met* leader	pJC1_tRNAi_ deletion	FW088	TTAACTAATACGACTCACT ATAGGGTCTTATAACAGTT TAATGAAACGTAAAC
		Sa.R_met-sRNA	GAAAAAATAAAAAAAGCT TCCGTCCTTCG
T7 short *met* leader	pJC1_tRNAi_ deletion	FW130	TTAACTAATACGACTCACT ATAGGGATTCTTTACGCAC GATTTTTTGTT
		Sa.R_met-sRNA	GAAAAAATAAAAAAAGCT TCCGTCCTTCG
T7 short *met* leader Ter_destab	pBASE_Ter_d estab	FW130	TTAACTAATACGACTCACT ATAGGGATTCTTTACGCAC GATTTTTTGTT
		FW159	GAAAAAATAAAAAAAGAG TCGTTGAATCGTCA
T7 short *met* leader Ter_mutated_1	2.2 kb overlap PCR *met* leader Ter_mutated_1 fragment	FW130	TTAACTAATACGACTCACT ATAGGGATTCTTTACGCAC GATTTTTTGTT
		FW169	GAAAAAATAAAAAAAGGA TCGTTGCCTCGT
T7 short *met* leader Ter_mutated_2	pBASE_Ter_ mutated_2	FW130	TTAACTAATACGACTCACT ATAGGGATTCTTTACGCAC GATTTTTTGTT
		FW211	GAAAAAATAAAAAAAGCT TCCGTGCTTCGT
T7 short *met* leader Ter_mutated_3	pBASE_Ter_ mutated_3	FW130	TTAACTAATACGACTCACT ATAGGGATTCTTTACGCAC GATTTTTTGTT
		FW212	GAAAAAATAAAAAAAGCT TCCGTGCCTCGT
T7 short *met* leader Ter_mutated_4	pBASE_Ter_ mutated_4	FW130	TTAACTAATACGACTCACT ATAGGGATTCTTTACGCAC GATTTTTTGTT
		FW213	GAAAAAATAAAAAAAGCT TCCTGGCTTCGT

Table 11. continued.

Purpose	Template	Name	Sequence
ds DNA probes			
met leader	Newman	Sa_lgsm02_Fow	ATGTATTCTAAATGAGTCAGACAACC
		Sa_lgsm02_Rev	CCGTCCTTCGTACCCGAATGA
metI	Newman	Sa_lgsm02-Lext_Fow	ACATCAAGTGGAATGTCAGCCA
		Sa_0431_R	CTATTGGTGAAAGTGTTGCGCCA
metI 5’	Newman	FW137	
		Sa_0431-R_RT	CGAATGATGCAATACCATGCTCA
metC	Newman	Sa_0430_F	GCTCGAACAAATCGAGGGTGCCA
		Sa_0430_R	ACGAAAGCCAATAACGGCAC
metC 3’	Newman	FW140	GCCTCCTTTAATGCGTATTTGAT
		FW141	GCTGATGAGTCTAAAGCACAA
metF 3’	Newman	FW138	CTCCTTGTGAGCAGTAATAGATT
		FW139	GGTATTAACACTGACGGTGAT
metE	Newman	Sa_metE_F	TGATGGTCGTAATGTATGGGCA
		Sa_metE_R	CGTTTGTTCTTCCAATCTGCACG
mdh	Newman	FW051	GCAACTTGGGTTGATTTAACGCAT
		FW052	GCCACGAGTTGGTAATTGATCTA
Cloning *met* leader mutants			
pBASE_*met* leader+1kb flanking (pFW001)	Newman	FW099	AGTATAAGATCTCGCTCAATGCGTAAATGCAAAGTT
		FW100	GTGATAAGATCTCCTACGATTTAATTGTTCAA TTA
pBASE_ΔAntiTer&Ter	pFW001	DSt003	CTTATAGGAGGGTCTTAATATGAAGGATACA
		DSt004	GTTATTCCATCGCTGAAATAACCTTATTCAGTA

Table 11. continued.

Purpose	Template	Name	Sequence
Cloning *met* leader mutants (continued)			
1.7 kb fragment pBASE_Ter_destab	pFW001	Sa_Ter401_out 1	CATTCCTTGACGATTCAACG ACTCTTTTTTTATTTTTTC
		FW107	GGCGAGTTACATGATCCCCC ATGTTGT
7.1 kb fragment pBASE_Ter_destab	pFW001	Sa_Ter427_out 2	AAAGAGTCGTTGAATCGTCA AGGAATGAATCGGATAAAA AG
		FW108	GGGGGATCATGTAACTCGCC TTGAT
800 bp 3' fragment *met* leader Ter_mutated_1	pBASE_T er_destab	FW099	AGTATAAGATCTCGCTCAAT GCGTAAATGCAAAGTT
		FW166	GGGATTCATTCCCTGACGAG GCAACGATCCTTTTTTT
1.4 kb 5' fragment *met* leader Ter_mutated_1	pBASE_T er_destab	FW100	GTGATAAGATCTCCTACGAT TTAATTGTTCAATTA
		FW165	CGTCAGGGAATGAATCCCAG AAAAAGCAACAATCCTTATG TT
2.2 kb overlap PCR *met* leader Ter_mutated_1 fragment	800 bp 3' fragment *met* leader Ter_mutat ed_1 and 1.4 kb 5' fragment *met* leader Ter_mutat ed_1	FW099	AGTATAAGATCTCGCTCAAT GCGTAAATGCAAAGTT
		FW100	GTGATAAGATCTCCTACGAT TTAATTGTTCAA TTA
1.7 kb fragment pBASE_Ter_mutated _2	pFW001	FW204	GCTTTTTATCCGATTCATTCG GGTACGAAGCACGGAA
		FW107	GGCGAGTTACATGATCCCCC ATGTTGT
7.1 kb fragment pBASE_Ter_mutated _2	pFW001	FW203	GCTTCGTACCCGAATGAATC GGATAAAAAGCACGAAA
		FW108	GGGGGATCATGTAACTCGCC TTGAT

Table 11. continued.

Purpose	Template	Name	Sequence
Cloning *met* leader mutants (continued)			
1.7 kb fragment pBASE_Ter_mutated_3	pFW001	FW206	GCTTTTTATCCGATTCATTCGGGTACGAGGCACGGAA
		FW107	GGCGAGTTACATGATCCCCCATGTTGT
7.1 kb fragment pBASE_Ter_mutated_3	pFW001	FW205	GCCTCGTACCCGAATGAATCGGATAAAAAGCACGAAA
		FW108	GGGGGATCATGTAACTCGCCTTGAT
1.7 kb fragment pBASE_Ter_mutated_4	pFW001	FW208	TGGCTTTTTATCCGATTCATTCGGGTACGAAGCCAGGAA
		FW107	GGCGAGTTACATGATCCCCCATGTTGT
7.1 kb fragment pBASE_Ter_mutated_4	pFW001	FW207	TGGCTTCGTACCCGAATGAATCGGATAAAAAGCCAGAAA
		FW108	GGGGGATCATGTAACTCGCCTTGAT
pBASE_SC2_metleader+1kb flanking	pFW001	DSt001	GCGAAACATAAGCTTTCGTCCTTTTTATCC
		DSt002	CCTTTATTTGTTATTCCATCGCTGAAATAACC
pBASE_SC4_metleader+1kb flanking	pFW001	Sa-TB-gg361cc_1out	AAAGGTCCTACCGCGAAACATAAGC
		Sa-TB-gg361cc_2out	TTCGCGGTAGGACCTTTATTTGTTATTCCA
pBASE_SC5_metleader+1kb flanking	pFW001	Sa-TB_cc365gg_1out	AAAGGTGGTAGGGCGAAACATAAGC
		Sa-TB-cc365gg_2out	TTCGCCCTACCACCTTTATTTGTTATTCCATCG
pBASE_SC7_metleader+1kb flanking	pFW001	Sa-TB-G362C_1out	AAAGGTCGTACCGCGAAACATAAGC
		Sa-TB-G362C_2out	TTCGCGGTACGACCTTTATTTGTTATTCCA

Table 11. continued.

Purpose	Template	Name	Sequence
Cloning pEB01-met leader-metI			
met leader-metI sequence (from -35 until nt 215 of metI)	Newman	FW198	AATTATGGATCCCCACTTGA TGTAGCGAATGATGCAATA
		FW199	AATTATGGATCCGTTGACAA ATCTTTTTTTACTCTGTAA
Cloning pJC1_tRNAi_deletion			
Cloning 4.5 kb fragment pJC1_tRNAi_deletion	pJC1-MetTBox-metleader-cl-pR-eYFP	FW19	GGGGCGTACGAAAACGCTA CGTTCCAAAATGTGG
		FW26	GCGATCGCGTATTTCGTCTC GCTCAGGCGCAAT
Cloning 5.2 kb fragment pJC1_tRNAi_deletion	pJC1-MetTBox-metleader-cl-pR-eYFP	FW27	GCCTGAGCGAGACGAAATA CGCGATCGCTGTTA
		FW28	GGTGGTTCAAATCCGCCTCC CGCAA CGTACGGTTTTT
NTML RNase mutants: transposon insertion verification			
Mini-III		FW150	CCATTGACCTTAGCATATAT GGGA
		Buster (NTML)	GCTTTTTCTAAATGTTTTTTA AGTAAATCAAGTAC
PNPase		FW151	CCTGGTGACGATGCAACATT
		Buster (NTML)	GCTTTTTCTAAATGTTTTTTA AGTAAATCAAGTAC
RNase R		FW152	GAAGAGATTATTAATCAACC TGAA
		Buster (NTML)	GCTTTTTCTAAATGTTTTTTA AGTAAATCAAGTAC
YhaM		FW153	CGCTAGTCTAATTTGGTTGA CT
		Buster (NTML)	GCTTTTTCTAAATGTTTTTTA AGTAAATCAAGTAC
RNase M5		FW154	GGACGAGATGATACTGA
		Upstream	CTCGATTCTATTAACAAGGG

Table 11. continued.

Purpose	Template	Name	Sequence
Cloning for Mdh overexpression			
pET28_His_Nde _mdh_Not1	Newman	DSt015	CCTGTACATATGATGACACA ATATCCTTTATG
		DSt016	TAGTTAGCGGCCGCTTAGTC ATTTGATGGTTTAATT
pET28a_His_kynB	*P. aeruginosa* ATCC15442	DSt021	AATGTACATATGATGACTTC GCTCCGCTACTGGGA
		DSt022	TAGTTACTCGAGTTACTCCG CGGTAGGCAG
pET28a_mdh_ His71Ser	pET28_His_N de _mdh_Not1	FW78	CTCGACAAATGAAATTGGTG CATCAATGTGA
		FW79	GATGCACCAATTTCATTTGT CGAGAATAAACG
pET28a_mdh_ His71Ser_Glu198Ser	pET28a_mdh_ His71Ser	FW80	GAATATAACGTGAGCCAACT AAATCACCATTT
		FW81	GATTTAGTTGGCTCACGTTA TATTCTTGGTCA
Cloning for *mdh* variants chromosomal integration plasmids			
pBASE_mdh	Newman	DSt014	ATTATAAGATCTCCGGATTT ACCAACAACAACTATTGGAT
		DSt023	ATTAGCAGATCTGCTATGAA AGGTGGCTTGCCA
pBASE_mdh_del	pBASE_mdh	FW76	GTAATAAAAATCACCCGTTT TTAGTTTA
		FW77	GATTTTTATTACCCAATAAA TCCATAAAC
pBASE_mdh_His71Ser	pBASE_mdh	FW78	CTCGACAAATGAAATTGGTG CATCAATGTGA
		FW79	GATGCACCAATTTCATTTGT CGAGAATAAACG
pBASE_mdh_Glu198S er	pBASE_mdh	FW80	GAATATAACGTGAGCCAACT AAATCACCATTT
		FW81	GATTTAGTTGGCTCACGTTA TATTCTTGGTCA
pBASE_mdh_His71Ser _Glu198Ser	pBASE_mdh_ His71Ser	FW80	GAATATAACGTGAGCCAACT AAATCACCATTT
		FW81	GATTTAGTTGGCTCACGTTA TATTCTTGGTCA
2.8 kb fragment pBASE mdh Phe32Trp	pBASE_mdh	FW133	CAAACTCACTCCAACGTGGT ATTTCCGGA
		FW108	GGGGGATCATGTAACTCGCC TTGAT
7 kb fragment pBASE mdh Phe32Trp	pBASE_mdh	FW134	CGGAAATACCACGTTGGAGT GAGTTTGAAAA
		FW107	GGCGAGTTACATGATCCCCC ATGTTGT

Tabel. 11 continued.

Purpose	Template	Name	Sequence
Cloning for BTHS (Mdh project)			
pKNT25_mdh	Newman	FW182	ATTAGCTCTAGATATGACAC AATATCCTTTATGGCA
		FW183	ATTAGCGGTACCAAGTCATT TGATGGTTTAATTGCA
pKT25C_mdh*	Newman	FW182	ATTAGCTCTAGATATGACAC AATATCCTTTATGGCA
		FW184	ATTAGCGGTACCTTAGTCAT TTGATGGTTTAATTGCA
pUT18N_mdh	Newman	FW182	ATTAGCTCTAGATATGACAC AATATCCTTTATGGCA
		FW183	ATTAGCGGTACCAAGTCATT TGATGGTTTAATTGCA
pUT18C_mdh*	Newman	FW182	ATTAGCTCTAGATATGACAC AATATCCTTTATGGCA
		FW184	ATTAGCGGTACCTTAGTCAT TTGATGGTTTAATTGCA
pUT18N_metI	Newman	FW170	ATTAGCTCTAGATATGAAGG ATACACAGTTAGCCCAA
		FW171	ATTAGCGGTACCCATACAAT CTCTCCAATCTGAGCT
pUT18C_metI*	Newman	FW170	ATTAGCTCTAGATATGAAGG ATACACAGTTAGCCCAA
		FW172	ATTAGCGGTACCTCATACAA TCTCTCCAATCTGAGCT
pUT18N_metC	Newman	FW173	ATTAGCTCTAGATATGACAC TTTCAAAAGAGACAGA
		FW174	ATTAGCGGTACCAATCTTTC AATTGTGTGAGGAATTGA
pUT18C_metC*	Newman	FW173	ATTAGCTCTAGATATGACAC TTTCAAAAGAGACAGA
		FW175	ATTAGCGGTACCTTATCTTT CAATTGTGTGAGGAA
pUT18N_metF	Newman	FW176	ATTAGCTCTAGAAATGAGTC AATTCCTCACACAATTGA
		FW177	ATTAGCGGTACCCATAATAT TGCCTCCTTGTGAGCA
pUT18C_metF*	Newman	FW176	ATTAGCTCTAGAAATGAGTC AATTCCTCACACAATTGA
		FW178	ATTAGCGGTACCTCATAATA TTGCCTCCTTGTGA

Tabel. 11 continued.

Purpose	Template	Name	Sequence
Colony PCR for BTHS (Mdh project)			
pKNT25 constructs		B2H_fow	GGCACGACAGGTTTCCCGA
		p25N_seq(a)	CCTTGATGCCATCGAGTACG GC
pKT25C constructs		B2H_fow	GGCACGACAGGTTTCCCGA
		pKT25_rev	GGCGATTAAGTTGGGTAACG CCA
pUT18N constructs		B2H_fow	GGCACGACAGGTTTCCCGA
		p18C-seq(a)	GTTGGCGGGTGTCGGGGCTG
pUT18C constructs		B2H_fow	GGCACGACAGGTTTCCCGA
		p18C-seq(a)	GTTGGCGGGTGTCGGGGCTG
Sequencing for BTHS (Mdh project)			
pKNT25 constructs		p25N_seq(a)	CCTTGATGCCATCGAGTACG GC
		p18C_seq(a)	GTTGGCGGGTGTCGGGGCTG
pKT25C constructs		B2H_fow	GGCACGACAGGTTTCCCGA
		p25C_seq(s)	CGGCGGATATCGACATGTTC GCC
		pKT25_rev	GGCGATTAAGTTGGGTAACG CCA
pUT18N constructs		B2H_fow	GGCACGACAGGTTTCCCGA
		p18N-seq(a)	GGAACGGGCGCCGGCGCGA GC
		p18C-seq(a)	GTTGGCGGGTGTCGGGGCTG
pUT18C constructs		B2H_fow	GGCACGACAGGTTTCCCGA
		p18C-seq(s)	GAGCGGACGTTCGAAGTT
		p18C-seq(a)	GTTGGCGGGTGTCGGGGCTG

5.1.8. Radioactive nucleotides

Radioactive nucleotides were purchased from HARTMANN ANALYTIC GmbH (Brunswick, GER).

Table 12. List of radioactive nucleotides and the designated use.

Radioactive nucleotide	Activity	Concentration	Purpose
[γ32P]-ATP (cat. no. SRP-501)	6000 Ci/mmol	10 µCi/µl	ssDNA probe labelling, end labelling of RNA
[α32P]-dCTP (cat. no. SRP-205)	3000 Ci/mmol	10 µCi/µl	dsDNA probe labelling

5.1.9. Plasmids

General plasmids

Table 13. List of general plasmids used in this work. In case of shuttle vectors selection is detailed for Gram-negative and Gram-positive bacteria.

Plasmid name	Properties	Size (bp)	Selection	Reference
pBASE6	ori ColE1, antisense *secY* under Pxyl/tet for counter selection	6,600	Gram (-): Amp (100) Gram (+): Cm (30)	(Geiger et al., 2012)
pGEM®-T Easy Vector System I	ori pBR322, 3´-T overhang, system for the cloning of PCR products, blue/white screening	3,015	Gram (-): Amp (100)	Promega
pCR-XL-2-TOPO™	ori pUC, *lac* promoter, (linearized and topoisomerase 1-activated)	3,960	Gram (-): Amp (100), Kana (50)	ThermoFisher Scientific Inc. (K8050-10, Invitrogen™)
pEB01	ori ColE1 (*E. coli*), ori pT181 (Gram+), *bla* (AmpR), *cat* (CmR), MCS to express gene of interest under native promoter, (pCN47 vector with *ermC* exchanged by *cat*)	5,580	Gram (-): Amp (100) Gram (+): Cm (30)	(Oun et al., 2013)
pJC1-MetTBox-metleader-cl-pR-eYFP	initiator tRNA NWMN_tRNA23, met-leader (T-Box), metI 30 bp, cl repressor with LVA-fast degradation tag, eYFP under pR promoter, bla truncated?, kana, orfX, repA, per	9,552	Gram (-): Kana (50) Gram (+): Kana (25)	R. Mahr (unpublished)
pET28a(+)	overexpression vector for, e.g. *E.coli* BL21 (H17) (T7 polymerase expressing host), T7 promoter + *lac* operator (IPTG induction), N-terminal His-tag/thrombin/T7-tag, optional C-terminal His-tag	5,369	Gram (-): Kana (50)	Novagen®
pKT25-zip	*lac* operator, *lac* promoter, ori p15A (*E. coli*), *bla* (AmpR), MCS downstream of T25 adenylate cyclase fragment, leucine zipper of GCN4 is genetically fused in frame to the T25 fragment, high copy, vector serves as positive control in BACTH when co-transformed with pUT18C-zip	3,556	Gram (-): Kana (50)	Euromedex; BACTH (Bacterial Adenylate Cyclase Two-Hybrid) System Kit

Table 13. continued.

Plasmid name	Properties	Size (bp)	Selection	Reference
pUT18C-zip	*lac* operator, *lac* promoter, ori pBR322 (*E. coli*), *bla* (AmpR), MCS downstream of T18 adenylate cyclase fragment, leucine zipper of GCN4 is genetically fused in frame to the T18 fragment, high copy, vector serves as positive control in BACTH when co-transformed with pKT25-zip	3,119	Gram (-): Amp (100)	Euromedex; BACTH (Bacterial Adenylate Cyclase Two-Hybrid) System Kit
pKT25 (p25C)	*lac* operator, *lac* promoter, ori p15A (*E. coli*), *bla* (AmpR), MCS downstream of T25 adenylate cyclase fragment to generate protein of interest with N-terminal fusion to T25, low copy	3442	Gram (-): Kana (50)	as above
pKNT25 (p25N)	*lac* operator, *lac* promoter, ori p15A (*E. coli*), *bla* (AmpR), MCS upstream of T25 adenylate cyclase fragment to generate protein of interest with C-terminal fusion to T25, low copy	3469	Gram (-): Kana (50)	as above
pUT18N (p18N)	*lac* operator, *lac* promoter, ori pBR322 (*E. coli*), *bla* (AmpR), MCS upstream of T18 adenylate cyclase fragment to generate protein of interest with C-terminal fusion to T18, high copy,	3023	Gram (-): Amp (100)	as above
pUT18C (p18C)	*lac* operator, *lac* promoter, ori pBR322 (*E. coli*), *bla* (AmpR), MCS downstream of T18 adenylate cyclase fragment to generate protein of interest with N-terminal fusion to T18, high copy,	3017	Gram (-): Amp (100)	as above

Plasmids generated in this work

Table 14. List of plasmids generated in this work. The internal strain collection number (ISC Nr.) of the Ziebuhr group strain collection is given. It refers to the *E. coli* strain containing the respective plasmid. In case of shuttle vectors selection is detailed for Gram-negative and Gram-positive bacteria.

Plasmid name	**Properties**	**Size (bp)**	**Selection**	**ISC Nr. (*E. coli*)**
pBASE_*met* leader+1kb flanking (pFW001)	pBASE6 with wild type *met* leader sequence and 1 kb flanking regions	8,849	Gram (-): Amp (100) Gram (+): Cm (30)	FW55
pBASE_ΔAntiTer&Ter	pFW001 with ΔAntiTer&Ter *met* leader	8,761	as above	FW56
pBASE_Ter_destab	pFW001 with Ter_destab *met* leader	8,849	as above	FW68
pBASE_SC2_metleader+ 1kb flanking	pFW001 with SC2 *met* leader	8,842	as above	FW57
pBASE_SC4_metleader+ 1kb flanking	pFW001 with SC4 *met* leader	8,849	as above	FW59
pBASE_SC5_metleader+ 1kb flanking	pFW001 with SC5 *met* leader	8,849	as above	FW60
pBASE_SC7_metleader+ 1kb flanking	pFW001 with SC7 *met* leader	8,849	as above	FW58
pGEM-T-easy +Ter_mutated_1	Ter_mutated_1 *met* leader	5,284	Gram (-): Amp (100)	FW80
pBASE6_Ter_mutated_1	pFW001 with Ter_mutated_1 *met* leader	8,849	Gram (-): Amp (100) Gram (+): Cm (30)	FW81
pBASE_Ter_mutated_2	pFW001 with Ter_mutated_2 *met* leader	8,849	as above	FW103
pBASE_Ter_mutated_3	pFW001 with Ter_mutated_3 *met* leader	8,849	as above	FW101
pBASE_Ter_mutated_4	pFW001 with Ter_mutated_4 *met* leader	8,849	as above	FW102
pEB01-met leader-metI	*met* leader sequence from -35 signal to 5'-region of *metI* (215 nt)	6,296	as above	FW95
pJC1_tRNAi_deletion	pJC1 with *met* leader, *yfp* and *cI* repressor, deletion of $tRNA_i$ gene	9,472	Gram (-): Kana (50) Gram (+): Kana (25)	FW6
pBASE_mdh	pBASE6 with wild type *mdh* sequence and 1 kb flanking regions	9,763	as above	DS10

Table 14. continued.

Plasmid name	Properties	Size (bp)	Selection	ISC Nr. (*E. coli*)
pBASE_mdh_del	pBASE6 with 1 kb flanking regions of *mdh* (NWMN_0347) with *mdh* sequence deleted	9,010	as above	DS11
pBASE_mdh_His71Ser	pBASE6 with *mdh* Glu198Ser sequence and 1 kb flanking regions	9,763	as above	FW36
pBASE_mdh_Glu198Ser	pBASE6 with *mdh* His71Ser sequence and 1 kb flanking regions	9,763	as above	FW37
pBASE_mdh_His71Ser_ Glu198Ser	pBASE6 with *mdh* His71Ser&Glu198Ser sequence and 1 kb flanking regions	9,763	as above	FW38
pBASE mdh Phe32Trp	pBASE6 with *mdh* Phe32Trp sequence and 1 kb flanking regions	9,763	as above	ER21
pET28_His_Nde _mdh_Not1	*S. aureus mdh* (NWMN_0347) with N-terminal His-tag	6,058	Kana (50)	DS3
pET28a_mdh_ His71Ser_Glu198Ser	catalytically inactive *S. aureus* Mdh (His71Ser_Glu198Ser) with N-terminal His-tag	6,058	as above	FW41
pET28_His_kynB	*P. aeruginosa kynB* with N-terminal His-tag	5,938	as above	DS9
pKNT25_mdh	*S. aureus mdh* (NWMN_0347) with T25 cyclase fragment fused to *mdh* C-terminus for Bacterial 2 Hybrid System (BACTH)	4,187	Amp (100)	FW86
pKT25C_mdh*	*S. aureus mdh* (NWMN_0347) with T25 cyclase fragment fused to *mdh* N-terminus for BACTH	4,213	as above	FW87
pUT18N_mdh	*S. aureus mdh* (NWMN_0347) with T18 cyclase fragment fused to *mdh* C-terminus for BACTH	3,767	as above	-
pUT18C_mdh*	*S. aureus mdh* (NWMN_0347) with T18 cyclase fragment fused to *mdh* N-terminus for BACTH	3,762	as above	FW92

Table 14. continued.

Plasmid name	Properties	Size (bp)	Selection	ISC Nr. (*E. coli*)
pUT18N_metI	*S. aureus metI* (NWMN_0351) with T18 cyclase fragment fused to *metI* C-terminus for BACTH	4,118	as above	FW88
pUT18C_metI*	*S. aureus metI* (NWMN_0351) with T18 cyclase fragment fused to *metI* N-terminus for BACTH	4,113	as above	FW85
pUT18N_metC	*S. aureus metC* (NWMN_0350) with T18 cyclase fragment fused to *metC* C-terminus for BACTH	4,175	as above	-
pUT18C_metC*	*S. aureus metC* (NWMN_0350) with T18 cyclase fragment fused to *metC* N-terminus for BACTH	4,170	as above	FW91
pUT18N_metF	*S. aureus metF* (NWMN_0349) with T18 cyclase fragment fused to *metF* C-terminus for BACTH	4,854	as above	FW94
pUT18C_metF*	*S. aureus metF* (NWMN_0349) with T18 cyclase fragment fused to *metF* N-terminus for BACTH	4,851	as above	FW89

5.1.10. Bacterial strains

Bacterial strains (general)

Table 15. List of bacterial strains used in this work (general). The internal strain collection number (ISC Nr.) of the Ziebuhr group strain collection is given.

Strain	Characteristics	Reference	ISC Nr.
E. coli			
DC10B	*E. coli* DH10B Δ*dcm* (cytosine methylase deficient) for direct cloning into staphylococci	(Monk and Foster, 2012; Monk et al., 2012)	H47
DH5α	common cloning host, *lacZ* negative, used for blue-white screening		H16
BTH101	Δ*cya* (*F⁻, cya-99, araD139, galE15, galK16, rpsL1, hsdR2, mcrA1, mcrB1*), Strep(50)	(unpublished, D. Ladant), Reference referring to 'unpublished': (Ouellette et al., 2017)	H80
BL21 (DE3)	Expression host; F- *ompT hsdSB*(r-Bm-B) *dcm gal* λ (DE3)	Merck Biosciences	H17
S. aureus			
RN4220	restriction-deficient derivative of *S. aureus* 8325-4, cloning host	(Nair et al., 2011)	H1
Newman	methicillin-sensitive isolate, NCTC 8178	(Baba et al., 2008; Duthie and Lorenz, 1952)	H29
Newman 106	RNase J2 mutant *rnjB*::pMUTIN, Erm(5)	(Schoenfelder et al., 2013)	H35
Newman 107	RNase III mutant *rnc*::pMUTIN, Erm(5)	(Schoenfelder et al., 2013)	H36
Newman 217	RNase Y mutant, *rny*::*ermC*, Erm(5)	(Marincola et al., 2012)	H40
SA564RD Δ*pyr*FE ('PR01')	hsdR type III mutant (restriction deficient), pyrimidine auxotroph,	(Redder and Linder, 2012)	H67
SA564RD Δ*pyrFE* ΔRNaseJ1	PR01 RNase J1 mutant, Δ*rnjA*,	(Redder and Linder, 2012)	H68
SA564RD Δ*pyrFE* ΔRNaseJ2	PR01 RNase J2 mutant, Δ*rnjB*,	(Redder and Linder, 2012)	H70
SA564RD Δ*pyrFE* ΔRNaseJ1/J2	PR01 RNase J1/J2 double mutant, Δ*rnjA*::*ermC*, Δ*rnjB*, Erm (10)	(Redder and Linder, 2012)	H71

Table 15. continued.

Strain	Characteristics	Reference	ISC Nr.
***S. aureus* (continued)**			
USA_300 JE2	*S. aureus* USA_300_LAC cured from a macrolide resistance and a cryptic plasmid	(Kennedy et al., 2010)	H60
USA_300 JE2 Mini-RNase III mutant (NE664)	Transposon insertion within RNase gene at position 575873, transposable element contains *gfp*, R6K and *ermC*, Erm(10)	(Bae et al., 2008b; Fey et al., 2013)	H74
USA_300 JE2 PNPase mutant (NE259)	Transposon insertion within RNase gene at position 1282378, transposable element contains *gfp*, R6K and *ermC*, Erm(10)	(Bae et al., 2008b; Fey et al., 2013)	H75
USA_300 JE2 RNase R mutant (NE501)	Transposon insertion within RNase gene at position 851566, transposable element contains *gfp*, R6K and *ermC*, Erm(10)	(Bae et al., 2008b; Fey et al., 2013)	H76
USA_300 JE2 YhaM mutant (NE637)	Transposon insertion within RNase gene at position 1973412, transposable element contains *gfp*, R6K and *ermC*, Erm(10)	(Bae et al., 2008b; Fey et al., 2013)	H77
USA_300 JE2 RNase M5 mutant (NE905)	Transposon insertion within RNase gene at position 528892, transposable element contains *gfp*, R6K and *ermC*, Erm(10)	(Bae et al., 2008b; Fey et al., 2013)	H78
P. aeruginosa			
P. aeruginosa ATCC 15442	Broad spectrum of resistance to various commercial germicides, pyocyanin not produced	American Type Culture Collection (ATCC)	H58

Bacterial strains generated in this work

Table 16. List of bacterial strains generated in this work. The internal strain collection number (ISC Nr.) of the Ziebuhr group strain collection is given.

Strain	**Characteristics**	**Project (e.g. Mdh)**	**ISC Nr.**
***S. aureus* Newman**			
ΔAntiTer&Ter *met* leader	ΔAntiTer&Ter *met* leader mutant	*met* leader processing & 'ON'/'OFF' mutants	FW74
Ter_destab *met* leader	Ter_destab *met* leader mutant	as above	FW79
SC2 *met* leader	SC2 *met* leader mutant	as above	FW75
SC4 *met* leader	SC4 *met* leader mutant	as above	FW78
SC5 *met* leader	SC5 *met* leader mutant	as above	FW77
SC7 *met* leader	SC7 *met* leader mutant	as above	FW76
Ter_mutated_1 *met* leader	Ter_mutated_1 *met* leader mutant	as above	FW84
Ter_mutated_2 *met* leader	Ter_mutated_2 *met* leader mutant	*met* leader processing	FW111
Ter_mutated_3 *met* leader	Ter_mutated_3 *met* leader mutant	as above	FW110
Ter_mutated_4 *met* leader	Ter_mutated_4 *met* leader mutant	as above	FW112
+ pEB01-met leader-metI	Plasmid with *met* leader seq. from -35 signal to 5' of *metI* (215 nt)	*met* mRNA processing	FW100
Δ*mdh*	Deletion of *mdh* (NWMN_0347)	Mdh	H72
mdh E198S	catalytically inactive Mdh (Glu198Ser)	Mdh	FW52
mdh H71S&E198S	catalytically inactive Mdh (His71Ser_Glu198Ser)	Mdh	FW53
mdh H71S	catalytically inactive Mdh (His71Ser)	Mdh	FW54
mdh F32W	Putative substrate recognition deficient Mdh (Phe32Trp)	Mdh	ER24

Table 16. continued.

Strain	**Characteristics**	**Project (e.g. Mdh)**	**ISC Nr.**
Other *S. aureus* strains			
H67 (SA564RD Δ*pyr*FE ('PR01')) + pEB01-met leader-metI	Plasmid with *met* leader seq. from -35 signal to 5' of *metI* (215 nt)	*met* mRNA processing	FW96
H68 (SA564RD Δ*pyrFE* ΔRNaseJ1) + pEB01-met leader-metI	as above	*met* mRNA processing	FW97
H70 (SA564RD Δ*pyrFE* ΔRNaseJ2) + pEB01-met leader-metI	as above	*met* mRNA processing	FW98
H71 (SA564RD Δ*pyrFE* ΔRNaseJ1/J2) + pEB01-met leader-metI	as above	*met* mRNA processing	FW99
Strains to transduce into *S. aureus* Newman			
***S. aureus* RN4220**			
+pBASE_ΔAntiTer&Ter	pFW001 with ΔAntiTer&Ter *met* leader	*met* leader processing & 'ON'/'OFF' mutants	FW61
+pBASE_Ter_destab	pFW001 with Ter_destab *met* leader	as above	FW69
+pBASE_SC2_metleader+1kb flanking	pFW001 with SC2 *met* leader	as above	FW62
+pBASE_SC4_metleader+1kb flanking	pFW001 with SC4 *met* leader	as above	FW64
+pBASE_SC5_metleader+1kb flanking	pFW001 with SC5 *met* leader	as above	FW70
+pBASE_SC7_metleader+1kb flanking	pFW001 with SC7 *met* leader	as above	FW63
+pBASE6_Ter_mutated_1	pFW001 with Ter_mutated_1 *met* leader	as above	FW82
+pBASE_Ter_mutated_2	pFW001 with Ter_mutated_2 *met* leader	*met* leader processing	FW104
+pBASE_Ter_mutated_3	pFW001 with Ter_mutated_3 *met* leader	as above	FW105
+pBASE_Ter_mutated_4	pFW001 with Ter_mutated_4 *met* leader	as above	FW106

Table 16. continued.

Strain	Characteristics	Project (e.g. Mdh)	ISC Nr.
***S. aureus* RN4220 (continued)**			
+pBASE_mdh_del	pBASE6 with 1 kb flanking regions of *mdh* (NWMN_0347) with *mdh* sequence deleted	Mdh	DS12
+pBASE_mdh_His71Ser	pBASE6 with *mdh* Glu198Ser sequence and 1 kb flanking regions	as above	FW46
+pBASE_mdh_Glu198Ser	pBASE6 with *mdh* His71Ser sequence and 1 kb flanking regions	as above	FW47
+pBASE_mdh_His71Ser_Glu198Ser	pBASE6 with *mdh* His71Ser&Glu198Ser sequence and 1 kb flanking regions	as above	FW48
pBASE mdh Phe32Trp	pBASE6 with *mdh* Phe32Trp sequence and 1 kb flanking regions	as above	ER22
Strains to create chromosomal mutations/integrations/deletions (via double cross over)			
***S. aureus* Newman**			
+pBASE_ΔAntiTer&Ter	pFW001 with ΔAntiTer&Ter *met* leader	*met* leader processing& 'ON'/'OFF' mutants	FW65
+pBASE_Ter_destab	pFW001 with Ter_destab *met* leader	as above	FW73
+pBASE_SC2_metleader+1kb flanking	pFW001 with SC2 *met* leader	as above	FW66
+pBASE_SC4_metleader+1kb flanking	pFW001 with SC4 *met* leader	as above	FW71
+pBASE_SC5_metleader+1kb flanking	pFW001 with SC5 *met* leader	as above	FW72
+pBASE_SC7_metleader+1kb flanking	pFW001 with SC7 *met* leader	as above	FW67
+pBASE6_Ter_mutated_1	pFW001 with Ter_mutated_1 *met* leader	as above	FW83
+pBASE_Ter_mutated_2	pFW001 with Ter_mutated_2 *met* leader	as above	FW107

Table 16. continued.

Strain	Characteristics	Project (e.g. Mdh)	ISC Nr.
***S. aureus* Newman (continued)**			
+pBASE_Ter_mutated_3	pFW001 with Ter_mutated_3 *met* leader	*met* leader processing	FW108
+pBASE_Ter_mutated_4	pFW001 with Ter_mutated_4 *met* leader	as above	FW109
+pBASE_mdh_del	pBASE6 with 1 kb flanking regions of *mdh* (NWMN_0347) with *mdh* sequence deleted	Mdh	DS13
+pBASE_mdh_His71Ser	pBASE6 with *mdh* Glu198Ser sequence and 1 kb flanking regions	as above	FW49
+pBASE_mdh_Glu198Ser	pBASE6 with *mdh* His71Ser sequence and 1 kb flanking regions	as above	FW50
+pBASE_mdh_His71Ser_Glu198Ser	pBASE6 with *mdh* His71Ser&Glu198Ser sequence and 1 kb flanking regions	as above	FW51
+pBASE mdh Phe32Trp	pBASE6 with *mdh* Phe32Trp sequence and 1 kb flanking regions	as above	ER23
***E. coli* BL21 (DE3)**			
+pET28_His_Nde _mdh_Not1	*S. aureus mdh* (NWMN_0347) with N-terminal His-tag for overexpression	Mdh	DS3
+pET28_His_kynB	*P. aeruginosa kynB* with N-terminal His-tag for overexpression	Mdh	DS9
+pET28a_mdh_ His71Ser_Glu198Ser	catalytically inactive *S. aureus* Mdh (His71Ser_Glu198Ser) with N-terminal His-tag for overexpression	Mdh	FW41

Table 16. continued.

Strain	Characteristics	Project (e.g. Mdh)	ISC Nr.
***E. coli* DC10B**			
+pBASE_*met* leader+1kb flanking (pFW001)	pBASE6 with wild type *met* leader sequence and 1 kb flanking regions	*met* leader processing & 'ON'/'OFF' mutants	FW55
+pBASE_ΔAntiTer&Ter	pFW001 with ΔAntiTer&Ter *met* leader	as above	FW56
+pBASE_Ter_destab	pFW001 with Ter_destab *met* leader	as above	FW68
+pBASE_SC2_metleader+1kb flanking	pFW001 with SC2 *met* leader	as above	FW57
+pBASE_SC4_metleader+1kb flanking	pFW001 with SC4 *met* leader	as above	FW59
+pBASE_SC5_metleader+1kb flanking	pFW001 with SC5 *met* leader	as above	FW60
+pBASE_SC7_metleader+1kb flanking	pFW001 with SC7 *met* leader	as above	FW58
+pGEM-T-easy+Ter_mutated_1	Ter_mutated_1 *met* leader	as above	FW80
+pBASE6_Ter_mutated_1	pFW001 with Ter_mutated_1 *met* leader	as above	FW81
+pBASE_Ter_mutated_2	pFW001 with Ter_mutated_2 *met* leader	*met* leader processing	FW103
+pBASE_Ter_mutated_3	pFW001 with Ter_mutated_3 *met* leader	as above	FW101
+pBASE_Ter_mutated_4	pFW001 with Ter_mutated_4 *met* leader	as above	FW102
+pEB01-met leader-metI	*met* leader sequence from -35 signal to 5'-region of *metI* (215 nt)	*met* mRNA processing	FW95
+pJC1_tRNAi_deletion	pJC1 with *met* leader, *yfp* and *cI* repressor, deletion of $tRNA_i$ gene		FW6
+pBASE_mdh	pBASE6 with wild type *mdh* sequence and 1 kb flanking regions	Mdh	DS10
+pBASE_mdh_del	pBASE6 with 1 kb flanking regions of *mdh* (NWMN_0347) with *mdh* sequence deleted	as above	DS11

Table 16. continued.

Strain	Characteristics	Project (e.g. Mdh)	ISC Nr.
***E. coli* DC10B (continued)**			
+pBASE mdh Phe32Trp	pBASE6 with *mdh* Phe32Trp sequence and 1 kb flanking regions	Mdh	ER21
+ pKTN25_mdh	*S. aureus mdh* (NWMN_0347) with T25 cyclase fragment fused to *mdh* C-terminus for Bacterial 2 Hybrid System (BACTH)	as above	FW86
+ pKT25C_mdh*	*S. aureus mdh* (NWMN_0347) with T25 cyclase fragment fused to *mdh* N-terminus for BACTH	as above	FW87
+ pUT18C_mdh*	*S. aureus mdh* (NWMN_0347) with T18 cyclase fragment fused to *mdh* N-terminus for BACTH	as above	FW92
+ pUT18N_metI	*S. aureus metI* (NWMN_0351) with T18 cyclase fragment fused to *metI* C-terminus for BACTH	as above	FW88
+ pUT18C_metI*	*S. aureus metI* (NWMN_0351) with T18 cyclase fragment fused to *metI* N-terminus for BACTH	as above	FW85
+ pUT18C_metC*	*S. aureus metC* (NWMN_0350) with T18 cyclase fragment fused to *metC* N-terminus for BACTH	as above	FW91
+ pUT18C_metF*	*S. aureus metF* (NWMN_0349) with T18 cyclase fragment fused to *metF* N-terminus for BACTH	as above	FW89

Table 16. continued.

Strain	Characteristics	Project (e.g. Mdh)	ISC Nr.
***E. coli* DH5α (continued)**			
+pET28_His_Nde_mdh_Not1	*S. aureus mdh* (NWMN_0347) with N-terminal His-tag	Mdh	DS5
+pET28_His_kynB	*P. aeruginosa kynB* with N-terminal His-tag for overexpression	as above	DS8
+pET28a_mdh_ His71Ser_Glu198Ser	catalytically inactive *S. aureus* Mdh (His71Ser_Glu198Ser) with N-terminal His-tag for overexpression	as above	FW45
+pBASE_mdh_His71Ser	pBASE6 with *mdh* Glu198Ser sequence and 1 kb flanking regions	as above	FW43
+pBASE_mdh_Glu198Ser	pBASE6 with *mdh* His71Ser sequence and 1 kb flanking regions	as above	FW44
+pBASE_mdh_His71Ser_Glu198Ser	pBASE6 with *mdh* His71Ser&Glu198Ser sequence and 1 kb flanking regions	as above	FW45

5.1.11. Solid and liquid growth media

Growth media were set up as listed in **Tab. 17**. Preparation of chemically defined medium (CDM) is detailed in a separate section. For solid growth media antibiotics were added before pouring, if applicable. Liquid media were stored at RT (except for CDM); solid media at 4°C for several months.

Components of general solid and liquid growth media

Used growth media are listed below. For pouring LB-, BHI- and TSB-agar plates 1.5% (w/v) agar was added to the media components and the volume adjusted to 400 or 800 ml with purified ('VE') H_2O. LB-soft agar was prepared in a total volume of 80 ml purified ('VE') H_2O and contained 0.6%(w/v) agar. This soft agar was stored solidified at room temperature and liquefied prior to use in a microwave.

Table 17. List of media used.

Media/Agar	Components	Amount	Manufacturer
Luria-Bertani (LB) broth	Yeast extract NaCl Tryptone/Peptone ex casein	0.5 % (w/v) 0.5 % (w/v) 1 %	Carl Roth GmbH + Co. KG
Brain Heart Infusion (BHI) broth		According to manufacturer's instructions	Carl Roth GmbH + Co. KG
Trypticase™ Soy Broth (TSB)		According to manufacturer's instructions	Becton Dickinson (BD) BBL™
LB-Soft Agar (80 ml)	Yeast extract NaCl Tryptone/Peptone ex casein Agar-agar	0.4 g 0.4 g 0.8 g 0.48 g	
Sheep Blood Agar	Yeast extract NaCl Tryptone/Peptone ex casein Sheep blood Agar-agar	0.5 % (w/v) 0.5 % (w/v) 1 % 5 % (v/v) 1.5% (w/v)	Carl Roth GmbH + Co. KG Elocin Lab, steril, defibriniert
Agar-agar, granulated			Carl Roth GmbH + Co. KG or BD Difco™

Chemically Defined Medium (CDM)

We have modified the original recipe from Greifswald according to our needs (Gertz et al., 1999; Mäder et al., 2016). The components listed in **Tab. 18** were mixed in the listed order to obtain the chemically defined medium and filled up with sterile ddH_2O to the designated volume. Medium was sterile-filtered into 500 ml single-use bottles with filter system (Corning) and was stored at 4° C. The 2x Basic Medium contained 25mM Na_2HPO_4*$2H_2O$, 20 mM KH_2PO_4, 3.3 mM $MgSO_4$, 18.5 mM NH_4Cl and 17 mM NaCl. The composition of the amino acids solutions, the vitamin mix and riboflavin is detailed in **Tab. 19**. All components were sterile filtered, except for glucose solution, sodium citrate tribasic dihydrate solution and ddH_2O that were autoclaved.

Table 18. List of components and their final concentrations in CDM.

Component	Endconcentration in CDM
2x Basic Medium	1x
Glucose solution (1 M)	75 mM
Sodium Citrate Tribasic Dihydrate solution (1 M)	0.142 mM
Amino Acids (see below)*	1 mM (except for cysteine with 1.2 mM, tyrosine with 0.1 mM)
Vitamin Mix (see below) (10,000x)	3x
Riboflavin (see below) (1,000x)	3x
Trace Metal Mix A5 with Co (1,000x)	1x
$NiCl_2$*$6H_2O$ (1,000x, 0.5 mM)	1x
$FeCl_3$ (in 1N HCl) solution (10,000x, 0.5 mM)	1.5x
NaOH (10,000x 1N)	1.5x

* Methionine was omitted in 'CDM -MET'

Table 19. List of amino acid solutions and components of vitamin mix for CDM. For 'CDM -MET' methionine was omitted from the medium. Riboflavin was set up as separate solution.

Amino acids (50 mM, each)
Alanine and glycine
Arginine
Asparainge and glutamine
Aspartic acid
Cysteine (60 mM)
Glutamic acid
Isoleucine
Leucine
Lysine
Methionine
Phenylalanine, tryptophan, histidine
Proline
Serine
Threonine
Tyrosine (5 mM)
Valine

Vitamine	10.000x [mM]
4-Aminobenzoic acid	2.9
Ca-D-Pathothenic acid (B5)	2.1
Cyanocobalamin (B12)	0.36
D-Biotine (B7)	0.4
Nicotinamid (B3)	8.1
Pyridoxine hydrochloride (B6)	6.2
Thiamine hydrochloride (B1)	2.9
	1000x [mM]
Riboflavine (B2)	0.2

For the protein (quantification) experiments (see **section 3.5, page 61 ff.**) L-arginine HCl (^{13}C,^{15}N) and L-lysine HCl (^{13}C, ^{15}N) were purchased from Silantes GmbH. These 'heavy' amino acids were added to the CDM instead of their 'light' variants, when indicated.

5.1.12. Antibiotics and analogues

Table 20. List of stocks and working solutions of antibiotics and ATc.

Antibiotic (abbreviation, manufacturer, Cat.-No.)	Solvent	Stock conc. [mg/ml]	Working conc. [µg/ml]
Ampicillin (Amp; Carl Roth GmbH + Co. KG, K029.2)	ddH_2O	100	100
Chloramphenicol (Cm; Carl Roth GmbH + Co. KG, 3886.2)	70% EtOH	30 or 10	30 or 10
Erythromycin (Erm; AppliChem GmbH, A2275.0005)	70% EtOH		
Kanamycin sulfate (Kana, Carl Roth GmbH + Co. KG, T832.2)	ddH_2O	50	50 or 25
Rifampicin (Rif; Sigma-Aldrich Chemie GmbH, R3501-1G)	DMSO	100	100
Streptomycin sulphate (Strep, Carl Roth GmbH + Co. KG, 0236.3)	ddH_2O	100	50
Anhydro-tetracycline (ATc; Sigma-Aldrich Chemie GmbH, 37919-100MG-R)	70% EtOH	100 µg/ml	50 ng/ml

5.1.13. Software for in silico predictions, data analysis and graphical representation

Table 21. List of software used for *in silico* predictions, data analysis and graphical representation.

Software	Purpose	Manufacturer
Blastx	Nucleotide and amino acid sequence comparison	NCBI (gish 1993) (Gish and States, 1993) (https://blast.ncbi.nlm.nih.gov/Blast.cgi) (last accessed 27.01.2020)
CLC Main Workbench, vers. 6.8.4	Sequencing data analysis, genome and plasmid visualisation	CLC bio (http://www.clcbio.com/) (last accessed 27.01.2020)
GraphPad Prism, vers. 6.0.4.0	Generating data graphs	GraphPad Software, Inc. (www.graphpad.com) (last accessed 27.01.2020)
graphical codon usage analyser 2.0	Identifying rare codons in gene sequences	http://gcua.schoedl.de/sequentialex.html (last accessed 27.01.2020)
Fiji (Fiji is Just ImageJ)	Image processing and Northern blot band quantification	(Schindelin 2012) (Schindelin et al., 2012) (https://imagej.net/Fiji) (last accessed 27.01.2020)

Table 21. continued.

Software	Purpose	Manufacturer
Inkscape, vers. 0.92.3	Creating illustrations	(https://www.inkscape.org) (last accessed 11.02.2020)
PyMOL™ vers. 2.1.1	Creating 3D protein structure images	Schrödinger, LLC
Typhoon FLA 7000, vers. 1.2	Radioactive signal detection from Northern blots, etc.	GE Healthcare
mfold	Prediction of RNA secondary structures	Zuker 2003 (Zuker, 2003) (http://unafold.rna.albany.edu/?q=mfold/RNA-Folding-Form) (last accessed 11.02.2020)
Jalview	graphical representation of alignments	Waterhouse 2009 (Waterhouse et al., 2009) (http://www.jalview.org/) (last accessed 11.02.2020)
MUSCLE (**MU**ltiple **S**equence **C**omparison by **L**og-**E**xpectation)	Generation of nucleotide and amino acid sequence alignments	Madeira 2019 (Madeira et al., 2019) (https://www.ebi.ac.uk/Tools/msa/muscle/) (last accessed 11.02.2020)
Protein Molecular Weight Calculator	Prediction of mass (kDa) of proteins	https://www.sciencegateway.org/tools/proteinmw.htm (last accessed 11.02.2020)
UNICORN 7.0	Control software for ÄKTA protein purification system	GE Healthcare
VARNA (Visualization Applet for RNA)	Drawing RNA secondary structure models	Darty 2009 (Darty et al., 2009) (http://varna.lri.fr/) (last accessed 11.02.2020)

5.1.14. RNA secondary structure modelling using mfold with constraints

The 2D structural model of the *met* leader was built based on the structural information obtained by in-line probing, augmented by computational folding predictions using the mfold algorithm on the mfold web server (http://unafold.rna.albany.edu/?q=mfold/RNA-Folding-Form) (Zuker, 2003). The experimental data were entered into the programme as constraints to eventually build the *met* leader RNA secondary structure model (see **Fig. 7 B**).

The bases could be forced to be single-stranded by entering the constraint in the format of ‘P i 0 k’ in the mfold programme. ‘P’ means in the syntax ‘prohibiting a string of consecutive bases from pairing’, ‘i’ details the first nucleotide to be single-stranded, ‘k’ is the number of consecutive bases that are forced to be single-stranded. For example: P 1 0 26 means that the first 26 nucleotides of the entered sequence should be forced to be single-stranded. P 67 0 5 means that the nucleotides 67 to 71 of the entered sequence should be forced to be single-stranded. The *met* leader sequence was divided into nt 1-129, nt 130-163, nt 164-205 and nt 206-440 to be entered into the mfold programme with the respective constraints listed in **Tab. 22**.

Table 22. List with *met* leader segments, sequences, constraints and resulting 2D structure used to build 2D model.

nts	Sequence	Constraints	2D structure in dot-bracket format (Vienna)
1-129	GUCUUAUAACAGUUUAAUGAAACGUAAA CACAAUAAAGAGGAAAGUAAAACACACC CUGCUUAUACAGAGAGUCUUUAGUAGCU GAGAGAAGAUUUUGAAAGCGUGUUUGAA AAUGGCCUUGGAGUGUU	P 1 0 26 P 67 0 5 P 78 0 11	..........................(((((......((((......((((((.....((((.........((((((...........)))))).....)))))))))))..... ...))))...)))))
130-163	GAUGCCAAUAUGAGGUGUCUACGGGUUC GCCCGU	P 1 0 3 P 7 0 7 P 26 0 4	...(((.......)))....(((((....)))))
164-205	UAUAGCGAUACAGUAUUAACAUUGAUGU UAAAUGGCGUACUG	P 7 0 2	..........((((((...((((.......))))..))))))
206-440	GAUUCUUU ACGCACGAUUUUUUGUUAAUAAGUAUGG GAUAGCACAUUACUAUAUCCUUACUUAC UGACUUUAAUUGUGAUAAUUGUUCAGUA AGCAUAUUUACUUUUAAUGCGUACUGAA UAAGGUUAUUUCAGCGAUGGAAUAACAA AUAAAGGUGGUACCGCGAAACAUAAGCU UUCGUCCUUUUUAUCCGAUUCAUUCGGG UACGAAGGACGGAAGCUUUUUUUAUUUU UUC	P 1 0 11 P 33 0 1 P 41 0 7 P 119 0 5 P 164 0 1 P 167 0 4 P 172 0 2 P 223 0 13	....(((((((....((((.((((...((((((... ....))))))..)))).))))...))))))) .........(((((.((((...........)))).)))))......(((((((((....))))))))).... ...((.....))...........((((((((((((. (((((((.....))))))).)))))))))))) ....
1-440 (assembled)	GUCUUAUAACAGUUUAAUGAAACGUAAA CACAAUAAAGAGGAAAGUAAAACACACC CUGCUUAUACAGAGAGUCUUUAGUAGCU GAGAGAAGAUUUUGAAAGCGUGUUUGAA AAUGGCCUUGGAGUGUUGAUGCCAAUAU GAGGUGUCUACGGGUUCGCCCGUUAUAG CGAUACAGUAUUAACAUUGAUGUUAAAU GGCGUACUGGAUUCUUUACGCACGAUUU UUUGUUAAUAAGUAUGGGAUAGCACAUU ACUAUAUCCUUACUUACUGACUUUAAUU GUGAUAAUUGUUCAGUAAGCAUAUUUAC UUUUAAUGCGUACUGAAUAAGGUUAUUU CAGCGAUGGAAUAACAAAUAAAGGUGGU ACCGCGAAACAUAAGCUUUCGUCCUUUU UAUCCGAUUCAUUCGGGUACGAAGGACG GAAGCUUUUUUUAUUUUUUC	-	..........................(((((......((((......((((((.....((((.........((((((...........)))))).....)))))))))))..... ...))))...)))))...(((.......)))....(((((....)))))..........((((((...((((. ......))))..))))))...........(((((((. ...((((.((((...((((((...........))))))..)))).))))...)))))))..........(((((.((((...........)))).)))))......(((((((((....)))))))))........((.....)) ...........((((((((((((.(((((((.... .))))))).))))))))))))).............. .

5.1.15. Rifampicin quantification using Fiji

Fiji software was used for quantification of Northern blot bands obtained from rifampicin assays. The procedure is described online (https://di.uq.edu.au/community-and-alumni/sparq-ed/sparq-ed-services/using-imagej-quantify-blots).

Probe signals were displayed in tiff files. These files were opened in Fiji and the region of interest was selected by using the rectangle tool covering the band of interest. After measuring the last band, the signals were plotted and the background noise was removed by closing the area under the curve. The enclosed areas under the curves were measured by the programme. The data were exported from the results table. Percentage of transcript remaining was calculated by setting the t0 value (derived from the t0 band signal of the rifampicin assay) as 100 %. 5S rRNA signals were quantified. Only, if values were equal for all time points, signals of *met* leader transcripts were quantified. The 'percentrage of transcript remaining' was plotted against time to obtain the graphs shown in **Figs. 9 B** and **A2.**

5.2. Microbiological methods

5.2.1. Bacterial culturing and storage

Growth conditions

E. coli strains were streaked on LB agar and grown in LB medium, when not otherwise stated. *S. aureus* strains were streaked on TSB agar, when not otherwise stated.

For overnight cultures 5 ml of medium were filled in 8 ml glass test tubes with cap and were inoculated with bacteria from an agar plate by using a sterile pipette tip. If not stated otherwise, bacteria were grown in a medium to flask volume ratio of 1:5.

S. aureus strains were grown in chemically defined medium (CDM) with (CDM +MET) or without methionine (CDM -MET) when not otherwise stated. For strains carrying resistance genes, antibiotics were used at the concentrations specified in **Tab. 20**.

Bacteria from overnight cultures (CDM +MET) were diluted to an initial optical density at 600 nm (OD_{600}) of 0.05 in fresh medium and grown with shaking at 180 rpm at 37° C to mid-exponential growth phase. For methionine-deprived (-MET) conditions bacteria were then washed twice with 1x PBS, resuspended in CDM -MET and incubated for 2 hours with shaking at 180 rpm at 37° C.

For growth experiments using the automatised microplate reader (TECAN system) bacteria from overnight cultures (CDM +MET) were washed twice with 1x PBS, resuspended in 2x Basic medium and diluted to an initial optical density at 600 nm (OD_{600}) of 0.05 in CDM with (+MET) or without methionine (-MET) and incubated in the TECAN system at 37° C and shaking. For details see **section 5.2.2, page 147**.

For Rifampicin assays under methionine-deprived conditions, bacteria from overnight cultures (CDM +MET) were washed twice with 1x PBS, resuspended in 2x Basic medium and diluted to an initial optical density at 600 nm (OD_{600}) of 0.05 in CDM without methionine (-MET). Bacteria were grown with shaking at 180 rpm at 37° C to mid-exponential phase.

For long-term growth experiments bacteria from overnight cultures (CDM +MET) were washed twice with 1x PBS, resuspended in 2x Basic medium and diluted to an initial optical density at 600 nm (OD_{600}) of 0.05 in CDM with (+MET) or without methionine (-MET) and incubated with shaking at 250 rpm for 20 days. Bacteria were grown in 50 ml tubes with the lid not tightly screwed to allow aeration. The medium to tube volume ratio was initially 1:2.5.

For protein (quantification) experiments bacteria from overnight cultures (CDM +MET) were washed twice with 1x PBS, resuspended in 2x Basic medium and diluted in CDM -MET to an initial optical density at 600 nm (OD600) of 0.05. Bacteria were grown with shaking at 180 rpm at 37° C to mid-exponential growth phase. Then bacteria were washed once with CDM -MET without arginine and lysine and were resuspended in CDM -MET with 1 mM 'heavy' arginine (L-arginine HCl (^{13}C, ^{15}N), Silantes GmbH) and 'heavy' lysine (L-lysine HCl (^{13}C, ^{15}N), Silantes GmbH) (instead of the normal 'light' (^{12}C, ^{14}N) arginine and lysine), t0 sample was taken and methionine to a final concentration of 10 mM was added. Bacteria were incubated with shaking at 180 rpm at 37° C. Samples were taken 15, 30, 60 and 240 min after methionine addition. Samples were immediately put on ice and split in two. One half was immediately pelleted, 1x washed with ice-cold TE-buffer (10 mM Tris (pH 8.0), 1 mM EDTA) supplemented with cOmplete™, EDTA-free Protease Inhibitor Cocktail (Roche) according to manufacturer's instructions), pellet was snap-frozen in liquid nitrogen and stored at -80° C until further processing described in **paragraph Sample preparation for proteomics, page 186**. The other half of the sample was treated as described in **section 5.4.1, page 162 ff.** In addition, the experiment was performed *vice versa* (switch from 'heavy' arginine and lysine to 'light' arginine and lysine containing CDM -MET). Number of biological replicates per time point: 4 (2x 'light' > 'heavy', 2x 'heavy' > 'light').

Cryostocks
Cryostocks were established for long-term storage of bacterial strains at -80° C. Either bacteria were grown overnight in liquid culture and then 850 µl culture were mixed with 550 µl 86 % sterile glycerol and frozen down to -80° C or bacteria were streaked out on an agar plate, incubated overnight and then scraped off the plate using an inoculation loop and suspended in 1 ml of a 2:1 medium to 86 % glycerol mixture. Stock was frozen down to -80° C.

5.2.2. Growth curves and CFU determination

The growth dynamics of the *met* leader and the *mdh* mutants were investigated using a minimal volume approach in an automatised microplate reader (TECAN system). Bacterial cultures with a start OD_{600} of 0.05 were set up as detailed above and 100 µl were transferred into a well of a 96-well plate. Each strain was set up in triplicate. The TECAN system allows orbital shaking of the plate at a set temperature. Shaking duration was set to 900 seconds with a shaking amplitude of 3 mm, temperature was set to 37° C. Measurement took place over 48 hours. The microplate reader measured the OD_{595} before start of incubation and then every 30 minutes and saved the obtained values in a Microsoft Excel table. Values of triplicates per time point were averaged and means were plotted against time to to create the growth curves.

For the long-term experiment 1 ml of undiluted or 1:10 dilutions of the cultures were measured using a spectrophotometer to determine the OD_{600} after 0, 24, and 48 hours, then after 4, 8, 12, 16 and 20 days. Obtained values were plotted against time to create the growth curves.

For CFU determination 20 µl of the undiluted and serially diluted culture were dropped on an TSB agar plate and spread by tilting the plate from left to right several times while keeping it constantly tilted to allow flowing of the culture. Plates were allowed to dry for 5 to 10 min and then incubated overnight at 37° C. Next morning colonies were counted and CFU/20 µl was calculated considering the respective dilution factor. In a next step, the values of the dilutions were averaged and the CFU/ml was calculated using the mean. Mean was derived from 3 or 4 values, depending on whether the undiluted part had a countable number of colonies. The dilutions plated ranged from 10^{-1} to 10^{-7} depending on the OD_{600} and the previous CFU/ml. (OD_{600} ~0.05: 10^{-3}-10^{-5}, ~0.5: 10^{-4}-10^{-6}, ≥2.0: 10^{-5}-10^{-7}).

5.2.3. Nebraska Transposon Mutant Library (NTML)

Five RNase mutants of the NTML were used in this thesis (see **section 3.3.4**, **page 49 ff.** and **Tab. 15**).

'In an effort to enhance the research capabilities of the staphylococcal research community, the CSR has generated a collection of sequence-defined transposon (Tn) insertion mutants of *Staphylococcus aureus* (*S. aureus*) termed the Nebraska Transposon Mutant Library [(NTML)]. This collection of strains contains mutant derivatives of USA300 LAC in which individual genes have been disrupted by the insertion of the mariner Tn *bursa aurealis*. By determining the nucleotide sequences of the junction fragments containing the end of the Tn and the flanking DNA, the insertion sites have been identified for each mutant in the collection. […]. The ultimate goal is to generate mutations in each of the approximately 2,000 non-essential genes in the genome and make these mutants available for experimental analysis. The Nebraska Transposon Mutant Library (https://app1.unmc.edu/fgx/) is a sequence-defined Tn insertion library of *S. aureus* in which each of the approximately 2,000 non-essential genes in the genome are disrupted via mariner Tn mutagenesis. […] The data associated with each mutant were obtained directly from the USA300_FPR3757 genome sequence (NCBI reference sequence NC_007793).' (https://www.unmc.edu/pathology/csr/research/library.html).

The NTML Screening Array for phenotype screens consists of 1,920 transposon (Tn) mutants of the NTML collection. These mutant strains have not had their Tn-insertion site re-sequenced to confirm the identity of each mutation. Therefore, location of the Tn-insertion in the respective gene needed to be confirmed by PCR with a gene-specific primer (see **Tab. 11**) and a primer binding in the Tn sequence. Depending on the orientation of the Tn the Upstream ('plus') or Buster ('minus') primer was used. For a detailed description see https://app1.unmc.edu/fgx/methods.html.

5.3. Basic Molecular Biological Methods

5.3.1. Plasmid DNA preparation

Plasmid DNA from *E. coli* was either extracted using the 'Quick and Dirty' method or using the NucleoSpin® Plasmid Kit (Macherey-Nagel). For high yields and transformation of plasmid into *Staphylococcus* the 'Quick and Dirty' method was used, for restriction digestion reactions and cloning, plasmid DNA was isolated using the kit to obtain higher purity.

Extraction of plasmid DNA from E. coli using the 'Quick and Dirty' method

A 5ml overnight culture with LB medium supplemented with the required antibiotic was inoculated with bacteria from an agar plate and incubated at 37° C and shaking at 220 rpm. 2 ml of the overnight culture were centrifuged for 1 min at 13,300 rpm and RT, supernatant was discarded, cell pellet resuspended in 200 µl 'buffer I' and reaction inverted several times. Then 200 µl of 'buffer II' were added, reaction inverted several times and incubated for 5 min at RT. Following, 200 µl 'buffer III' were added, reaction inverted several times and incubated for 5 min at RT. Reaction was centrifuged for 10 min at 14,000 rpm and RT, supernatant transferred into a fresh 1.5 ml tube (~600 µl) (if necessary, step was repeated with 5 min centrifugation to increase purity) and DNA precipitated with 0.8 x volumes isopropanol. DNA was pelleted by centrifugation for 10 min at 14,000 rpm and RT, supernatant discarded and washed with 500 µl 70 % ethanol. After centrifugation for 5 min at 14,000 rpm and RT supernatant was discarded, pellet was air-dried or dried at 37° C and subsequently redissolved in 50 µl ddH_2O. DNA concentration and quality was determined by measuring an aliquot of the sample with a spectrophotometer (NanoDrop). DNA was stored at -20° C until use.

Extraction of plasmid DNA from E. coli using a kit

Plasmid DNA from *E. coli* was isolated using the NucleoSpin® Plasmid Kit according to manufacturer's instructions.

5.3.2. Extraction of genomic DNA from *Staphylococcus*

A 5ml overnight culture with LB medium supplemented with 1% (w/v) glycine was inoculated with bacteria from an agar plate and incubated at 37° C and shaking at 220 rpm. 2 ml of the overnight culture were centrifuged for 1 min at 13,300 rpm and RT, supernatant was discarded and cell pellet resuspended in 1 ml TE buffer and pelleted again. Then pellet was resuspended in 100 µl TS buffer (10mM Tris pH7.5, 25% Saccharose), 15 µl 0.5 M EDTA (pH 8.0) and 10 µl lysostaphin (2 mg/ml) were added and mixed by flicking the tube. Reaction was incubated for 20-30 min at 37° C until it became viscous. Following, 375 µl TE buffer, 225 µl 10 % (w/v) SDS solution and 20 µl proteinase K (5 mg/ml) were added and mixed by inverting several times. Reaction was incubated for 30 min at 55° C. After incubation 150 µl sodium perchlorate (5 M) were added, mixed by inverting and then 450 µl (0.5x of total volume) of a chloroform/isoamylalcohol 24:1 mix were added under a fume hood. Then reaction was vigorously shaken for 1 h and 30 min using a vortexer with rack adapter at maximum speed. Subsequently, reaction was centrifuged for 10 min at 14,000 rpm and RT. Upper aqueous phase was transferred into two fresh 1.5 ml tubes (~2x 400 µl) and centrifuged for 5 min at 14,000 rpm and RT, supernatant was transferred into fresh 1.5 ml tubes again and centrifuged for 5 min at 14,000 rpm and RT to increase purity. DNA was precipitated with 2x volumes ethanol (~800 µl per tube), centrifuged for 10 min at 14,000 rpm and RT and DNA pellet washed with 500 µl 70 % ethanol. After centrifugation for 5 min at 14,000 rpm and RT supernatant was discarded, pellet was air-dried or dried at 37° C and subsequently redissolved in 50 µl TE buffer. DNA concentration and quality was determined by measuring a 1:10 diluted aliquot of the sample with a spectrophotometer (NanoDrop). DNA was stored at 4° C until use.

5.3.3. Polymerase Chain Reaction (PCR)

Polymerase chain reaction (PCR) was used to amplify specific regions of any template DNA (e.g. chromosomal DNA, plasmid DNA).

For routine PCR amplification (e.g colony PCR) of DNA with sizes up to 6 kb, DreamTaq DNA polymerase was used. For longer amplicons or when high fidelity of the DNA sequence was required the Phusion High-Fidelity DNA polymerase was used due to its proof-reading function. PCR products were stored at -20°C or analysed directly by gel electrophoresis.

DreamTaq PCR:

PCR reaction (1x):		Final concentration
	5 µl 10x DreamTaq Green Buffer	1x
	1 µl 10 mM dNTP mix (10 mM each)	200 µM
	1 µl 10 µM primer 1	200 nM
	1 µl 10 µM primer 2	200 nM
	0.2 µl Dream Taq polymerase	1 U
	Template DNA	10-100 ng for plasmid DNA, 400 ng for chromosomal DNA, 2 µl supernatant of colony preparation
	ddH_2O ad 50 µl	

PCR programme:	95° C	2 min (for colony PCR 5 min)
	95° C	30 sec
	TA° C*	30 sec — 35x
	72° C	1min/1 kb
	72° C	5 min
	15° C ∞	∞
*Annealing temperature: Tm (melting temperature) of primer with lower Tm minus 5° C		

Phusion PCR:

PCR reaction (1x):		Final concentration
	10 µl 5x Phusion Green Buffer HF or GC	1x
	1 µl 10 mM dNTP mix (10 mM each)	200 µM
	1 µl 10 µM primer 1	200 nM
	1 µl 10 µM primer 2	200 nM
	0.5 µl Phusion polymerase	1 U
	Template DNA	10-100 ng for plasmid DNA, 400 ng for chromosomal DNA, 2 µl supernatant of colony preparation
	ddH_2O ad 50 µl	

PCR programme:	98° C	30 sec (for colony PCR 5 min)
	98° C	10 sec
	TA° C*	30 sec — 35x
	72° C	15-30 sec/1kb
	72° C	10 min
	15° C ∞	∞
*Annealing temperature: Tm of primer with lower Tm plus 3° C		

Colony PCR for testing of clones after transformation or transduction

Clones from *E. coli* transformations (see **paragraph Heat-shock method (for *E. coli* transformation), page 159**) were saved on an agar plate by picking the colony with a pipette tip and streaking it on agar. Then tip with remaining bacteria was transferred into PCR tube pre-filled with PCR master mix and bacteria were brayed directly in the PCR tube. The initial denaturation step of the PCR was 5 min to lyse bacteria and release the template DNA.

Clones from *S. aureus* transformations (see **paragraph Electroporation (for *S. aureus* transformation), page 159 ff.**) were saved on an agar plate by picking the colony with a pipette tip and streaking it on agar. Then tip with remaining bacteria was transferred into a 1.5 ml reaction tube pre-filled with 20 µl ddH_2O and bacteria were resuspended/brayed. Suspension was boilt at 95° C for 7 minutes, immediately chilled on ice, vortexed and boilt again for 7 minutes and chilled. Following, suspension was spun down for 1 min at 13,300 rpm and room temperature and 2 µl of supernatant containing the template DNA were used for PCR.

5.3.4. Agarose gel electrophoresis

Agarose gel electrophoresis was carried out in 1x TAE buffer to size-separate DNA fragments amplified by PCR or generated by enzymatic digestion. Gels were run in 1X TAE buffer for 30 min to 1 hour at 120-130 V. The run time was adjusted according to the desired separation of fragments. Percentage of agarose used depended on the size of the DNA. Routinely, 1 % agarose gels were used to separate DNA from 0.5-10 kb. To prepare an agarose gel, the agarose was boiled in 1X TAE buffer until agarose was completely dissolved using a microwave. The solution cooled down to approx. 50°C while stirring on a magnetic stirrer before Midorigreen was added (4 µl/ 100 ml). Mix was poured into a prepared tray with built-in comb. The agarose gel polymerised at least 20 min at room temperature prior to usage for electrophoresis. After polymerisation agarose gels could be stored wrapped in cling film for several weeks at 4°C or directly used for electrophoresis. 5 µl of PCR reaction or size marker were loaded per lane. For enzymatic reactions total volume was loaded (20 µl). The result was visualised and documented with a UV imaging system.

5.3.5. Preparation of DNA for Sanger Sequencing

DNA was prepared according to the instructions of the 'Microsynth Seqlab' company that was as follows: The total reaction volume of 15 µl had to contain 30 pmol of the sequencing primer, 22.5 ng/100 bp of the DNA (PCR product) to be sequenced and ddH_2O to fill up the volume. The reaction had to be set up in a 1.5 ml reaction tube stickered with the pre-paid barcode label and registered online at the company's homepage before sample collection by the company. Sequencing results were obtained routinely the next day by downloading the files from the web server. Sequencing data were analysed using the software CLC Main Workbench.

5.3.6. Restriction digestion, vector dephosphorylation, DNA ligation

Restriction digestion reactions
Restriction digestion reactions were set up according to manufacturer's instructions (ThermoScientific for the FastDigest restriction enzymes, or else NEB). A standard reaction with plasmid DNA contained 1 µg plasmid DNA, 2 µl 10x FastDigest Green Buffer or 2x NEB CutSmart buffer, 1 µl of the respective enzymes (single or double digest reaction) and ddH_2O to a final volume of 20 µl. Reaction was incubated at 37° C (if not otherwise required) for 1 hour and subsequently dephosphorylated (see below).

A standard reaction with PCR products contained 10 µl unpurified PCR product, 2 µl 10x FastDigest Green Buffer, 1 µl of the respective enzymes (single or double digest reaction) and ddH_2O to a final volume of 30 µl. Reaction was incubated at 37° C (if not otherwise required) for 1 hour. A DpnI digestion reaction with the FastDigest enzyme was set up accordingly. When using the NEB DpnI, 1 µl of enzyme was added directly to the PCR reaction and incubated at 37° C for 1 hour. Reactions were cleaned up using the innuPREP PCRpure kit.

Vector dephosphorylation reactions
Plasmid linearisation by restriction digestion was followed by a dephosphorylation reaction to prevent self-religation of the vector backbone without including the insert. Either Antarctic Phosphatase (AnP, NEB) or Alkaline Phosphatase from Calf Intestine (CIP, NEB) were used. Reaction was set up according to manufactuer's instructions: 17 µl of the unpurified restriction digestion reaction (see above), 2 µl 10x AnP Buffer or 10x CutSmart Buffer and 1 µl AnP or CIP. Reaction was incubated for at least 1 hour at 37° C and cleaned up using the innuPREP PCRpure Kit.

DNA ligation reactions
Usually, the QuickLigation kit (NEB) was used for ligation reactions according to manufacturer's instructions. For ligations difficult to achieve the T4-ligase (NEB) was used at 16°C in an overnight reaction according to manufacturer's instructions.

5.3.7. Cloning and mutagenesis

Two different cloning techniques were used for the generation of plasmids. Either the conventional 'cut-and-paste' method using restrictions enzymes and ligases or the '*in vivo E. coli* cloning' (iVEC) method were employed (Nozaki and Niki, 2019). PCR Site-directed mutagenesis methods in combination with iVEC were used to introduce point mutations, insertions or deletions into a plasmid sequence.

Plasmid construction
All plasmids and oligonucleotides are listed in **Tab. 14** and **11**, respectively. Used enzymes are listed in **Tab. 10**, used kits are listed in **Tab. 9**.

pBASE *met* leader mutant vectors
Vector pBASE_met leader+1kb flanking (pFW001) was generated by amplifying the *met* leader sequence with its 1kb flanking regions with polymerase chain reaction (PCR) using genomic DNA of *S. aureus* Newman as template. PCR product was digested with BglII and cloned into pBASE6. The resulting plasmid, pFW001, was verified by Sanger sequencing and used as template for outward PCRs to generate plasmids pBASE_ΔAntiTer&Ter, pBASE_SC2_metleader+1kb flanking, pBASE_SC4_metleader+1kb flanking, pBASE_SC5_metleader+1kb flanking and pBASE_SC7_metleader+1kb flanking. PCR products were DpnI-digested, cleaned up using the innuPREP PCRpure kit (Analytikjena) and used for a ligation reaction. (Note that an actual ligation cannot take place due to the blunt end and tri-phosphate nature of the PCR products. However, iVEC turend out to be more efficient in presence of the ligation buffer. In later cloning approaches the ligase was omitted from the 'ligation' reaction.) The resulting plasmids were verified by Sanger sequencing.

Vectors pBASE_Ter_destab, pBASE6_Ter_mutated_ 2, 3 and 4 were generated by PCR site-directed mutagenesis amplifying the pFW001 vector in two fragments that overlapped in the ampicillin resistance cassette and in the region containing the point mutations introduced by

the primers. The 1.7 kb and the 7.1 kb fragments were DpnI-digested, cleaned up using the innuPREP PCRpure kit and used for a 'ligation' reaction (see above). The resulting plasmid was verified by Sanger sequencing.

Vector pBASE6_Ter_mutated_1 was generated in several steps because cloning as described above was unsuccessful. First two fragments overlapping in the region containing the point mutations introduced by the primers were amplified by PCR using the pBASE_Ter_destab plasmid as template. The 800 bp-fragment contained a BglII restriction site, the 3' flanking region of the *met* leader and the 3' region of the *met* leader, the 1.4 kb-fragment contained a BglII restriction site, the 5'-flanking region of the *met* leader and most of the *met* leader sequence (both fragments overlapped in the Terminator region). PCR reactions were treated with DpnI and cleaned up using the innuPREP PCRpure kit. 50-100 ng of each fragment were used as template for an overlap PCR using the primers FW099 and FW100. The resulting 2.2 kb fragment was size-separated from unwanted PCR products via gel electrophoresis, cut out from the agarose gel and purified using the NucleoSpin® Gel and PCR Clean-up kit (Machery-Nagel). Purified fragment was subjected to A-tailing using Dream-Taq polymerase, following manufacturer's instructions, for cloning into the pGEM-T-easy vector. The resulting plasmid, pGEM-T-easy+Ter_mut_1, was verified by Sanger sequencing and treated with BglII to cut out the Ter-mut_1+1kb_flanking region fragment. pBASE6 vector was linearised using BglII and dephosphorylated using CIP according to manufacturer's instructions. The fragment and the linearised vector were size-separated on an agarose gel, cut out from gel and purified using the NucleoSpin® Gel and PCR Clean-up kit. The fragment was cloned into pBASE6. The resulting plasmid pBASE6_Ter_mutated_1 was verified by Sanger sequencing.

pEB01-met leader-metI

Vector pEB01-met leader-metI was generated by amplifying the *met* leader sequence (from the -35 signal on) until nt 215 of *metI* with PCR using genomic DNA of *S. aureus* Newman as template. PCR product was digested with BamHI and cloned into pEB01. The resulting plasmid was verified by Sanger sequencing.

pJC1_tRNAi_deletion

Vector pJC1_tRNAi_deletion was generated by amplifying the pJC1-MetTBox-metleader-cl-pR-eYFP vector in two fragments that overlapped in the kanamycin resistance cassette. The

5.2 kb fragment included the 3'-end of the tRNA sequence on the non-overlapping end that was subsequently removed by Pfl23II digestion. The 4.5 kb fragment had a flanking Pfl23II restriction site on the non-overlapping end. Both fragments were DpnI- and Pfl23II-digested, cleaned up using the innuPREP PCRpure kit and used for a ligation reaction. The resulting plasmid was verified by Sanger sequencing.

pBASE mdh mutant vectors

Vector pBASE_*mdh* was generated by amplifying the *mdh* sequence with its 1kb flanking regions with polymerase chain reaction (PCR) using genomic DNA of *S. aureus* Newman as template. PCR product was digested with BglII and cloned into pBASE6. The resulting plasmid, pBASE_mdh, was verified by Sanger sequencing and used as template for an outward PCR to generate plasmid pBASE_mdh_del. PCR product was DpnI- and BglII-digested, cleaned up using the innuPREP PCRpure kit and used for a ligation reaction. The resulting plasmid was verified by Sanger sequencing.

Vectors pBASE_mdh_His71Ser and pBASE_mdh_Glu198Ser were generated by PCR site-directed mutagenesis. Outward PCR using pBASE_mdh as template resulted in a linearised vector with overlapping ends in the region containing the point mutations introduced by the primers. PCR products were DpnI-digested, cleaned up using the NucleoSpin® Gel and PCR Clean-up kit and used for a ligation reaction. (Note that an actual ligation cannot take place due to the blunt end and tri-phosphate nature of the PCR products. However, iVEC turend out to be more efficient in presence of the ligation buffer. In later cloning approaches the ligase was omitted from the 'ligation' reaction.) The resulting plasmids were verified by Sanger sequencing.

Vector pBASE_mdh_His71Ser&Glu198Ser was generated by PCR site-directed mutagenesis. Outward PCR using pBASE_mdh_His71Ser as template resulted in a linearised vector with overlapping ends in the region containing the point mutations introduced by the primers. PCR product was DpnI-digested, cleaned up using the NucleoSpin® Gel and PCR Clean-up kit and used for a 'ligation' reaction (see above). The resulting plasmid was verified by Sanger sequencing.

Vector pBASE_mdh Phe32Trp was generated by PCR site-directed mutagenesis amplifying the pBASE_mdh vector in two fragments that overlapped in the ampicillin resistance cassette and in the region containing the point mutations introduced by the primers. The 2.8 kb and the

7 kb fragments were DpnI-digested, cleaned up using the innuPREP PCRpure kit and used for a 'ligation' reaction (see above). The resulting plasmid was verified by Sanger sequencing.

pET28a vectors

Vector pET28_His_Nde_mdh_Not1 was generated by amplifying the *mdh* sequence with PCR using genomic DNA of S. aureus Newman as template. PCR product was digested with NotI and NdeI and cloned into pET28a. The resulting plasmid was verified by Sanger sequencing.

Vector pET28_his_kynB was generated by amplifying the *knyB* sequence with PCR using genomic DNA of *P. aeruginosa* ATCC 15442 as template. PCR product was digested with XhoI and NdeI and cloned into pET28a. The resulting plasmid was verified by Sanger sequencing.

Vector pET28a_mdh_His71Ser was generated by PCR site-directed mutagenesis. Outward PCR using pET28_His_Nde_mdh_Not1 as template resulted in a linearised vector with overlapping ends in the region containing the point mutations introduced by the primers. PCR products was DpnI-digested, cleaned up using the NucleoSpin® Gel and PCR Clean-up kit and used for a ligation reaction. (Note that an actual ligation cannot take place due to the blunt end and tri-phosphate nature of the PCR products. However, iVEC turend out to be more efficient in presence of the ligation buffer. In later cloning approaches the ligase was omitted from the 'ligation' reaction.) The resulting plasmid was verified by Sanger sequencing.

Vector pET28a_mdh_His71Ser_Glu198Ser was generated as described above. Plasmid pET28a_mdh_His71Ser was used as template.

BTHS vectors

Vectors pKNT25_mdh, pKT25C_mdh*, pUT18N_mdh, pUT18C_mdh*, pUT18N_metI, pUT18C_metI*, pUT18N_metC, pUT18C_metC*, pUT18N_metF and pUT18C_metF* were generated by amplifying the respective gene sequence (*mdh*, *metI*, *metC*, *metF*) with flanking XbaI and KpnI restriction sites with polymerase chain reaction (PCR) using genomic DNA of *S. aureus* Newman as template. For the C-terminal fusion constructs the stop codon of the gene sequence was deleted by designing primers accordingly. PCR products were digested with XbaI and KpnI and cloned into the applicable backbone vector(s) (pKNT25, pKT25C, pUT18N or pUT18C). The resulting plasmids were verified by Sanger sequencing.

5.3.8. Genetic manipulation of bacteria

Bacteria were genetically modified by introducing plasmids via transformation or transduction or by subsequently inserting, deleting or exchanging sequences on the bacterial chromosome via allelic replacement. Methods used to genetically modify bacteria are described in the following sections.

5.3.9. Preparation of competent cells

Chemically competent E. coli cells
Bacteria from overnight cultures (5 ml LB medium) were diluted to an initial optical density at 600 nm (OD_{600}) of 0.05 in 200 ml fresh medium and grown with shaking at 180 rpm at 37° C to an OD_{600} of 0.5-0.7. The bacteria were incubated on ice for 10-15 min, transferred into pre-cooled 50 m tubes and centrifuged for 10 min at 4,000 xg and 4° C. Supernatants were discareded and pellets resuspended in 25 ml ice-cold sterile 0.1 M $CaCl_2$ solution, each, on ice, followed by a 20-minute incubation on ice. Then bacteria were centrifuged for 10 min at 4,000 xg and 4° C, supernatants were discareded and pellets resuspended in 2.5 ml ice-cold sterile 0.1 M $CaCl_2$/15 % glycerol solution, each, on ice, followed by a 15-minute incubation on ice. 100 µl aliquots of competent bacteria were transferred into pre-cooled 1.5 ml tubes on ice and stored at -80° C until use.

Electro-competent S. aureus cells
Preparation of electro-competent S. aureus cells for long-term storage

Bacteria from overnight cultures (5 ml TSB medium) were diluted 1:100 with fresh medium to a final volume of 100 ml and grown with shaking at 180 rpm at 37° C to an OD_{600} of 0.6-0.7. Cultures were transferred into 50 ml tubes and centrifuged for 5 min at 4,000 xg and room temperature. Pellet were washed with sterile ddH_2O, centrifuged for 5 min at 4,000 xg and room temperature and then washed 3 times with 20 ml sterile 10 % glycerol solution. Subsequently, pellets were resuspended in 10-15 ml sterile 10 % glycerol solution and incubated at room temperature for 15 min. Then bacteria were centrifuged for 7 min at 4,000xg and pellets were resuspended in 1 ml sterile 10 % glycerol solution, aliquots of 70 µl were stored at -80°C until use.

Freshly prepared electro-competent S. aureus cells

When electro-competent *S. aureus* cells were needed from a strain rarely transformed, electro-competent bacteria were set up freshly for immediate use. Bacteria from overnight cultures (5 ml BHI medium) were diluted to an initial optical density at 600 nm (OD_{600}) of 0.05 in 5 ml fresh medium and grown with shaking at 180 rpm at 37° C to an OD_{600} of 1.0-2.0. Bacteria from 4 ml culture were harvested in a single 2 ml tube, by repeated centrifugation (2x for 1 min at 10,000 rpm, supernatant was discareded after each centrifugation step): Then pellet was washed five times with 2 ml sterile ddH_2O, centrifugation for 30 seconds at 10,000 rpm. Then pellet was resuspended in 70 µl sterile ddH_2O. Preparation was immediately used for electroporation (see **paragraph Electroporation (for *S. aureus* transformation), page 159**). When multiple 70 µl electro-competent *S. aureus* preparations were needed, culture was scaled up accordingly and cells were harvested in separate 2 ml tubes.

5.3.10. Plasmid transformation and transduction

Heat-shock method (for E. coli transformation)

E. coli strains were transformed with a vector using the heat-shock method. Chemically competent bacteria (see **paragraph Chemically competent E. coli cells, page 158**) were quickly thawed on ice, mixed with 10-50 ng of a vector or ligation reaction and incubated on ice for 20-30 min. Then, bacteria were incubated for 90 sec at 42° C, immediately put back on ice for 1-2 min and 1 ml LB medium was added. After that bacteria were incubated for 45 min to 1 h at 37° C and vigorous shaking. Subsequently, 100 µl of the bacterial suspension were plated on LB agar supplemented with the antibiotic the transformed vector confers resistance to and the remaining suspension was spun down for 1 min at 13,000 rpm, ~ 850 µl supernatant was discarded, bacteria resuspended in rest volume and plate on agar as above. Agar plates were incubated at 37° C overnight. After successful transformation colonies appeared. Colonies were tested for presence of plasmid of interest by colony PCR (see **paragraph Colony PCR for testing of clones after transformation or transduction, page 152**).

Electroporation (for S. aureus transformation)

S. aureus strains were transformed with a vector using the electroporation method. Used plasmids were always purified from *E. coli* DC10B to allow direct transformation into *S. aureus* strains other than RN4220. Electro-competent bacteria (see **paragraph Electro-**

competent *S. aureus* cells, page 158 ff.) were either thawed for 15 min at room temperature or immediately used (freshly prepared electro-competent cells), mixed with 5 µg of a vector (in a final volume of 20 µl) and incubated at room temperature for 15 min. Then mixture was transferred into an electroporation cuvette (long electrode, red lid, 1 mm gap, Cell Projects Ltd.) and a pulse of 1.8 kV was applied. Immediately after pulsing, 150 µl TSB were added to the cuvette, mixture was transferred into a 1.5 ml tube and incubated at 37° C and shaking at approx. 180 rpm for 1 hour. Subsequently, ~125 µl of mixture were plated on BHI agar with lower antibiotic concentration (e.g. Cm 10) and the remaining mixture on BHI agar with higher antibiotic concentration (e.g. Cm 30). Agar plates were incubated at 37° C for 2-3 days. After successful transformation colonies appeared. Colonies were tested for presence of plasmid of interest by colony PCR (see **paragraph Colony PCR for testing of clones after transformation or transduction, page 152**).

Phage transduction
Phage lysate preparation

For introduction of plasmids into *S. aureus* strain Newman phage transduction was employed. To obtain phage lysate with the respective plasmid, a *S. aureus* RN4220 strain containing the plasmid of interest was grown in 20 ml LB medium supplemented with the required antibiotic at 37° C and shaking overnight. Then 100 µl of a 1 M $CaCl_2$ solution were added to the culture (final concentration: 5 mM) and mixed. Following, 300 µl of the culture were transferred into a 15 ml tube, 100 µl of Phage φ11 preparation (10^{-2},10^{-1} or 10^{0} phage dilution in phage buffer) added, briefly vortexed and incubated for 3.5-4 hours at room temperature. In parallel a control reaction without phage was set up. After incubation cultures were mixed with 4 ml LB softagar (at 55° C), plated onto BHI agar supplemented with the required antibiotic and incubated overnight at 37° C. Next day, plate with phages was checked for clearing due to plaque formation. If a difference between phage and control plate was visible, 2 ml of phage buffer were added to the phage plate and the soft agar was carefully scratched off the solid agar. The buffer and soft agar were then transferred into a 50 ml tube and centrifuged for 20 min at 4696 xg and room temperature. Supernatant was sterile-filtered via a 0.45 µm and ensuing via a 0.2 µm pore membrane to remove all bacteria from the phage lysate. Phage lysates were immediately used for phage transduction or stored at 4° C until use.

Phage transduction

Bacteria to be transduced were grown in 10 ml LB medium in a 100 ml flask overnight at 37° C and shaking. Then 50 µl of a 1 M $CaCl_2$ solution were added to the culture (final concentration: 5 mM) and mixed. Following, 300 µl of the culture were transferred into a 15 ml tube, incubated for 2 minutes at 52° C in a water bath to shut down bacterial restriction systems and immediately 100 µl of the prepared phage lysate were added. The culture was briefly vortexed and incubated for 45 minutes at room temperature. In parallel a control reaction without phage lysate was set up. After incubation cultures were mixed with 3 ml LB softagar supplemented with 20 mM trisodium citrate (60 µl of 1 M trisodium citrate solution for 3 ml softagar) (at 55° C), plated onto BHI agar supplemented with the required antibiotic or on plain TSB agar for the control reaction and incubated for 1-2 days at 37° C. After successful transduction colonies appeared. Colonies were tested for presence of plasmid of interest by colony PCR (see **paragraph Colony PCR for testing of clones after transformation or transduction, page 152**). Control plate showed a bacterial lawn.

5.3.11. Allelic replacement ('double cross over')

Chromosomal integration or deletion of genes was accomplished via allelic replacement with inducible counter-selection ('double cross over') adapted from Bae & Schneewind (Bae and Schneewind, 2006). The pBASE6 *S. aureus/E. coli* shuttle vector has been used. The vector containing the sequence to be chromosomally integrated and 1 kb of its flanking region, or in the case of a deletion only the 1 kb flanking region, was cloned as described in **section 5.3.7., page 154 ff.** The vector was either introduced into the *S. aureus* strain of interest via electroporation or phage transduction. Bacteria were grown overnight in 10 ml TSB medium supplemented with chloramphenicol (30 µg/ml, Cm30) to prevent vector loss in a 250 ml shaking flask with vigorous shaking at 37° C. Part of the culture was streaked out with an inoculation loop on a pre-warmed (43° C) TSB agar plate supplemented with Cm30 and immediately incubated at 43° C overnight to induce vector insertion into the chromosome. Vector replication is inhibited at 43° C. Therefore, the vector with the chloramphenicol resistance cassette can be only propagated when integrated into the chromosome. Next day a big, well isolated colony was used to inoculate 5 ml TSB supplemented with Anhydrotetracycline (50 ng/ml, ATc) in a culture tube wrapped in aluminium foil. Bacteria were grown overnight at 30° C and vigorous shaking. ATc is very light sensitive and induces

expression of the *secY* antisense transcript via the Pxyl/tetO promoter from the vector. SecY is essential in *S. aureus*, the antisense transcript prevents its expression. Due to that ATc stimulates vector excision and allows only growth of cells that have excised the vector from the chromosome ('counter-selection'). The overnight culture was diluted 10^{-4} to 10^{-6} with sterile 1x PBS depending on the OD and 100 µl were plated on a TSB agar plate supplemented with ATc (50 ng/ml). Incubation overnight at 37° C was strictly performed in the dark to prevent ATc degradation. Next day 10-30 big colonies were picked and streaked out on TSB and TSB supplemented with Cm30 and incubated overnight. Colonies that grew only on plain TSB were tested for successful allelic replacement by colony PCR and subsequent sequencing of the region of interest.

Testing for spontaneous agr mutations after 'double cross over'

All *met* leader mutants obtained by allelic replacement were tested for spontaneous *agr* mutations as described by (Adhikari et al., 2007). Because the 'double cross over' procedure seems to facilitate spontaneous *agr* mutations (personal communication Gabriella Marincola, Würzburg). *S. aureus* RN4220 was streaked in a vertical line on a blood agar plate, then all strains to be tested were streaked from the margin of the plate at a right angle into the RN4220. As reference strain *S. aureus* Newman was used. Plates were incubated at 37° C overnight and inspected for changes in haemolysis patterns. All tested mutants were negative for *agr* mutations.

5.4. RNA Techniques

Reagents and buffers were either bought 'RNase-free' or set up with DEPC-treated ddH_2O. DEPC water was set up according to manufacturer's instructions. During all RNA-related work, special care was taken to maintain RNase-free conditions by cleaning devices, pipettes and surfaces regularly with RNase-ZAP® and changing gloves frequently. Unless otherwise indicated, RNA was kept on ice during procedures to avoid degradation and stored at -80° C.

5.4.1. Total RNA extraction

Total RNA from staphylococci was extracted using the hot phenol method. Samples were kept on ice during the whole extraction process unless otherwise specified. Bacteria were grown to

the indicated growth phase, 7.5 to 10 ml of culture were harvested and mixed with 0.2x volumes of ice-cold RNA Stop Mix solution (95 % pure ethanol and 5 % Roti®-Aqua-Phenol, v/v) and kept on ice (max. 1 h) until spin-down for 10 min at 3,500 rpm and 4° C. Supernatant was discarded and cell pellets were frozen-down and stored at -80° C until RNA extraction. Samples were thawed on ice, pellets were resuspended in 750 µl TE-buffer and suspension transferred into a Lysing Matrix E tube (MP). Cells were mechanically disrupted using the FastPrep (MP) device at maximum force (6.5) for 2x 30 seconds. Samples were immediately chilled on ice for 5 minutes and subsequently spun down for 30 sec at 13,000 rpm and 4° C. In total, about 600 µl supernatant were transferred into a fresh reaction tube, mixed with 60 µl 10 % (w/v) SDS and incubated for 2 min at 64° C in a waterbath, then mixed with 66 µl 1M sodium acetate. 750 µl Roti®-Aqua-Phenol was added to the sample, mixed by inversion and incubated for 10 min at 64° C with mixing every minute. Following samples were cooled down on ice for 2 min and spun down for 15 min at 13,000 rpm and 4° C. Upper aqueous phase was transferred into Phase Lock Gel Heavy tubes (5Prime) prefilled with 750 µl chloroform and vigorously shaken for 1-2 min. After a 12-minute spin at 13,000 rpm and 15° C upper aqueous phase was either transferred into 2 fresh reaction tubes for ensuing overnight precipitation with ethanol or in 1 fresh tube for ensuing isopropanol precipitation.

Ethanol precipitation: RNA was precipitated overnight at -20° C with 4.67x volumes 30:1 ethanol/sodium acetate mix.

Isopropanol precipitation: RNA was precipitated at room temperature for 10 min with equal volume of isopropanol and 0.1x volume 3M sodium acetate.

Precipitation reaction was centrifuged for 30-45 min at 14,000 rpm and 4° C, RNA pellet washed once with 900 µl ice-cold 70-75% ethanol and dried at room temperature or 37° C. RNA was redissolved in 40-80 µl RNase-free dH_2O with incubation for 5 min at 65° C and shaking at 1,000 rpm using a heating block. RNA concentration and quality was determined by measuring a 1:10 diluted aliquot of the sample with a spectrophotometer (NanoDrop). RNA was stored at -80° C until use.

5.4.2. Denaturing polyacrylamide gel electrophoresis (PAGE)

Unless otherwise specified 10 µg of total RNA was size separated on a 5 % polyacrylamide gel with 7M urea for analysis of the *met* leader RNA. One gel consisted of 60 ml PAA premix

(5 % of 40 % PAA solution (19:1 acrylamide/bis-acrylamide), 7 M urea, 10 % 10x TBE buffer and purified ('VE') H_2O), 600 µl 10 % APS and 60 µl TEMED. RNA was mixed with 2x RNA gel loading dye, incubated for 2 min at 95° C and chilled on ice before loading. Electrophoresis proceeded at 300 V for 2h and 45 min in 1x TBE buffer at room temperature. Ensuing RNA was subjected to Northern blotting (see below).

5.4.3. Denaturing (formaledehyde) agarose gel electrophoresis

10 µg of total RNA was size separated on a 1.2 % denaturing agarose gel for analysis of RNA species longer than 500 nt (*met* operon mRNA). 150 ml gel consisted of 1.8 g agarose (1.2 %), 15 ml 10x MOPS buffer (1x), 4.5 ml 37 % formaldehyde solution (1.11 %) and 130.5 ml DEPC water. For RNA visualisation 6 µl Midorigreen were added to the gel preparation. RNA was mixed with 2x RNA gel loading dye, incubated for 2 min at 95° C and chilled on ice before loading. Electrophoresis proceeded at 100 V for 3 h and 30 min in 1x MOPS buffer at room temperature. Ensuing separation and integrity of the RNA was documented by UV imaging and subjected to Northern blotting (see below).

5.4.4. Northern Blotting and analysis

Total RNA separated by size on a polyacrylamide gel was transferred onto a nylon membrane (Amersham Hybond-XL, GE Healthcare) using the wet electroblotting technique. RNA was transferred onto membrane at 50 V for 1 h and 15 min at 4° C in 1x TBE buffer. After blotting RNA was cross-linked to membrane with 2x 120 mJ UV light.

Total RNA separated by size on an agarose-formaldehyde gel was transferred onto a nylon membrane (Amersham Hybond-XL, GE Healthcare) by either using upward capillary transfer or by rapid downward transfer with a 10x SSC (saline sodium citrate) buffer. When using the upward capillary transfer method, blotting was allowed to run overnight (around 15 h), when using the rapid downward transfer, blotting proceeded for 2 h and 30 min. After blotting RNA was cross-linked to membrane with 2x 120 mJ UV light.

5.4.5. Radioactive probe and marker labelling

For detection of *met* RNAs radioactively labelled double-stranded (ds) DNA probes were used. 25 ng of a column-purified PCR product was mixed with ddH_2O and 2.5 µl primer solution to a final volume of 9 µl, incubated for 2 min at 95° C and chilled on ice. Then 5 µl 3x labelling buffer, 1 µl Klenow-fragment and 1.5-2.5 µl [α-^{32}P]-dCTP were added, mixed and incubated for 30 min to 1 h at 37° C. Reaction was cleaned up via a G-25 column (illustra MicroSpin G-25 column, GE Healthcare) according to manufacturer's instructions to remove unincorporated dCTPs and stored at -20° C until use.

For detection of 16S or 5S rRNA radioactively labelled single-stranded (ss) DNA probes were used. 0.5 µl of 10 µM ssDNA (with a 5'-monophosphate) were mixed with 7 µl ddH_2O, incubated for 1 min at 95° C and chilled on ice. Then 1 µl T4 DNA polynucleotide kinase buffer A, 0.5 µl T4 DNA polynucleotide kinase (PNK, NEB) and 1 µl [γ-^{32}P]-ATP were added and mixed. Reaction was incubated for 1 h at 37° C, following for 5 min at 95° C to heat-inactivate the PNK and then cleaned up via a G-25 column (illustra MicroSpin G-25 column, GE Healthcare) according to manufacturer's instructions to remove unincorporated γATPs and stored at -20° C until use.

The pUC8 marker was radioactively labelled to be run on denaturing PAA gel for size estimation of RNA species. 15 µl of the pUC8 marker ready-to-use mix (Fermentas) were incubated at 95° C for 1 min and chilled on ice. Then 2 µl T4 DNA polynucleotide kinase buffer A, 1 µl T4 DNA polynucleotide kinase (PNK, NEB) and 2 µl [γ-^{32}P]-ATP were added and mixed. Reaction was incubated for 1 h at 37° C, following for 5 min at 95° C to heat-inactivate the PNK and then cleaned up via a G-50 column (illustra MicroSpin G-50 column, GE Healthcare) according to manufacturer's instructions to remove unincorporated γATPs. 2x RNA gel loading dye was added in equal volume (50 µl) and marker was stored at -20° C until use.

5.4.6. Rifampicin RNA stability assays

To determine the stability of the *met leader* and *met* operon RNA in *Staphylococcus aureus*, bacteria were grown to an OD_{600} of 1.5 to 2.0 (mid-exponential phase) and treated with rifampicin to a final concentration of 100 µg/ml. Samples were taken for RNA isolation at

indicated time point following rifampicin addition (unless otherwise specified: after 0, 0.5, 1, 2, 4, 8, 16 and 32 min) as described in **section 5.4.1, page 162 ff**.

5.4.7. In-line probing

In-line probing was used to determine the secondary structure of the *met* leader RNA. *In vitro* transcribed RNA of either the full-length (440 nt) or a shortened (237 nt) *met* leader version were used for in-line probing. Column-purified PCR products containing a T7 promoter sequence immediately upstream of the *met* leader sequence were used as template for *in vitro* transcription. To increase transcription efficacy, the full-length *met* leader template sequence contains two additional 5'-guanosines and the shortened *met* leader one additional 5'-guanosine.

In vitro transcription was carried out using the T7 Mega Script Kit according to the manufacturer's instructions for short transcripts. Following, template DNA was digested by incubation with 1 µl Turbo DNase for 15 min at 37° C, reaction volume was increased to 100 µl with RNase-free water and RNA was purified with 100 µl phenol chloroform isoamylalcohol solution (P/C/I, 25:24:1) in a PLG heavy tube. After vigorous shaking reaction was centrifuged for 12 min at 13,000 rpm and 15° C and upper aqueous phase cleaned up via a G-25 column (illustra MicroSpin G-25 column, GE Healthcare) according to manufacturer's instructions. RNA was precipitated with 300 µl 30:1 ethanol/sodium acetate mix for 2 to 3 h at -80° C or overnight at -20° C. When precipitated at -80° C solution was thawed on ice for 20 to 30 min prior to centrifugation for 30 min at 14,000 rpm and 4° C. RNA pellet was washed with 100 µl 70-75 % ethanol, centrifuged for 10 min at 14,000 rpm and 4° C and then dried at room temperature. To redissolve the RNA 33 µl RNase-free dH2O were added and solution was incubated for 5 min at 65 and 1,000 rpm in a heating block and vortexed one to two times in between. RNA concentration and quality was determined by measuring a 1:10 diluted and an undiluted aliquot of the sample with a spectrophotometer (NanoDrop). 10 µM stock solutions of the *in vitro* transcribed RNA were set up with RNase-free water for downstream application and stored at -80° C until use.

End labelling of the *in vitro* transcribed RNA with radioactive [γ-^{32}P]-ATP required preceding dephosphorylation to obtain a 5'-monophosphate. 20 pmol *in vitro* transcribed RNA were mixed with 15 µl RNase-free dH_2O, incubated at 95° C for 1 min and chilled on ice. Then 2 µl 10x CIP (alkaline phosphatase calf intestinal, NEB) reaction buffer and 2 µl CIP were added

and reaction was incubated for 1 h at 37° C. Ensuing reaction volume was increased to 110 µl with RNase-free water and RNA purified with 110 µl phenol/chloroform/isoamylalcohol solution (25:24:1) in a PLG heavy tube. After vigorous shaking reaction was centrifuged for 12 min at 13,000 rpm and 15° C and upper aqueous phase was transferred into a fresh tube. 1.1 µl GlycoBlue (15 mg/ml, Ambion) were added and RNA was precipitated with 300 µl 30:1 ethanol/sodium acetate mix for 3 h at -80° C or overnight at -20° C. RNA was cleaned up and redissolved in 16 µl RNase-free ddH_2O as described above. RNA concentration was determined by measuring an undiluted aliquot of the sample with a spectrophotometer (NanoDrop).

For labelling of the RNA, radioactive [γ-^{32}P]-ATP should be as fresh as possible (preferably usage before calibration date) to allow later on easy detection of weaker bands on the in-line gel as well. 20 pmol of dephosphorylated *in vitro* transcribed RNA mixed with RNase-free water to a final volume of 15 µl were incubated at 95° C for 1 min and chilled on ice. Then 2 µl 10x PNK buffer A, 1 µl PNK and 2 µl [γ-^{32}P]-ATP were added and incubated for 1 h at 37° C. Labelling reaction was cleaned up via a G-25 column (illustra MicroSpin G-25 column, GE Healthcare) according to manufacturer's instructions and mixed with 20 µl 2x RNA gel loading dye. Sample was incubated at 95° C for 1 min, chilled on ice and loaded in two lanes of a denaturing 5 or 6 % PAA gel with 7 M urea and deep wells. Electrophoresis proceeded at 300 V for 1h and 45 min in 1x TBE buffer at room temperature. Subsequently, bands of wanted RNA (entire transcript) were excised from gel, transferred into a reaction tube and 750 µl RNA elution buffer were added. RNA was eluted from gel by incubation at 8° C and 850 rpm overnight in a heating and cooling block with shaking function. Then reaction was briefly centrifuged, about 700 µl supernatant was transferred into a PLG heavy tube prefilled with 750 µl phenol/chloroform/isoamylalcohol solution (25:24:1) and vigorously shaken. After centrifugation for 12 min at 13,000 rpm and 15° C upper aqueous phase was transferred equally into 2 fresh tubes and RNA was precipitated with 1 ml absolute ethanol for at least 3 h or overnight at -20° C. RNA was spun down for 30 min at 13,000 rpm and 4° C, pellet was air-dried and then redissolved in 25-50 µl RNase-free water. When the signal detected with the Geiger counter was less than 1,000 counts per second, the RNA was regarded as weakly labelled and double the quantity was used for the in-line probing reaction. RNA concentration was determined by measuring an undiluted aliquot of the sample with a spectrophotometer (NanoDrop) and a 0.2 pmol/µl stock was set up with RNase-free ddH_2O.

For the in-line probing reaction 0.2 pmol [γ-^{32}P]-ATP labelled RNA was mixed with RNase-free water to a final volume of 5 µl and incubated at 95° C for 1 min, then chilled on ice for 5

min and subsequently incubated at 37° C for 15 min. After addition of 5 µl 2x in-line reaction buffer reaction was incubated for 40 h at room temperature. Then 10 µl 2x colourless gel loading solution were added to in-line probing reaction and kept on ice until loading.
For the ladder and control reactions 0.2 pmol [γ-^{32}P]-ATP labelled RNA was used. To prepare the T1 ladder 0.2 pmol [γ-^{32}P]-ATP labelled RNA was mixed with 8 µl RNA sequencing buffer, incubated for 1 min at 95° C and immediately chilled on ice for 2 min. Then 1 µl RNase T1 (0.1 U/µl, 1:10 diultion of stock was set up with RNase-free water) was added, reaction incubated for 5 min at 37° C and stopped by adding 12 µl 2x RNA gel loading dye. Ladder was kept on ice until loading.
To prepare the OH ladder 0.2 pmol [γ-^{32}P]-ATP labelled RNA was mixed with 9 µl alkaline hydrolysis buffer, incubated for 5 min at 95° C and reaction stopped by adding 12 µl 2x RNA gel loading dye. Ladder was kept on ice until loading.

To prepare the control (RNA integrity) reaction 0.2 pmol [γ-^{32}P]-ATP labelled RNA was mixed with 9 µl RNase-free dH_2O, 12 µl 2x RNA gel loading dye was added and control reaction was kept on ice until loading.
10 µl of the in-line, ladder and control reactions were loaded per lane of a denaturing PAA sequencing gel with 7 M urea, respectively. 4, 5, 6 and 10 % PAA gels were used to obtain satisfying size separation of the complete RNA molecule. One gel consisted of 50 ml PAA premix (4, 5, 6 or 10 % of a 40 % PAA solution (19:1 acrylamide/bis-acrylamide), 7 M urea, 10 % 10x TBE buffer and purified ('VE') water), 500 µl 10 % APS and 50 µl TEMED. Gel was pre-warmed to 40-45° C by running in 1x TBE buffer for 1 h at 40 W. Then samples were loaded and electrophoresis proceeded at 40 W for 1 to 4 h (depending on PAA percentage and region of the RNA molecule supposed to be well separated) in 1x TBE buffer at room temperature. Ensuing gel was transferred onto blotting paper (Whatman), dried for 45 min at 80° C with a vacuum applied and exposed to a storage phosphor screen for 1 to 2 days. Screen was read out using the Typhoon FLA 7000 phosphor imaging system.

Table 23. List of *in vitro* transcription product for in-line probing with respective primers used for PCR template.

Name	Primer pair	PCR product [bp]	RNA length [nt]	M.W. [g/mol] RNA
Full-length *met* leader	FW088 Sa.R_met-sRNA	464	440	141,316
Short *met* leader	FW130 Sa.R_met-sRNA	259	236	75,949
Short *met* leader Ter_destab	FW130 FW159	259	236	75,689
Short *met* leader Ter_mutated	FW130 FW169	259	236	75,926
Short *met* leader Ter_mutated_2	FW130 FW211	259	236	75,949
Short *met* leader Ter_mutated_3	FW130 FW212	259	236	75,965
Short *met* leader Ter_mutated_4	FW130 FW213	259	236	75,949

5.4.8. cRACE

cRACE (rapid amplification of cDNA ends from circularised RNA) has been performed to determine the TSS (transcriptional start site), the 3'-end of the *met* leader RNA and in a separate experiment to characterise the transcript detected in the Δ*rnjA* strain containing the plasmid pEB01-met leader-metI (FW97) with a *metI*-specific probe (see **Fig. 14 B**).

TSS and 3'-end determination of *met* leader RNA

15 µg of total RNA isolated as described in **section 5.4.1, page 162 ff.** was mixed with RNase-free water to a total volume of 38 µl, incubated for 5 min at 65° C and chilled on ice. Then 5 µl 10x rDNase I buffer, 5 µl rDNase I (Ambion) and 2 µl SUPERase*In (Ambion) were added and reaction incubated for 1 h at 37° C. Following, 50 µl RNase-free dH2O were added and RNA was purified with 100 µl phenol/chloroform/isoamylalcohol solution (25:24:1) in a PLG heavy tube. After vigorous shaking reaction was centrifuged for 12 min at 13,000 rpm and 15° C, upper aqueous phase was transferred into fresh reaction tube and RNA was precipitated with 250 µl 30:1 ethanol/sodium acetate mix overnight at -80° C. Solution was thawed on ice for 30 min prior to centrifugation for 30-40 min at 14,000 rpm and 4° C. RNA pellet was washed with 250 µl 70-75 % ethanol, centrifuged for 10 min at 14,000 rpm and 4° C and then dried at room temperature. To redissolve the RNA 25 µl RNase-free ddH_2O prewarmed at 65° C were added.

RNA concentration and quality was determined by measuring a 1:10 diluted aliquot of the sample with a spectrophotometer (NanoDrop).

PCR was set up with 4 µl of 1:10 diluted RNA per reaction to check for efficiency of DNA digestion. Primers specific for 16S rRNA gene (16S_rDNA_F and Se16SrDNAR) and for the *met* leader (Sa_lgsm02-Fow and Sa_lgsm02_Rev) were used, T_A: 49° C, t_E: 1 min and T_A: 54° C and t_E: 45 sec, respectively. DreamTaq polymerase (Thermo Scientific) was used.

5 µg of DNase-treated RNA was dephosphorylated using RNA 5´ Pyrophosphohydrolase (RppH, NEB) to generate 5'- monophospated RNA that can be self-ligated with its 3'-end. RNA was mixed with 0.5 µl RiboLock (ThermoScientific), 5 µl 10x NEB buffer 2, 2 µl RppH and RNase-free water was added to a final volume of 50 µl. Reaction was incubated for 45 min at 37° C, following RNA was cleaned up as described above, but with overnight incubation at -20° C. Then RNA was redissolved in 13.5 µl RNase-free water prewarmed at 65° C, denatured for 2 min at 70° C and chilled on ice. For ligation of RNAs' 5'- and 3'-ends 2 µl 10x ligation buffer, 2 µl T4 RNA ligase (10 U/µl) and 1 µl RiboLock were added and reaction incubated overnight at 16° C. Circularised RNA was cleaned up as described above with precipitation over day for 4 h at -80° C, redissolved in 10 µl RNase-free water and RNA concentration was determined by measuring a 1:10 diluted aliquot of the sample with a spectrophotometer (NanoDrop).

2 µg circularised RNA was used for cDNA synthesis. RNA was mixed with 20 pmol of a *met* leader RNA-specific primer (FW144), 1 µl of a 10 mM dNTP mix and RNase-free water was added to a final volume of 14.5 µl. Then reaction was incubated for 5 min at 65° C and chilled on ice. Following, 4 µl of 5x Reverse Transcriptase buffer, 0.5 µl of RiboLock and 1 µl of RevertAid Premium Reverse Transcriptase (ThermoScientific) were added, reaction was incubated for 30 min at 50° C and Reverse Transcriptase was heat-inactivated by incubation of 5 min at 80° C.

1 µl of undiluted, 1:10 and 1:20 diluted cDNA were used in PCR. *met* leader specific primers FW144 and FW145 were used for amplification with DreamTaq polymerase, T_A: 48° C, t_E: 30 sec. PCR of 3 dilutions were pooled and cleaned up via a column. DNA concentration was determined by measuring an aliquot of the sample with a spectrophotometer (NanoDrop). PCR products were cloned into the pGEM-T-easy vector system I (Promega) with a 6:1 insert to vector ratio. DNA concentration of the PCR product was regarded as ten times less than measured, as residual RNA seemed to bias the measurement. Ligation reaction was set up according to manufacturer's instructions and transformed into *E. coli* DC10B.

Colony PCR was set up with transformants using the universal vector primers M13_Fow and M13_Rev to amplify the insertion region, T_A: 45° C, t_E: 45 sec. All PCR products that resulted from non-empty vectors were cleaned up and prepared for sequencing as described in **section 5.3.5, page 153**. Primer M13_Fow was used for sequencing. Sequences were analysed using the CLC Main Workbench software.

Δ*rnjA* mutant transcript characterisation

cRACE was performed as described above with total RNA of strain Δ*rnjA* containing the plasmid pEB01-met leader-metI (FW97). Primer FW156 was used for cDNA synthesis and primers FW156 and FW157 for PCR, T_A: 46° C, t_E: 1 min.

5.4.9. 5' RACE

5' RACE (rapid amplification of cDNA ends) has been performed to determine the 5'-ends of the *met* operon mRNA processing intermediates. 10 µg of untreated total RNA were used for RNA adapter ligation. The untreated RNA sample allowed to detect only processed RNAs and not primary transcripts as only processed RNAs contain a 5'-monophosphate required for RNA adapter ligation. RNA was mixed with 400 pmol RNA adapter primer, volume was adjusted to 66.2 µl with RNase-free ddH_2O, incubated for 5 min at 95° C and chilled on ice. For ligation of RNAs' 5'-end with the RNA adapter 8 µl 10x ligation buffer, 4 µl T4 RNA ligase (10 U/µl), 0.8 µl ATP (75 mM) and 1 µl BSA were added and reaction incubated for 1 h at 37° C. RNA was cleaned up as described above after adjusting volume to 100 µl with RNase-free ddH_2O with precipitation overnight at -20° C. To redissolve the RNA 10 µl RNase-free ddH_2O were added. Subsequently, RT-PCR was set up for cDNA synthesis. 5 µl of RNA was mixed with 20 pmol of a *met* operon mRNA-specific primer (FW161 binding within *metF* or FW200 binding within *metI*) (see **Fig. 12**), 1 µl of a 10 mM dNTP mix and RNase-free water was added to a final volume of 14.5 µl. Then reaction was incubated for 5 min at 65° C and chilled on ice. Following, 4 µl of 5x Reverse Transcriptase buffer, 0.5 µl of RiboLock and 1 µl of RevertAid Premium Reverse Transcriptase (ThermoScientific) were added, reaction was incubated for 1 h at 50° C and Reverse Transcriptase was heat-inactivated by incubation of 5 min at 80° C.
1 µl of 1:10 and 1:20 diluted cDNA were used in PCR. *met* operon specific primer FW149 or Sa_lgsm02_Lext_rev and an RNA adapter specific primer were used for amplification with the Platinum SuperFi Green PCR Master Mix (Thermo Scientific) according to manufacturer's

instructions, T_A: 59.9° C, t_E: 2 min 30 sec (cDNA synthesis with FW161) or 30 sec (cDNA synthesis with FW200). PCR of 2 dilutions were pooled and cleaned up using the PureLink kit supplied with the TOPO™-XL-2 complete PCR Cloning Kit (Thermo Scientific) according to manufacturer's instructions. DNA concentration was determined by measuring an aliquot of the sample with a spectrophotometer (NanoDrop). PCR products were cloned into the pCR-XL-2-TOPO vector with a 1:1 insert to vector ratio. DNA concentration of the PCR product was regarded as ten times less than measured, as residual RNA seemed to bias the measurement. Cloning reaction was set up according to manufacturer's instructions and transformed into One Shot™ OmniMAX™ 2 $T1^R$ competent cells via heat shock. 2 µl of cloning reaction were mixed with competent cells briefly thawed on ice, incubated on ice for 20-30 min and heat-shocked for 30 sec at 42° C. Then cells were kept on ice for 2 min, 225 µl S.O.C. medium was added and bacteria incubated for 45 min to 1 hour at 37° C and shaking at 225 rpm. Bacteria were plated on LB-agar supplemented with 50 µg/ml kanamycin and 1 mM IPTG. Colony PCR was set up with transformants using the universal vector primers M13_Fow and M13_Rev to amplify the insertion region. For 5' RACE set up with primer FW161, Phusion polymerase (ThermoScientific) was used, T_A: 53° C, t_E: 2 min 30 sec. For 5' RACE set up with primer FW200 DreamTaq polymerase (ThermoScientific) was used, T_A: 45° C, t_E: 1 min 15 sec and 1 min30 sec, respectively. All PCR products that resulted from non-empty vectors were cleaned up and prepared for sequencing as described in **section 5.3.5, page 153**. Primer M13_Rev was used for sequencing, for PCR products longer than 1 kb addition sequencing reaction with the M13_Fow was set up. Sequences were analysed using the CLC Main Workbench software.

5.5. Protein Techniques

The following section was adapted from Daniela Steigerwald's and Esther Rogalski's master theses (Rogalski, 2017; Steigerwald, 2016). Wolfgang Kölmel provided the crystallisation statistic data.

5.5.1. (Over)expression and purification of His-tagged proteins

Mdh, Mdh His71Ser&Glu198Ser and KynB overexpressed in *E. coli* contained a 21 amino acids-long N-terminal tag (MGSS**HHHHHH**SSG*LVPRGS*HM) including the **hexa-histidine tag** and a *thrombin tag* (for proteolytic removal of the tag, if necessary) as encoded by the pET28a(+) vector system (Novagen®). The mass of the proteins was predicted including the tag: Mdh: 31.05 kDa, Mdh His71Ser&Glu198Ser: 30.96 kDa, KynB: 25.45 kDa using the Protein Molecular Weight Calculator (https://www.sciencegateway.org/tools/proteinmw.htm). Mdh expressed in *S. aureus* contained a C-terminal hexa-histidine tag. The mass of the protein was predicted including the tag: 29.58 kDa.

Overxpression and purification of N-terminally His-tagged proteins from E. coli

For overexpression in *E. coli* BL21 (DE3) of N-terminally His-tagged Mdh, Mdh His71Ser&Glu198Ser (double mutant) and KynB overnight cultures (30 ml LB-medium, supplemented with 0.5 % glucose and 30 µl kanamycin (50 mg/ml) were set up in a 250 ml flask and incubated at 37° C and shaking.

The next day, 20ml of the culture was diluted with 980 ml fresh LB-medium, supplemented with 0.5 % glucose and 980 µl kanamycin (50 mg/ml) (overnight culture to fresh media ratio 1:50) and incubated in a 2 l flask at 37° C shaking until OD_{600} of 0.6 was reached. 1 ml aliqot was taken as uninduced reference. In the remaining culture overexpression of was induced by adding 0.4 mM IPTG, culture was incubated at 20° C and shaking for around 20 h. Then cultures were transferred into BeckmanCoulter Avanti Centrifuge J-26XP buckets and centrifuged with the JLA 8.1000 rotor for 15 min at 5,000 rpm and 4 °C. The supernatant was discarded and the pellet resuspended in 20 ml of 1x PBS and transferred into 50 ml falcons and again centrifuged at 5000 rpm for 15 min and 4 °C then the pellet was weighed. Pellets with a weight between 2 g and 4 g were resuspended in 10 ml of 1x LEW buffer supplemented with 400 µl protease inhibitor solution (1 tablet cOmplete™, EDTA-free Protease Inhibitor Cocktail (Roche) solved in 2 ml of ddH_2O). Suspension was incubated on ice for 30 min and subsequently sonified 10x for 20 seconds at maximum power on ice. Then lysates were

centrifuged for 30 min at 10, 000 xg and 4 °C (Thermo Scientific Multifuge Heraeus X3R and the HighconicII Ch.0010478 rotor). Supernatant was decanted into a new 50 ml tube. His-tagged proteins were isolated using affinity chromatography (Protino® Ni-TED 2000 Packed Columns, Macherey-Nagel). The column was calibrated with 5 ml of 1x LEW buffer and the whole cell lysate was loaded onto the column, after flow-through column was washed with 20 ml of 1x LEW buffer followed by a washing step with 10 ml of 1x LEW buffer supplemented with 1 mM imidazole. Proteins were eluted from the column with 9 ml of 1x Elution buffer (1x LEW buffer supplemented with 250 mM imidazole) in 1 ml fractions. To remove the imidazole, elution fractions were pooled and dialysed overnight in 5 litre of a Na_2HPO_4/NaH_2PO_4 (pH 7.4) buffer at 4° C.

Following the dialysis, the samples were purified more profound over a size exclusion chromatography column (Column HiLoad 16/60 Superdex 75 pg) using the ÄKTA device with the UNICORN 7.0 software. 1 litre of degassed protein buffer (Na_2HPO_4/NaH_2PO_4, pH 7.4) was prepared by stirring the buffer for 2 h under vacuum. The volume of the protein sample was added up to 6 ml with the degassed protein buffer and centrifuged at 16,000 rpm for 30 min at 4 °C to ensure no precipitate was transferred onto the column. SDS-PAGE was performed to monitor the overexpression and purification process and to chose the SEC fractions for subsequent concentration for crystalliasation and use in *in vitro* assays (only SDS-PAGE results for SEC fractions are shown).

SEC fractions used for downstream applications: Mdh **A11 to B3**, Mdh His71Ser&Glu198Ser: **A12-B5**. Half of the protein solutions were aliquoted into 50 µl fractions, snap frozen in liquid nitrogen and stored at -80° C until use. The other half was concentrated with an Amicon Ultra-15 10 kDa flacon (Merck Millipore) to 18 mg/ml for crystallisation experiments.

SEC fractions of KynB used for in vitro assays: **A7 to B4**. Protein solution was aliquoted into 50 µl fractions, snap frozen in liquid nitrogen and stored at -80° C until use.

Expression and purification of C-terminally His-tagged Mdh from S. aureus

For expression in *S. aureus* Newman of C-terminally His-tagged Mdh an overnight culture (35 ml CDM +MET) was set up in a 250 ml flask and incubated at 37° C, shaking. The next day, the culture was washed twice with PBS, cell pellet was resuspended in 2x Basic Medium and two 500 ml cultures with CDM -MET and a start OD_{600} of 0.05 were set up. Cultures were incubated at 20° C, shaking for around 27 h (OD_{600} of 3.5). Then cultures were transferred into BeckmanCoulter Avanti Centrifuge J-26XP buckets and centrifuged with the JLA 8.1000 rotor for 15 min at 5,000 rpm and 4 °C. The supernatant was discarded and the pellet resuspended in 20 ml of 1x PBS and transferred into 50 ml falcons and again centrifuged at 5000 rpm for 15 min and 4 °C then the pellet was weighed. Pellets with a weight between 2 g and 4 g were resuspended in 10 ml of 1x LEW buffer supplemented with 400 µl protease inhibitor solution (1 tablet cOmplete™, EDTA-free Protease Inhibitor Cocktail (Roche) solved in 2 ml of ddH_2O). Suspension was incubated on ice for 30 min and subsequently transferred into a 50 ml Lysing Matrix E tube. Cells were mechanically disrupted using the FastPrep (MP) device at maximum force (6.5) for 2x 30 seconds. Samples were immediately chilled on ice for 5-10 minutes in between and after and subsequently centrifuged for 30 min at 10, 000 xg and 4 °C (Thermo Scientific Multifuge Heraeus X3R and the HighconicII Ch.0010478 rotor). Supernatant was decanted into a new 50 ml tube. His-tagged proteins were isolated using affinity chromatography (Protino® Ni-TED 2000 Packed Columns, Macherey-Nagel) as described above. (Note: as the column clogged during the purification process, extended centrifugation time, a filtration step and a bigger elution volume seem advisable).

SDS-PAGE was performed to monitor the expression and purification process and to chose the SEC fractions for subsequent use in *in vitro* assays (only Western blot results for SEC fractions are shown).

SEC fractions used for downstream applications: Mdh (expressed in *S. aureus*): **A9**.

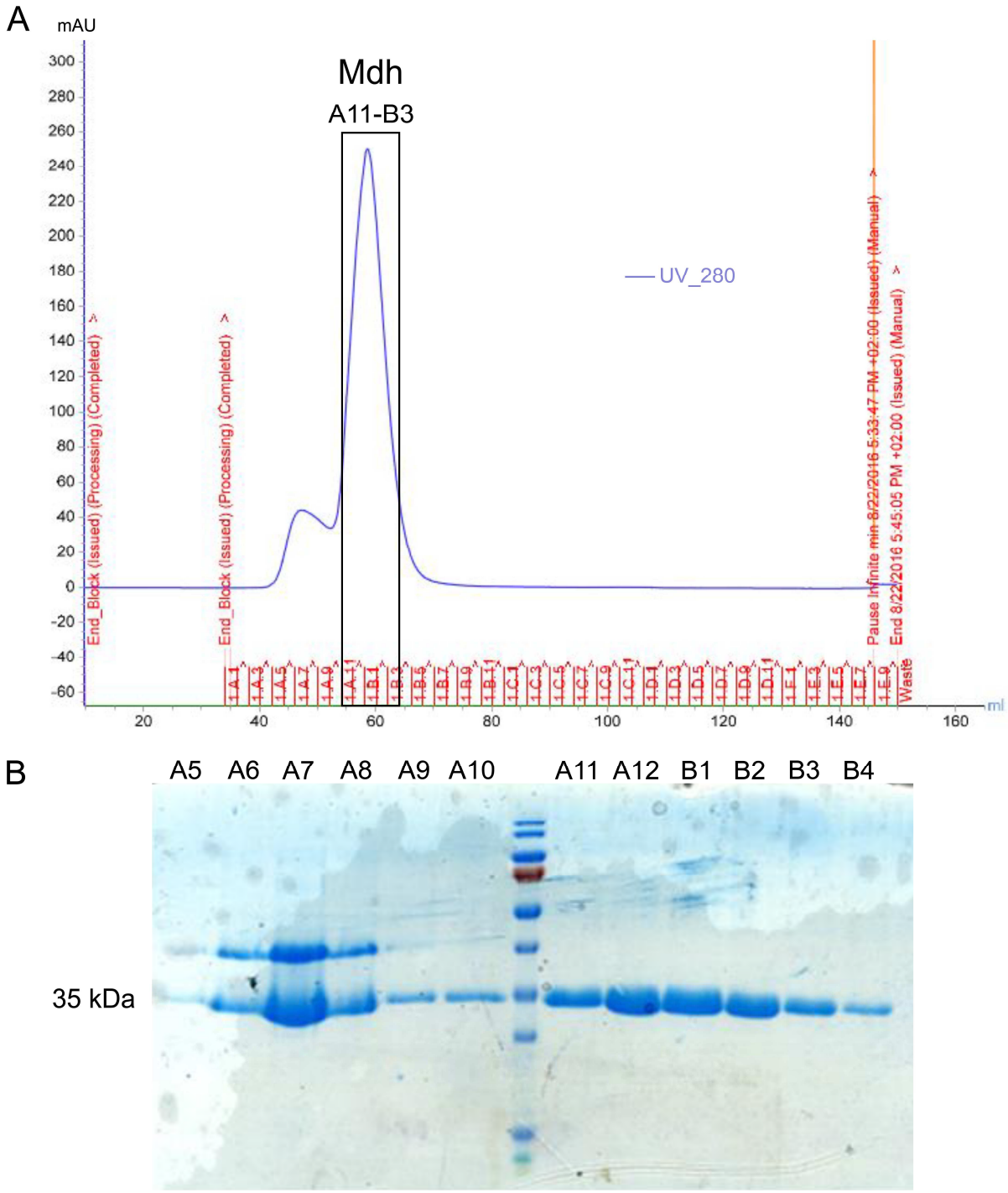

Figure 28. Chromatogram of size exclusion chromatography (SEC) and SDS-PAGE of Mdh fractions derived from SEC. (A) Absorption in mAU at 280 nm is plotted against the elution volume in ml. Collected fractions are specified on top of x-axis. Fractions used for downstream applications are highlighted by a box. **(B)** SDS-PAGE of aliquots from SEC fractions indicated above gel. Size of relevant band is indicated on the left. 12% SDS-polyacrylamide gel, coomassie-stained, size marker: Prestained Protein Ladder 10-180 kDa. For further details see (Steigerwald, 2016).

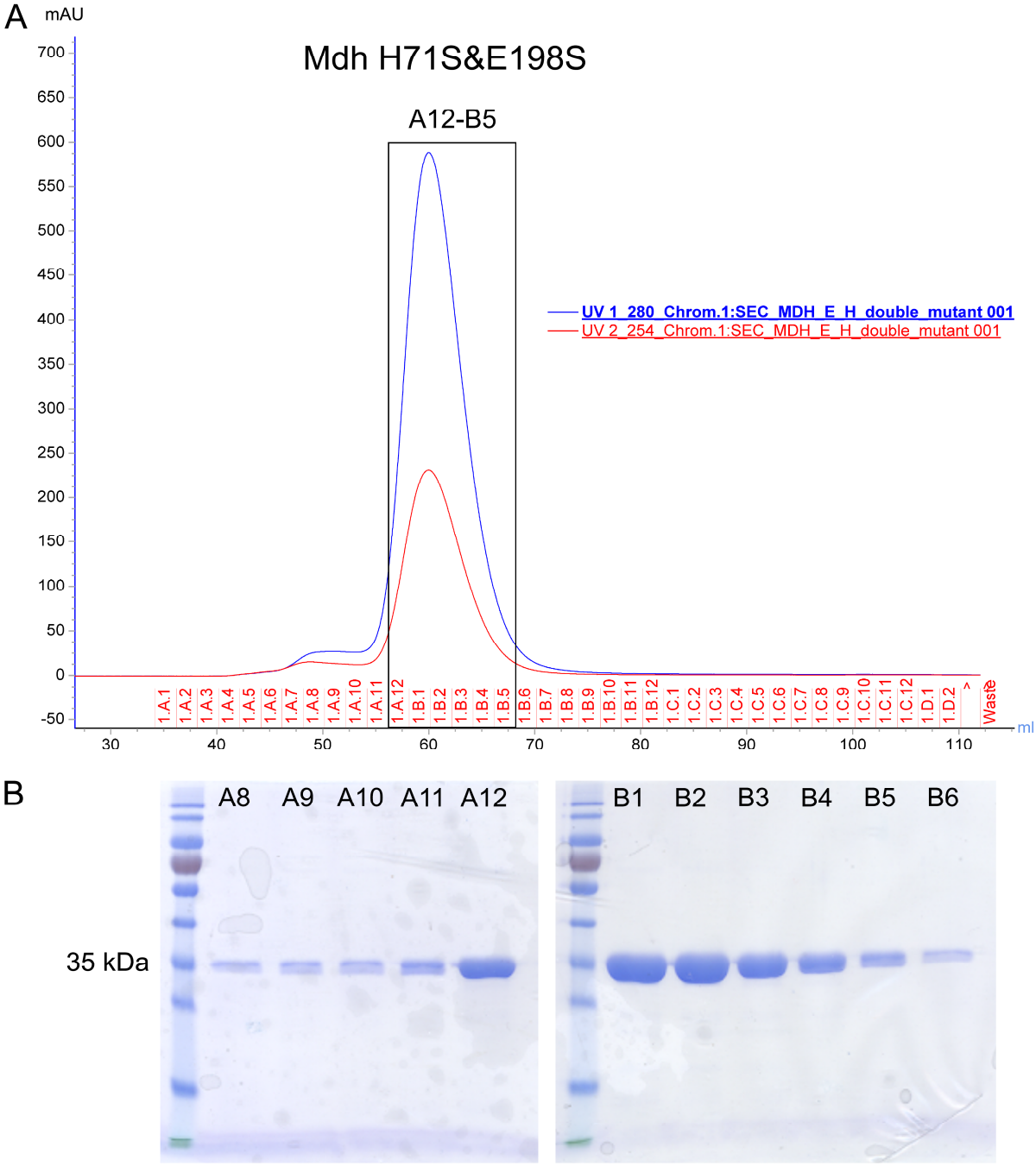

Figure 29. Chromatogram of size exclusion chromatography (SEC) and SDS-PAGE of Mdh His71Ser&Glu198Ser fractions derived from SEC. (A) Absorption in mAU at 280 nm (blue) and 254 nm (red) are plotted against the elution volume in ml. Collected fractions are specified on top of x-axis. Fractions used for downstream applications are highlighted by a box. **(B)** SDS-PAGE of aliquots from SEC fractions indicated above gel. Size of relevant band is indicated on the left. 12% SDS-polyacrylamide gel, coomassie-stained, size marker: Prestained Protein Ladder 10-180 kDa. For further details see (Rogalski, 2017).

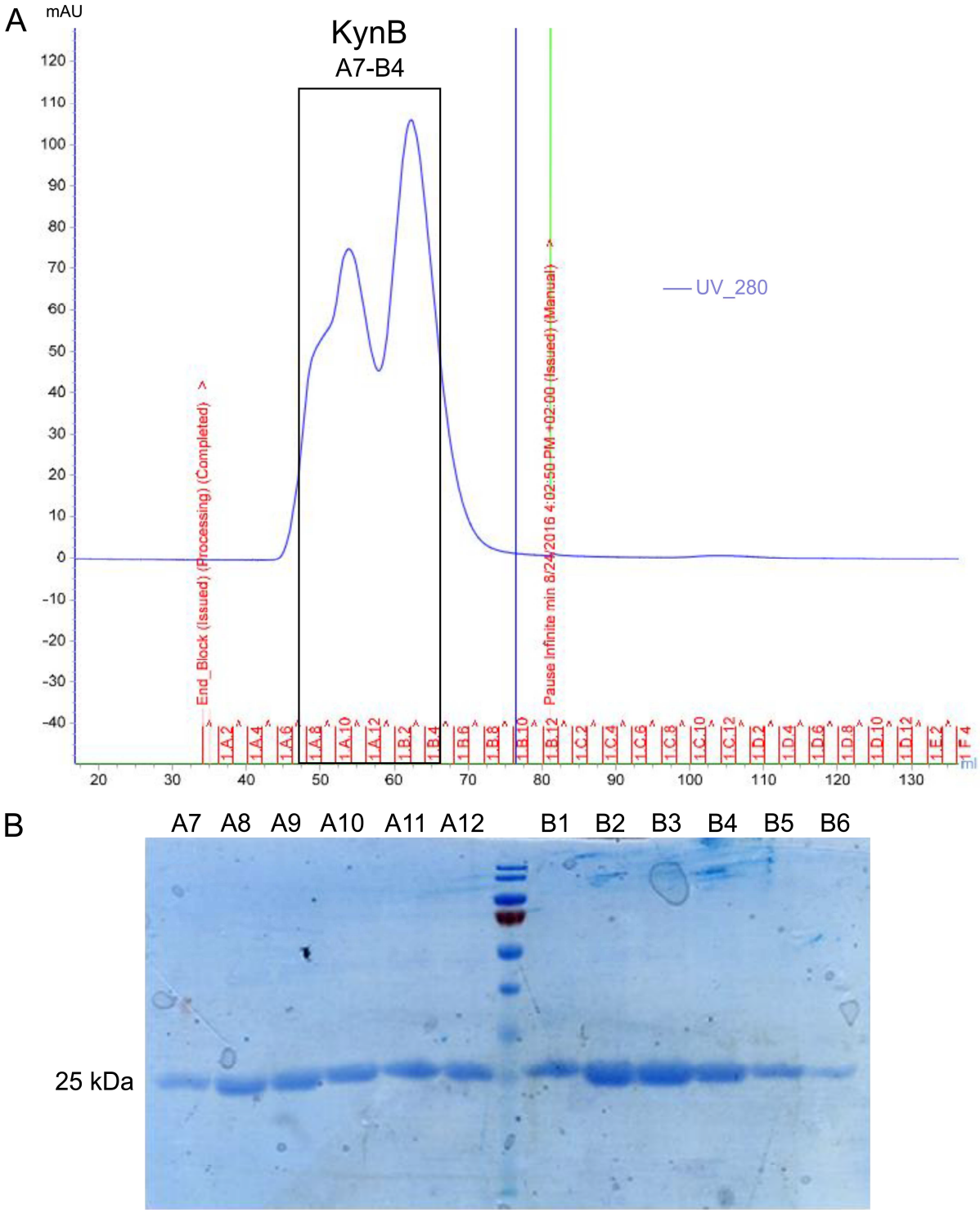

Figure 30. Chromatogram of size exclusion chromatography (SEC) and SDS-PAGE of KynB fractions derived from SEC. (A) Absorption in mAU at 280 nm is plotted against the elution volume in ml. Collected fractions are specified on top of x-axis. Fractions used for downstream applications are highlighted by a box. **(B)** SDS-PAGE of aliquots from SEC fractions indicated above gel. Size of relevant band is indicated on the left. 12% SDS-polyacrylamide gel, coomassie-stained, size marker: Prestained Protein Ladder 10-180 kDa. For further details see (Steigerwald, 2016).

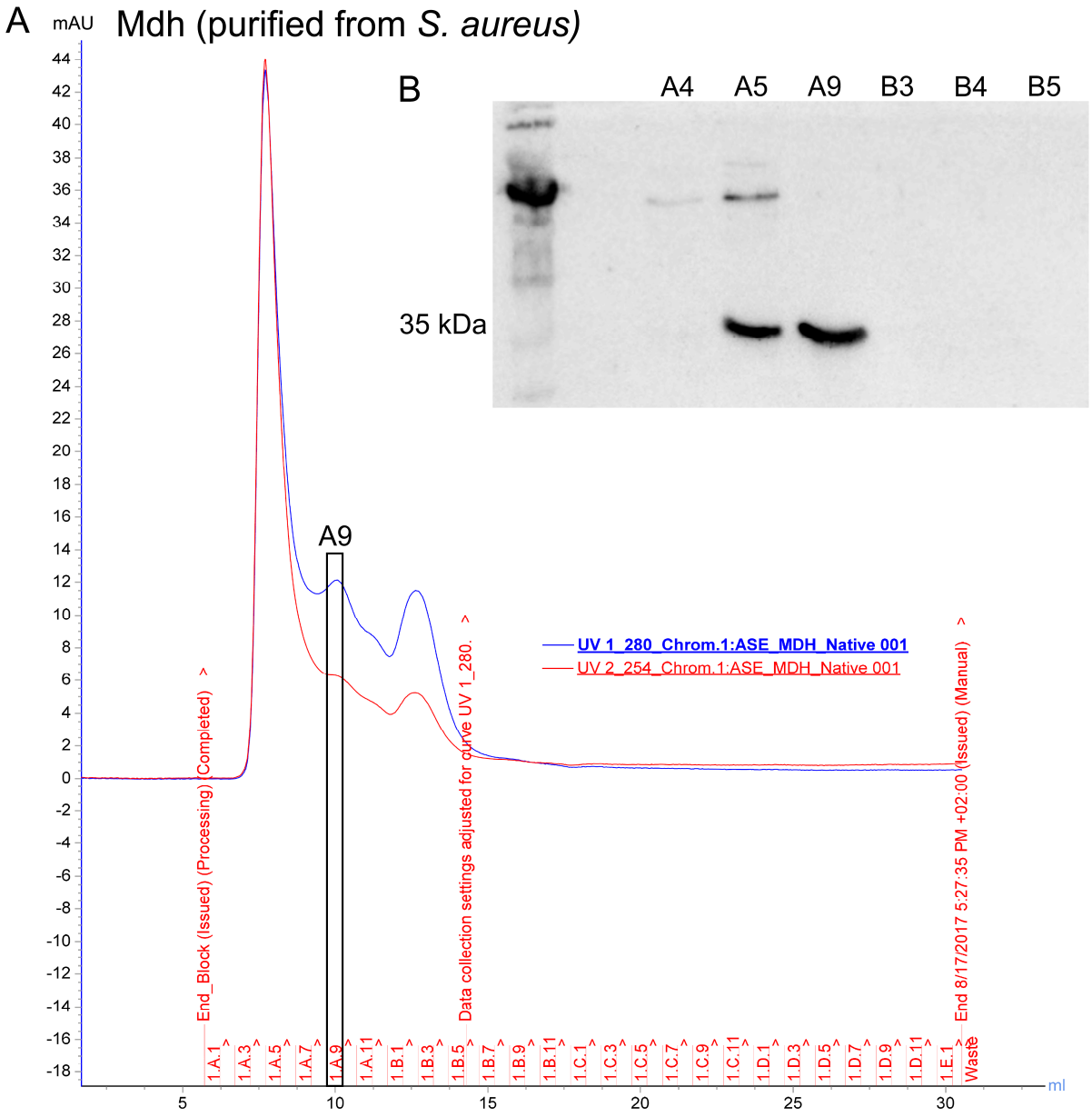

Figure 31. Chromatogram of size exclusion chromatography (SEC) and Western blot of Mdh (purified from *S. aureus)* fractions derived from SEC. (A) Absorption in mAU at 280 nm (blue) and 254 nm (red) are plotted against the elution volume in ml. Collected fractions are specified on top of x-axis. Fraction used for downstream applications is highlighted by a box. **(B)** Western blot of aliquots from SEC fractions indicated above blot using Anti-His-Tag (mouse) primary antibody. Size of relevant band is indicated on the left. (Rogalski, 2017).

5.5.2. Protein crystallisation and 3D structure resolving

Crystallisation of Mdh and Mdh His71Ser&Glu198Ser was achieved overnight at 20°C employing the sitting drop method in a 96 well format. Crystals were obtained by mixing equal volumes of the protein solution at a concentration of 18 mg/ml with a reservoir solution containing 100 mM bis-tris (pH 5.5), 30-300 mM ammonium acetate and 15-20 % PEG 10,000. All crystals were flash frozen in liquid nitrogen using the mother liquior containing additionally 40% PEG 400, as cryo protectant. Diffraction data were collected at the ESRF synchrotron radiation facility at Grenoble, France at the beamline ID23-2.

Data were integrated with XDS (Kabsch, 2010) and scaled with AIMLESS (Collaborative Computational Project, Number 4, 1994). The structure of Mdh was solved by molecular replacement using Phaser (McCoy, 2007) and the phases from the *L. aggregata* Isatin Hydrolase model (PDB entry 4M8D). The structure of Mdh His71Ser&Glu198Ser was solved by molecular replacement using the phases of the Mdh model. Manual model building was done in COOT (Emsley et al., 2010) and model refinement was carried out with PHENIX (Adams et al., 2010). Data collection and refinement statistics are summarized in **Tab. 24** (data provided by Wolfgang Kölmel).

Crystallographic statistics

Table 24. Crystallographic statistics.

Strucutre	**Mdh**	**Mdh His71Ser&Glu198Ser**
Data collection		
Wavelength (Å)	0.8729	0.980
Spacegroup	P 6522	P 6522
Unit cell parameters (Å)	a = 87.065, b = 87.065, c = 142.053, α = 90.0, β = 90.0, γ 0 120.0	a = 85.118, b = 85.118, c = 132.029, α = 90.0, β = 90.0, γ 0 120.0
Resolution range (Å)	43.53 - 1.99 (2.04 - 1.99)	49.18 - 1.80 (1.84 - 1.80)
Unique reflections	22260 (1575)	26936 (1546)
R_{merge}	0.194 (1.650)	0.139 (2.223)
R_{pim}	0.065 (0.627)	0.033 (0.540)
<I/σ (I)>	8.7 (1.1)	14.5 (1.4)
CC (1/2)	0.996 (0.373)	0.999 (0.897)
Multiplicity	9.4 (7.5)	19.2 (17.7)
Completeness (%)	99.5 (97.7)	100.0 (99.9)
Refinement		
Resolution range (Å)	43.50 - 1.99	49.177 - 1.80
Unique reflections	21127	26858
Number of atoms	2175	2184
R_{work}	0.168	0.167
R_{free}	0.219	0.213
Mean B-factor ($Å^2$)	25.55	27.13
RMS Deviations:		
Bond lengths (Å)	0.0224	0.007
Bond angles (°)	1.9880	0.998
Ramachandran statistics:		
Favored (%)	97.93	99.19
Allowed (%)	2.07	0.81
Outliers (%)	0.0	0.0

5.5.3. *In vitro* assays for Mdh substrate testing

In the initial *in vitro* assay, N-formyl-L-kynurenine (Santa Cruz Biotechnology) was tested as substrate for Mdh. L-kynurenine absorbes light at 365 nm, NFK does not. Therefore, cleavage of NFK to L-kynurenine and formate (anion of formic acid) could be measured by an increase in absorption at 365 nm over time with a spectrophotometer.

NFK was dissolved in 'protein reaction buffer' (Na_2HPO_4/NaH_2PO_4, pH7.4) to obtain a 100 mM solution. Mdh and KynB (heterologously overexpressed and purified from *E. coli* (as described in **paragraph Overxpression and purification of N-terminally His-tagged proteins from *E. coli*, page 173 ff.**)) were diluted with protein reaction buffer to a concentration of 5 ng/µl, 500 ng of enzyme were used per reaction. A 1 mM $ZnCl_2$ solution was set up with ddH_2O.

Reactions were set up in quartz cuvettes (Hellma®, Typ 104-QS SA 10 mm, Quarzglas Suprasil) for accurate measurements. Composition of reactions measured in this initial *in vitro* assay is detailed in **Tab. 25**. Absorption was measured every 30 seconds until 5 minutes after addition of Mdh or KynB (positive control), then absorption was measured every minute until 10 minutes after addition, then absorption was measured every 5 minutes until 30 minutes after addition of the enzyme. Absorption of the control reaction containing only NFK was measured 0 and 30 minutes after addition of NFK. Temperature during measurements ranged between 24 and 26° C.

Table 25. Composition of reaction for *in vitro* assay with NFK.

	Mdh	**KynB**	**Control**
Protein reaction buffer	380 µl	380 µl	480 µl
$ZnCl_2$ solution (1 mM)	20 µl	20 µl	20 µl
NFK (100 mM)	500 µl	500 µl	500 µl
Enzyme (5 ng/µl)	100 µl	100 µl	-
Total volume	**1000 µl**	**1000 µl**	**1000 µl**

In the coupled in vitro assay (see **Fig. 24 B**) the release of formate due to the cleavage of formylated amino acids by Mdh could be detected indirectly via the reduction of NAD^+ to NADH. The formic acid is converted to hydrogen ions and carbon dioxide by a formate dehydrogenase (FDH) in the presence of NAD^+ that is reduced to NADH. NADH absorbs light at a wavelength of 340 nm, the extinction at 340 nm increases with rising NADH levels. Therefore, the increase in extinction can be used as a proxy for the release of formate. Reaction

conditions were adapted from (Resch et al., 2005). NAD^+, all substrates to be tested (F-methionine, F-glutamic acid, Na-pyruvate) and formic acid were dissolved/diluted in 'protein reaction buffer' (Na_2HPO_4/NaH_2PO_4, pH7.4) to obtain 100 mM solutions. A 25 mM THF solution was set up with protein reaction buffer and 1 mM $ZnCl_2$ solution with ddH_2O. Formate dehydrogenase (FDH, ~50 U/ml) was purchased from Sigma-Aldrich as solution. 500 ng of 'Ec Mdh' (heterologously overexpressed and purified from *E. coli*) and 'Sa Mdh' (expressed and purified from S. aureus, see **paragraph Expression and purification of C-terminally His-tagged Mdh from *S. aureus*, page 175 f.**) were used per reaction. All reaction components except for FDH and the Mdh enyzmes were prewarmed at 30° C. Temperature during measurements ranged between 33 and 34° C.

As technical control, 1 mM free formic acid was used, absorption at 340 nm was measured every 30 seconds until 25 min after addition of formic acid, then 30, 40, 50 and 70 after addition. A reaction with formic acid without FDH was measured 0.5, 1, 15, 25 and 75 minutes after addition of formic acid to test for spontaneous reduction of NAD+. The reactions with F-methionine and Ec Mdh were measured in every 30 seconds until 10 min after addition of F-methionine or Ec Mdh, then reactions were measured 15, 20, 30, 40, 50 and 75 after addition (see **Fig. 24 D**, curves with crosses ('†')). This experiment was executed separately from the experiment detailed below. F-methionine, F-glutamic acid and Na-pyruvate were tested with Sa Mdh and with additional THF. Ec Mdh was tested with F-glutamic acid and Na- pyruvate in the presence of THF. In this experiment all reactions were preincubated for 40 min at 30° C in the dark prior to addition of the repective Mdh enzyme to allow conversion of formate already present in the reaction due to spontaneous degradation of the substrate. Composition of all reactions measured in the coupled *in vitro* assay is detailed in **Tab. 26**.

Table 26. Composition of reaction for coupled *in vitro* assay with F-methionine, F-glutamic acid and Na-pyruvate.

			Ctrl*	Ec Mdh	Sa Mdh	Ctrl THF	Ec Mdh	Sa Mdh
Substrate tested	Technical Ctrl		F-methionine					
Protein reaction buffer	960	970	940	925	930	900	885	890
$ZnCl_2$ solution (1 mM)	-	-	20	20	20	20	20	20
Formic acid (100 mM)	-	10	-	-	-	-	-	-
Substrate (100 mM)	-	-	10	10	10	10	10	10
NAD^+ (100 mM)	10	10	10	10	10	10	10	10
FDH (50 U/ml)	20	20	20	20	20	20	20	20
THF (25 mM)	-	-	-	-	-	40	40	40
					40 min preincubation at 30° C			
Enzyme (final amount 500 ng)	-	-	-	15 (0.03 mg/ml)	10 (0.05 mg/ml)	-	15 (0.03 mg/ml)	10 (0.05 mg/ml)
Total volume [µl]	**1000**	**1000**	**1000**	**1000**	**1000**	**1000**	**1000**	**1000**
Figure	24 C		24 D					

*Control reaction was set up for both experiments.

	Ctrl	Sa Mdh	Ctrl THF	Ec Mdh	Sa Mdh
Substrate tested	F-glutamic acid // Na-pyruvate				
Protein reaction buffer	940	930	900	885	890
$ZnCl_2$ solution (1 mM)	20	20	20	20	20
Substrate (100 mM)	10	10	10	10	10
NAD^+ (100 mM)	10	10	10	10	10
FDH (50 U/ml)	20	20	20	20	20
THF (25 mM)	-	-	40	40	40
40 min preincubation at 30° C					
Enzyme (final amount 500 ng)	-	10 (0.05 mg/ml)	-	15 (0.03 mg/ml)	10 (0.05 mg/ml)
Total volume [µl]	**1000**	**1000**	**1000**	**1000**	**1000**
Figure	24 E // F				

5.5.4. Protein-protein interaction studies (bacterial two-hybrid system)

The bacterial two-hybrid system was used to detect interaction of Mdh with enzymes of the *met* operon and to confirm Mdh's dimerization (see **Fig. 25 B**). Plasmids detailed in **Tab. 27** were cotransformed into *E. coli* BTH101, 5 ng per plasmid were transformed. 100 µl of transformation suspensions were plated on LB agar supplemented with 100 µg/ml ampicillin, 50 µg/ml kanamycin and 50 µg/ml streptomycin and plates were incubated for 48 hours at 30° C. For the screening assay 1 ml LB medium containing 100 µg/ml Amp, 50 µg/ml Kana, 50 µg/ml Strep and 0.5 mM IPTG was inoculated with 6 colonies of the cotransformation plate

in a MASTERBLOCK® 96 well plate. For each cotransformation 3x 1 ml culture was set up (in total 18 colonies). Cultures were incubated overnight at 30° C and shaking. The next morning 2 µl of each culture was spottet onto a LB agar plate supplemented with 100 µg/ml Amp, 50 µg/ml Kana, 50 µg/ml Strep, 0.5 mM IPTG and 40 µg/ml X-gal and plate was incubated for 24 hours at 30° C. A colour change from white to blue of the spot during incubation indicated interaction of enzymes encoded by the genes cotransformed with the two respective plasmids.

Table 27. Cotransformation scheme for BTHS. Information on plasmids can be found in **Tab. 14**.

	pKNT25_mdh	**pKT25C_mdh***	**pKT25C_zip**	**pKNT25**
pUT18N_mdh	co	co		
pUT18C_mdh*	co	co		
pUT18N_metI	co	co		
pUT18C_metI*	co	co		
pUT18N_metC	co	co		
pUT18C_metC*	co	co		
pUT18N_metF	co	co		
pUT18C_metF*	co	co		
pUT18C_zip			co	
pUT18C				co

5.5.5. Proteomics

Protein preparation and downstream procedures for proteomics were carried out by our collaborators of the Becher group in Greifswald. The respective contributions are detailed in **chapter 6, page 188 f. 'Contributions by Others'**.

Sample preparation for proteomics

Cell pellets were resuspended in TE-buffer (50 mM Tris-HCl pH 7.25, 10 mM EDTA) and disrupted with 0.1 mm glass beads and a homogenizer (4 cycles of 30 seconds at 6.5 m/s). Between each cycle, samples were placed on ice for 5 minutes. Glass beads were removed by centrifugation and lysates were subsequently transferred to a new reaction tube. Protein concentration was determined with Roti-Nanoquant (Roth) according to the manufacturer's protocol. For in solution digest 100 µg protein were reduced with 500 mM tris(2-carboxyethyl)phosphine for 45 minutes at 65 °C and subsequently alkylated with 500 mM iodoacetamide in the dark for 15 minutes at room temperature before digestion was performed with trypsin (protein-to-enzyme-ratio 200:1) at 37 °C for 14 h. Digestion was stopped by lowering the pH to 2 by adding trifluoroacetic acid before samples were desalted via C18 columns (Millipore ZipTips) according to the manufacturer's protocol.

LC–MS/MS measurements

Tryptic peptides were separated by liquid chromatography (LC) and measured online by ESI-mass spectrometry. LC–MS/MS analyses were performed with an EASY-nLC 1200 coupled to an Orbitrap Orbitrap Elite (Thermo Fisher Scientific). Peptides were loaded on a self-made analytical column (3 µm particles, Dr. Maisch GmbH, OD 360 µm, ID 100 µm, length 20 cm) and eluted by a binary nonlinear gradient of 5–53% acetonitrile in 0.1% acetic acid over 180 min with a flow rate of 300 nl min^{-1}. For MS analysis a full scan in the Orbitrap (m/z 300–1700) with a resolution of 60,000 was followed by CID MS/MS experiments of the twenty most abundant precursor ions acquired in the linear ion trap.

Proteome data processing

Relative protein quantification was achieved using the MaxQuant software (version 1.6.1.0.) (Cox and Mann, 2008) and the Andromeda plug-in (Cox et al., 2011). The *.raw files were searched against an *Staphylococcus aureus* strain Newman database (downloaded from Uniprot at July 15, 2018, 2,584 entries). Additionally, MaxQuant's generic contamination list was included during the search. Database search was performed with following parameters:

digestion mode, trypsin/P with up to 2 missed cleavages; variable modifications, methionine oxidation and acetylation of protein N-termini, a maximal number of 5 modifications per peptide and activated 'match-between-runs' feature. The false discovery rates of peptide spectrum match and protein were set to 0.01. Only unique peptides were used for protein quantification. The identified proteins from MaxQuant output files were filtered for contaminants, only identified by site and reverse hits with the Perseus software (v. 1.6.1.3). Proteins were accepted if at least two unique peptides could be identified in at least two of the three biological replicates. The LFQ-values were log2-transformed, exported and used for statistical analysis using TM4 (Saeed et al., 2003). Statistical significance required a p-value < 0.01 in an ANOVA applying standard Bonferroni correction. For comparison of protein amounts within one sample the intensities of all identified peptides were normalized by dividing the respective intensity by the median of all peptide intensities of the same condition. According to Silva et al. the normalized intensities of the three most abundant peptides of a proteins were summed to obtain the final quantitative value (Silva et al., 2006).

6. Contributions by Others

The work described in this doctoral thesis was conducted under the supervision of PD Dr Wilma Ziebuhr at the Institute of Molecular Infection Biology (IMIB) at the Julius-Maximilians-Universität Würzburg, Würzburg, Germany.

Parts of this work which have been conducted in collaborations or were carried out by students under my supervision are detailed below:

Chapter 3.5 The *met* operon on protein level

Dr Sandra Maaß (Becher group, Microbial Proteomics, Institute of Microbiology, Universität Greifswald) processed the samples for proteomics, performed the LC–MS/MS measurements and did the proteome data processing. Data analysis was carried out in collaboration with Dr Sandra Maaß and **Prof Dr Dörte Becher** (Microbial Proteomics, Institute of Microbiology, Universität Greifswald).

Chapter 3.7 Mdh (metal-dependent hydrolase): the unknown of the *met* operon

Daniela Steigerwald (Master programme Biochemistry at Julius-Maximilians-Universität Würzburg) worked in the laboratory under my supervision from April to November 2016 and concluded her work by submitting the master thesis entitled 'Characterization of the *mdh* gene in the methionine synthesis operon of *Staphylococcus aureus'* (Steigerwald, 2016).

Daniela Steigerwald

- cloned the plasmid for chromosomal deletion of *mdh* (pBASE_mdh_del) and generated the Δ*mdh* mutant in *S. aureus* (internal strain collection number: DS11)
- generated the plasmids for overexpression of N-terminally His-tagged Mdh (pET28_His_Nde_mdh_Not1) and KynB of *P. aeruginosa* (pET28_His_kynB)
- overexpressed and purified N-terminally His-tagged Mdh and KynB (affinity chromatography)
- performed the initial *in vitro* assay experiments with N-formylkynurenine (see **Fig. 24 A**)

Esther Rogalski (Master programme Biology at Julius-Maximilians-Universität Würzburg) worked in the laboratory under my supervision from February to October 2017 and concluded her work by submitting the master thesis entitled 'Charakterisierung der metallabhängigen Hydrolase (Mdh) im Methionin-Biosyntheseoperon von *Staphylococcus aureus'*(Rogalski, 2017).

Esther Rogalski

- cloned the plasmid for chromosomal integration of *mdh* Phe32Trp (pBASE mdh Phe32Trp) and generated the mutant in *S. aureus* (internal strain collection number: ER24)
- performed the growth experiments with the *mdh* mutants in *S. aureus* (see **Fig. 23**)
- overexpressed and purified N-terminally His-tagged Mdh His71Ser&Glu198Ser (affinity chromatography)
- cloned the plasmid for chromosomal integration and subsequent (over)expression of C-terminally His-tagged Mdh in *S. aureus* (pBASE 3´(C-Term) His-mdh) and generated the *S. aureus* strain (internal strain collection number: ER16)
- (over)expressed and purified C-terminally His-tagged Mdh from *S. aureus* (ER16) (affinity chromatography)
- performed the *in vitro* assay experiments with Mdh purified from *E. coli* and *S. aureus* with F-methionine, F-glutamic acid and Na-pyruvate (see **Fig. 24 D-F**)
- analysed the distance between *metE* and *mdh* in 10 staphylococcal species (*S. lugdunensis*, *S. carnosus*, *S. haemolyticus*, *S. aureus*, *S. xylosus*, *S. saprophyticus S. epidermidis*, *S. pasteuri*, *S. warneri, S. scuri*)

Matthias Peindl (Master programme Biomedicine at Julius-Maximilians-Universität Würzburg) worked in the laboratory under my supervision from April to June 2018 and concluded his work by an oral presentation.

Matthias Peindl

- cloned the plasmids for the protein-protein interaction studies (bacterial-two-hybrid system (BTHS)) of Mdh with MetI, MetC and MetF (pKNT25_mdh, pKT25C_mdh*, pUT18N_mdh, pUT18C_mdh*, pUT18N_metI, pUT18C_metI*, pUT18N_metC, pUT18C_metC*, pUT18N_metF, pUT18C_metF*)
- performed the BTHS assays (see **Fig. 25 B**)

Dr Yesid Ramiréz (formerly Kisker group, Rudolf-Virchow-Zentrum (RVZ), initially suggested crystallisation of Mdh, supervised Daniela Steigerwald and Esther Rogalski during size exclusion chromatography (SEC), performed crystallisation of Mdh and Mdh His71Ser&Glu198 and obtained the diffraction data.

Dr Wolfgang Kölmel (Kisker group, Rudolf-Virchow-Zentrum (RVZ), Würzburg) and Dr Yesid Ramiréz solved the crystal structure of Mdh and Mdh His71Ser&Glu198Ser, suggested generation of the His71Ser, Glu198Ser and His71Ser&Glu198Ser Mdh mutants and proposed the presented catalytic mechanism of Mdh (see **Fig. 22 D**). Dr Wolfgang Kölmel hypothesised residue Phe32 to be involved in substrate recognition and suggested generation of the Phe32Trp Mdh mutant.

General:

The plasmids and bacterial strains provided by collaborators are listed in **Tabs. 13** and **15**.

7. References

Adams, P.D., Afonine, P.V., Bunkóczi, G., Chen, V.B., Davis, I.W., Echols, N., Headd, J.J., Hung, L.-W., Kapral, G.J., Grosse-Kunstleve, R.W., et al. (2010). PHENIX: a comprehensive Python-based system for macromolecular structure solution. Acta Crystallogr. D Biol. Crystallogr. *66*, 213–221.

Adhikari, R.P., Arvidson, S., and Novick, R.P. (2007). A Nonsense Mutation in *agrA* Accounts for the Defect in *agr* Expression and the Avirulence of *Staphylococcus aureus* 8325-4 traP::kan. Infect. Immun. *75*, 4534–4540.

Ananthanarayan, R. (2006). Chapter 22: *Staphylococcus*. In Ananthanarayan and Paniker's Textbook of Microbiology, (Orient Blackswan), pp. 192–201.

Anderson, K.L., Roberts, C., Disz, T., Vonstein, V., Hwang, K., Overbeek, R., Olson, P.D., Projan, S.J., and Dunman, P.M. (2006). Characterization of the *Staphylococcus aureus* Heat Shock, Cold Shock, Stringent, and SOS Responses and Their Effects on Log-Phase mRNA Turnover. J. Bacteriol. *188*, 6739–6756.

Anderson, K.L., Roux, C.M., Olson, M.W., Luong, T.T., Lee, C.Y., Olson, R., and Dunman, P.M. (2010). Characterizing the Effects of Inorganic Acid and Alkaline Shock on the *Staphylococcus aureus* Transcriptome and Messenger RNA Turnover. FEMS Immunol. Med. Microbiol. *60*, 208–250.

Anupam, R., Nayek, A., Green, N.J., Grundy, F.J., Henkin, T.M., Means, J.A., Bergmeier, S.C., and Hines, J.V. (2008). 4,5-Disubstituted oxazolidinones: High affinity molecular effectors of RNA function. Bioorg. Med. Chem. Lett. *18*, 3541–3544.

Anupama, K., Leela, J.K., and Gowrishankar, J. (2011). Two pathways for RNase E action in *Escherichia coli in vivo* and bypass of its essentiality in mutants defective for Rho-dependent transcription termination. Mol. Microbiol. *82*, 1330–1348.

Asmari, M., Ratih, R., Alhazmi, H.A., and El Deeb, S. (2018). Thermophoresis for characterizing biomolecular interaction. Methods *146*, 107–119.

Auger, S., Yuen, W.H., Danchin, A., and Martin-Verstraete, I. (2002). The *metIC* operon involved in methionine biosynthesis in *Bacillus subtilis* is controlled by transcription antitermination. Microbiol. Read. Engl. *148*, 507–518.

Baba, T., Bae, T., Schneewind, O., Takeuchi, F., and Hiramatsu, K. (2008). Genome sequence of *Staphylococcus aureus* strain Newman and comparative analysis of staphylococcal genomes: polymorphism and evolution of two major pathogenicity islands. J. Bacteriol. *190*, 300–310.

Bae, T., and Schneewind, O. (2006). Allelic replacement in *Staphylococcus aureus* with inducible counter-selection. Plasmid *55*, 58–63.

Bae, T., Glass, E.M., Schneewind, O., and Missiakas, D. (2008a). Generating a collection of insertion mutations in the *Staphylococcus aureus* genome using bursa aurealis. Methods Mol. Biol. Clifton NJ *416*, 103–116.

Bae, T., Glass, E.M., Schneewind, O., and Missiakas, D. (2008b). Generating a collection of insertion mutations in the *Staphylococcus aureus* genome using *bursa aurealis*. Methods Mol. Biol. Clifton NJ *416*, 103–116.

Båga, M., Göransson, M., Normark, S., and Uhlin, B.E. (1988). Processed mRNA with differential stability in the regulation of *E. coli* pilin gene expression. Cell *52*, 197–206.

Barber, M. (1947). Staphylococcal Infection due to Penicillin-resistant Strains. Br. Med. J. *2*, 863–865.

Bäsell, K., Otto, A., Junker, S., Zühlke, D., Rappen, G.-M., Schmidt, S., Hentschker, C., Macek, B., Ohlsen, K., Hecker, M., et al. (2014). The phosphoproteome and its physiological dynamics in *Staphylococcus aureus*. Int. J. Med. Microbiol. *304*, 121–132.

Bastard, K., Perret, A., Mariage, A., Bessonnet, T., Pinet-Turpault, A., Petit, J.-L., Darii, E., Bazire, P., Vergne-Vaxelaire, C., Brewee, C., et al. (2017). Parallel evolution of non-homologous isofunctional enzymes in methionine biosynthesis. Nat. Chem. Biol. *13*, 858–866.

Battaglia, R.A., Grigg, J.C., and Ke, A. (2019). Structural basis for tRNA decoding and aminoacylation sensing by T-box riboregulators. Nat. Struct. Mol. Biol. *26*, 1106–1113.

Belasco, J.G., Beatty, J.T., Adams, C.W., Gabain, A. von, and Cohen, S.N. (1985). Differential expression of photosynthesis genes in *R. capsulata* results from segmental differences in stability within the polycistronic *rxcA* transcript. Cell *40*, 171–181.

Bjerregaard-Andersen, K., Sommer, T., Jensen, J.K., Jochimsen, B., Etzerodt, M., and Morth, J.P. (2014). A Proton Wire and Water Channel Revealed in the Crystal Structure of Isatin Hydrolase. J. Biol. Chem. *289*, 21351–21359.

Blount, K.F., Megyola, C., Plummer, M., Osterman, D., O'Connell, T., Aristoff, P., Quinn, C., Chrusciel, R.A., Poel, T.J., Schostarez, H.J., et al. (2015). Novel Riboswitch-Binding Flavin Analog That Protects Mice against *Clostridium difficile* Infection without Inhibiting Cecal Flora. Antimicrob. Agents Chemother. *59*, 5736–5746.

Boël, G., Letso, R., Neely, H., Price, W.N., Wong, K.-H., Su, M., Luff, J.D., Valecha, M., Everett, J.K., Acton, T.B., et al. (2016). Codon influence on protein expression in *E. coli* correlates with mRNA levels. Nature *529*, 358–363.

Bolten, C.J., Schröder, H., Dickschat, J., and Wittmann, C. (2010). Towards methionine overproduction in *Corynebacterium glutamicum*--methanethiol and dimethyldisulfide as reduced sulfur sources. J. Microbiol. Biotechnol. *20*, 1196–1203.

Bonnin, R., A, M., Bouloc, P., Bonnin, R., A, M., and Bouloc, P. (2015). RNA Degradation in *Staphylococcus aureus*: Diversity of Ribonucleases and Their Impact. Int. J. Genomics Int. J. Genomics *2015, 2015*, e395753.

Bouvier, M., and Carpousis, A.J. (2011). A tale of two mRNA degradation pathways mediated by RNase E. Mol. Microbiol. *82*, 1305–1310.

Brar, G.A., and Weissman, J.S. (2015). Ribosome profiling reveals the what, when, where, and how of protein synthesis. Nat. Rev. Mol. Cell Biol. *16*, 651–664.

Breaker, R.R. (2011). Prospects for Riboswitch Discovery and Analysis. Mol. Cell *43*, 867–879.

Busch, A., Richter, A.S., and Backofen, R. (2008). IntaRNA: efficient prediction of bacterial sRNA targets incorporating target site accessibility and seed regions. Bioinforma. Oxf. Engl. *24*, 2849–2856.

Cantor, J.R., Abu-Remaileh, M., Kanarek, N., Freinkman, E., Gao, X., Louissaint, A., Lewis, C.A., and Sabatini, D.M. (2017). Physiologic Medium Rewires Cellular Metabolism and Reveals Uric Acid as an Endogenous Inhibitor of UMP Synthase. Cell *169*, 258-272.e17.

Carafa, Y. d'Aubenton, Brody, E., and Thermes, C. (1990). Prediction of rho-independent *Escherichia coli* transcription terminators: A statistical analysis of their RNA stem-loop structures. J. Mol. Biol. *216*, 835–858.

Carpousis, A.J. (2007). The RNA Degradosome of *Escherichia coli*: An mRNA-Degrading Machine Assembled on RNase E. Annu. Rev. Microbiol. *61*, 71–87.

Chambers, H.F., and DeLeo, F.R. (2009). Waves of Resistance: *Staphylococcus aureus* in the Antibiotic Era. Nat. Rev. Microbiol. *7*, 629–641.

Chang, A.T., and Nikonowicz, E.P. (2013). Solution NMR determination of hydrogen bonding and base pairing between the *glyQS* T box riboswitch Specifier domain and the anticodon loop of tRNAGly. FEBS Lett. *587*, 3495–3499.

Chetnani, B., and Mondragón, A. (2017). Molecular envelope and atomic model of an anti-terminated *glyQS* T-box regulator in complex with tRNAGly. Nucleic Acids Res. *45*, 8079–8090.

Chiang, P.K., Gordon, R.K., Tal, J., Zeng, G.C., Doctor, B.P., Pardhasaradhi, K., and McCann, P.P. (1996). S-Adenosylmethionine and methylation. FASEB J. Off. Publ. Fed. Am. Soc. Exp. Biol. *10*, 471–480.

Collaborative Computational Project, Number 4 (1994). The CCP4 suite: programs for protein crystallography. Acta Crystallogr. D Biol. Crystallogr. *50*, 760–763.

Commichau, F.M., Rothe, F.M., Herzberg, C., Wagner, E., Hellwig, D., Lehnik-Habrink, M., Hammer, E., Völker, U., and Stülke, J. (2009). Novel Activities of Glycolytic Enzymes in *Bacillus subtilis*: INTERACTIONS WITH ESSENTIAL PROTEINS INVOLVED IN mRNA PROCESSING. Mol. Cell. Proteomics *8*, 1350–1360.

Condon, C., Putzer, H., and Grunberg-Manago, M. (1996). Processing of the leader mRNA plays a major role in the induction of *thrS* expression following threonine starvation in *Bacillus subtilis*. Proc. Natl. Acad. Sci. *93*, 6992–6997.

Connelly, C.M., Numata, T., Boer, R.E., Moon, M.H., Sinniah, R.S., Barchi, J.J., Ferré-D'Amaré, A.R., and Schneekloth, J.S. (2019). Synthetic ligands for PreQ 1 riboswitches provide structural and mechanistic insights into targeting RNA tertiary structure. Nat. Commun. *10*, 1501.

Copley, S.D. (2003). Enzymes with extra talents: moonlighting functions and catalytic promiscuity. Curr. Opin. Chem. Biol. *7*, 265–272.

Cox, J., and Mann, M. (2008). MaxQuant enables high peptide identification rates, individualized p.p.b.-range mass accuracies and proteome-wide protein quantification. Nat. Biotechnol. *26*, 1367–1372.

Cox, J., Neuhauser, N., Michalski, A., Scheltema, R.A., Olsen, J.V., and Mann, M. (2011). Andromeda: A Peptide Search Engine Integrated into the MaxQuant Environment. J. Proteome Res. *10*, 1794–1805.

Dar, D., and Sorek, R. (2018). Extensive reshaping of bacterial operons by programmed mRNA decay. PLOS Genet. *14*, e1007354.

Dar, D., Shamir, M., Mellin, J.R., Koutero, M., Stern-Ginossar, N., Cossart, P., and Sorek, R. (2016). Term-seq reveals abundant ribo-regulation of antibiotics resistance in bacteria. Science *352*, aad9822.

Darty, K., Denise, A., and Ponty, Y. (2009). VARNA: Interactive drawing and editing of the RNA secondary structure. Bioinforma. Oxf. Engl. *25*, 1974–1975.

Deana, A., and Belasco, J.G. (2005). Lost in translation: the influence of ribosomes on bacterial mRNA decay. Genes Dev. *19*, 2526–2533.

Deana, A., Celesnik, H., and Belasco, J.G. (2008). The bacterial enzyme RppH triggers messenger RNA degradation by 5′ pyrophosphate removal. Nature *451*, 355–358.

Deigan, K.E., and Ferré-D'Amaré, A.R. (2011). Riboswitches: Discovery of Drugs That Target Bacterial Gene-Regulatory RNAs. Acc. Chem. Res. *44*, 1329–1338.

Díaz-Sáez, L., Srikannathasan, V., Zoltner, M., and Hunter, W.N. (2014). Structures of bacterial kynurenine formamidase reveal a crowded binuclear zinc catalytic site primed to generate a potent nucleophile. Biochem. J. *462*, 581–589.

Dortet, L., Anguel, N., Fortineau, N., Richard, C., and Nordmann, P. (2013). *In vivo* acquired daptomycin resistance during treatment of methicillin-resistant *Staphylococcus aureus* endocarditis. Int. J. Infect. Dis. *17*, e1076–e1077.

Dreyfus, M. (2009). Chapter 11 Killer and Protective Ribosomes. In Progress in Molecular Biology and Translational Science, (Academic Press), pp. 423–466.

Durand, S., and Condon, C. (2018). RNases and Helicases in Gram-Positive Bacteria. Microbiol. Spectr. *6*.

Durand, S., Gilet, L., Bessières, P., Nicolas, P., and Condon, C. (2012a). Three Essential Ribonucleases—RNase Y, J1, and III—Control the Abundance of a Majority of *Bacillus subtilis* mRNAs. PLOS Genet. *8*, e1002520.

Durand, S., Gilet, L., and Condon, C. (2012b). The essential function of *B. subtilis* RNase III is to silence foreign toxin genes. PLoS Genet. *8*, e1003181.

Duthie, E.S., and Lorenz, L.L. (1952). Staphylococcal Coagulase: Mode of Action and Antigenicity. Microbiology, *6*, 95–107.

Emsley, P., Lohkamp, B., Scott, W.G., and Cowtan, K. (2010). Features and development of Coot. Acta Crystallogr. D Biol. Crystallogr. *66*, 486–501.

Espah Borujeni, A., Channarasappa, A.S., and Salis, H.M. (2014). Translation rate is controlled by coupled trade-offs between site accessibility, selective RNA unfolding and sliding at upstream standby sites. Nucleic Acids Res. *42*, 2646–2659.

Falconer, R.J. (2016). Applications of isothermal titration calorimetry – the research and technical developments from 2011 to 2015. J. Mol. Recognit. *29*, 504–515.

Ferla, M.P., and Patrick, W.M. (2014). Bacterial methionine biosynthesis. Microbiol. Read. Engl. *160*, 1571–1584.

Fey, P.D., Endres, J.L., Yajjala, V.K., Widhelm, T.J., Boissy, R.J., Bose, J.L., and Bayles, K.W. (2013). A genetic resource for rapid and comprehensive phenotype screening of nonessential *Staphylococcus aureus* genes. MBio *4*, e00537-00512.

Figaro, S., Durand, S., Gilet, L., Cayet, N., Sachse, M., and Condon, C. (2013). *Bacillus subtilis* Mutants with Knockouts of the Genes Encoding Ribonucleases RNase Y and RNase J1 Are Viable, with Major Defects in Cell Morphology, Sporulation, and Competence. J. Bacteriol. *195*, 2340–2348.

Figge, R.M. (2007). Methionine Biosynthesis in *Escherichia col i*and *Corynebacterium glutamicum*. In Amino Acid Biosynthesis ~ Pathways, Regulation and Metabolic Engineering, V.F. Wendisch, ed. (Berlin, Heidelberg: Springer Berlin Heidelberg), pp. 163–193.

Foster, T.J. (2004). The *Staphylococcus aureus* "superbug." J. Clin. Invest. *114*, 1693–1696.

Francklyn, C.S., and Mullen, P. (2019). Progress and challenges in aminoacyl-tRNA synthetase-based therapeutics. J. Biol. Chem. *294*, 5365–5385.

Freyer, M.W., and Lewis, E.A. (2008). Isothermal Titration Calorimetry: Experimental Design, Data Analysis, and Probing Macromolecule/Ligand Binding and Kinetic Interactions. In Methods in Cell Biology, (Academic Press), pp. 79–113.

Frohlich, K.M., Weintraub, S.F., Bell, J.T., Todd, G.C., Väre, V.Y.P., Schneider, R., Kloos, Z.A., Tabe, E.S., Cantara, W.A., Stark, C.J., et al. (2019). Discovery of Small-Molecule Antibiotics against a Unique tRNA-Mediated Regulation of Transcription in Gram-Positive Bacteria. ChemMedChem *14*, 758–769.

Fuchs, S., Mehlan, H., Bernhardt, J., Hennig, A., Michalik, S., Surmann, K., Pané-Farré, J., Giese, A., Weiss, S., Backert, L., et al. (2018). AureoWiki‑The repository of the *Staphylococcus aureus* research and annotation community. Int. J. Med. Microbiol. *308*, 558–568.

Fuhrmann, M., Hausherr, A., Ferbitz, L., Schödl, T., Heitzer, M., and Hegemann, P. (2004). Monitoring dynamic expression of nuclear genes in *Chlamydomonas reinhardtii* by using a synthetic luciferase reporter gene. Plant Mol. Biol. *55*, 869–881.

Gan, J., Tropea, J.E., Austin, B.P., Court, D.L., Waugh, D.S., and Ji, X. (2006). Structural Insight into the Mechanism of Double-Stranded RNA Processing by Ribonuclease III. Cell *124*, 355–366.

Garrey, S.M., and Mackie, G.A. (2011). Roles of the 5′-phosphate sensor domain in RNase E. Mol. Microbiol. *80*, 1613–1624.

Geiger, T., Goerke, C., Fritz, M., Schäfer, T., Ohlsen, K., Liebeke, M., Lalk, M., and Wolz, C. (2010). Role of the (p)ppGpp Synthase RSH, a RelA/SpoT Homolog, in Stringent Response and Virulence of *Staphylococcus aureus*. Infect. Immun. *78*, 1873–1883.

Geiger, T., Francois, P., Liebeke, M., Fraunholz, M., Goerke, C., Krismer, B., Schrenzel, J., Lalk, M., and Wolz, C. (2012). The Stringent Response of *Staphylococcus aureus* and Its Impact on Survival after Phagocytosis through the Induction of Intracellular PSMs Expression. PLoS Pathog. *8*.

Gertz, S., Engelmann, S., Schmid, R., Ohlsen, K., Hacker, J., and Hecker, M. (1999). Regulation of σB-dependent transcription of *sigB* and *asp23* in two different *Staphylococcus aureus* strains. Mol. Gen. Genet. MGG *261*, 558–566.

Gioia, D., Bertazzo, M., Recanatini, M., Masetti, M., and Cavalli, A. (2017). Dynamic Docking: A Paradigm Shift in Computational Drug Discovery. Molecules *22*, 2029.

Gish, W., and States, D.J. (1993). Identification of protein coding regions by database similarity search. Nat. Genet. *3*, 266–272.

Gophna, U., Bapteste, E., Doolittle, W.F., Biran, D., and Ron, E.Z. (2005). Evolutionary plasticity of methionine biosynthesis. Gene *355*, 48–57.

Goulding, C.W., Postigo, D., and Matthews, R.G. (1997). Cobalamin-Dependent Methionine Synthase Is a Modular Protein with Distinct Regions for Binding Homocysteine, Methyltetrahydrofolate, Cobalamin, and Adenosylmethionine. Biochemistry *36*, 8082–8091.

Greene, R.C. (1996). Biosynthesis of Methionine. In *Escherichia Coli* and *Salmonella*, (Washington, D.C.: ASM Press), pp. 542–560.

Grigg, J.C., and Ke, A. (2013). Structural Determinants for Geometry and Information Decoding of tRNA by T Box Leader RNA. Structure *21*, 2025–2032.

Grigg, J.C., Chen, Y., Grundy, F.J., Henkin, T.M., Pollack, L., and Ke, A. (2013). T box RNA decodes both the information content and geometry of tRNA to affect gene expression. Proc. Natl. Acad. Sci. *110*, 7240–7245.

Grosdidier, A., Zoete, V., and Michielin, O. (2007). EADock: Docking of small molecules into protein active sites with a multiobjective evolutionary optimization. Proteins Struct. Funct. Bioinforma. *67*, 1010–1025.

Grundy, F.J., and Henkin, T.M. (1993). tRNA as a positive regulator of transcription antitermination in *B. subtilis*. Cell *74*, 475–482.

Grundy, F.J., and Henkin, T.M. (1994). Conservation of a Transcription Antitermination Mechanism in Aminoacyl-tRNA Synthetase and Amino Acid Biosynthesis Genes in Gram-positive Bacteria. J. Mol. Biol. *235*, 798–804.

Grundy, F.J., and Henkin, T.M. (1998). The S box regulon: a new global transcription termination control system for methionine and cysteine biosynthesis genes in Gram-positive bacteria. Mol. Microbiol. *30*, 737–749.

Grundy, F.J., and Henkin, T.M. (2003). The T box and S box transcription termination control systems. Front. Biosci. J. Virtual Libr. *8*, d20-31.

Grundy, F.J., and Henkin, T.M. (2004). Kinetic Analysis of tRNA-Directed Transcription Antitermination of the *Bacillus subtilis glyQS* Gene *In Vitro*. J. Bacteriol. *186*, 5392–5399.

Gu, B., Kelesidis, T., Tsiodras, S., Hindler, J., and Humphries, R.M. (2013). The emerging problem of linezolid-resistant *Staphylococcus*. J. Antimicrob. Chemother. *68*, 4–11.

Guédon, E., Sperandio, B., Pons, N., Ehrlich, S.D., and Renault, P. (2005). Overall control of nitrogen metabolism in *Lactococcus lactis* by CodY, and possible models for CodY regulation in Firmicutes. Microbiology *151*, 3895–3909.

Haaber, J., Penadés, J.R., and Ingmer, H. (2017). Transfer of Antibiotic Resistance in *Staphylococcus aureus*. Trends Microbiol. *25*, 893–905.

Hacham, Y., Gophna, U., and Amir, R. (2003). *In Vivo* Analysis of Various Substrates Utilized by Cystathionine γ-Synthase and O-Acetylhomoserine Sulfhydrylase in Methionine Biosynthesis. Mol. Biol. Evol. *20*, 1513–1520.

Hanson, G., and Coller, J. (2018). Codon optimality, bias and usage in translation and mRNA decay. Nat. Rev. Mol. Cell Biol. *19*, 20–30.

Henkin, T.M., and Grundy, F.J. (2006). Sensing Metabolic Signals with Nascent RNA Transcripts: The T Box and S Box Riboswitches as Paradigms. Cold Spring Harb. Symp. Quant. Biol. *71*, 231–237.

Henkin, T.M., Glass, B.L., and Grundy, F.J. (1992). Analysis of the *Bacillus subtilis tyrS* gene: conservation of a regulatory sequence in multiple tRNA synthetase genes. J. Bacteriol. *174*, 1299–1306.

Herzberg, C., Weidinger, L.A.F., Dörrbecker, B., Hübner, S., Stülke, J., and Commichau, F.M. (2007). SPINE: A method for the rapid detection and analysis of protein–protein interactions in vivo. PROTEOMICS *7*, 4032–4035.

Ho, J.M., Bakkalbasi, E., Söll, D., and Miller, C.A. (2018). Drugging tRNA aminoacylation. RNA Biol. *15*, 667–677.

Hollands, K., Proshkin, S., Sklyarova, S., Epshtein, V., Mironov, A., Nudler, E., and Groisman, E.A. (2012). Riboswitch control of Rho-dependent transcription termination. Proc. Natl. Acad. Sci. *109*, 5376–5381.

Iost, I., and Dreyfus, M. (1995). The stability of *Escherichia coli lacZ* mRNA depends upon the simultaneity of its synthesis and translation. EMBO J. *14*, 3252–3261.

Jackson, C.J., Gillam, E.M.J., and Ollis, D.L. (2010). 9.20 - Directed Evolution of Enzymes. In Comprehensive Natural Products II, H.-W. (Ben) Liu, and L. Mander, eds. (Oxford: Elsevier), pp. 723–749.

Jäger, W., Schäfer, A., Pühler, A., Labes, G., and Wohlleben, W. (1992). Expression of the *Bacillus subtilis sacB* gene leads to sucrose sensitivity in the gram-positive bacterium *Corynebacterium glutamicum* but not in *Streptomyces lividans*. J. Bacteriol. *174*, 5462–5465.

Jevons, M.P. (1961). "Celbenin" - resistant Staphylococci. Br. Med. J. *1*, 124–125.

Jia, X., Zhang, J., Sun, W., He, W., Jiang, H., Chen, D., and Murchie, A.I.H. (2013). Riboswitch Control of Aminoglycoside Antibiotic Resistance. Cell *152*, 68–81.

Johnston, M., Jankowski, D., Marcotte, P., Tanaka, H., Esaki, N., Soda, K., and Walsh, C. (1979). Suicide inactivation of bacterial cystathionine gamma-synthase and methionine gamma-lyase during processing of L-propargylglycine. Biochemistry *18*, 4690–4701.

Kabsch, W. (2010). XDS. Acta Crystallogr. D Biol. Crystallogr. *66*, 125–132.

Kahl, B.C., Becker, K., and Löffler, B. (2016). Clinical Significance and Pathogenesis of Staphylococcal Small Colony Variants in Persistent Infections. Clin. Microbiol. Rev. *29*, 401–427.

Kahn, D., Fromant, M., Fayat, G., Dessen, P., and Blanquet, S. (1980). Methionyl-Transfer-RNA Transformylase from *Escherichia coli*. Eur. J. Biochem. *105*, 489–497.

Kaleta, C., Schäuble, S., Rinas, U., and Schuster, S. (2013). Metabolic costs of amino acid and protein production in *Escherichia coli*. Biotechnol. J. *8*, 1105–1114.

Kennedy, A.D., Otto, M., Braughton, K.R., Whitney, A.R., Chen, L., Mathema, B., Mediavilla, J.R., Byrne, K.A., Parkins, L.D., Tenover, F.C., et al. (2008). Epidemic community-associated methicillin-resistant *Staphylococcus aureu*s: Recent clonal expansion and diversification. Proc. Natl. Acad. Sci. *105*, 1327–1332.

Kennedy, A.D., Porcella, S.F., Martens, C., Whitney, A.R., Braughton, K.R., Chen, L., Craig, C.T., Tenover, F.C., Kreiswirth, B.N., Musser, J.M., et al. (2010). Complete Nucleotide Sequence Analysis of Plasmids in Strains of *Staphylococcus aureus* Clone USA300 Reveals a High Level of Identity among Isolates with Closely Related Core Genome Sequences. J. Clin. Microbiol. *48*, 4504–4511.

Khemici, V., Prados, J., Linder, P., and Redder, P. (2015). Decay-Initiating Endoribonucleolytic Cleavage by RNase Y Is Kept under Tight Control via Sequence Preference and Sub-cellular Localisation. PLoS Genet *11*, e1005577.

Killiny, N. (2018). Generous hosts: Why the larvae of greater wax moth, *Galleria mellonella* is a perfect infectious host model? Virulence *9*, 860–865.

Kim, H.K., Missiakas, D., and Schneewind, O. (2014). Mouse models for infectious diseases caused by *Staphylococcus aureus*. J. Immunol. Methods *410*, 88–99.

Klein, D.J., Schmeing, T.M., Moore, P.B., and Steitz, T.A. (2001). The kink-turn: a new RNA secondary structure motif. EMBO J. *20*, 4214–4221.

Kokai-Kun, J.F. (2008). The Cotton Rat as a Model for *Staphylococcus aureu*s nasal colonization in humans: cotton rat *S. aureus* nasal colonization model. Methods Mol. Biol. Clifton NJ *431*, 241–254.

Korostelev, A., Trakhanov, S., Laurberg, M., and Noller, H.F. (2006). Crystal Structure of a 70S Ribosome-tRNA Complex Reveals Functional Interactions and Rearrangements. Cell *126*, 1065–1077.

Kreuzer, K.D., and Henkin, T.M. (2018). The T-Box Riboswitch: tRNA as an Effector to Modulate Gene Regulation. Microbiol. Spectr. *6*.

Krismer, B., Liebeke, M., Janek, D., Nega, M., Rautenberg, M., Hornig, G., Unger, C., Weidenmaier, C., Lalk, M., and Peschel, A. (2014). Nutrient Limitation Governs *Staphylococcus aureus* Metabolism and Niche Adaptation in the Human Nose. PLOS Pathog. *10*, e1003862.

Kurnasov, O., Jablonski, L., Polanuyer, B., Dorrestein, P., Begley, T., and Osterman, A. (2003). Aerobic tryptophan degradation pathway in bacteria: novel kynurenine formamidase. FEMS Microbiol. Lett. *227*, 219–227.

Laalami, S., Bessières, P., Rocca, A., Zig, L., Nicolas, P., and Putzer, H. (2013). *Bacillus subtilis* RNase Y Activity *In Vivo* Analysed by Tiling Microarrays. PLOS ONE *8*, e54062.

Laalami, S., Zig, L., and Putzer, H. (2014). Initiation of mRNA decay in bacteria. Cell. Mol. Life Sci. *71*, 1799–1828.

Latif, H., Szubin, R., Tan, J., Brunk, E., Lechner, A., Zengler, K., and Palsson, B.O. (2015). A streamlined ribosome profiling protocol for the characterization of microorganisms. BioTechniques *58*, 329–332.

Lechner, S., Lewis, K., and Bertram, R. (2012). *Staphylococcus aureus* Persisters Tolerant to Bactericidal Antibiotics. J. Mol. Microbiol. Biotechnol. *22*, 235–244.

Lehnik-Habrink, M., Pförtner, H., Rempeters, L., Pietack, N., Herzberg, C., and Stülke, J. (2010). The RNA degradosome in *Bacillus subtilis*: identification of CshA as the major RNA helicase in the multiprotein complex. Mol. Microbiol. *77*, 958–971.

Lehnik-Habrink, M., Newman, J., Rothe, F.M., Solovyova, A.S., Rodrigues, C., Herzberg, C., Commichau, F.M., Lewis, R.J., and Stülke, J. (2011a). RNase Y in *Bacillus subtilis*: a Natively Disordered Protein That Is the Functional Equivalent of RNase E from *Escherichia coli*. J. Bacteriol. *193*, 5431–5441.

Lehnik-Habrink, M., Schaffer, M., Mäder, U., Diethmaier, C., Herzberg, C., and Stülke, J. (2011b). RNA processing in *Bacillus subtilis*: identification of targets of the essential RNase Y. Mol. Microbiol. *81*, 1459–1473.

Leibig, M., Liebeke, M., Mader, D., Lalk, M., Peschel, A., and Götz, F. (2011). Pyruvate Formate Lyase Acts as a Formate Supplier for Metabolic Processes during Anaerobiosis in *Staphylococcus aureus*. J. Bacteriol. *193*, 952–962.

Leyn, S.A., Suvorova, I.A., Kholina, T.D., Sherstneva, S.S., Novichkov, P.S., Gelfand, M.S., and Rodionov, D.A. (2014). Comparative Genomics of Transcriptional Regulation of Methionine Metabolism in Proteobacteria. PLoS ONE *9*.

Li, S., Su, Z., Lehmann, J., Stamatopoulou, V., Giarimoglou, N., Henderson, F.E., Fan, L., Pintilie, G.D., Zhang, K., Chen, M., et al. (2019). Structural basis of amino acid surveillance by higher-order tRNA-mRNA interactions. Nat. Struct. Mol. Biol. *26*, 1094–1105.

Li, Y., Sun, Y., Ison, C., Levine, M.M., and Tang, C.M. (2004). Vaccination with Attenuated *Neisseria meningitidis* Strains Protects against Challenge with Live Meningococci. Infect. Immun. *72*, 345–351.

Linder, P., Lemeille, S., and Redder, P. (2014). Transcriptome-Wide Analyses of 5′-Ends in RNase J Mutants of a Gram-Positive Pathogen Reveal a Role in RNA Maturation, Regulation and Degradation. PLOS Genet. *10*, e1004207.

Lioliou, E., Sharma, C.M., Caldelari, I., Helfer, A.-C., Fechter, P., Vandenesch, F., Vogel, J., and Romby, P. (2012). Global Regulatory Functions of the *Staphylococcus aureus* Endoribonuclease III in Gene Expression. PLOS Genet. *8*, e1002782.

Lost, I., and Dreyfus, M. (1994). mRNAs can be stabilized by DEAD-box proteins. Nature *372*, 193–196.

Lowy, F.D. (1998). *Staphylococcus aureus* Infections. N. Engl. J. Med. *339*, 520–532.

Macalino, S.J.Y., Gosu, V., Hong, S., and Choi, S. (2015). Role of computer-aided drug design in modern drug discovery. Arch. Pharm. Res. *38*, 1686–1701.

Mackie, G.A. (1998). Ribonuclease E is a 5′-end-dependent endonuclease. Nature *395*, 720–724.

Madeira, F., Park, Y.M., Lee, J., Buso, N., Gur, T., Madhusoodanan, N., Basutkar, P., Tivey, A.R.N., Potter, S.C., Finn, R.D., et al. (2019). The EMBL-EBI search and sequence analysis tools APIs in 2019. Nucleic Acids Res. *47*, W636–W641.

Mader, D., Liebeke, M., Winstel, V., Methling, K., Leibig, M., Götz, F., Lalk, M., and Peschel, A. (2013). Role of N-terminal protein formylation in central metabolic processes in *Staphylococcus aureus*. BMC Microbiol. *13*, 7.

Mäder, U., Nicolas, P., Depke, M., Pané-Farré, J., Debarbouille, M., Kooi-Pol, M.M. van der, Guérin, C., Dérozier, S., Hiron, A., Jarmer, H., et al. (2016). *Staphylococcus aureus* Transcriptome Architecture: From Laboratory to Infection-Mimicking Conditions. PLOS Genet. *12*, e1005962.

Majerczyk, C.D., Dunman, P.M., Luong, T.T., Lee, C.Y., Sadykov, M.R., Somerville, G.A., Bodi, K., and Sonenshein, A.L. (2010). Direct Targets of CodY in *Staphylococcus aureus*. J. Bacteriol. *192*, 2861–2877.

Malkowski, S.N., Spencer, T.C.J., and Breaker, R.R. (2019). Evidence that the nadA Motif is a Bacterial Riboswitch for the Ubiquitous Enzyme Cofactor NAD. RNA N. Y. N.

Mann, M., Wright, P.R., and Backofen, R. (2017). IntaRNA 2.0: enhanced and customizable prediction of RNA-RNA interactions. Nucleic Acids Res. *45*, W435–W439.

Marincola, G., Schäfer, T., Behler, J., Bernhardt, J., Ohlsen, K., Goerke, C., and Wolz, C. (2012). RNase Y of *Staphylococcus aureus* and its role in the activation of virulence genes. Mol. Microbiol. *85*, 817–832.

Mathy, N., Bénard, L., Pellegrini, O., Daou, R., Wen, T., and Condon, C. (2007). 5′-to-3′ Exoribonuclease Activity in Bacteria: Role of RNase J1 in rRNA Maturation and 5′ Stability of mRNA. Cell *129*, 681–692.

Mathy, N., Hébert, A., Mervelet, P., Bénard, L., Dorléans, A., Sierra-Gallay, I.L. de la, Noirot, P., Putzer, H., and Condon, C. (2010). *Bacillus subtilis* ribonucleases J1 and J2 form a complex with altered enzyme behaviour. Mol. Microbiol. *75*, 489–498.

Matsui, M., and Corey, D.R. (2017). Non-coding RNAs as drug targets. Nat. Rev. Drug Discov. *16*, 167–179.

McCown, P.J., Corbino, K.A., Stav, S., Sherlock, M.E., and Breaker, R.R. (2017). Riboswitch diversity and distribution. RNA *23*, 995–1011.

McCoy, A.J. (2007). Solving structures of protein complexes by molecular replacement with Phaser. Acta Crystallogr. D Biol. Crystallogr. *63*, 32–41.

Meinnel, T., Mechulam, Y., and Blanquet, S. (1993). Methionine as translation start signal: A review of the enzymes of the pathway in *Escherichia coli*. Biochimie *75*, 1061–1075.

Merino, E., and Yanofsky, C. (2005). Transcription attenuation: a highly conserved regulatory strategy used by bacteria. Trends Genet. *21*, 260–264.

Meyer, H., Liebeke, M., and Lalk, M. (2010). A protocol for the investigation of the intracellular *Staphylococcus aureus* metabolome. Anal. Biochem. *401*, 250–259.

Michalik, S., Bernhardt, J., Otto, A., Moche, M., Becher, D., Meyer, H., Lalk, M., Schurmann, C., Schlüter, R., Kock, H., et al. (2012). Life and Death of Proteins: A Case Study of Glucose-starved *Staphylococcus aureus*. Mol. Cell. Proteomics *11*, 558–570.

Monk, I.R., and Foster, T.J. (2012). Genetic manipulation of Staphylococci-breaking through the barrier. Front. Cell. Infect. Microbiol. *2*, 49.

Monk, I.R., Shah, I.M., Xu, M., Tan, M.-W., and Foster, T.J. (2012). Transforming the untransformable: application of direct transformation to manipulate genetically *Staphylococcus aureus* and *Staphylococcus epidermidis*. MBio *3*.

Morikawa, K., Ohniwa, R.L., Ohta, T., Tanaka, Y., Takeyasu, K., and Msadek, T. (2010). Adaptation beyond the Stress Response: Cell Structure Dynamics and Population Heterogeneity in *Staphylococcus aureus*. Microbes Environ. *25*, 75–82.

Morrison, J.M., Anderson, K.L., Beenken, K.E., Smeltzer, M.S., and Dunman, P.M. (2012). The Staphylococcal Accessory Regulator, SarA, is an RNA-Binding Protein that Modulates the mRNA Turnover Properties of Late-Exponential and Stationary Phase *Staphylococcus aureus* Cells. Front. Cell. Infect. Microbiol. *2*.

Mosteller, R.D., and Yanofsky, C. (1970). Transcription of the tryptophan operon in *Escherichia coli*: Rifampicin as an inhibitor of initiation. J. Mol. Biol. *48*, 525–531.

Mudd, E.A., Krisch, H.M., and Higgins, C.F. (1990). RNase E, an endoribonuclease, has a general role in the chemical decay of *Escherichia coli* mRNA: evidence that rne and ams are the same genetic locus. Mol. Microbiol. *4*, 2127–2135.

Mulhbacher, J., St-Pierre, P., and Lafontaine, D.A. (2010a). Therapeutic applications of ribozymes and riboswitches. Curr. Opin. Pharmacol. *10*, 551–556.

Mulhbacher, J., Brouillette, E., Allard, M., Fortier, L.-C., Malouin, F., and Lafontaine, D.A. (2010b). Novel Riboswitch Ligand Analogs as Selective Inhibitors of Guanine-Related Metabolic Pathways. PLoS Pathog *6*, e1000865.

Nahvi, A., Sudarsan, N., Ebert, M.S., Zou, X., Brown, K.L., and Breaker, R.R. (2002). Genetic Control by a Metabolite Binding mRNA. Chem. Biol. *9*, 1043–1049.

Nahvi, A., Barrick, J.E., and Breaker, R.R. (2004). Coenzyme B12 riboswitches are widespread genetic control elements in prokaryotes. Nucleic Acids Res. *32*, 143–150.

Nair, D., Memmi, G., Hernandez, D., Bard, J., Beaume, M., Gill, S., Francois, P., and Cheung, A.L. (2011). Whole-genome sequencing of *Staphylococcus aureus* strain RN4220, a key laboratory strain used in virulence research, identifies mutations that affect not only virulence factors but also the fitness of the strain. J. Bacteriol. *193*, 2332–2335.

Newbury, S.F., Smith, N.H., and Higgins, C.F. (1987). Differential mRNA stability controls relative gene expression within a polycistronic operon. Cell *51*, 1131–1143.

Newman, J.A., Hewitt, L., Rodrigues, C., Solovyova, A.S., Harwood, C.R., and Lewis, R.J. (2012). Dissection of the Network of Interactions That Links RNA Processing with Glycolysis in the *Bacillus subtilis* Degradosome. J. Mol. Biol. *416*, 121–136.

Novick, R.P. (2003). Autoinduction and signal transduction in the regulation of staphylococcal virulence. Mol. Microbiol. *48*, 1429–1449.

Nozaki, S., and Niki, H. (2019). Exonuclease III (XthA) Enforces *In Vivo* DNA Cloning of *Escherichia coli* To Create Cohesive Ends. J. Bacteriol. *201*, e00660-18.

Ogston, A. (1882). Micrococcus Poisoning. J. Anat. Physiol. *17*, 24–58.

Orac, C.M., Zhou, S., Means, J.A., Boehm, D., Bergmeier, S.C., and Hines, J.V. (2011). Synthesis and Stereospecificity of 4,5-Disubstituted Oxazolidinone Ligands Binding to T-box Riboswitch RNA. J. Med. Chem. *54*, 6786–6795.

Ouellette, S.P., Karimova, G., Davi, M., and Ladant, D. (2017). Analysis of Membrane Protein Interactions with a Bacterial Adenylate Cyclase–Based Two-Hybrid (BACTH) Technique. Curr. Protoc. Mol. Biol. *118*, 20.12.1-20.12.24.

Oun, S., Redder, P., Didier, J.-P., François, P., Corvaglia, A.-R., Buttazzoni, E., Giraud, C., Girard, M., Schrenzel, J., and Linder, P. (2013). The CshA DEAD-box RNA helicase is important for quorum sensing control in *Staphylococcus aureus*. RNA Biol. *10*, 157–165.

Paul, B.D., and Snyder, S.H. (2012). H_2S signalling through protein sulfhydration and beyond. Nat. Rev. Mol. Cell Biol. *13*, 499–507.

Pedersen, M., Nissen, S., Mitarai, N., Svenningsen, S.L., Sneppen, K., and Pedersen, S. (2011). The Functional Half-Life of an mRNA Depends on the Ribosome Spacing in an Early Coding Region. J. Mol. Biol. *407*, 35–44.

Perkins, K.R., Atilho, R.M., Moon, M.H., and Breaker, R.R. (2019). Employing a ZTP Riboswitch to Detect Bacterial Folate Biosynthesis Inhibitors in a Small Molecule High-throughput Screen. ACS Chem. Biol.

Pertzev, A.V., and Nicholson, A.W. (2006). Characterization of RNA sequence determinants and antideterminants of processing reactivity for a minimal substrate of *Escherichia coli* ribonuclease III. Nucleic Acids Res. *34*, 3708–3721.

Pohl, K., Francois, P., Stenz, L., Schlink, F., Geiger, T., Herbert, S., Goerke, C., Schrenzel, J., and Wolz, C. (2009). CodY in *Staphylococcus aureus*: a Regulatory Link between Metabolism and Virulence Gene Expression. J. Bacteriol. *191*, 2953–2963.

Proctor, R.A., Kriegeskorte, A., Kahl, B.C., Becker, K., Löffler, B., and Peters, G. (2014). *Staphylococcus aureus* Small Colony Variants (SCVs): a road map for the metabolic pathways involved in persistent infections. Front. Cell. Infect. Microbiol. *4*.

Prud'homme-Généreux, A., Beran, R.K., Iost, I., Ramey, C.S., Mackie, G.A., and Simons, R.W. (2004). Physical and functional interactions among RNase E, polynucleotide phosphorylase and the cold-shock protein, CsdA: evidence for a 'cold shock degradosome.' Mol. Microbiol. *54*, 1409–1421.

Ratnayake-Lecamwasam, M., Serror, P., Wong, K.-W., and Sonenshein, A.L. (2001). *Bacillus subtilis* CodY represses early-stationary-phase genes by sensing GTP levels. Genes Dev. *15*, 1093–1103.

Redder, P., and Linder, P. (2012). New Range of Vectors with a Stringent 5-Fluoroorotic Acid-Based Counterselection System for Generating Mutants by Allelic Replacement in *Staphylococcus aureus*. Appl. Environ. Microbiol. *78*, 3846–3854.

Regulski, E.E., and Breaker, R.R. (2008). In-line probing analysis of riboswitches. Methods Mol. Biol. Clifton NJ *419*, 53–67.

Reiter, N.J., Osterman, A., Torres-Larios, A., Swinger, K.K., Pan, T., and Mondragón, A. (2010). Structure of a bacterial ribonuclease P holoenzyme in complex with tRNA. Nature *468*, 784–789.

Rekand, I.H., and Brenk, R. (2017). Ligand design for riboswitches, an emerging target class for novel antibiotics. Future Med. Chem. *9*, 1649–1663.

Resch, A., Rosenstein, R., Nerz, C., and Götz, F. (2005). Differential Gene Expression Profiling of *Staphylococcus aureus* Cultivated under Biofilm and Planktonic Conditions. Appl. Environ. Microbiol. *71*, 2663–2676.

Roberts, C., Anderson, K.L., Murphy, E., Projan, S.J., Mounts, W., Hurlburt, B., Smeltzer, M., Overbeek, R., Disz, T., and Dunman, P.M. (2006). Characterizing the Effect of the *Staphylococcus aureus* Virulence Factor Regulator, SarA, on Log-Phase mRNA Half-Lives. J. Bacteriol. *188*, 2593–2603.

Rodionov, D.A., Vitreschak, A.G., Mironov, A.A., and Gelfand, M.S. (2004). Comparative genomics of the methionine metabolism in Gram-positive bacteria: a variety of regulatory systems. Nucleic Acids Res. *32*, 3340–3353.

Rogalski, E. (2017). Charakterisierung der metallabhängigen Hydrolase (Mdh) im Methionin-Biosyntheseoperon von *Staphylococcus aureus*. Master Thesis (Study programme Biology). Julius-Maximilians Universität Würzburg.

Rollins, S.M., Grundy, F.J., and Henkin, T.M. (1997). Analysis of cis-acting sequence and structural elements required for antitermination of the *Bacillus subtilis tyrS* gene. Mol. Microbiol. *25*, 411–421.

Romilly, C., Chevalier, C., Marzi, S., Masquida, B., Geissmann, T., Vandenesch, F., Westhof, E., and Romby, P. (2012). Loop-loop interactions involved in antisense regulation are processed by the endoribonuclease III in *Staphylococcus aureus*. RNA Biol. *9*, 1461–1472.

Roux, C.M., DeMuth, J.P., and Dunman, P.M. (2011). Characterization of Components of the *Staphylococcus aureus* mRNA Degradosome Holoenzyme-Like Complex. J. Bacteriol. *193*, 5520–5526.

Saad, N.Y., Stamatopoulou, V., Brayé, M., Drainas, D., Stathopoulos, C., and Becker, H.D. (2013). Two-codon T-box riboswitch binding two tRNAs. Proc. Natl. Acad. Sci. *110*, 12756–12761.

Saeed, A. i., Sharov, V., White, J., Li, J., Liang, W., Bhagabati, N., Braisted, J., Klapa, M., Currier, T., Thiagarajan, M., et al. (2003). TM4: A Free, Open-Source System for Microarray Data Management and Analysis. BioTechniques *34*, 374–378.

Salis, H.M. (2011). Chapter two - The Ribosome Binding Site Calculator. In Methods in Enzymology, C. Voigt, ed. (Academic Press), pp. 19–42.

Salis, H.M., Mirsky, E.A., and Voigt, C.A. (2009). Automated design of synthetic ribosome binding sites to control protein expression. Nat. Biotechnol. *27*, 946–950.

Schindelin, J., Arganda-Carreras, I., Frise, E., Kaynig, V., Longair, M., Pietzsch, T., Preibisch, S., Rueden, C., Saalfeld, S., Schmid, B., et al. (2012). Fiji: an open-source platform for biological-image analysis. Nat. Methods *9*, 676–682.

Schoenfelder, S.M.K. (2006). Suche nach kleinen regulatorischen RNAs im Genom von *Staphylococcus epidermidis*. Diploma Thesis. Julius-Maximilians Universität Würzburg.

Schoenfelder, S.M.K. (2011). Gene expression control in healthcare-associated Staphylococci: Characterisation of a T-box regulatory RNA element governing methionine biosynthesis gene transcription. Doctoral Thesis. Queen's University Belfast.

Schoenfelder, S.M.K., Marincola, G., Geiger, T., Goerke, C., Wolz, C., and Ziebuhr, W. (2013). Methionine Biosynthesis in *Staphylococcus aureus* Is Tightly Controlled by a Hierarchical Network Involving an Initiator tRNA-Specific T-box Riboswitch. PLOS Pathog. *9*, e1003606.

Seidel, S.A.I., Wienken, C.J., Geissler, S., Jerabek-Willemsen, M., Duhr, S., Reiter, A., Trauner, D., Braun, D., and Baaske, P. (2012). Label-Free Microscale Thermophoresis Discriminates Sites and Affinity of Protein–Ligand Binding. Angew. Chem. Int. Ed. *51*, 10656–10659.

Seif, E., and Altman, S. (2008). RNase P cleaves the adenine riboswitch and stabilizes *pbuE* mRNA in Bacillus subtilis. RNA *14*, 1237–1243.

Shahbabian, K., Jamalli, A., Zig, L., and Putzer, H. (2009). RNase Y, a novel endoribonuclease, initiates riboswitch turnover in *Bacillus subtilis*. EMBO J. *28*, 3523–3533.

Sharova, L.V., Sharov, A.A., Nedorezov, T., Piao, Y., Shaik, N., and Ko, M.S.H. (2009). Database for mRNA Half-Life of 19 977 Genes Obtained by DNA Microarray Analysis of Pluripotent and Differentiating Mouse Embryonic Stem Cells. DNA Res. Int. J. Rapid Publ. Rep. Genes Genomes *16*, 45–58.

Sherlock, M.E., Sudarsan, N., and Breaker, R.R. (2018). Riboswitches for the alarmone ppGpp expand the collection of RNA-based signaling systems. Proc. Natl. Acad. Sci. *115*, 6052–6057.

Sherwood, A.V., Grundy, F.J., and Henkin, T.M. (2015). T box riboswitches in Actinobacteria: Translational regulation via novel tRNA interactions. Proc. Natl. Acad. Sci. *112*, 1113–1118.

Sherwood, A.V., Frandsen, J.K., Grundy, F.J., and Henkin, T.M. (2018). New tRNA contacts facilitate ligand binding in a *Mycobacterium smegmatis* T box riboswitch. Proc. Natl. Acad. Sci. 201721254.

Shivers, R.P., and Sonenshein, A.L. (2004). Activation of the *Bacillus subtilis* global regulator CodY by direct interaction with branched-chain amino acids. Mol. Microbiol. *53*, 599–611.

Silva, J.C., Gorenstein, M.V., Li, G.-Z., Vissers, J.P.C., and Geromanos, S.J. (2006). Absolute Quantification of Proteins by LCMSE : A Virtue of Parallel ms Acquisition. Mol. Cell. Proteomics *5*, 144–156.

Silvian, L.F., Wang, J., and Steitz, T.A. (1999). Insights into editing from an ile-tRNA synthetase structure with tRNAile and mupirocin. Science *285*, 1074–1077.

Sørensen, M.A., Fehler, A.O., and Svenningsen, S.L. (2018). Transfer RNA instability as a stress response in *Escherichia coli*: Rapid dynamics of the tRNA pool as a function of demand. RNA Biol. *15*, 586–593.

Stamatopoulou, V., Apostolidi, M., Li, S., Lamprinou, K., Papakyriakou, A., Zhang, J., and Stathopoulos, C. (2017). Direct modulation of T-box riboswitch-controlled transcription by protein synthesis inhibitors. Nucleic Acids Res. *45*, 10242–10258.

Steigerwald, D. (2016). Characterization of the *mdh* gene in the methionine synthesis operon of *Staphylococcus aureus*. Master Thesis (Study programme Biochemistry). Julius-Maximilinas Universität Würzburg.

Steitz, J.A. (1969). Polypeptide chain initiation: nucleotide sequences of the three ribosomal binding sites in bacteriophage R17 RNA. Nature *224*, 957–964.

Suddala, K.C., and Zhang, J. (2019). An evolving tale of two interacting RNAs—themes and variations of the T-box riboswitch mechanism. IUBMB Life *71*, 1167–1180.

Suddala, K.C., Cabello-Villegas, J., Michnicka, M., Marshall, C., Nikonowicz, E.P., and Walter, N.G. (2018). Hierarchical mechanism of amino acid sensing by the T-box riboswitch. Nat. Commun. *9*, 1896.

Svenningsen, S.L., Kongstad, M., Stenum, T.S., Muñoz-Gómez, A.J., and Sørensen, M.A. (2017). Transfer RNA is highly unstable during early amino acid starvation in *Escherichia coli*. Nucleic Acids Res. *45*, 793–804.

Taboada, B., Ciria, R., Martinez-Guerrero, C.E., and Merino, E. (2012). ProOpDB: Prokaryotic Operon DataBase. Nucleic Acids Res. *40*, D627–D631.

Trübe, P., Hertlein, T., Mrochen, D.M., Schulz, D., Jorde, I., Krause, B., Zeun, J., Fischer, S., Wolf, S.A., Walther, B., et al. (2019). Bringing together what belongs together: Optimizing murine infection models by using mouse-adapted *Staphylococcus aureus* strains. Int. J. Med. Microbiol. *309*, 26–38.

Vitreschak, A.G., Mironov, A.A., Lyubetsky, V.A., and Gelfand, M.S. (2008). Comparative genomic analysis of T-box regulatory systems in bacteria. RNA *14*, 717–735.

Vogel, U., and Jensen, K.F. (1994). The RNA chain elongation rate in *Escherichia coli* depends on the growth rate. J. Bacteriol. *176*, 2807–2813.

Wang, H., Fischmann, T.O., Balibar, C.J., Xiao, L., Galgoci, A.M., Malinverni, J.C., Mayhood, T., Villafania, A., Nahvi, A., Murgolo, N., et al. (2015). Selective small-molecule inhibition of an RNA structural element. Nature *526*, 672–677.

Wang, J., Henkin, T.M., and Nikonowicz, E.P. (2010). NMR structure and dynamics of the Specifier Loop domain from the *Bacillus subtilis tyrS* T box leader RNA. Nucleic Acids Res. *38*, 3388–3398.

Waterhouse, A.M., Procter, J.B., Martin, D.M.A., Clamp, M., and Barton, G.J. (2009). Jalview Version 2—a multiple sequence alignment editor and analysis workbench. Bioinformatics *25*, 1189–1191.

Welch, W., Ruppert, J., and Jain, A.N. (1996). Hammerhead: fast, fully automated docking of flexible ligands to protein binding sites. Chem. Biol. *3*, 449–462.

Wencker, F., and Ziebuhr, W. (2017). Chapter 13: Methionine Synthesis in Microbes. In The Handbook of Microbial Metabolism of Amino Acids, (Oxfordshire, UK: CABI), pp. 179–197.

Wertheim, H.F., Melles, D.C., Vos, M.C., van Leeuwen, W., van Belkum, A., Verbrugh, H.A., and Nouwen, J.L. (2005). The role of nasal carriage in *Staphylococcus aureus* infections. Lancet Infect. Dis. *5*, 751–762.

Whitfield, C.D., Steers, E.J., and Weissbach, H. (1970). Purification and Properties of 5-Methyltetrahydropteroyltriglutamate-Homocysteine Transmethylase. J. Biol. Chem. *245*, 390–401.

Wienken, C.J., Baaske, P., Rothbauer, U., Braun, D., and Duhr, S. (2010). Protein-binding assays in biological liquids using microscale thermophoresis. Nat. Commun. *1*, 1–7.

Williams, R.E.O. (1963). Healthy Carriage of *Staphylococcus aureus*: Its Prevalence and Importance. Microbiol. Mol. Biol. Rev. *27*, 56–71.

Winkler, W.C., Grundy, F.J., Murphy, B.A., and Henkin, T.M. (2001). The GA motif: an RNA element common to bacterial antitermination systems, rRNA, and eukaryotic RNAs. RNA *7*, 1165–1172.

Winkler, W.C., Nahvi, A., Roth, A., Collins, J.A., and Breaker, R.R. (2004). Control of gene expression by a natural metabolite-responsive ribozyme. Nature *428*, 281–286.

Yarchuk, O., Iost, I., and Dreyfus, M. (1991). The relation between translation and mRNA degradation in the *lacZ* gene. Biochimie *73*, 1533–1541.

Zhang, J., and Ferré-D'Amaré, A.R. (2013). Co-crystal structure of a T-box riboswitch stem I domain in complex with its cognate tRNA. Nature *500*, 363–366.

Zhang, J., and Ferré-D'Amaré, A.R. (2015). Structure and mechanism of the T-box riboswitches. Wiley Interdiscip. Rev. RNA *6*, 419–433.

Zhang, J., and Ferré-DAmaré, A.R. (2016). Trying on tRNA for Size: RNase P and the T-box Riboswitch as Molecular Rulers. Biomolecules *6*, 18.

Zhang, J., Chetnani, B., Cormack, E.D., Alonso, D., Liu, W., Mondragón, A., and Fei, J. (2018). Specific structural elements of the T-box riboswitch drive the two-step binding of the tRNA ligand. ELife *7*, e39518.

Zhou, S., Means, J.A., Acquaah-Harrison, G., Bergmeier, S.C., and Hines, J.V. (2012). Characterization of a 1,4-disubstituted 1,2,3-triazole binding to T box antiterminator RNA. Bioorg. Med. Chem. *20*, 1298–1302.

Ziehler, W.A., and Engelke, D.R. (2000). Probing RNA Structure with Chemical Reagents and Enzymes. Curr. Protoc. Nucleic Acid Chem. *00*, 6.1.1-6.1.21.

Zubieta, C., Arkus, K.A.J., Cahoon, R.E., and Jez, J.M. (2008). A Single Amino Acid Change Is Responsible for Evolution of Acyltransferase Specificity in Bacterial Methionine Biosynthesis. J. Biol. Chem. *283*, 7561–7567.

Zuker, M. (2003). Mfold web server for nucleic acid folding and hybridization prediction. Nucleic Acids Res. *31*, 3406–3415.

Euromedex BACTH Manual. BACTH System Kit (Bacterial Adenylate Cyclase Two-Hybrid System Kit) www.euromedex.com

7.1. Online sources

graphical codon usage analyser 2.0: http://gcua.schoedl.de/sequentialex.html
(last accessed 10.02.2020)
Kyoto Encyclopedia of Genes and Genomes (KEGG): https://www.kegg.jp/
(last accessed 10.02.2020)
Manual for blot quantification unsing ImageJ: https://di.uq.edu.au/community-and-alumni/sparq-ed/sparq-ed-services/using-imagej-quantify-blots (last accessed 10.02.2020)
mfold web server: http://unafold.rna.albany.edu/?q=mfold/RNA-Folding-Form
(last accessed 10.02.2020)
MUSCLE (**MU**ltiple **S**equence **C**omparison by **L**og- **E**xpectation): http://www.ebi.ac.uk/Tools/msa/muscle/ (last accessed 10.02.2020)
NCBI Taxonomy Browser: https://www.ncbi.nlm.nih.gov/Taxonomy/Browser/wwwtax.cgi
(last accessed 10.02.2020)
NTML: https://www.unmc.edu/pathology/csr/research/library.html
(last accessed 10.02.2020)
NTML function genomics explorer, Methods: https://app1.unmc.edu/fgx/methods.html
(last accessed 10.02.2020)
NTML function genomics explorer, Tn insertion map: https://app1.unmc.edu/fgx/
(last accessed 10.02.2020)
S. aureus expression data browser: http://genome.jouy.inra.fr/cgi-bin/aeb/index.py
(last accessed 10.02.2020)

8. Appendix

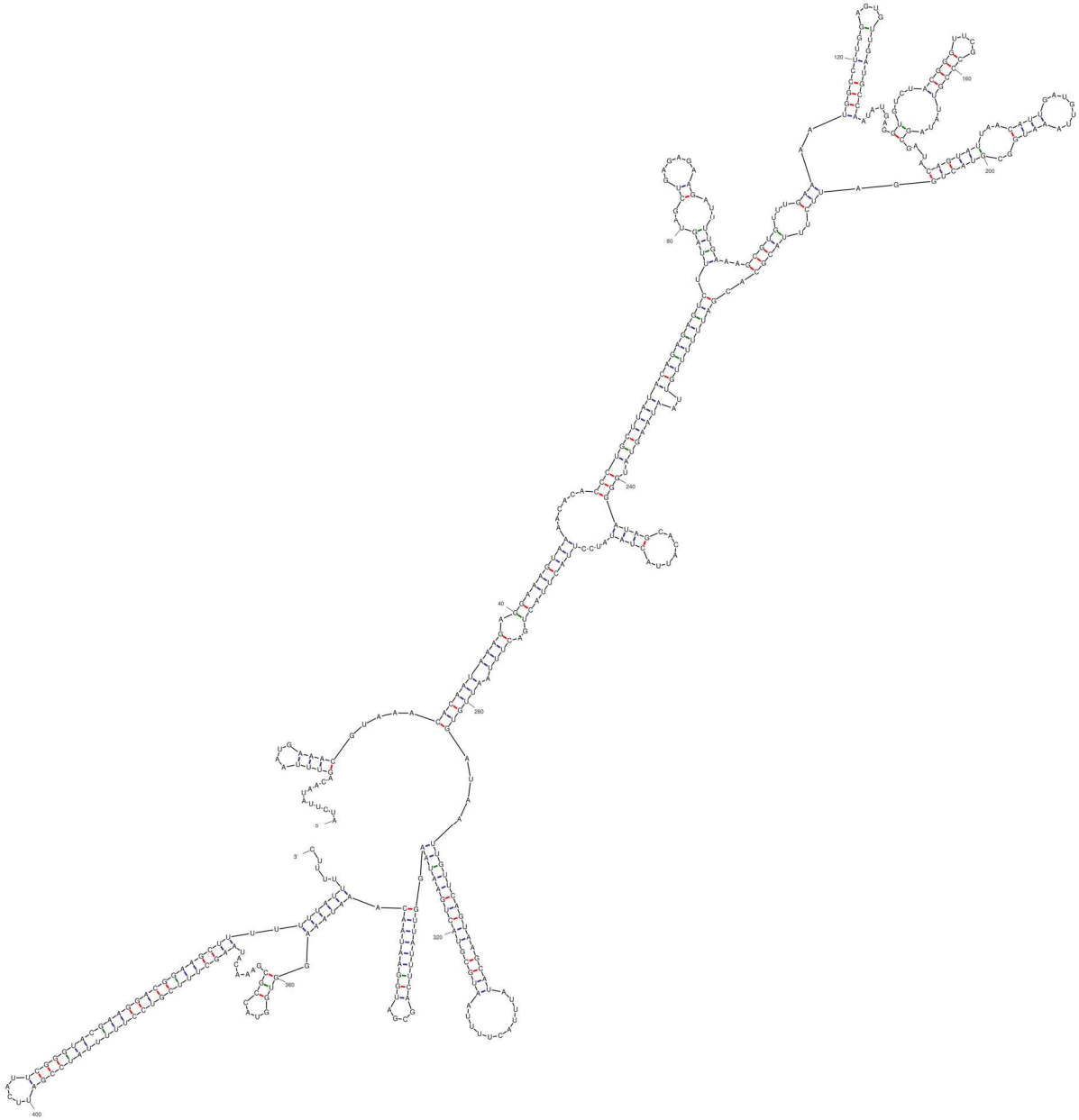

Figure A1. Secondary structure of *met* leader predicted by mfold. Complete sequence of *S. aureus met* leader was entered into mfold and secondary structure was predicted. Structure #1 was chosen (Zuker, 2003).

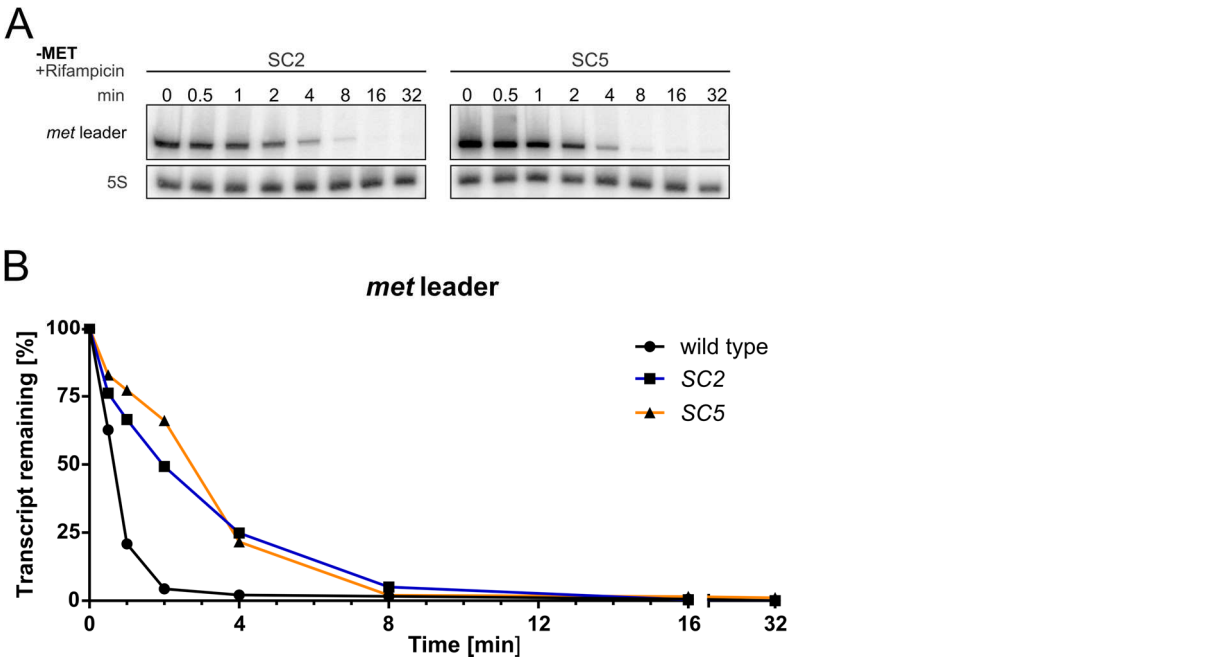

Figure A2. The *met* leader mutants SC2 and SC5 have an increased *met* leader stability compared to the wild type. (A) Total RNA isolated from *S. aureus* Newman *met* leader mutants SC2 and SC5 grown in CDM with methionine, then washed and shifted for two hours into CDM without methionine ('-MET'). Samples were taken over a time course of rifampicin addition (0-32 min). RNA was run on a denaturing 5 % PAA 7 M Urea gel and blotted onto a nylon membrane. Northern blot was hybridised with a *met* leader-specific probe and subsequently re-hybridised with a 5S rRNA-specific probe as loading control. **(B)** Quantification of *met* leader transcript levels over time from rifampicin stability assays shown in (A) and *S. aureus* Newman wild type RNA shown in **Fig. 9**.

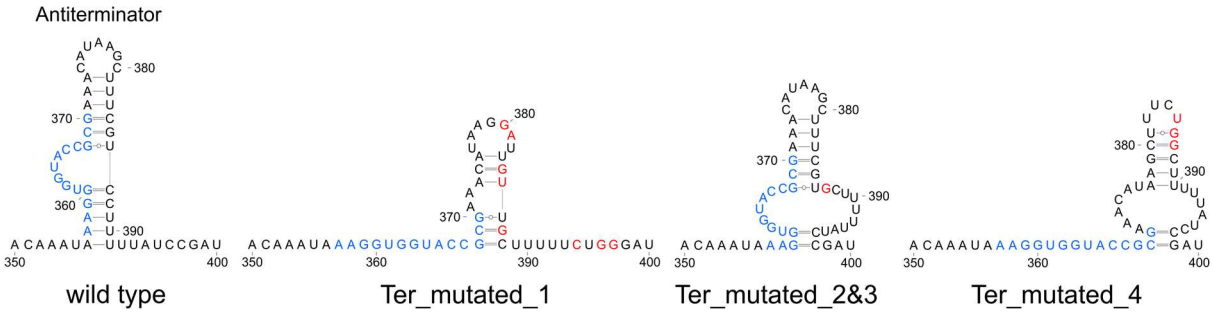

Figure A3. Predicted secondary structures of Antiterminator region of *met* leader mutants Ter_mutated_1 and Ter_mutated_2, 3, 4. Secondary structures predicted with mfold (Zuker, 2003) of Antiterminator region in *met* leader of wild type and Ter_mutated mutants. T-box sequence is highlighted in blue, point mutations introduced are shown in red.

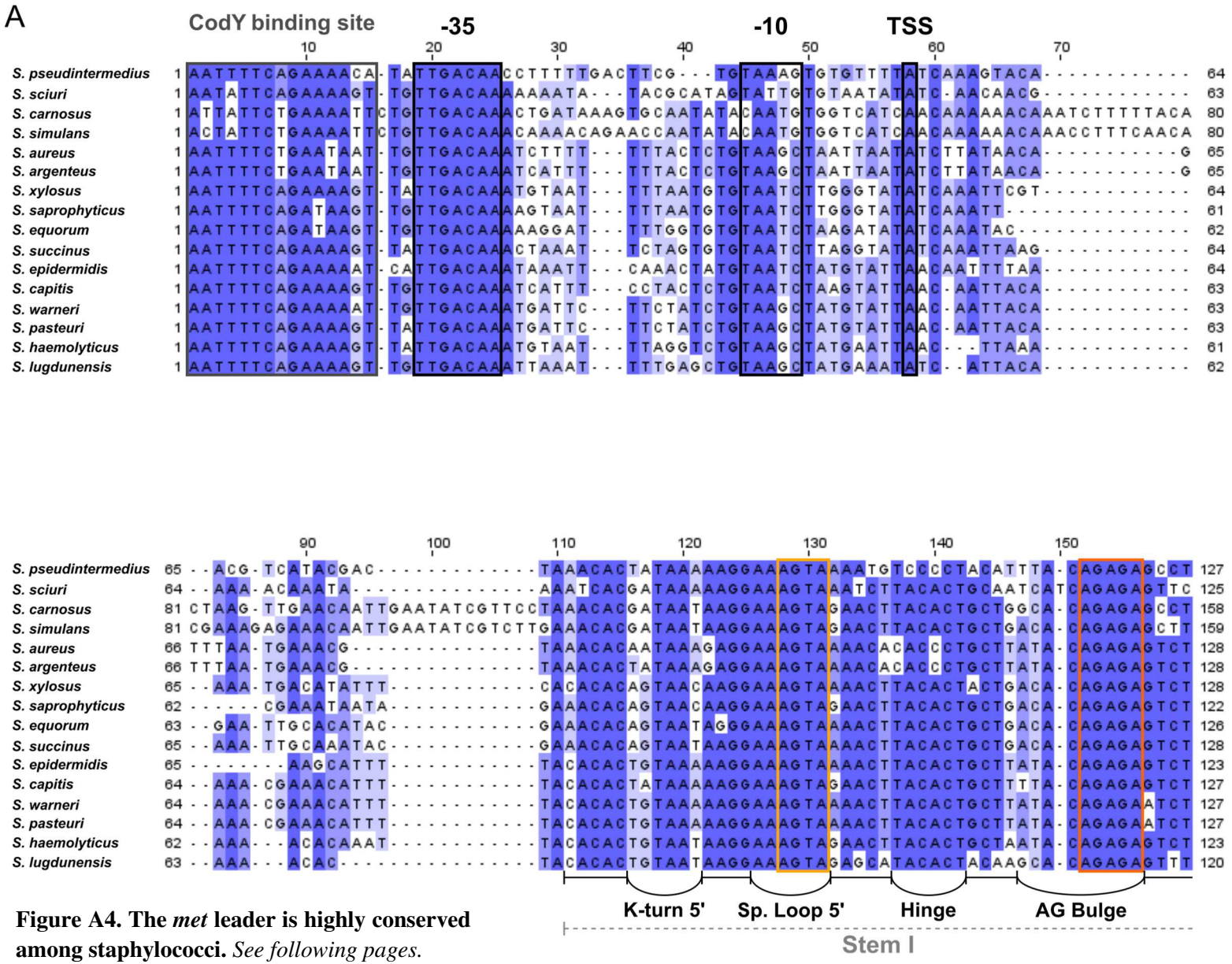

Figure A4. The *met* leader is highly conserved among staphylococci. *See following pages.*

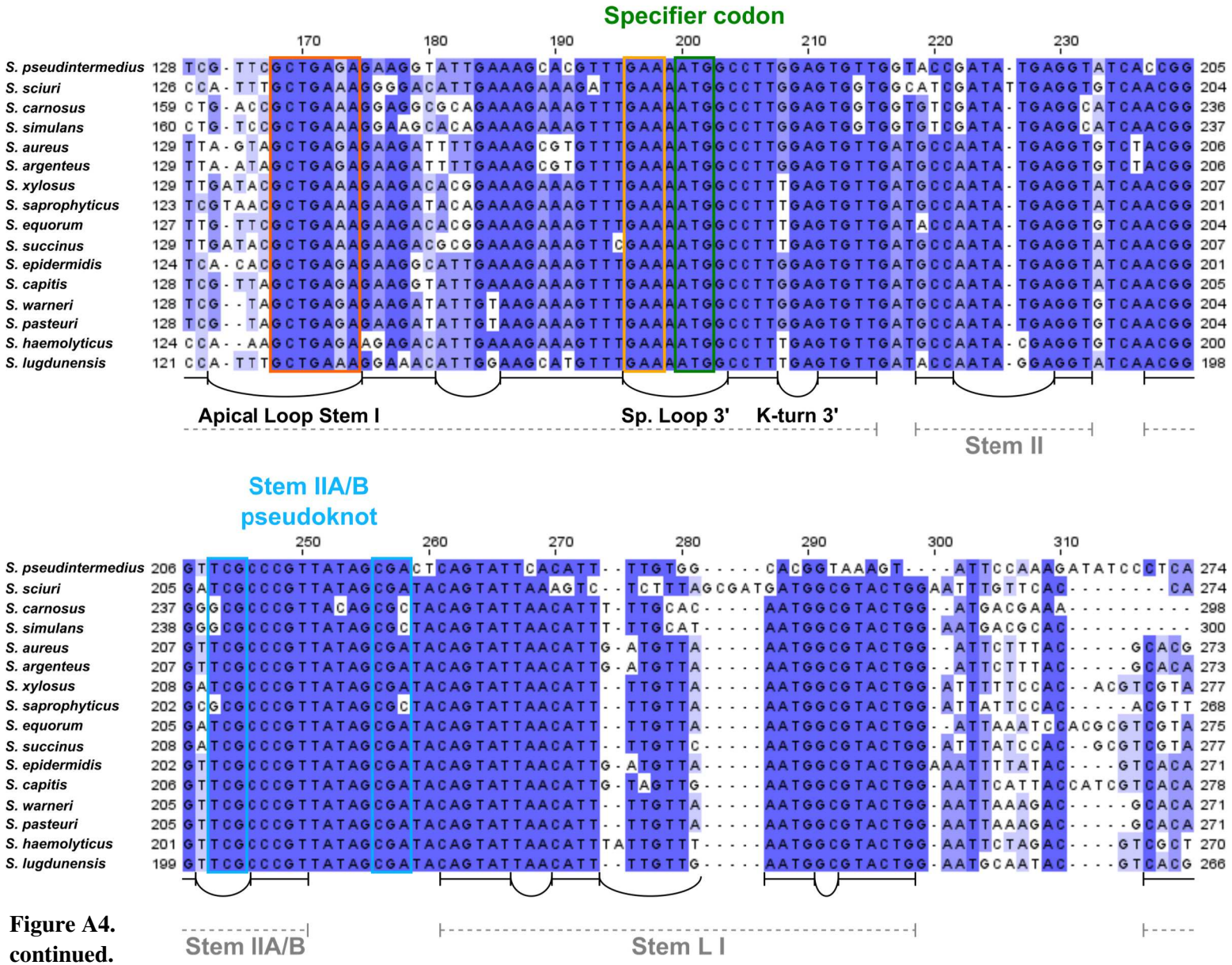

Figure A4. continued.

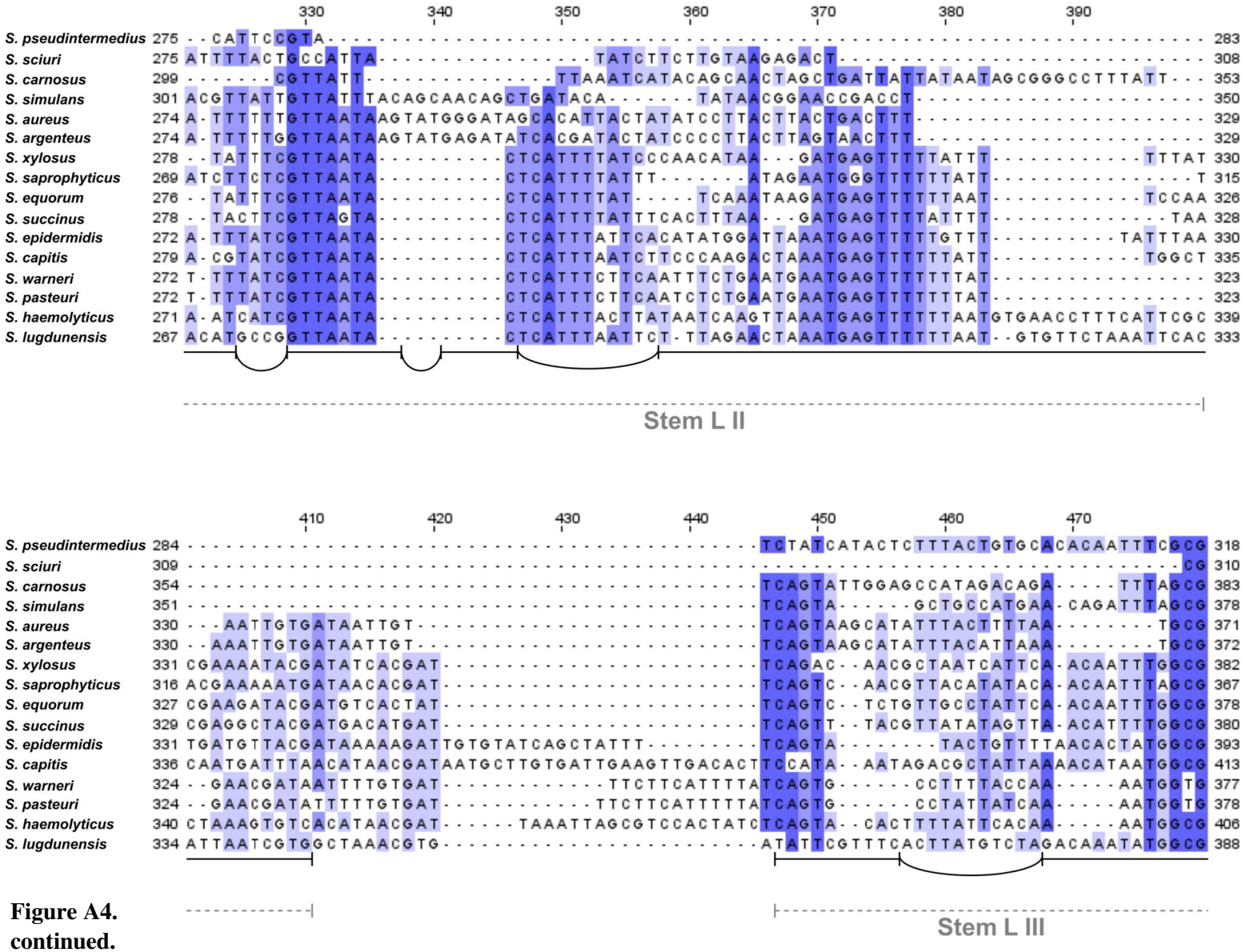

Figure A4. continued.

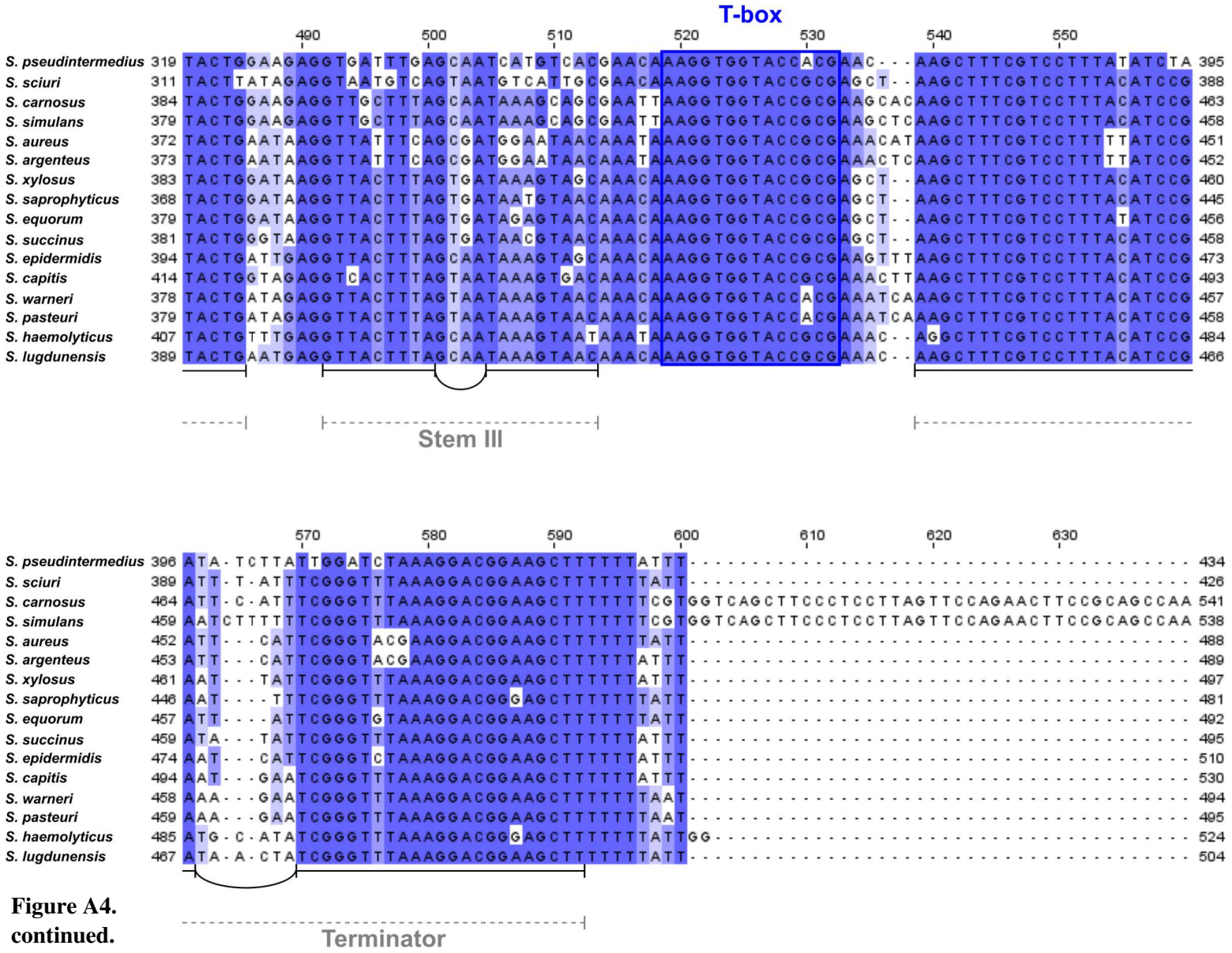

Figure A4. continued.

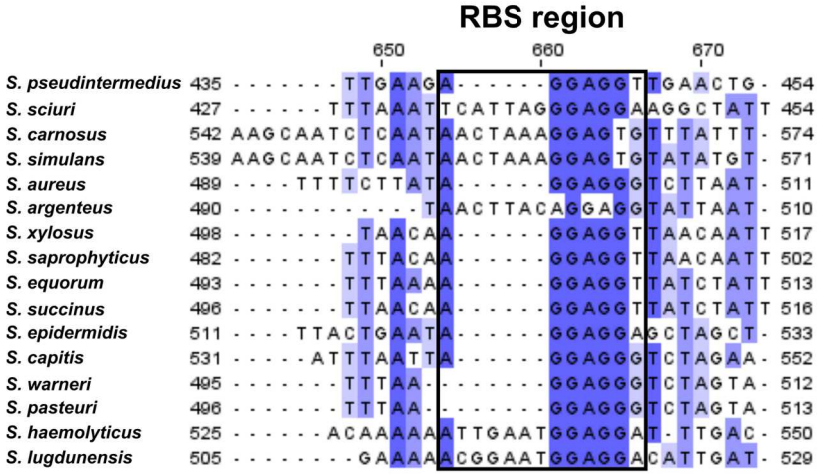

B

Staphylococcal species	Length [nt] *met* leader
S. sciuri	378
S. pseudintermedius	384
S. saprophyticus	432
S. argenteus	438
S. simulans	440
*S. aureus**	440
S. carnosus	443
S. equorum	443
S. succinus	445
S. pasteuri	446
S. warneri	446
S. xylosus	446
S. lugdunensis	452
*S. epidermidis**	459
S. haemolyticus	470
S. capitis	482

* experimentally validated
(this work, Schoenfelder et al., 2013)

Figure A4. continued.
(A) Alignment of *met* leader and its adjacent sequences of 16 staphylococcal species. All structural and sequence information given are according to findings in *S. aureus*. CodY binding site sequence is boxed in grey, -35, -10, TSS and RBS region are boxed in black, 'AGTA' sequence interacting with 'GAA' within Specifier Loop are boxed in light orange, 'AGAGA' motif of AG Bulge interacting with 'GCTGAGA' sequence of apical loop of Stem I are boxed in dark orange, Specifier codon is boxed in green, 'TCG' potentially interacting with 'CGA' to form Stem IIA/B pseudoknot are boxed in light blue, T-box sequence is boxed in dark blue. Below each alignment row secondary structure of the sequence is given: bars represent double-stranded stem regions, bows represent single-stranded regions forming loops, loops of special interest in Stem I are named, grey dashed bars indicate the whole region comprising a certain stem structure. Sequences were aligned using MUSCLE (**MU**ltiple **S**equence **C**omparison by **L**og- **E**xpectation), graphical representation of alignments was done with Jalview (Waterhouse et al., 2009). Nucleotides shaded in dark blue: > 80 % of aligned nucleotides at this position agree with the consensus sequence, in blue > 60 % and in light blue > 40 %, nucleotides that differ from consensus are not shaded. **(B)** Staphylococcal species sorted by size of the predicted *met* leader according to the alignment. For *S. aureus* and *S. epidermidis* existence of the *met* leader RNA has been experimentally validated, indicated by an asterisk (*).

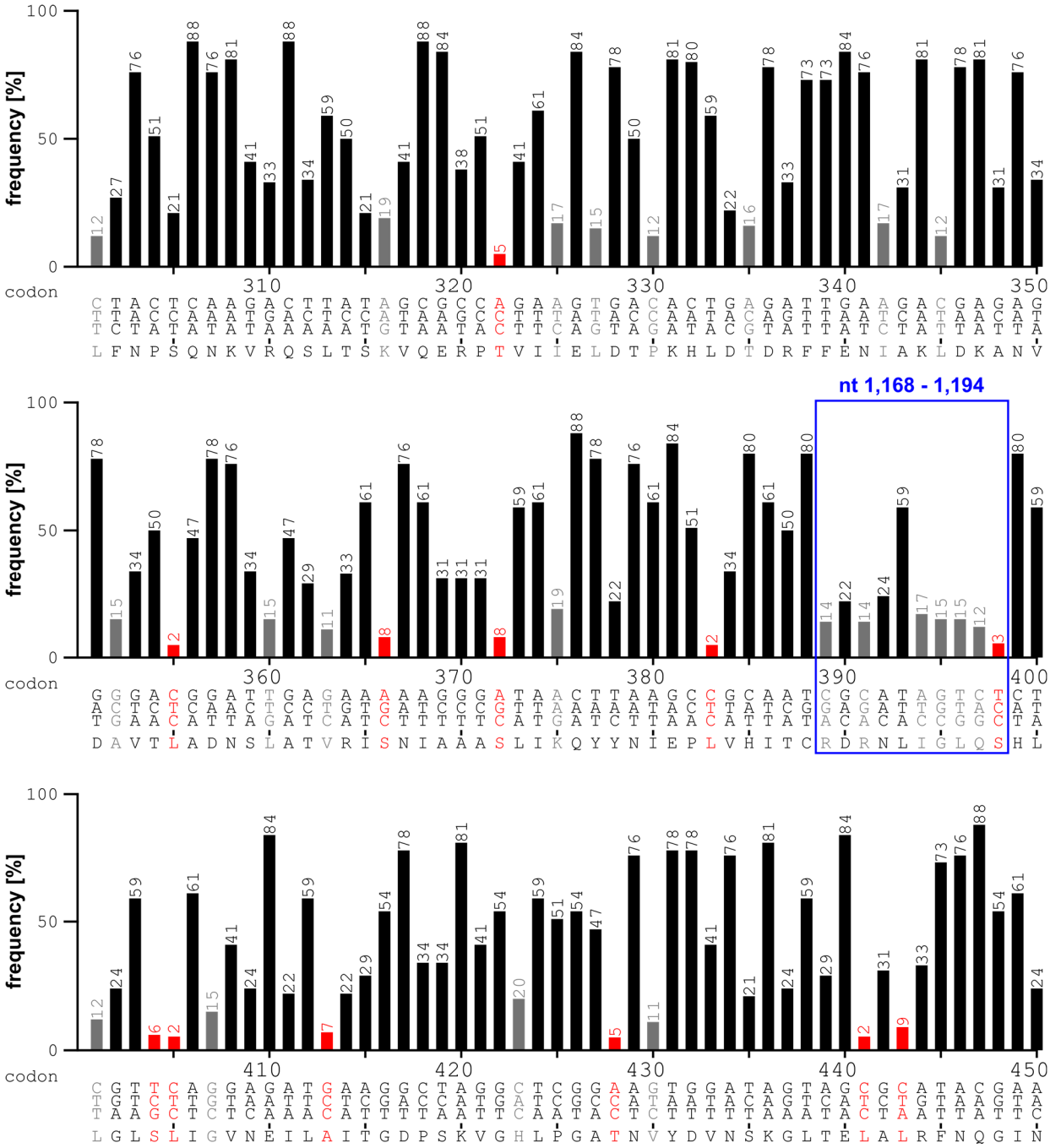

Figure A5. Stretch of rare codons present within last 800 nts of *metF*. Frequency of each codon from 300-450 (= nt 900-1,350) of *metF* is given in percent ('%') for *S. aureus*. 'AUG' would have a frequency of 100 % because it is the only base triplet coding for methionine. A frequency of 80 % means that the respective codon is used by *S. aureus* in 80 % of cases, when the particular amino acid is encoded. Therefore, this codon would be regarded as frequent. Codons with frequencies below 20 % (grey) and 10 % (red) are regarded as rare codons. Region of nt 1,168-1,194 (= codons 389-398) within *metF*, where 29 % of 5'-ends were detected with 5' RACE is highlighted by a blue box. Base triplet and amino acid in single letter code is given for each position.

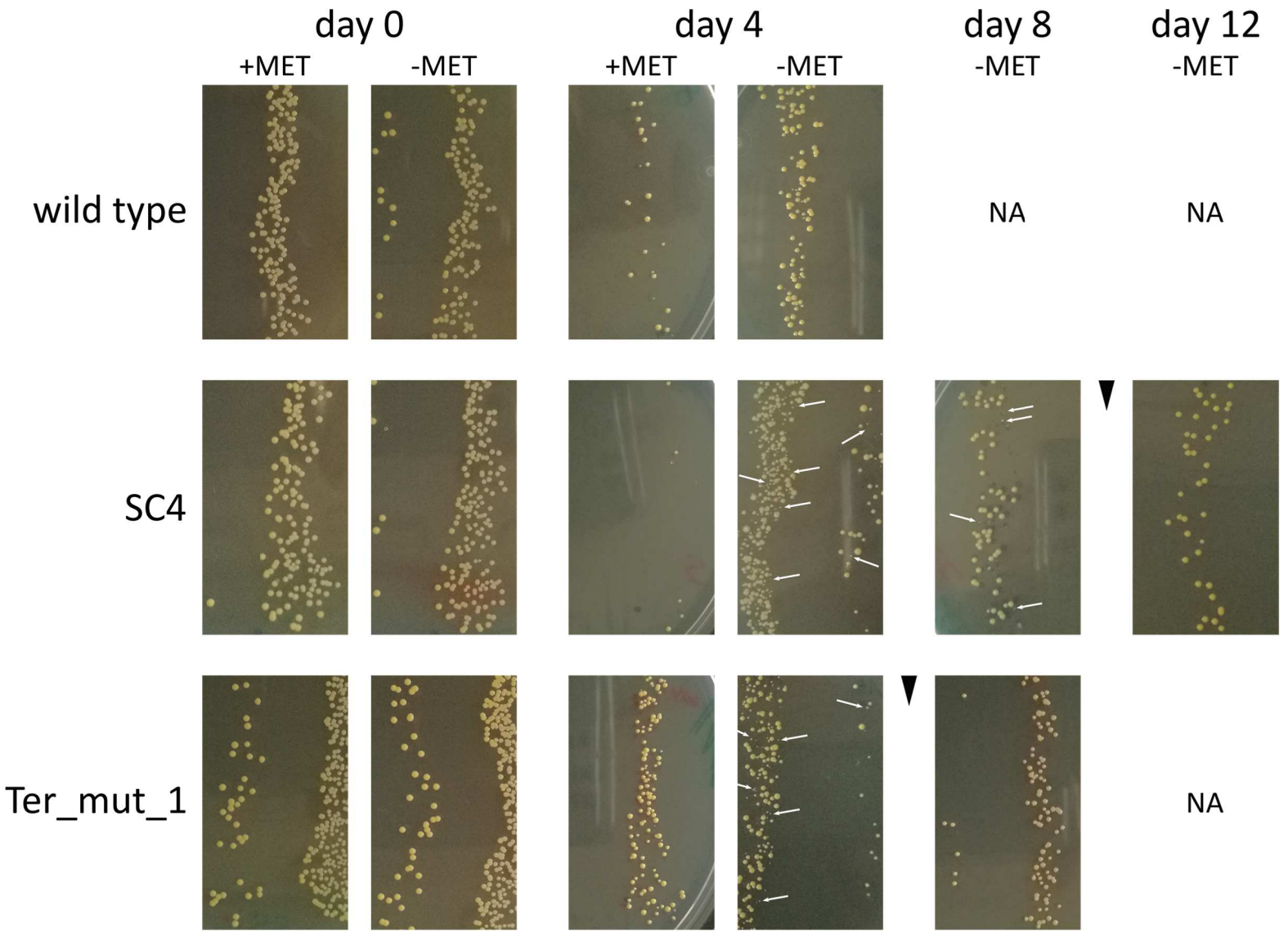

Figure A6. *(see next page).*

Figure A6. Influence of long-term cultivation on *met* leader 'OFF' mutants SC4 and Ter_mutated_1 under methionine-deprived conditions. Colony images of *S. aureus* Newman and its isogenic *met* leader 'OFF' mutants SC4 and Ter_mutated_1 grown in CDM with ('+MET') and without ('-MET') methionine and plated on TSB agar at time points indicated for CFU determinations. White arrows indicate potential small colony variant-like phenotypes. Black arrowheads symbolise onset of growth in the culture. For details see text. NA: not applicable as CFU was 0. Ter_mutated_1 abbreviated as 'Ter_mut_1'.

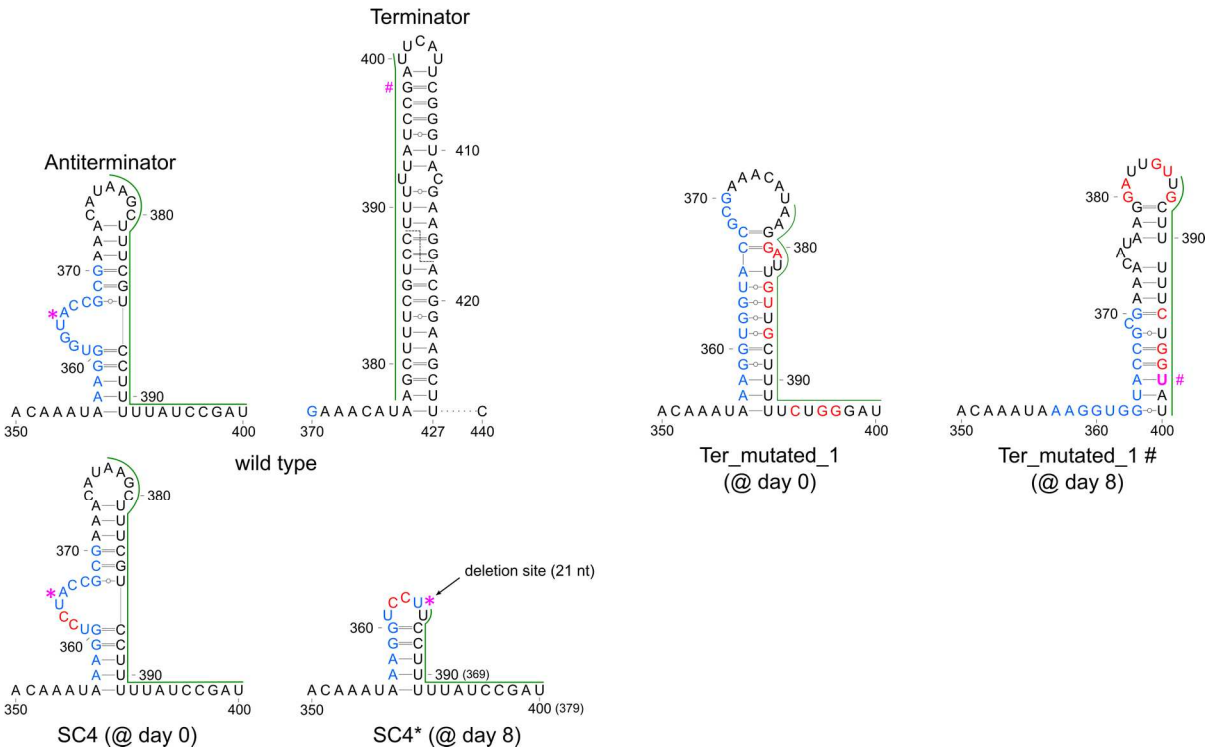

Figure A7. Mutations acquired during long-term cultivation under methionine-deprived conditions in *met* leader 'OFF' mutants SC4 and Ter_mutated_1 likely enable operon activation. Predicted secondary structures of region 350-400 of *met* leader in 'OFF' mutants at days 0 and 8. Antiterminator and Terminator structures of the wild type are shown for comparison. T-box sequence or parts thereof are shown in blue. Point mutations compared to the wild type sequence are highlighted in red. Region comprising the 5'-half of the Terminator stem is indicated by a green line. Magenta asterisk (*) marks the deletion site of 21 nucleotides in the SC4 sequence after 8 days of incubation (SC4*). Magenta hashtag (#) marks the position of the G to U point mutation in the Ter_mutated_1 sequence after 8 days (Ter_mutated_1 #). For details see text. Structures were predicted with mfold (Zuker, 2003).

9. Curriculum Vitae

10.Publication List

The listed publications, not directly related to the doctoral thesis, were released during the doctoral research work:

Schoenfelder, S.M.K., Lange, C., Prakash, S.A., Marincola, G., Lerch, M.F., **Wencker, F.D.R.**, Förstner, K.U., Sharma, C.M., and Ziebuhr, W. (2019). The small non-coding RNA RsaE influences extracellular matrix composition in *Staphylococcus epidermidis* biofilm communities. PLOS Pathogens 15, e1007618.

Marincola, G., **Wencker, F.D.R.**, and Ziebuhr, W. (2019). The Many Facets of the Small Non-coding RNA RsaE (RoxS) in Metabolic Niche Adaptation of Gram-Positive Bacteria. Journal of Molecular Biology 431, 4684–4698.

Lerch, M.F., Schoenfelder, S.M.K., Marincola, G., **Wencker, F.D.R.**, Eckart, M., Förstner, K.U., Sharma, C.M., Thormann, K.M., Kucklick, M., Engelmann, S., et al. (2019). A non-coding RNA from the intercellular adhesin (ica) locus of *Staphylococcus epidermidis* controls polysaccharide intercellular adhesin (PIA)-mediated biofilm formation. Molecular Microbiology.

The following book chapter related to the doctoral thesis was published:

Wencker, F., and Ziebuhr, W. (2017). Methionine Synthesis in Microbes. In The Handbook of Microbial Metabolism of Amino Acids, (Oxfordshire, UK: CABI), pp. 179–197.

The following manuscript related to the doctoral thesis is in preparation:

Wencker, F.D.R., Marincola, G., Schoenfelder, S.M.K., Maaß, S., Becher, D. and Ziebuhr, W. Another layer of complexity in *Staphylococcus aureus* methionine biosynthesis control: Unusual RNase III-driven T-box riboswitch processing determines *met* operon mRNA stability and decay

Previous publication:

The listed study was published prior to the beginning of, and is unrelated to, the doctoral thesis:

Pulcini, C., **Wencker, F.**, Frimodt-Møller, N., Kern, W.V., Nathwani, D., Rodríguez-Baño, J., Simonsen, G.S., Vlahović-Palčevski, V., Gyssens, I.C., Gyssens, I.C., et al. (2015). European survey on principles of prudent antibiotic prescribing teaching in undergraduate students. Clinical Microbiology and Infection 21, 354–361.

11.Acknowledgements

I thank PD Dr Wilma Ziebuhr for her supervision, support and scientific curiosity, and for encouraging me to present my work at many national and international conferences. I gathered a lot of valuable experiences during my PhD, working on a topic I am still enthusiastic about.

I would like to express my gratitude to my thesis committee Prof Dr Caroline Kisker and PD Dr Knut Ohlsen for their suggestions, guidance and support during my whole PhD.

I thank Dr Gabriella Marincola for her persistence to push things forwards, for her scientific advice anytime I needed it and for being a true friend. And of course for coffee, pizza and her 'athletic effort' during harvesting the bacteria for the 'big protein experiment'.

A big thanks to my master students Daniela Steigerwald, Esther Rogalski and Matthias Peindl for their efforts on the Mdh project and 'teaching' me how to supervise.

I thank Dr Yesid Ramiréz for offering to take Mdh (purified by Daniela) and 'just give it a try, if it crystallises'. It did marvellously. Funny enough that it all started with dancing salsa.

I thank Dr Wolfgang Kölmel for solving the crystal structure with Yesid, for suggesting several mutants and for answering all my questions regarding proteins and crystallisation that came up during the writing process.

I would like to thank Dr Sandra Maaß for processing the protein samples, analysing the data with me and answering all my proteomics questions.

Furthermore, I thank Dr Sonja Schönfelder for remembering everything she previously ever did on the *met* leader project and for intense discussions on the topic.

I am grateful to Dr Maike Lerch who told me on my first day 'don't trust anyone [regarding accuracy]'. This advice saved me weeks of errant work already more than once.

I want to thank Dr Tan Hock Siew (Patrick) for initial training and 'special tricks' with the in-line probing method.

Thanks to Prof Dr Peter Redder for visiting my poster on my very first conference and offering his RNase J mutants.

I thank Lukardis Wencker, Michael Epple and Dieter Filser for proofreading.

I am deeply grateful to my family for their mental support and the certainty that they are always there for me. I particularly thank my mother who all along encouraged me to cut my own path.

I thank Dieter for listening, taking the load off me, for helping me to maintain a certain level of work-life balance and loving me the way I am.

And last but not least, I thank my biology teachers Ms Mitze-Baumeister and Mr Mitze who infected me with their excitement for biology.